Solute Mixing in Full-Scale Constructed Wetlands: Seasonal Variation of Vegetation & Hydraulic Performance

Vasiliki Ioannidou (MSc, MEng)

Thesis

Submitted in fulfilment of the requirements for the degree of Doctor of Philosophy

University of Warwick, School of Engineering

June, 2017

Contents

List of Figures

List of Tables

List of Publications

Parts of this thesis have been published by the author:

Peer-reviewed Journals:

1. **Ioannidou, V.G**. & Pearson, J.M. The effects of flow rate and seasonal vegetation variation on the longitudinal mixing characteristics and other hydraulic parameters in a full-scale constructed farm wetland. (Under review).

Peer-reviewed Conferences:

1. **Ioannidou, V.G**. & Pearson, J.M. (2017). Case Studies Investigating Hydraulic Parameters in Full-Scale Constructed Wetlands. *Environmental Water Resources Association (EWRA), 10th World Congress,* Athens, Greece, 5-9 July, 2017.
2. **Ioannidou, V.G.** & Pearson, J.M. (2015). Seasonal effects of vegetation and flow rate on mixing and pollutant transport in constructed wetlands. Proceedings of the WETPOL Conference, "6th International Symposium on Wetland Pollutant Dynamics and Control Annual Conference of the Constructed Wetland Association".

Posters:

1. Ramos, A.M., **Ioannidou, V.G.**, Whelan, M.J., Villa, R., Guymer, I. & Jefferson, B. (2015). Evaluating the potential of constructed wetlands for attenuating metaldehyde losses from agricultural land to surface waters. *SETAC Europe 25th Annual Meeting, 3-7 May, Barcelona*.

2. Ramos, A.M., **Ioannidou, V.G**., Whelan, M.J., Villa, R., Guymer, I. & Jefferson, B. (2015). Evaluating the potential of constructed wetlands for attenuating metaldehyde losses from agricultural land to surface waters. *WETPOL 2015, 6th International Symposium on Wetland Pollutant Dynamics and Control Annual Conference of the Constructed Wetland Association*.

Acknowledgements

I am grateful to my supervisor, Dr Jonathan Pearson, for his supervision, wholehearted support and undivided attention to my PhD study. His fieldwork and ethical support, encouragement and guidance was invaluable during my PhD studentship. His friendly and supportive personality, along with his educational attitude fosters inspiration and will always follow my professional pursuits. It was a real pleasure to collaborate with such a person.

I acknowledge the School of Engineering for their financial support during the 3-year period of this PhD and their support for disseminating my work in conferences. In addition to this, I need to thank the Graduate School and their student support services, which were very crucial and valuable during my PhD studentship, and the University's Senior Tutor.

I am particularly thankful to the technical support I received from Mr Ian Bayliss (Water Laboratory) for my fieldwork experiments, and also to the technical support from the Structures Laboratory staff regarding surveying equipment, as well as the Stores staff for providing essential equipment for my fieldwork visits. Furthermore, I feel the need to express my gratitude to my colleagues, who so nicely embraced and supported me, either by escorting me for my fieldwork activities, or by collaborating and exchanging views with me. The outcome of this kind interaction was admittedly far more beneficial.

I would like to express my special appreciation to my main collaborators in the RSPB Farm (Knapwell, Cambridgeshire) where my experiments took place, and particularly to Mr Ian Dillon, and Mr Derek Gruar. They were friendly, polite, over-supportive and proactive with us. Support in lifting and transferring equipment on the muddy soil were most helpful to the nature of this experimental fieldwork. Their support was further important including removal of our vehicles when stuck into the muddy farm tracks, and help with giving power to our vehicle battery when it ran out. Guys, you are the ideal collaborators! Furthermore, much appreciation is expressed toward The Coal Authority staff (Mansfield) for their nice research collaboration, and support during the experiments in A-WMTS (Derbyshire). Additionally, I

acknowledge the research collaboration with Andre Ramos (Cranfield University) and the rainfall data sharing at the RSPB Farm, and Dr Mick Whelan (Leicester University) for providing two Venturi flumes at the RSPB site.

I owe special gratitude to my friends in my hometown Florina, all my friends around Greece, and to the special friendships I made during my studentship, for their emotional and ethical support, their encouragement, advice and guidance.

Finally, I wish to thank my parents, family members and special friends, without whose support this work could not be fulfilled.

Declaration

This thesis is submitted to the University of Warwick in support of my application for the degree of Doctor of Philosophy. It has been composed by myself and has not been submitted in any previous application for any degree.

Abstract

Within the last decades the importance of sustainable treatment technologies, such as constructed wetlands (CWs) and vegetated ponds, has raised due legislation (e.g. WFD), directing toward green infrastructure to mitigate water pollution. The efficiency of pond and CW treatment systems depends on the internal hydrodynamics and mixing interactions between water and aquatic vegetation. In order to contribute to the current knowledge of how emergent real vegetation affects solute mixing, and physical flow characteristics in full-scale aqueous systems, an understanding and quantification of those processes and interactions was sought under the: i) natural seasonal vegetation and flow rate variation in two CWs, and ii) physical flow characteristics in overall six different full-size treatment units.

To address these issues, outdoor tracer field studies were undertaken in each treatment unit. Regarding the seasonal plant variation, an intelligent automated tracer injection system was developed to achieve autonomous remote measurements in two CWs, vegetated by Phragmites australis, in different seasons and flow rates. Experiments involved measurements of longitudinal mixing, physical flow characteristics and vegetation characteristics in different plant ages and various discharges.

It was shown that seasonal vegetation variation influences the longitudinal mixing coefficient by up to four times, and the physical flow characteristics by increasing the flow resistance and creating stagnant backwaters at the end of plant cycle, achieving reduction of the peak concentration by three times. Longitudinal mixing decreased with discharge in all plant ages. Furthermore, it was shown that internal design (i.e. bed topography or vegetation distribution) overwhelm the seasonal plant variation effects on mixing and flow characteristics. Moreover, relative comparison of outlet configuration, inflow conditions, and internal features, between the six different treatment units demonstrated an increase in residence time by up to three times. Results underlined the importance of investigating hydrodynamics and physics of flow in full-size units to enhance treatment efficiency and predictions of water quality models.

Notation

Roman Symbols

A	Cross-sectional area
A_R	Aspect Ratio
A_s	Surface Area (m^2)
B	Channel breadth
B_p	Plant biomass
c	Concentration of the diffused solute entering
C	Actual tracer concentration
$\bar{C}$	Concentration if the tracer impulse were instantly mixed within the tank
C_0	Initial tracer concentration
C_D	Canopy drag coefficient
C_e	Coefficient of discharge for the V-notch weir
C_{ft}	Free-flow coefficient for the Venturi flume
C_{peak}	Peak concentration of the RTD (ppb)
d_m	Average stem diameter
D_f	Dispersive fraction
D_m	Measured longitudinal dispersion coefficient (m^2/s)
D_p	Predicted longitudinal dispersion coefficient (m^2/s)
D_x	Longitudinal dispersion coefficient (m^2/s)
e_m	Molecular diffusion coefficient
h	Mean water depth (m)
H	Average stem height (m)
h_e	Effective head for the V-notch weir (m)
h_u	Water depth in ft on Venturi flume (ft)
h_v	Measured head on V-notch weir (m)
J_x	Rate of molecular conveyance across the unit area
K_e	Mass exchange coefficient between main flow and dead zone
K_h	Head correction factor for the V-notch weir
K_{oc}	Soil partition coefficient
K_y	Transverse mixing coefficient (m^2/s)
L	Length (m)
L_x	Longitudinal distance

M_0 Zeroth moment, corresponding to the area under the distribution curve

M_1 First moment, corresponding to the centroid of the distribution curve

M_2 Second moment, corresponding to the variance of the distribution curve

Mo Morril mixing index given by t_{90}/t_{10}

n_{ft} Exponent depending on the flume size (Venturi flume)

N Number of CSTRs

NR* Stem Reynolds number

N_d Number of data

N_t Stem population density (Number of plants per square meter)

Q Flow rate (l/s)

$Q_{d.g}$ Flow rate measured through dilution gauging

Q_f Flow rate in cfs (cubic foot per second) in the Venturi flume

Q_{norm} Non-dimensionalised Q using

Q_{trans} Flow rate measured using the pressure transducer

R Ripe radius

Re Reynolds number

s Tracer concentration departing the dead zone

S_A Short-circuiting index given by t_{16}/t_{50}

S_B Short-circuiting index given by t_{16}/t_n

S_C Short-circuiting index given by t_{50}/t_n

S_S Source term related to the 1D advection-dispersion equation

t_0 Time zero at which tracer is released

t_1 Time at which the tracer plume has been advected downstream after injection

t'_1 First arrival time of tracer

t_{10} 10^{th} percentile of tracer having passed through the outlet

t_{16} 16^{th} percentile of tracer having passed through the outlet

t_{50} 50^{th} percentile of tracer having passed through the outlet

t_{90} 90^{th} percentile of tracer having passed through the outlet

t_m Centroid tracer concentration time

t_n Nominal or theoretical residence time. Volumetric travel time

t_p Time of the peak tracer outflow concentration

T Residence time from ADZ model

u Flow velocity in the longitudinal direction (m/s)

u* Bed shear velocity

u,v,w Velocity component for each axial direction x,y,z repsectively

V Volume (m^3)

V_{eff}	Effective water volume (m^3)
W	Width (m)
x,y,z	The three axial directions

Greek Symbols

α	Frontal area per canopy volume
α_n	Short-circuiting index given by $1-t_m/t_n$
Γ_c	Ratio of common boundary region between main flow and dead zone
Γ_c	Ratio of common boundary region to the dead zone volume
δ	Discrete-time corresponding to the time delay $\tau/\Delta t$
δ_e	penetration length into the canopy
ΔS	Average spacing between the plant elements
Δt	Time step used in the ADZ model
ε	Turbulent diffusion coefficient (m^2/s)
ε_{r0}	Transverse mixing coefficient (m^2/s)
ε_x, ε_y, ε_z	Turbulent diffusion coefficients of the x,y,z axial directions respectively
η	Vegetation porosity
η_g	Vegetation porosity for zero stems deflection (upright stems)
η_{dc}	Vegetation porosity for full stems deflection (fully deflected stems)
θ	V-notch weir angle in rad
λ	Hydraulic efficiency
λ_d	Discrepancy ratio
ν	Kinematic viscosity of water
ν_{winter}	Kinematic viscosity of water during winter season
ν_{summer}	Kinematic viscosity of water during summer season
σ^2	Variance of trace impulse
σ_s	Sinuosity of stream
τ	Time delay from ADZ model
Φ	Plant solid volume fraction

Abbreviations

ADE	Advection Diffusion Equation
ADZ	Aggregated Dead Zone
AR	Agricultural Runoff
A-WMTS	A-Winning Minewater Treatment Scheme
BMP	Best Management Practices
BOD	Biological Oxygen Demand
CFD	Computer Fluid Dynamics
COD	Chemical Oxygen Demand
CPW	Coffee Processing Wastewater
CRTD	Cumulative Residence Time Distribution
CSTR	Continuous Stirred Tank Reactor
CW	Constructed Wetland
DO	Dissolved Oxygen
DWF	Dry Weather Flow
EA	Environment Agency
FWS	Free-Water Surface
HRT	Hydraulic Residence Time
HSF	Horizontal Subsurface Flow
K	Potassium
MAE	Mean Absolute Error
MW	Minewater
NH_4	Ammonia
NO_3^-	Nitrate
NW	North Wetland
OP	Organophosphorus
P	Phosphorus

ppb	Parts per billion
PF	Plug Flow
RMS	Root Mean Square
RSPB	Royal Society for the Protection of Birds
RTD	Residence Time Distribution
RWT	Rhodamine WT
SF	Subsurface Flow
SW1	South Wetland 1
SW2	South Wetland 2
SWs	South Wetlands
TN	Total Nitrogen
TN_4^+	Total Ammonium
TP	Total Phosphorus
TSS	Total Suspended Solids (or Sediments)
VSF	Vertical Subsurface Flow
WA	Watershed Area (or Catchment Area)
W.L.	Water Level
WFD	Water Framework Directive
WW	Wastewater

1. Introduction

1.1. Preface & Motivation

Global water contamination is gaining increasing importance at an international level. Mitigation of water pollution has become a priority for the environmental management nowadays, as water resources become severely contaminated due to various anthropogenic activities. As a consequence, there is an increasing engagement to set and advance regulations and policies internationally to protect drinking water quality (2006/7/EC) (European Commission, 2006), and aquatic ecosystems, as enacted by the EU Water Framework Directive (2000/60/EC) (European Commission, 2000). In England and Wales, less than 25% of the freshwater environments have been regarded to be healthy under the European Water Framework Directive (WFD) (Mackenzie & Mcllwraith, 2015). Particularly though, diffuse water pollution from agriculture, is considered one of the most important sources of waterways contamination (EPA, 2014; Mackenzie & Mcllwraith, 2015). Agricultural runoff, as a non-point source of pollution, contributes to surface and ground water deterioration (Hammer, 1992; Locke et al, 2011) that can lead to serious environmental and economic consequences (Wu et al, 2013a).

Many stakeholders have shown their interest in the increasing contamination of the natural water recipients and drinking water supplies. Environmental managers require information about urban and agricultural runoff pollution to preserve standards; the farming community (i.e. farm advisers, and farmers), various regulators (i.e. Environment Agency, and Chemical Regulatory Directorate), and modellers need information to conform to the environmental regulations and water quality criteria. Moreover, utility managers use information related to travel time and quality of the treated effluents entering watercourses.

Effective water management is needed to alleviate the stresses on water as a resource, which is related to the economic value of water, to human health through access to good quality

of drinking water supplies, and to degradation of aquatic ecosystems. Therefore, understanding the spread of contamination in waterways is of high importance. Within the environmental context, it has been observed that ecological engineering resources, as the SuDS, are capable of mitigating pollution and of providing water purification (Wu et al, 2013a). Integration of natural drainage systems, such as constructed wetlands (CWs), vegetated ponds, swamps, permeable pavements and more, are used to manage flood incidents and to treat contamination in the source (Scholz et al 2007; Woods-Ballard et al, 2007). Increased interest has raised in CWs, because of the multiple benefits they afford, including low energy and cost input, water quality enhancement, flood moderation, and environmental amenities (Vymazal, 2010).

Prediction of the downstream pollution levels poses a current challenge to designers and modellers of CWs. Understanding and knowledge around mixing processes in vegetated flows is still an area of research, especially in full-scale units. The presence of vegetation influences mixing properties in wetlands, whilst non-idealised geometrical shapes and channel irregularities contribute to non-uniform flow fields. Moreover, treatment efficacy is related to hydraulic residence time (hence water movement), thus discharge of effluents at shorter residence times than the designed is undesirable. Furthermore, treatment efficacy is linked to mixing processes, since pollutant concentrations downstream are expected to abate through spread and dilution, and through degradation. The impact of vegetation growth and ageing on mixing characteristics is an area that has been overlooked. Understanding how pollution transports in vegetated flows under the natural ageing on the actual site will provide information that has been restricted by studies using artificial vegetation or conducted in idealised small-scale laboratory conditions.

1.2. Aims & Objectives of the Thesis

The primary aim of this study is to experimentally investigate the impact of vegetation growth and ageing on mixing characteristics and on flow structure on the actual site in full-size constructed wetlands, and to investigate these characteristics under different flow rates.

Secondly, the physics and hydraulic behaviour of different full-scale systems across the UK were examined to conduct a comparative evaluation of parameters affecting their hydraulic performance and mixing processes.

The objectives of this thesis are to:

- Contribute to the body of knowledge by providing mixing coefficients within emergent, real vegetated flows on the actual site under seasonal plant growth and discharge variation.
- Investigate the physical flow and mixing characteristics under the seasonal plant variation and under discharge variation.
- Apply and assess the current theoretical understandings developed in idealised conditions for real vegetation on the actual site, thus including the field effects.
- Evaluate the effect of size of a treatment unit on the contaminant dispersion, and thus on treatment efficiency.
- Understand the effect of various design parameters on hydraulic performance, and contribute to the current knowledge of design guides to improve treatment efficacy.
- Underline the importance of investigating hydrodynamics and physics of flow in treatment units, besides the sole focus on treatment performance.

1.3. Structure of the Thesis

This thesis comprises of eight chapters, with a summary of the main points covered at the beginning of each chapter.

- Chapter 1 is the introductory chapter, illustrating the motivation and the main focus of this research, as well as the aims, objectives and structure of this thesis.
- Chapter 2 presents the literature review, which focuses on two main subjects areas: firstly, constructed wetlands' competency to treat agricultural runoff pollution, and secondly, fundamentals of physical flow characteristics and pollutant transport in

open channels and in vegetated flows. At the end of the chapter a research proposal is included, defining the research questions of this thesis.

- Chapter 3 describes the field methodology and experimental setup of the two wetlands for which seasonal vegetation variation was monitored, namely South Wetland 1 and South Wetland 2.
- Results and individual discussion of each of the two main experimental sites, South Wetland 1 and South Wetland 2, are included in Chapter 4. This chapter also introduces results related to the connecting stream (as the two wetlands are in-series arrangement), as a base case of no vegetation.
- Chapter 5 includes a comparative summary of the results discussed and interpreted in Chapter 4.
- Additional applications of four full-scale investigated aqueous systems are presented in Chapter 6. This includes presentation of the experimental setup, results and discussion of each aqueous system individually, referring to two CWs and two lagoons.
- A comparative evaluation and summary taking into account the six aqueous systems examined in this thesis is presented in Chapter 7. This incorporates the two constructed wetlands presented in Chapter 4, as well as the four additional aqueous systems presented in Chapter 6.
- Chapter 8 presents the main conclusions extracted from this research, and provides recommendations for future work.

The thesis includes an Appendix section containing:

- Appendix I: Material related to Chapter 3: *Methodology*.
- Appendix II: Material related to Chapter 4: *Experimental Results*.
- Appendix III: Material related to Chapter 5: *Summary of SW1 & SW2 Results & Discussion*.
- Appendix IV: Material related to Chapter 6: *Further Applications & Experimental Results*.

2. Literature Review

2.1. Overview

The scope of this study is the quantification and description of the transportation and mixing processes of solute pollutants through full-scale constructed wetlands (CWs), and the exploration of the seasonal vegetation impact on mixing characteristics, flow pattern, and hydraulic performance. This literature review investigates the hydrodynamic (transport and mixing) processes in wetlands, with particular emphasis on water flow movement and mixing processes in vegetated flows.

Section 2.1 provides an overview explaining the aims of this chapter. Section 2.2 introduces the diffuse pollution from agricultural runoff and the associated water quality challenges arising from nutrients and pesticides application. Section 2.3 introduces CWs as a means of green technology to abate diffuse pollution from agricultural runoff. Particular review is carried out to underline CWs' competency to mitigate various agricultural pollutants. Section 2.4 presents hydraulic performance related parameters and mixing processes in open channel flow. Section 2.5 discusses the flow and mixing processes in vegetated flows. Section 2.6 provides a summary of the main conclusions of this literature review. Section 2.7 presents the research proposal of this study.

When a contaminant enters a CW, there are several factors that contribute to the transport, dispersion, breakdown and removal degree of the pollutant. A CW consists of plants, support medium (soil), microorganisms (microbial community) and sediments. Although all of the above components play an important role in the pollutant removal, the governing factor is the water movement in the system, as it is linked directly with the hydraulic residence time (HRT), thus the treatment efficiency. As such, hydraulics and physics of flow are very important parameters to understand and explore in a CW, because they relate to the treatment performance. Fundamental factors that influence the hydraulic performance of a system include: HRT, short-circuiting, mixing and dispersion, vegetation, and removal

processes. As illustrated in Figure 1, vegetation, local topography and the CW shape affect the HRT and hence the pollutant treatment, via different processes, i.e. mixing, dead water, flow shear velocity, shot-circuiting.

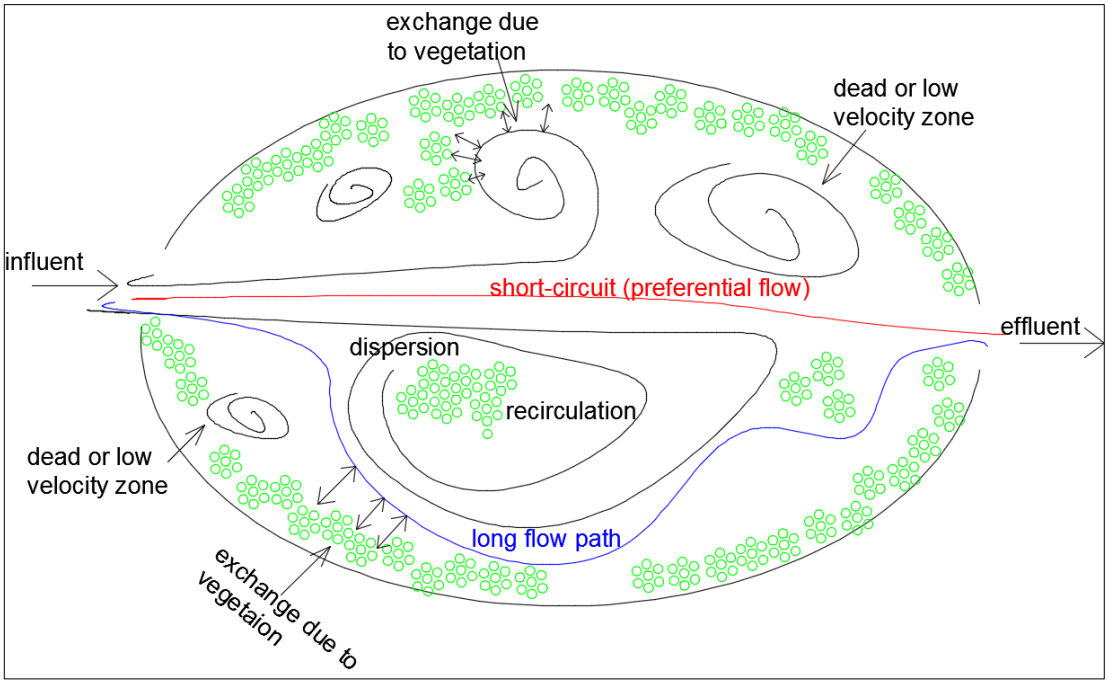

Figure 1: Main hydraulic processes existing in a wetland or pond include dispersion, recirculation, diverse flow paths (short-circuit, shorter or longer paths), dead zones and exchange zones due to vegetation.

This study quantifies and describes the hydraulic and mixing properties of CWs and assesses the role and effect of macrophytes on hydrodynamics to add knowledge on the seasonal operation and performance of CW guides. In order to increase the CWs' treatment efficiency, a sound understanding of the internal hydraulics and physics is required. This incorporates quantification of mixing and dispersion processes, short-circuit paths and stagnant zones, HRT, and understanding of seasonal plant variation and hydrology effects on those processes. This can be achieved by implementing in-situ tracer tests. The product of tracer tests is the residence time distribution (RTD) curves, which provide information about the system's dominant processes, the HRT, peak concentration of pollutant, overall mixing, as well as indications of short-circuiting and dead zones in the wetland. Overall, both the HRT and the degree of mixing assist in the evaluation of the CW removal efficacy. The intended results of this research are to quantify and describe the physical processes (mixing, HRT,

effective volume, hydraulic efficiency) of full-scale CWs, and the influence of seasonal vegetation and flow rate variations on the physical processes and on mixing characteristics, and to add knowledge on the current operational standards of CWs.

2.2. Agricultural Runoff & Non-Point Source Pollution

Water pollution has come at the forefront of the environmental management, as water becomes severely contaminated due to various human activities, which entails significant impact on the aquatic ecosystems and on human health. As a consequence, there is an increasing engagement at a global level to set and advance regulations and policies to protect drinking water quality (2006/7/EC) and aquatic ecosystems, as enacted by the EU Water Framework Directive (2000/60/EC).

Surface runoff is a central component of the water cycle, and can be transferred through confined, discrete conveyance means, *point source*, or can be diffused onto surfaces, *non-point source* (NPS), including land runoff, storm water discharges, drainage, seepage (Reichenberger et al, 2007; EPA, 2016). However, surface water contamination, spread via agricultural NPS runoff, is the leading remaining source resulting into water quality challenges, and posing concern for the fisheries, wildlife and drinking water supplies (EPA, 2016).

Agricultural runoff is the runoff of agrochemicals, i.e. fertilisers and pesticides, discharging into surface waters, and is the major avenue of diffuse pollution (Fulton et al, 1999). Modern agriculture invariably applies fertilisers (i.e. nutrients) and pesticides to achieve and secure high crop yields, and to protect crops from diseases and insects. Agricultural diffuse runoff contributes to large discharges of fertilisers, pesticides and suspended solids downstream of the agricultural catchments, or into aquatic ecosystems adjacent to rural areas (Fulton et al, 1999). The impact of agricultural runoff has profound adverse effects on wildlife and aquatic ecosystems, as being discharged in estuaries, and on human health via drinking water supply (Hammer, 1992; Locke et al, 2011; EPA, 2014). As a consequence, surface and ground water deterioration due to agricultural diffuse runoff may lead to serious environmental and

economic consequences (Wu et al, 2013a). Hence, there is a growing research interest around mitigation of NPS pollution over the last two decades (Yanhua et al, 2012). The types of pollutants related to agricultural runoff are fertilisers and pesticides, introduced in Section 2.2.1 and 2.2.2 respectively.

2.2.1. Fertilisers

Fertilisers contain various nitrogen and phosphorous forms, and constitute key pollutants in diffuse agricultural runoff (Mitsch et al, 2000; Poe et al, 2003). Problems associated with elevated loads of fertilisers' application are well documented to cause eutrophication, excessive phytoplankton production and hypoxia (deficiency of dissolved oxygen (DO) of surface water courses), and consequently ecosystem disturbance (Beutel et al, 2009; Borgvang & Tjomsland, 2001; Coffey, 1997; Faulwetter et al, 2009; Jordan et al 2003; Kiely, 1997; Koskiaho et al, 2003; Volkmar & Dahlgren, 2006). However, in addition this, nutrients induce groundwater pollution, especially in water intended for drinking purposes (Beutel et al, 2009; Coffey, 1997). The associated drinking water treatment involves high cost processes (Kiely, 1997), and as a consequence, agricultural runoff NPS pollution impacts on the ecosystems function, but also on the economic value of clean water (Stanton & Taylor, 2012).

Concerning nitrogen, and particularly free ammonia, acute toxic levels are caused into aquatic life and fish, especially in vegetated aquatic recipients (Shilton, 2005), whereas, nitrate (NO_3^-) is also liable for the aforementioned problems. Elevated levels of NO_3^- are associated with cause of methemoglobinemia or 'blue baby' syndrome in infants (Horne, 2002; Masters, 1991; Knobeloch et al, 2000; Saunders & Kalff, 2001). Remarkably, it is reported that 40-60% of the total nitrogen (TN) fertiliser field application amount is ultimately used by crops, whilst the rest is lost either as runoff or seeps into soil layers ending into groundwater (Coffey, 1997). Furthermore, it is reported that the origin of 90% of the nitrogen losses leaching via agricultural runoff in Europe is NO_3^- (Billy et al, 2013; Tournebize et al, 2015). Nevertheless, phosphorous (P) is the prime cause of eutrophication, with all the previously mentioned ecological and financial consequences involved (Borgvang &

Tjomsland, 2001; Koskiaho et al, 2003; Lu et al, 2009; Dunne et al, 2015; Johannensson et al, 2015).

As a consequence of nutrients implications on estuarine habitat and environment, the European Directive 2000/60/CE has designated regulation and goals related to acceptable ecological standards in rivers and estuaries. Within the best management practice (BMP) context to support this goal, this literature review targets at the potential of CWs to mitigate agricultural runoff (discussed in Sections 2.3.1 and 2.3.2).

2.2.2. Pesticides

Pesticides are chemical compounds broadly used in modern agriculture to improve crop production and to secure high yields and profits. Runoff from agricultural fields is the primary source of pesticide transport to surface waters (Norwell et al, 1999). Pesticides are classified into various categories based on the targeting enemy type, i.e. herbicides, insecticides, fungicides, bactericides, disinfectants, and more. For the majority of pesticides applied, loss via runoff is regarded the most serious route of diffuse pollution transport, followed by loss via erosion (Reichenberger et al, 2007).

The largest pesticide losses are observed to occur due to intense storm events succeeding pesticides' field application (Branger et al, 2009; Gregoire et al, 2009; Kladivko et al, 2001; Schulz, 2004). Today, there is growing concern about the effects of pesticide agricultural runoff on human health, estuarine habitat, and groundwater (Bollmann et al, 2014; Feng et al, 2011; Tao & Fletcher, 2013; Runes et al, 2003; Tediosi et al, 2012; Tournebize et al, 2013; Veolia Water Technologies, 2014; Zhang et al, 2011; Zhang & Zhang 2011).

Ample research has been conducted to understand the mechanisms of several insecticides and herbicides over the last three decades (Miller, 1986; Gao, 1998b; Schulz & Peall, 2001; Locke et al, 2011). Schulz (2004) underpins that so far most attention has been paid to insecticides, due to the increased toxicity they cause onto invertebrates and fish. Baker in 1992 observed elevated application of herbicides – particularly four times higher herbicide application since 1966 – and stressed the need for immediate mitigation strategies to avoid

health and environmental risks. Reichenberger et al (2007) reported the utilisation of CWs as an effective means of pesticide load reduction, and noted the gap in knowledge around moderately and weakly sorbing pesticides mitigation capacity via CWs, underpinning that CWs efficiency had been tested mainly for strongly sorbing pesticides.

Most significant factors linked to pesticide transport through runoff comprise (Norwell et al, 1999):

- Climate, (i.e. duration, amount, and intensity of rainfall; the timing of rainfall relating to pesticide application) (Section 2.3.3.2)
- Soil characteristics (i.e. soil texture and organic material content, slope and topography of the ground) (Section 2.3.3.3)
- The physical and chemical properties of the pesticide itself (water solubility, sorption properties, persistence K_{oc}) (Section 2.3.3.4)
- Agricultural management practices (pesticide application rate, application placement – soil surface or foliar) way of application (drift, pellets, etc.).

The above factors together with hydraulics and vegetation are discussed in Sections 2.3.3.1 to 2.3.3.5. Generally, the longer a pesticide stays in the system the higher the degradation rate achieved. Depending on the solubility degree of a pesticide degradation is not always achieved. Therefore, appropriate sampling rate is required during storm events following their field application to provide useful insights of their removal rate through CWs.

To preserve public health and groundwater quality against pesticide runoff impact, the European Drinking Water Directive (98/83/EC) has established stringent limitation of 0.1 µg/l of any individual pesticide as a maximum detection limit in potable water. The emerging problem so far is identified in specific pesticides – such as carbetamide, clopyralid, imazalil, metaldehyde, propyzamide, pendimethalin, terbuconazole – whose detected concentration in potable water exceeds the allowable (Tao & Fletcher, 2013; Lv et al, 2016; Tediosi et al, 2012; Veolia Water Technologies, 2014). For example, metaldehyde has captured the interest since 2008, when the UK Environment Agency (EA) emphasized the elevated levels detected in potable water supply (Tao & Fletcher, 2013). In addition to this, standard treatment

processes fail to remove metaldehyde from potable water, entailing the immediate need to resolve the problem (Tao & Fletcher, 2013; Veolia Water Technologies, 2014). The challenge reaches the drinking water supply companies, which either have to deal with high energy consumption and costs for drinking water treatment, or find it impossible to remove some pesticides with the state-of-the-art technological processes.

Therefore, it is inferred that the elevated costs and energy input requirement involved in the agricultural runoff water treatment is a great driver to search and investigate alternative options that are capable of mitigating or removing NPS contaminants in a way that is equally efficient with conventional treatment systems, but also cheaper. One such technology is the constructed wetlands, discussed in Section 2.3.

2.3. Constructed Wetlands

This section reviews various types of CWs applied for agricultural runoff, it showcases the to-date CW studies related to agricultural runoff mitigation, and it reviews the CWs' treatment efficiency to remove agricultural runoff pollutants. Finally, this section reviews the factors influencing CWs' treatment performance and the related removal and transport mechanisms.

Constructed wetlands (CWs) are engineered systems using natural processes through plants, soil and microbial consortia, to support treatment of polluted water (Kadlec & Knight, 1996). At the outset of this review, it would be helpful to distinguish between ponds and wetlands, because they provide dissimilar hydraulic and hydrological characteristics, and eventually different water quality processes. Thus, according to Persson et al. (1999), ponds are typically small man-made open-water bodies demonstrating little water stage fluctuation. Vegetation is generally limited to emergent aquatic macrophytes, growing to the margins of the pond (called marginal vegetation), and to potential submerged plantation in the open water. On the other hand, CWs are described as shallow detention systems, experiencing occasionally intermittent flow, leading thereby to wet and dry periods in the system. Additionally, CWs are normally vegetated with emergent aquatic plants (Persson et al, 1999).

Wetlands afford a wide range of regulatory functions, comprising control of pollutant transport, water quality enhancement, flood mitigation, storm water retention and biodiversity productivity (Verhoeven & Setter, 2010). Natural processes taking place in wetlands contribute to the mitigation of nutrients, pesticides, heavy metals, pathogens, BOD and COD.

Particularly in agricultural runoff, the chief associated contaminants comprise nutrients, pesticides and particulate matter (Wauchope, 1978; Wallach, 1991). The main natural wetland processes conducive to reduction of eutrophication and toxicity caused by nutrients involve adsorption, plant uptake, sediment retention and denitrification (Haygarth & Jarvis, 2002; Rodgers & Dunn, 1992), while regarding pesticides, the chief processes involved are sorption and degradation. Within the set agro-environmental policy context, CWs are largely preferred to ponds, because of the multiple privileges and auxiliary services they offer, beyond the water quality enhancement (Koskiaho et al, 2003). Wetlands provide a rich spectrum of values, linked to population, ecosystem and global perspectives. The ecosystem values of wetlands refer to storm abatement, flood moderation, groundwater recharge, aesthetics and water quality enhancement. In terms of global and local profits, wetlands are considered as potentially pivotal elements contributing to sustain the cycles of carbon dioxide, methane and nitrogen (Kadlec & Knight, 1996; Mitsch & Gosselink, 2007; Shutes et al, 2010).

The majority of the to-date bibliography and research on CWs refers to wastewater treatment (WWT), originating from urban, industrial and mining activities (Locke et al, 2011). The scientifically established utilisation of wetlands for WWT commenced in Germany in the 1950s (Editorial, 2009), whereas the scientific interest of CWs utilisation for purifying diffuse agricultural runoff commenced in 1980s (Schulz, 2004; Locke et al, 2011; Bodin et al, 2012).

Complying with the stringent regulations designated in the framework directives about surface, ground, and drinking water quality, and estuary ecosystem standards, CWs have nowadays emerged as an increasingly popular measure against NPS agricultural pollution.

The investigation and assessment of CWs' treatment efficiency to abate nutrient and pesticides compounds has increased in recent years.

2.3.1. Types of CWs applied for Agricultural Runoff Mitigation

CWs are categorised into free-water surface (FWS) or subsurface-flow (SF) systems (Reed, 1990), where the SF systems are further subdivided into vertical (VSF) and horizontal (HSF), depending on the direction of the flow path. The various common types of CWs are illustrated in Figure 2, and are classified based on how the water flows into them.

In FWS CWs water flows freely in the system and mainly above the substrate medium, mimicking the natural wetland (Hammer, 1992; Mitsch & Gosselink, 2007). Native clay or soil are generally the substrate materials used (Hammer, 1992). In SF CWs the water passes laterally and entirely through the porous substrate medium, thus free water is not visible (Hammer, 1992; Mitsch & Gosselink, 2007). Typical substrate media in SF CWs include various sizes of gravel (Hammer, 1992). SF CWs are more similar to wastewater treatment plants than wetlands (Mitsch & Gosselink, 2007), hence this technology has been largely developed and applied for WWT.

The majority of to-date literature about any wetland type refers to wastewater treatment (Kadlec, 2009; Kotti et al, 2010), with the most commonly employed types being FWS and HSF wetlands. According to Kadlec (2009), various factors contribute to the decision making of the wetland type – e.g. cost, functionality, size – but with respect to removal efficacy, it has been observed that FWS tend to produce higher removal rates in total suspended solids (TSS), ammonia (NH_4), total phosphorous (TP) and total nitrogen (TN). Furthermore, FWS CWs afford a better habitat for particular flora and fauna species, because of the water ponding effect during most of the year (Mitsch & Gosselink, 2007). On the other hand, HSF systems exhibit higher removal capacities for nitrate (NO_3^-) and pathogens, mainly due to the anoxic conditions, which promote denitrification (Fennel et al, 2009; Reed & Brown, 1995). In terms of capital and operational cost, FWS CWs provide a much cheaper option compared to HSF CWs. Finally, FWS wetlands afford greater development of biodiversity and natural habitat compared to HSF systems (Kadlec, 2009).

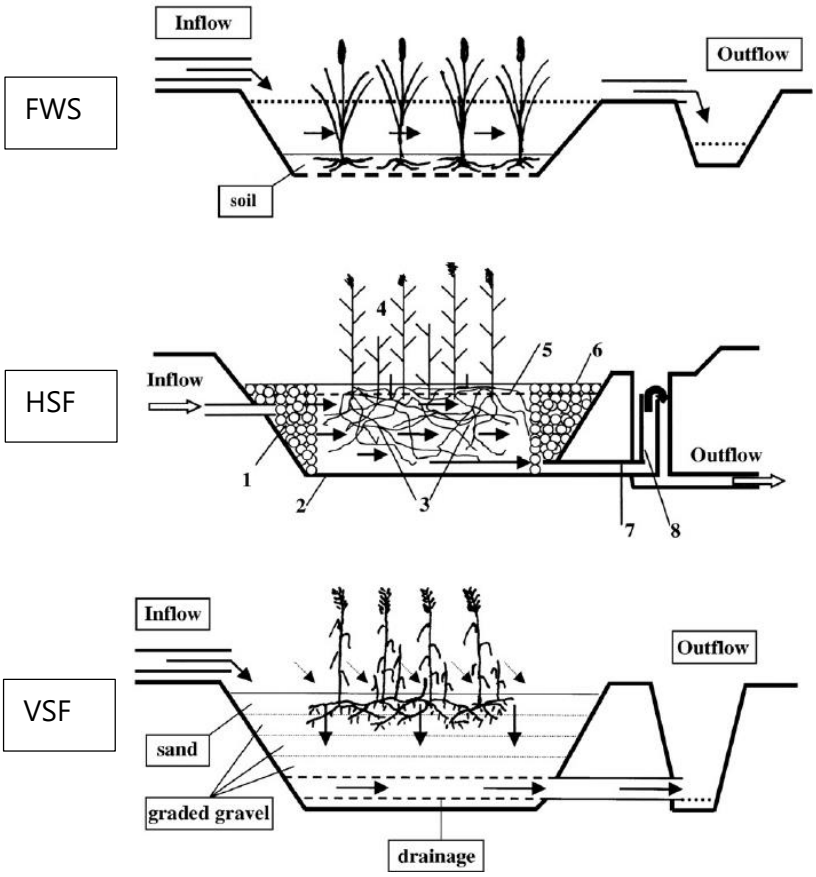

Figure 2: Different types of constructed wetlands sorted according to the water flow type (i.e. FWS, HSF, VSF) within the system. (Adapted from Vymazal, 2007).

Another CW classification relies on the vegetation morphology (see Figure 3), and refers to (Mitsch & Gosselink, 2007):

i. Free floating macrophyte systems. The floating leaves are either free/unattached or they are anchored.
ii. Emergent macrophyte systems. The stems and leaves are above the water surface.
iii. Submerged macrophyte systems. They grow completely below the water surface.
iv. Algae, which is a cellular plant form commonly called as moss.

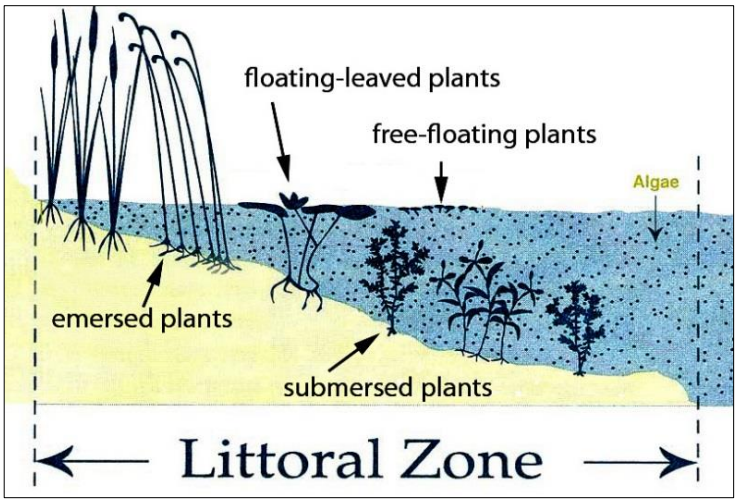

Figure 3: Classification of wetland vegetation based on its morphology may include floating leaves, emergent vegetation, submerged vegetation, and algae (Taken from http://plants.ifas.ufl.edu/).

The general design pattern of CWs varies for each type. FWS CWs are shallow systems with sealed bottom, by clay or geotextile. They consist of a soil layer which supports the rooting system for macrophyte development. FWS wetlands often encompass all the macrophyte types (Mitsch & Gosselink, 2007). Besides, the design of VSF CWs comprises gravel or sand layers on the vertical direction, with size gradient towards the bottom (Vymazal et al, 2006). Water moves by gravity vertically through the porous media. Common reeds is the most popular species used in this system. VSF CWs involve the lowest area demand, but higher operational costs compared to the other two CW types (Vymazal et al, 1998, Cooper, 1999). Regarding HSF CWs, fundamental design employs gravel or soil as substrate medium, and plants, usually common reeds (Vymazal et al, 2006). Free water is not visible in HSF systems, while water moves horizontally and through the porous media pores (substrate) (Vymazal et al, 1998). Overall, SF wetlands utilize solely emergent macrophytes (Mitsch & Gosselink, 2007).

From the above, it is understood that the selection of the CW type depends on the aim of the desired work. As a general norm, WWT works often prefer the HSF CWs. Nonetheless, in the case of an effluent type other than sewage, e.g. urban or agricultural runoff, FWS wetlands would provide the most suitable option both in terms of low machinery input demand, and low cost requirements according to the to-date literature.

2.3.2. CWs efficiency

CWs are considered a promising means of water pollution mitigation and management, as their application covers a broad spectrum of effluent types, i.e. urban and agricultural runoff, municipal, and industrial wastewater, and more. This section presents conducted research to date on pilot or full-scale, laboratory or outdoor CW units treating various pollutants (mainly focused on agricultural runoff), and provides CWs treatment performance. Table 2.1 assembles CW treatment efficiencies indicating the CW type (number of cells, vegetation coverage col. (1)), CW size & location col. (2), effluent type col. (3), CW dimensions col. (4), removal percentage col. (5), and citation col. (6)).

As mentioned in the introduction of Section 2.3, most to-date published bibliography is on CWs treating wastewater effluents, as the interest in CWs treating agricultural runoff effluents rose later (Schulz, 2004; Locke et al, 2011; Bodin et al, 2012). Retention and fate of sediments and nutrients via CWs have been investigated quite thoroughly so far, and there is a good understanding around the related processes, however, the same cannot be argued about other agrochemicals (Shulz & Peall, 2001; Gregoire et al, 2009). In particular, beyond laboratory mesocosm studies on pesticides, there are very few field studies conducted in CWs and providing quantitative results (Gregoire et al, 2009). As such, Table 2.1 summarises recent research work undertaken to attest the treatment efficiency of various CW types, mainly focused on agricultural runoff effluents.

Table 2.1: Studies undertaken in CWs for agricultural runoff mitigation, reporting their type, scale, location, dimensions, pollutant removal, and citation.

(1)	(2)	(3)	(4)	(5)	(6)
Type of CW	**Size – Scale, Location**	**Effluent Type**	**Dimensions (in m)**	**Pollutant Removal %**	**Reference**
FWS (EM) [4 CWs]	Pilot – scale, USA	AR (0.8), UA (0.2)	20000 – 35000 m^2, 1 (D)	TSS: 76 – 99% NO_3-N: 39-99% TP: 52-99%	Hey et al, 1994
HSF (EM) [4 CWs]	Pilot – scale, Brazil	CPW	0.5*2.0*0.6 (L*W*D)	BOD: 86% COD: 90%	Rossmann et al, 2013
SF (EM)	Pilot – scale, India	CPW	0.6*0.2*0.3 (L*W*D)	BOD: 98% COD: 97% TSS: 90%	Selvamurugan et al, 2010
FWS (EM) [5 CWs]	Pilot – scale, Greece	WW	3.40*0.85*0.10 (L*W*D)	BOD: 78% COD: 68% TP: 52% Orthophosphate: 56% Ammonia: 54%	Kotti et al, 2010
FWS (EM) [2 CWs]	Full – scale, USA	AR	180*30*0.45 (L*W*D)	Atrazine: 70-89% Fluorometuron: 58-81%	Locke et al, 2011

VSF (EM)	Pilot – scale (Lab), China	AR	0.5*0.4 (D*d)	TP: 3-21%	Wu et al, 2013b
FWS (EM)	Full – scale, China	AR	2800 m^2	TP: 59%	Lu et al, 2009
FWS (EM)	Pilot – scale, Canada	AR	9.29 m^2	P: 41% NO_3-N:	Yates & Prasher, 2009
FWS (EM)	Full – scale, Switzerland	AR	2350 m^2, 0.6 (D)	TP: 23%	Reinhardt et al, 2005
FWS (EM) [4 CWs]	Full – scale, Norway	AR	350-900 m^2	TP: 21-44%	Braskerud, 2002
FWS (SUB) [9 CWs]	Mesocosm, USA	AR	4.7*0.8*1 (L*W*D)	TP: 50-79%	Dierberg et al, 2002
3 SF & 1 FWS (EM)	Full – scale, Norway	AR	40*3 (L*W)	NO_3^-: 0 – 90.5% (based on trench & season)	Søvik & Mørkved, 2008
FWS (EM) [10% coverage]	Full – scale	AR	860 m^2, 50 (D)	NO_3^-: 50±18%	Tournebize et al, 2015
FWS (EM) [6 CWs]	Full – scale, USA	AR	16000 m^2	TN: > 60% NO_3^-: 90%	Beutel et al, 2009
FWS (EM)	Full – scale, France	AR	12000 m^2, 0.1-1 (D),	NO_3^-: 90%	Mander et al, 2015
FWS (EM)	Full – scale, USA	AR	13000 m^2	TN_4^+: 25% NO_3^-: 52% TP: 27% TN: 14% TSS: 13%	Jordan et al, 2003
FWS (EM) [7 CWs]	Full – scale, USA	AR	23000-1500000 m^2, 0.5-1.5 m (D)	TSS: 31–96% NO_3^-: 22-99 %	Diaz et al, 2012
FWS (EM)	Full – scale, South Africa	AR	4400 m^2	TSS: 15-78% Orthophosphate: 54-75% NO_3^-: 70-84% Toxicity: 89% OP pesticides: 100% (dry & wet weather conditions)	Schulz & Peall, 2001
FWS [in series: 1 unplanted & 1 planted systems]	Pilot – scale, Australia	AR	Unplanted: 100 m^2; 1 m (D); Planted: 200 m^2; 0.5m (D).	Herbicides: fluometuron: 0-34%; Diuron: 27-55%; aldicard: 15-39%. Insecticides: endosulfan: 24% (unplanted), 27% (planted).	Rose et al, 2006
FWS (EM)	Full – scale, Italy	AR	3200 m^2	Nitrogen: 90%	Borin & Tocchetto (2007).
FWS (EM) [Aulnoy: in stream, 10% coverage; Bray: 3*in-series CWs, off-stream, 70% coverage)	Full – scale, France	AR	860 m^2, 0.5m (D); 1280 m^2, 0.2-0.8 m (D)	Pesticides: Aulnoy: 54%; Bray: 45%.	Tournebize et al, 2013
FWS [4 CWs; 50% planted; 50% unplanted]	Full – scale, Korea	AR	13294 m^2	TSS: 38% TN: 37% TP: 60%	Lee et al, 2015
FWS	Full – scale, Italy	AR	3200 m^2	Herbicides: metolachlor, terbuthylazine: 98%	Pappalardo et al, 2016
(SF) SFW & VSF (EM)	Pilot – scale, China	AR	0.6*0.8*0.5 (L*W*D)	Insecticides: endosulfan, chlorpyrifos, fenvalerate > 95%. Herbicides: diuron 45%.	Tang et al, 2016
FWS (EM) [2 CWs]	Full – scale, Norway	AR	Grautholen: 840 m^2, 100m (L); Lier: 1200 m^2.	7 pesticides: 3-67%	Blankenberg et al, 2006

L = Length, W = Width, D= Depth, d = diameter, EM = Emergent, SUB = Submerged, OP = Organophosphorus, AR = Agricultural Runoff, UA = Urban Activities, CPW = Coffee Processing Wastewater, WW = Municipal Wastewater. All units refer to m.

From Table 2.1, it is observed that to date, the most popular CW type for agricultural runoff mitigation is FWS. Full-scale units are increasingly employed and assessed for their treatment performance. Small-scale cells, such as mesocosm laboratory studies and pilot-scale units, undeniably serve successfully in the increase of current knowledge for the various CW components, e.g. plant species, and substrate material. Studies reported in Table 2.1, demonstrate encouraging treatment efficiencies for various agricultural runoff pollutants, but also underline variability in treatment rates, i.e. between systems, seasons, soils, areas/countries. Consequently, there is a wide spectrum of factors that affect the removal rate of agricultural runoff pollutants, which are discussed Section 2.3.3.

2.3.3. Factors affecting CWs performance & removal mechanisms

The overall CW efficiency is a joint function of biogeochemical transformation and hydraulic transport processes (Polprasert & Bhattarai, 1985). The physicochemical, environmental and biological processes occurring in CWs determine the removal efficiency of pollutants. Hence, there are various factors affecting CWs performance. Every pollutant is usually mitigated or removed through a combination of processes, which depends on the pollutant properties and on climatic factors (i.e. temperature, season), with great dependence on the HRT, which is the main focus of this review. Although the overriding influence on pollutants' removal in CWs is assigned to the movements of water (Kadlec, 1994; Min & Wise, 2009), there are yet other additional components contributing to pollution removal, including soil, sediments, microbes and macrophytes. Complex processes occur in the water treatment involving sedimentation, filtration, adsorption, plant uptake and degradation (Faulwetter et al, 2009; Vymazal, 2013). Overall, two main mechanisms determine a CW's treatment competence, namely plants-adsorption and microorganisms-degradation (Su et al, 2009). In this section, transfer and removal mechanisms are discussed, including vegetation, soil, sorption and degradation.

The basic components in a CW, i.e. plants, substrate, microbial community, and water, interact and interdepend to achieve treatment. Overall, soil is the medium that supports vegetation and microorganisms. Vegetation depends on the soil in order to develop the root

zone, necessary for removal processes operation. Vegetation also acts as a large biofilm for the microbial assemblage to develop, settle and treat pollutants. Importantly, each pollutant is affected by different factors and is removed by different processes. For instance, nitrogen removal is affected by seasonal variations and is mainly removed via plant uptake process, while pesticides are mainly ruled by sorption, and degradation processes, which depend on environmental factors, i.e. temperature. Contact with the atmospheric air is also a key aspect to transform pollutants (i.e. through photolysis). A synopsis of the transfer and transformation processes taking place between the major components of the system – water, air, soil and plants – is illustrated in Figure 4.

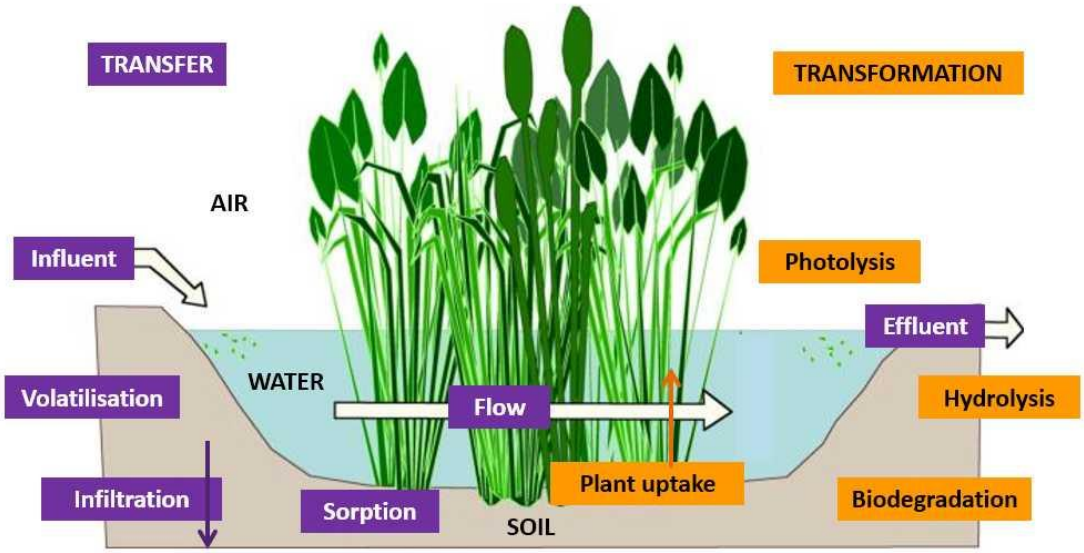

Figure 4: Schematic of pollutant transfer, transformation and removal mechanisms of agricultural runoff in emergent vegetated wetlands. (Adapted from: http://www.nurserymag.com/)

2.3.3.1. Vegetation

CW Vegetation, also known as macrophytes, constitutes an indispensable part of the system, providing multiple services. Firstly, macrophytes promote pollutant mitigation and removal via: i) plant uptake, sorption and degradation processes; ii) the habitat surfaces (biofilm) promoting microbial activity; and iii) the oxygen transport through the root system (fostering aerobic degradation) (Brix, 1994; Faulwetter, 2009; Rossmann et al, 2012; Stomp et al, 1994; Nepf, 2012, Vymazal, 2013). The presence of vegetation has a favourable effect on nitrogen

removal, as biofilm surface enhances plant uptake, and nitrification procedures (Fia et al, 2008; Weisner et al, 1994).

In addition to this, macrophytes offer stabilization of the bed surface, and channel bank erosion control (Brix, 1994; Nepf, 2012), while, they additionally reduce wind velocity, enhance suspended sediments settling and abate settling particles re-suspension (Brix, 1994; Vymazal, 2013). Plants also impede algae creation by attenuating light passage (Brix, 1994). The role of plants is considered outstanding and is deemed that even the dead standing plants function favourably, affording insulation coverage for the soil against ice during winter (Brix, 1994; Rossmann et al, 2012).

From a hydrodynamic perspective, HRT is affected by emergent vegetation, and increases with vegetation density (Jadhav & Buchberger, 1995), while it is reported that increased turbulence levels can potentially enhance nutrient uptake (Anderson & Charters, 1982). The role of plants in wetland hydraulics is discussed separately in Section 2.5.

There is still ongoing research trying to investigate, and elucidate the relation between the removal efficiency of certain plant species and certain target pollutants. That is because vegetation characteristics, i.e. plant morphology, species, biomass, are considered to be a factor that adjusts the removal rate. For example, Gottschall et al (2009) reported that wetlands planted with emergent macrophytes demonstrated higher nitrogen removal proportion than those planted with submersed macrophytes, while they additionally noticed that increased plant density attained higher nitrate removal rates, a finding that reinforces the importance of macrophytes role in treating nutrients. Besides, Dierberg et al (2002) examined and assessed mesocosm CW cells with submerged plant species, and found similar P removal efficiencies from the different tested plant species, but importantly noticed that submerged aquatic plants aggregated twice higher P mass compared to the soil accumulation process. Tanner (1996) studied and compared the growth and nutrient uptake capacities of eight emergent macrophyte species, and found that there is a wide variation in the overall nutrient uptake between different species, while he further noted that the high levels of TSS, BOD and P removal presented no significant affinity to plant species.

Furthermore, Wu et al (2013a) suggested that selection of plants with grand biomass capacity, and of media with large adsorption ability is central for the CW treatment competence of the specific pollutant in treatment. The plant biomass is related to the amount of nutrient uptake, assimilation of heavy metals, and to transpiration needs (Wang et al 2009; Wang et al 2012). For example, nitrogen storage capacity via plants is linked to the stem population density, N_t (stems/m^2), and to plant biomass height. In Europe, the predominant emergent plant species employed in CWs is Phragmites Australis (Vymazal, 2013). Phragmites has the required traits, i.e. quick growth and high stems, and has displayed higher plant biomass rates compared to other plant species, i.e. Iris psedacorous and Typha latifolia (Wang et al 2009; Gagnon et al, 2012).

The benefits of plants presence on ancillary services is increasingly demonstrated by various studies, which examined planted and plant-free cases. Significant difference in pesticide concentration abatement between planted and unplanted ponds has been observed (Rose et al, 2006; Tang et al, 2016; Tournebize et al, 2013), and has been demonstrated that planted systems show enhanced pesticide removal efficiencies (Schulz et al, 2003), and accelerated degradation rates (Sethunathan et al, 2004; Zablotowitcz et al, 1998). Wu et al (2013b) scrutinised the seasonal TP removal of four different plant species and of a non-vegetated cell in microcosm laboratory units. Plants effect on removal capacities was evidenced between the vegetated and non-vegetated cases, regardless the species, and with reference to the same seasons and testing conditions. Beutel et al (2009) investigated temperature and DO variation in unplanted and in planted wetlands, and concluded that planted systems achieved decrease in temperature and DO levels, both of which conditions encourage biological denitrification. Lu et al (2009) noticed that the chief P removal way was via plant harvest, attaining 58% reduction of the total P removal load. This result underlines the importance of selecting plants with grand biomass and P adsorption competence, and supports the fact that plant harvest can prevent from release of the adsorbed P back in the wetland water. This is further supported by Tang et al (2016), who investigated certain pesticides removal rates related to the addition of Fe-impregnated biochar in planted and unplanted pilot-scale units. Results evidenced highest efficiencies in the planted units, and

including the Fe-Biochar. This outcome supports that annual plant harvesting is desirable to prevent from pesticides discharge back to water via plants, as well as harvested plant waste recycling, via conversion to Fe-Biochar and reuse of that for enhancing the treatment efficacy (Tang et al, 2016).

From the above mentioned cases the predominance of vegetation on treatment efficacy is evidenced, while research gaps were provided for further optimisation of CW design to attain maximal treatment efficiencies of specific pollutants, i.e. research orientation towards plant species and morphologies (emergent or submerged) with respect to specific agrochemical pollutants and testing conditions. However, this information is given only as a reference to support and acknowledge the important role of vegetation in CWs, and such investigation is beyond the scope of this review.

2.3.3.2. Hydrology – Climate – Season

Hydrological and climatic factors (Persson & Wittgren, 2003), along with agrochemicals application and irrigation practices (Zhang et al, 2008; Bianchi & Harter, 2002), affect CWs treatment efficiency. Lee et al (2015) underlined that three climatic-related parameters – namely rainfall intensity and depth, and antecedent dry days – are pivotal in the removal mechanisms of NPS pollution.

Additional factor that influences CWs treatment performance is temperature, and is related to season and climate. Temperature affects plant development, microbial activity, and nutrients removal (Kuschk et al, 2003; Poach et al, 2004; Wu et al, 2013a). Overall, nutrients have demonstrated high dependence on plant uptake and soil accumulation processes (Borin & Tocchetto, 2007; Tanner et al, 2005; Wu et al, 2013a), as well as on temperature (Beutel et al, 2009; Kadlec, 2005; Koskiaho et al, 2003b; Lu et al, 2009; Mander et al, 2015; Søvik & Mørkved, 2008; Tournebize et al, 2016).

In very cold or icy conditions major removal processes may be considerably affected. Microbial consortia is associated to temperature, and drop in temperature decreases both microbial development and metabolic rates (Faulwetter, 2009). In addition to this, nitrification and degradation processes are susceptible to temperature (Blankenberg, 2006;

Gottschall, 2007). Therefore, climate factors have significant impact on the seasonal performance of CWs, and thus deceleration of nutrients and agrochemicals removal rates should be anticipated during winter period.

2.3.3.3. Soil

According to Stottmeister et al (2003) root zone is the active reaction area of CWs, where biological and physicochemical processes take place. Soil mainly serves as a supporting medium for plant growth and microbial consortia. CWs efficiency suggests dependence upon the substrate material though (Yates & Prasher, 2009). Yates & Prasher (2009) considered how two kind of substrates, namely sandy clay loam and sandy soil, affect the P retention in pilot-scale units (Table 2.1). Results showed no notable difference in capturing P between the two soil types, but they suggested that sandy soil appears as a more sustainable material in maintaining its properties as a P sink for longer (Yates & Prasher, 2009). Likewise, Stottmeister et al (2003) underlined the presence of a relationship between soil hydraulics and grain size distribution, noting that optimal results both on hydraulics and on pollutants removal might be produced using a combination of sand and gravel as a substrate.

Denitrification is a process that takes place in the vicinity of the substrate in CWs (Fennel et al, 2009; Reed & Brown, 1995). NO_3^- removal is principally achieved via denitrification, a process that requires anaerobic conditions to take place, while ammonia removal is accomplished via nitrification, which is an aerobic process (Bastviken et al, 2009; Faulwetter et al, 2009). As a biological process, denitrification is a function of temperature, DO levels, pH, and vegetation (Bachand & Horne, 2000; Beutel et al, 2009; Braskerud, 2002; Firestone, 1982), and generally increases with DO levels (Kadlec & Knight, 1996; Phipps & Crumpton, 1994), and drastically with temperature (Vymazal, 2007). This might explain why SF CWs display greater removal efficiency of NO_3^- (Reed & Brown, 1995).

2.3.3.4. Sorption

Sorption is determined as any accumulation of a dissolved organic chemical by solid particles (Nowell et al, 1999). In the case of pesticides, sorption is the dominant reaction and

transformation mechanism that affects pesticides fate (Miller, 1986). Environmental conditions, such as organic carbon content, temperature and pH have a considerable impact on the sorption process (Nowell et al, 1999; Gao, 1998a). Sorption is such a rigorous process that is able to affect also other processes responsible for the fate of a compound, including transport and degradation (Gao, 1998a). Pesticide adsorption in soil, and degradation constitute fundamental factors that determine the potential impact of pesticide application on water and environmental quality (Villaverde, 2008). Important factors that affect degradation process include pesticide format, micro-climate (i.e. hydrology, precipitation, temperature), and biological activity (Blankenberg, 2006). Table 2.2 presents the transfer and removal mechanisms that mainly contribute to abatement of NPS pesticide runoff.

Table 2.2: Transfer & removal mechanisms in wetlands conducive to NPS pesticide runoff mitigation (Adapted from Rodgers & Dunn, 1992).

Transfer mechanisms	**Removal mechanisms**
Flow	Volatilisation
Sorption	Photolysis
Solubility	Hydrolysis
Retention	Biotransformation
Infiltration	

The portion of organic carbon in a particle identifies the degree of sorption that some pesticides experience in that specific environment. Pesticides removal depends on a combination of transport and degradation processes, which is a function of the physicochemical properties of the specific pesticide (Crossan, 2002; Stangroom et al, 2000).

A soil partition coefficient normalized for fraction of organic content, K_{oc}, is used as a standard measure of the level at which a specific pesticide compound will sorb in water and soil. K_{oc} indicates the sorption and the mobility of a pesticide in the water environment, and is measured in days. Overall, compounds with higher K_{oc} are considered as highly sorbing (thus, lower solubility and more sticking ability in the sediment). In particular, based on the K_{oc} value, pesticides are classified as low sorbing when K_{oc} < 400ml/g, and highly sorbing when K_{oc} > 1000 ml/g (Tournebize et al, 2016).

As mentioned previously, seasonality, in terms of pesticide application period, constitutes another factor of the CW removal efficacy, mainly because pesticides' transfer and transformation procedures are related to season. Overall, based on their K_{oc} and physicochemical properties, each pesticide reacts differently, thus, the related transport mechanisms from soil to wetland via runoff might be different for each pesticide, even if they belong in the same category.

2.3.3.5. Hydraulics

Hydraulics is another factor controlling the CW treatment performance. The hydraulic residence time (HRT) dictates the removal efficiency, and is essentially linked to hydrological conditions, such as storm and dry weather conditions, and hydraulics, i.e. actual CW shape. Details about HRT are given in Section 2.4.2. Dierberg et al (2002) remarked higher TP removal rates for longer HRTs. Johannesson et al (2015) observed good affinity between P and TSS retention and CW aspect ratio, with higher aspect ratios recommended for greater removal. Therefore, it is inferred that the hydraulic design of a CW should not be overlooked.

The high potential of CWs to remove a diversity of pollutants was discussed in Section 2.3.2 (see Table 2.1). To date, a great deal of research in CWs and ponds has been directed towards treatment processes, i.e. biological and chemical, comparing in-/outgoing concentrations of pollutants. However, this approach treats the system as a black box, overlooking the hydraulics and the fact that water flow is regarded a key factor of the overall system performance (Polprasert & Bhattarai, 1985; Kadlec, 1994; Min & Wise, 2009). Thus, there has been less research dedicated to the hydraulic performance of CW systems, to the investigation of hydraulic processes in vegetated flows, and to the interdependence between hydraulic and water quality processes, all of which are intended to be covered in Sections 2.4-2.5, which pose the main research focus of this literature review and study.

2.4. Hydraulics & Pollutant Transport

The aim of this section is to provide a background description of various CW hydraulic performance related parameters, and to introduce principles of solute mixing in open channel flows.

2.4.1. Tracer tests

A tracer is a chemical substance that is introduced into the stream or wetland inflow to track the movement of the flow or pollutant through it and to monitor its concentration downstream. The types of tracers that are largely employed include fluorescent, chemical and radioactive tracers (Gordon et al, 2004). Particularly in CWs, the most frequently used tracers are: anion bromide, cation lithium and fluorescent dyes (Headley & Kadlec, 2007). Yet dyes are preferred in most cases, as they present zero natural background levels (i.e. conservative) and low detection limits, plus their relatively low cost (Headley & Kadlec, 2007).

Amongst fluorescent dyes, Rhodamine WT (RWT) is considered as one of the most suitable dyes for application in CWs (Smart & Laidlaw, 1977; Headley & Kadlec, 2007; Stern et al, 2001). Reviewing its properties, RWT is an organic fluorescent tracer, high soluble in water, easily detectable at low concentrations, conservative, with low biodegrade properties, and relatively harmless in low concentrations for the aquatic habitat and for the operators, and inexpensive (Smart & Laidlaw, 1977; Stern et al, 2001; Lin et al, 2003). Limitations of RWT application comprise application only for short term tests (i.e. less than week duration) and for relatively low organic environments, in order to avoid possible adsorption (Smart & Laidlaw, 1977; Headley & Kadlec, 2007; Plazas et al, 2009). RWT under particular conditions behaves non-conservatively; this occurs when it sorbs to sediments or degrades biologically or photochemically (Lin et al, 2003).

To conclude, tracer tests constitute an essential means of obtaining information about the hydraulic behaviour of CWs. Information obtained from tracer tests includes contaminant's HRT, dispersion and mixing, hydraulic efficiency, insights about short-circuiting and dead

zones. To achieve these, it is important to select the appropriate tracer according to the wetland's environment, nature of tests, and tracer's properties; otherwise, the estimated parameters from the tracer tests may fail to representatively describe the hydraulic behaviour and removal capacity of the system.

2.4.2. Hydraulic Residence Time (HRT)

Hydraulic and treatment performance are inextricably linked to each other to achieve pollutant removal in a CW. A key controlling component of the overall performance of the system is the water movement. Flow field and mixing of the water parcels, along with the time that each parcel spends in a wetland, identifies the contact and activity time for treating pollutants (Werner & Kadlec, 2000). Hydraulic residence time (HRT) suggests the period that the inflow stays in the system, determining the reaction time with the pollutants (Su et al, 2009). HRT plays crucial role in the treatment degree of the pollutant in concern, while it is often the case that longer HRT yields to higher removal rate (Lee et al, 2015; Stern et al, 2001; Pappalardo et al, 2016; Tournebize et al, 2016). HRT is also referred to as retention or detention time, where simple differentiation between the two terms is that retention refers to continual presence of water that fluctuates in stage and mainly aims at reducing contaminants loads, while detention refers to systems with temporary water (experiencing intermittent flow and dry-off periods) aiming at holding large amounts of water to delay and reduce the wave of runoff following storm events (Buccola & Spolek, 2011).

According to Walker (1998), the main factors influencing HRT are the hydrology and hydraulics. Hydrology refers to the temporal allocation of inflows, while hydraulics describe the flow paths and system layout during storm events. In addition to that, HRT is also affected by factors such as evapotranspiration, infiltration and wind. In terms of hydraulics, emergent vegetation, flow rate (Q) and aspect ratio (A_R), affect the HRT (Kadlec, 1990; Jadhav & Buchberger, 1995). It is observed that HRT increases with A_R for constant Q, surface area and vegetation density (Jadhav & Buchberger, 1995). More information about the relation between HRT and hydraulics in vegetated flows is provided in Section 2.5.

Evaluation of the hydraulic performance is most frequently achieved through interpretation of the residence time distributions (RTDs) (Danckwerts, 1953; Persson & Wittgren, 2003; Min et al, 2009). A RTD shows the system's outlet response to an instantaneous upstream tracer input (i.e. salts, fluorescent dyes, etc.), it describes the residence time, and represents the system's fundamental mixing response (Danckwerts, 1953).

Mass transport theory on water and wastewater treatment units, e.g. ponds and wetlands, has been traditionally based on two basic ideal conceptual approaches (or flow regimes), which are the plug flow (PF) and the complete mixing, i.e. continuously stirred tank reactors (CSTRs). Firstly, the PF model suggests that all the water parcels entering the wetland travel with the same uniform velocity, and remain in the system for exactly the same time, without experiencing any mixing. This unique exit time is known as the nominal or theoretical residence time, t_n, defined as the ratio of the total wetland volume to discharge (Equation 2.1). (Levenspiel, 1966). Hence, t_n describes the time that the system requires to discharge the entire volume.

The completely-mixed model is represented by a sequence of continuously stirred tank reactors (CSTRs), where water in the CSTR is instantly and evenly mixed throughout the system. If a wetland follows the CSTR pattern, it produces a distribution of retention times typical of an exponential decay curve (Danckwerts, 1953; Levenspiel, 1966). As seen in Figure 5, curve A represents the completely-mixed influent scenario (i.e. maximum dispersion) displaying the expected exponential decay curve shape, with the tail of the curve extending following an exponential line towards x axis. On the contrary, PF is expressed by curve F (see Figure 5) (uniform and stable flow velocity conditions). This is a vertical line to the x axis, indicating that all tracer parcels undergo the same travel velocity uniformly. For clarity reasons in Figure 5, x axis displays the ratio of the actual time (t) of a tracer concentration appearing at the outlet divided by the theoretical detention time (t_n) of the tank, while y axis states the ratio of the actual tracer concentration (C) divided by the concentration that would be acquired if the tracer impulse was mixed instantly within the tank ($\bar{C}$).

$$t_n = V_{tot} / Q \qquad \text{Equation 2.1}$$

in which t_n is the nominal residence time, V_{tot} is the total water volume of the wetland, and Q is the corresponding discharge.

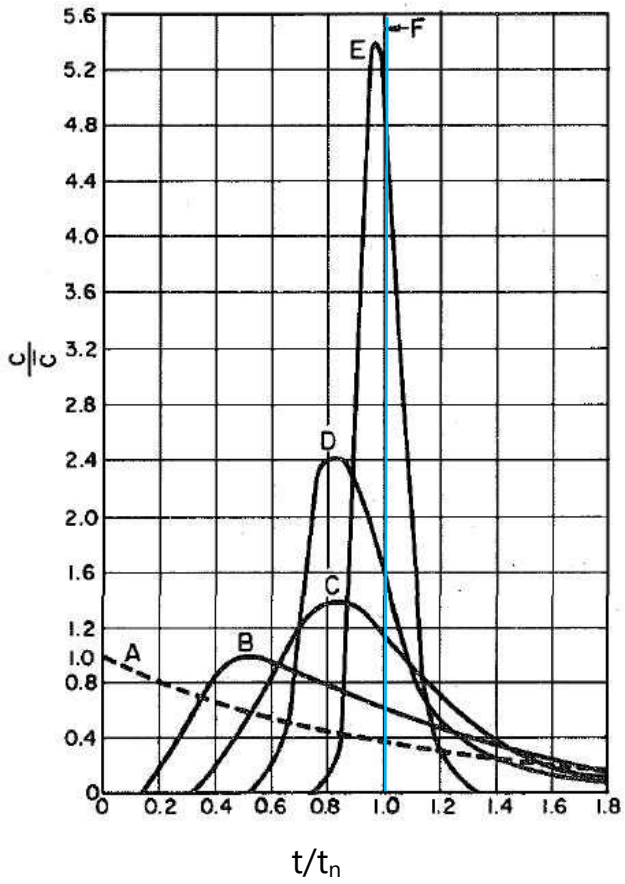

Figure 5: Dimensionless plot of dispersion showing characteristic dispersion curves for tanks. Curve A corresponds to the ideal dispersion of instantaneously & completely mixed influent. Vertical line F indicates the conditions in the tank for plug flow pattern (zero mixing). Intermediate degree of mixing is expressed by curves B-E (Adapted from Polpasert & Bhattarai, 1985).

However, in reality, the flow pattern inside a treatment unit, deviates from the above-mentioned ideal flow regimes, and usually results in lower treatment performance than the expected performance at the design stage (Kadlec, 1994; Bodin et al, 2012). Thus, the non-ideal flow patterns that occur in a dynamic system, e.g. CW, produce intermediate degree of mixing (Kadlec, 1994), hence a distribution of times for each parcel exiting the wetland. This is presented by curves B, C, D & E in Figure 5, laying between the two ideal flow patterns (i.e. curves A and F). Consequently, based on the mixing degree of the system, one should expect concentration-time distribution curves similar to cases B, C, D & E. As such, the actual

residence time (i.e. HRT) in a dynamic system is expressed as the mean residence time, which derives from the ratio of the mean volume of water to the mean discharge of the operating system (Kadlec, 1994). Thus, HRT can be thought as a measure of the variation of the residence time of the water coming into a wetland, where velocity profiles result into a distribution of residence times (Werner & Kadlec, 2000). Due to various factors, the theoretical and mean retention times are expected to be different in a dynamic (Figure 6).

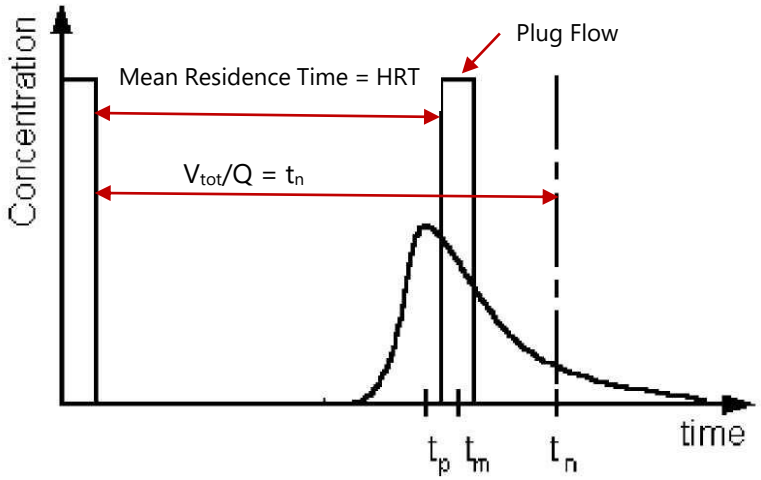

Figure 6: Concentration against Time plot obtained from a typical tracer test. Mean (t_m) and nominal (t_n) residence times are indicated, as well as Plug Flow pattern. Peak concentration time is denoted as t_p. (Adapted from Persson & Wittgren, 2003).

Causes of non-ideal flow distribution might include variation in flow velocities, different flow path lengths, and mixing processes (Holland et al, 2004). Figure 6 shows that during PF, the concentration-time distribution curve would resemble a spike, implying that all the incoming tracer parcels undergo the same retention period (Persson et al, 1999). However, under constantly stirred flow state, the concentration-time distribution is expressed by an exponential function where the outflow tracer concentration is decreased progressively (Persson et al, 1999) (see Figure 5 curve A). In reality though, the concentration-time plot normally generates skewed bell-shaped downstream distributions (Headley & Kadlec, 2007), while the tail of the curve extends as the flow state for the whole system reaches completely mixed conditions (Persson et al, 1999).

The plot that represents the concentration-time profile of the tracer in the exit of the system as a response to an instantaneous slug tracer injection is known as C-diagram, as shown in Figure 7. This plot gives insights of the nature of the water movement in the system, provided that the tracer used is conservative. Four fundamental mixing regimes (RTD curves) are represented by the C-diagrams in Figure 7. Moving from left to right, curve *a* represents plug flow, curve *b* plug flow with some longitudinal dispersion (i.e. very close to Gaussian-Fickian distribution), curve *c* corresponds to perfect mixing conditions, while curve *d* to a system with dead water zones and a restricted flow channel (Danckwerts, 1953). Time axis is normalised multiplying by $1/t_n$.

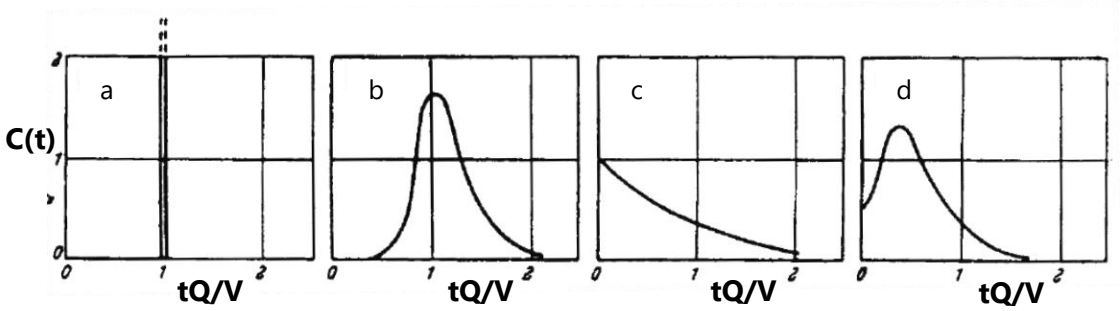

Figure 7: Typical C-diagrams for representative types of system. From left to right: plug flow, plug flow with some longitudinal dispersion, perfect mixing, and dead water. (Adapted from Danckwerts, 1953).

The cumulative residence time distribution (CRTD) is an alternative way of presenting the temporal concentration data. The concentration-time curve at the outlet of the system, as measuring concentration relative to the inlet tracer concentration, and time in reduced units (normalised time), is known as F-diagram (Levenspiel , 1966), as illustrated in Figure 8. Thus, the CRTD corresponds to the integral form of the RTD. The summation of the CRTD after being normalized produces unity. The CRTD approach has been utilized in water engineering to assess the performance of various aquatic systems and hydraulic structures, such as wetlands, ponds, storages tanks/reservoirs. Typical shapes of CRTDs (or F-diagrams) for representative types of a system are illustrated in Figure 8, where the flow regimes presented correspond to those of Figure 7.

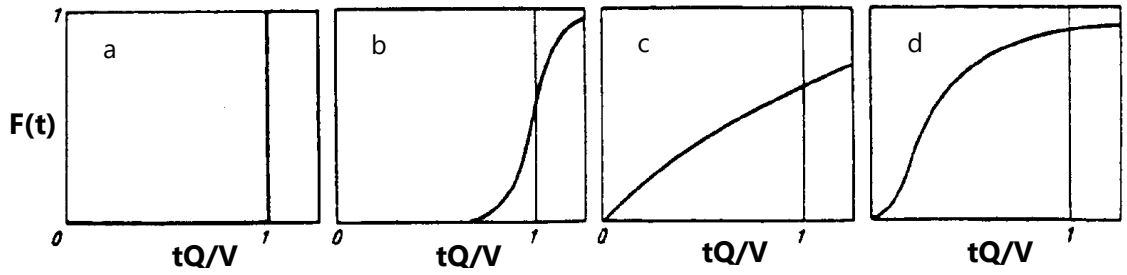

Figure 8: Typical F-diagrams for representative types of system. From left to right: plug flow, plug flow with some longitudinal dispersion, perfect mixing, and dead water. (Adapted from Danckwerts, 1953)

In order to quantify the key hydraulic parameters of a wetland, i.e. t_m (or HRT) and variance (σ^2) of the tracer impulse, the method of moments is commonly applied (Thackston et al, 1987; Kadlec, 1994; Rutherford, 1994; Kadlec & Knight, 1996; Holland et al, 2004; Seo et al, 2006; Bodin et al, 2012). According to that, the zeroth moment M_0 (Equation 2.2) corresponds to the area under the response curve; the first moment M_1 (Equation 2.3) describes the actual (or mean) residence time, t_m, determined as the centroid of the RTD. This is the average time that a tracer parcel expends in the wetland. For clarity reasons, for the rest of this thesis the HRT corresponds to the t_m. The second moment (Equation 2.4) is the temporal variance, σ^2, of the RTD, and describes the degree of spreading of the tracer response curve about the centroid (t_m).

$$M_0 = \int_{-\infty}^{\infty} c(x,t)dt \qquad \text{Equation 2.2}$$

$$M_1 = \int_{-\infty}^{\infty} t \cdot c(x,t)dt \qquad \text{Equation 2.3}$$

$$M_2 = \int_{-\infty}^{\infty} t^2 \cdot c(x,t)dt \qquad \text{Equation 2.4}$$

A simple approach to solve the definite integral of the response curve, i.e. the skewed bell-shaped curve in Figure 6, is the rectangle method. This approximation computes the area of the response curve by summing the sequential rectangles, resulting in Equation 2.5 - Equation 2.7. Therefore, the obtained properties from the moment analysis would be in simple mathematic terms as follows:

$$\text{Area} \rightarrow A = M_0 \qquad \text{Equation 2.5}$$

$$\text{Centroid} \rightarrow t_m = M_1 / M_0 \qquad \text{Equation 2.6}$$

$$\text{Variance} \rightarrow \sigma^2 = (M_2 / M_0) - t_m^2 \qquad \text{Equation 2.7}$$

From the moments' analysis calculation of the longitudinal dispersion coefficient, D_x, can be achieved (see Section 2.4.5.3). The degree of dispersion in a vessel or an aqueous system varies between plug flow (zero dispersion) and perfect mixing (infinity value of dispersion), as seen in Figure 5. The actual parameter that represents the dispersion is expressed by the dispersion number, *D/uL*, where: *D* is the dispersion coefficient; *L* is the length of the reactor; *u* is the fluid velocity (Levenspiel, 1966). By definition, lower dispersion number, entails lower dispersion in the system. The reciprocal of the dispersion number is known as Peclet number, *Pe=uL/D*, and describes the relative importance of advection and of dispersion in the system, where the advective scale is indicated by the nominator of the ratio. For *Pe*>>1, advection controls the transport; for *Pe*<<1, dispersion dominates and controls transport in the system.

TIS Model

An alternative mass transport model that has received attention, as it is considered to be capable of describing non-ideal flow characteristics, in contrast to the PF and CSTRs, is the tank in series (TIS). In the TIS approach, the CW is separated into a number of equally sized CSTR tanks, *N* (Levenspiel, 1966). In this way, a completely mixed reactor is represented by one TIS (N =1), while PF state corresponds to infinite number of TIS (N=∞), as seen in Figure 5, for the representative CRTD curves. A correspondence between the C-diagram and the *N* in the TIS model can be obtained. The number of corresponding TIS using the plume dimensionless variance obtained from the RTD can be determined as shown in Equation 2.8 (Levenspiel, 1966):

$$\sigma_\theta^2 = \frac{1}{N} \qquad \text{Equation 2.8}$$

where dimensionless variance is obtained as in Equation 2.9 (Kadlec & Wallace, 2009):

$$\sigma_\theta^2 = \frac{\sigma^2}{\bar{t}_m^2} \qquad \text{Equation 2.9}$$

This section introduced the RTD principles of a dynamic system and commonly applied models to represent the fluid flow. Section 2.4.3 describes a measure of characterising CW hydraulic performance and related parameters.

2.4.3. Hydraulic Efficiency

One measure to characterise CWs hydraulic performance is through the hydraulic efficiency, λ. Hydraulic performance is a broader notion that encompasses more features (or hydraulic phenomena) of the flow conditions, such as short-circuiting, recirculation, dead zones, while λ describes the capacity of a wetland to allocate flow uniformly within the volume it occupies, and to achieve satisfactory mixing or recirculation (Persson et al, 1999). In other words, λ incorporates both the deviations from the PF model, and the mixing degree. When λ is sufficiently high it is expected to allow greater contact time for the pollutants, enhancing the capacity to break them down. Factors affecting the λ include wetland shape (expressed as length to width ratio, L/W, or aspect ratio, A_R), bathymetry, vegetation characteristics, in-/outlet locations, as well as hydrological conditions (i.e. water depth, h, and flow rate, Q) (Persson et al, 1999; Holland et al, 2004).

Since both near PF state and effective volume, V_{eff}, utilisation contribute to a good λ and thus to an effective system operation, Persson et al (1999) introduced a practical measure for the hydraulic efficiency given in Equation 2.10. This formula incorporates the V_{eff} (see Equation 2.17) and the amount of mixing, expressed as N, where N=1 corresponds to fully mixed conditions and N=∞ signifies the PF pattern (Persson et al, 1999). Equation 2.10 can be applied to any wetland/pond and constitutes a common measure of comparison amongst different systems. The term λ_n means that hydraulic efficiency is measured using t_n.

$$\lambda_n = \mathrm{e}\left(1 - \frac{1}{\mathrm{N}}\right) = \frac{\mathrm{t_p}}{\mathrm{t_n}} \qquad \text{Equation 2.10}$$

Where: t_p denotes the time of the peak outflow concentration and t_n the nominal retention time (refer to Figure 6).

Computer simulations of various pond geometries and in-/outlet locations ran by Persson (2000) on thirteen hypothetical ponds, as shown in Figure 9, allowed to classify λ_n qualities,

as provided in Table 2.3. It should be noted that evapotranspiration and infiltration were not taken into consideration, and that tracer tests were simulated.

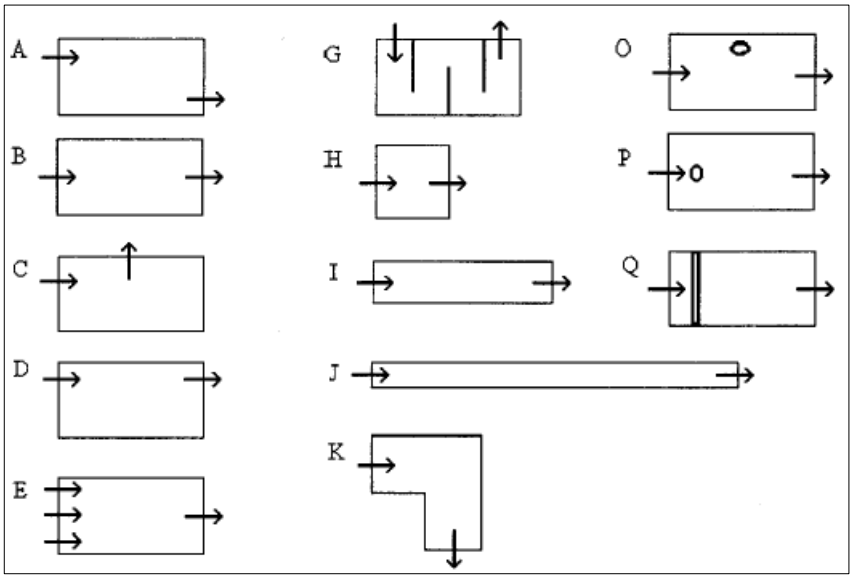

Figure 9: Different pond shapes, inlet-outlet geometries and obstruction designations for the 13 hypothetical pond cases simulated by Persson et al (1999).

Table 2.3: λ classification by Persson et al. (1999).

Quality of λ	Range factor
Good	λ>0.75
Satisfactory	0.5<λ≤0.75
Poor	λ≤0.5

The result of the hydraulic efficiency of the investigated cases in Figure 9 are registered in Table 2.4. Results propose that high λ values can be achieved using horizontally stretched ponds (case J), or baffled ponds (case P and Q), or even systems where the inflow is spread across the inlet (case E). Furthermore, it was revealed that the L/W (or A_R), plays a crucial role in wetlnads hydraulic efficacy. In particular, Persson (2000) found that A_R values smaller than 4:1 are expected to produce poor hydraulic efficiency. Incorporation of a small island or a submerged berm close to the inlet demonstrated considerably increased hydraulic efficacy potential (Persson et al, 1999). It was furthermore remarked that effective volume augments with A_R. The fact that the data of that study was not calibrated with data from existing ponds may indicate the need for investigating λ in full-scale units and comparing the results with

Persson et al's (1999) λ values (Table 2.3). Nevertheless, this initial theoretical approach provides valuable insights on the start of the investigation of hydraulic efficiency scenarios. It is also worhtnoty that that study did not look on vegetation characteristics investigation and its influence on the hydraulic efficiency.

Table 2.4: Ranking of hypothetical ponds according to λ (Adapted from Persson et al, 1999).

Category	Cases
Good	E, G & J
Satisfactory	P & Q
Poor	A, B, C, D, I, H, K, & O

Somes et al (1998) investigated the hydraulic efficiency of a natural wetland, and examined a basic case consisting of marginal vegetation. Furthermore, the authors produced five additional hypothetical simulated cases, modifying bathymetry, and vegetation layout. Results demonstrated that fully vegetated systems without any morphological alterations achieved doubled λ value compared to the unplanted case (base case). This result clearly evidences the crucial role of macrophytes in wetland hydraulic performance, recommending that fully vegetated wetlands may benefit more the λ compared to merely marginal vegetated units. Additionally, the authors found that bathymetry can play an important role in enhancing λ in fully vegetated systems. Bathymetry change can be achieved either by shaping the basin bed topography resembling trapezoidal cross sections, or by employing submerged aquatic benches. Although the authors exhort the convenience, reliability and success of using calibrated models to optimize wetland hydrodynamics, the emerging question is whether model simulations without calibration of models against empirical data can represent reliably and appropriately the actual hydraulic performance conditions of CWs. Furthermore, seasonal vegetation variation as a naturally occurring factor, alters the canopy morphology over different seasons, posing an element that was not examined in that work.

Koskiaho (2003) scrutinized the hydraulic patterns and performance of two CW–ponds, followed by computer simulations of a few further cases. The author simulated the tracer tests and employed the ratio of CW to watershed area (CW/WA), underpinning its importance in the retention performance. The two tested wetlands were designed to

accommodate and reduce flow velocities during flood periods, with the ultimate goal to accomplish high TSS retention. The designs of the two investigated CWs–ponds of Hovi and Alastaro, are shown in Figure 10 and Figure 11 respectively, indicating the in-/outlet locations and systems' geometries.

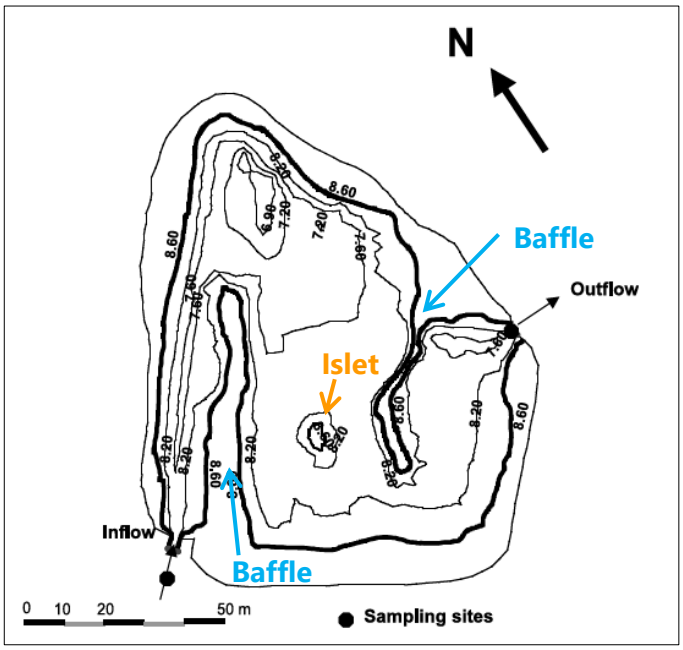

Figure 10: Schematic contour map of the Hovi CW, Finland. The map indicates the locations of inlet and outlet and sampling points for TSS analysis. The contour line 8.60 m in bold represents the shoreline of the pond during flood. (Adapted from Koskiaho, 2003).

Figure 10 depicts Hovi treatment unit, which constitutes the actual base case L_H1, consisting of two baffles and an islet. The hypothetical investigated case, L_H2, included no obstructions (no baffles or islets). λ evaluation was based on Equation 2.10 and t_p was obtained via simulated tracer tests. The obtained λ values evidenced that although the hypothetical case allows for larger water volume in the unit, obstruction inclusion increases the hydraulic efficiency more than 2.5 times, which is in accordance with Persson's (2000) results.

The Alastaro treatment unit examined by Koskiaho (2003) is illustrated in Figure 11. This is a rectangular shaped system with opposite corner to corner inlet and outlet design. The peculiarity of this unit is that it consists of two parts, the first of which is an open-water basin, while the second a shallow-planted area. The real case scenario, L_A1, is depicted in Figure 11; however, two hypothetical scenarios were ran; the first scenario was L_A2 with inlet-outlet

sited on the same side, and the second scenario was L_A3 for evenly distributed water at the inlet. The obtained λ for the hypothetical cases produced almost the same efficiency with L_A1, displaying a minimal increase in λ. Results suggest that for rectangular layouts the effects of location and width of inlet on hydraulic properties appear to be milder than in more squared layouts.

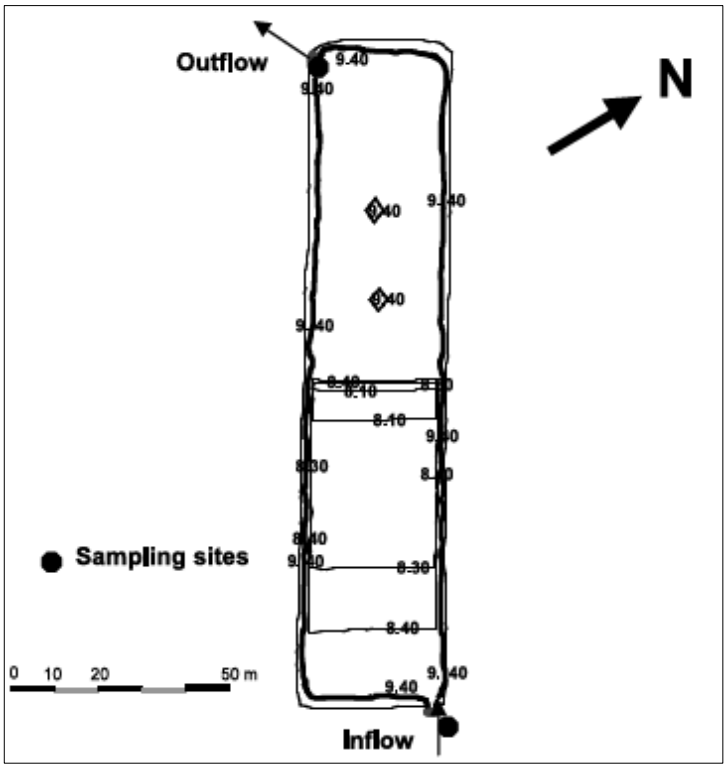

Figure 11: Schematic contour map of the Alastaro CW, Finland. The map indicates the locations of inlet and outlet, which is corner-corner. The contour line 9.40 m in bold represents the shoreline of the pond during flood. (Taken from Koskiaho, 2003).

Overall in Koskiaho's (2003) study, highest λ was obtained in L_H1 scenario. That unit had A_R = 4/1, which according to Persson et al (1999) is anticipated to produce poor hydraulic efficacy. The achieved λ ranged from 0.52 to 0.55, corresponding to satisfactory hydraulic efficiency though. Overall, Koskiaho's (2003) empirical results accord with Persson et al's (1999), advocating that elongated wetland shapes and use of islands improve λ.

Based on a stormwater pond suffering from water stagnation and short-circuiting, German et al (2005) employed numerical modelling to appraise the impact of alternative designs on the treatment and hydraulic efficiency. The original pond design is illustrated in Figure 12

(Left), divided into two parts, by a causeway; an island is placed at the second part of the pond, and outflow is discharged via two identical culverts. The four simulated scenarios are presented in Figure 12 from left to right, including: i) exclusion of the island; ii) installation of baffles; iii) creation of a culvert under the causeway; iv) creation of four culverts under the causeway.

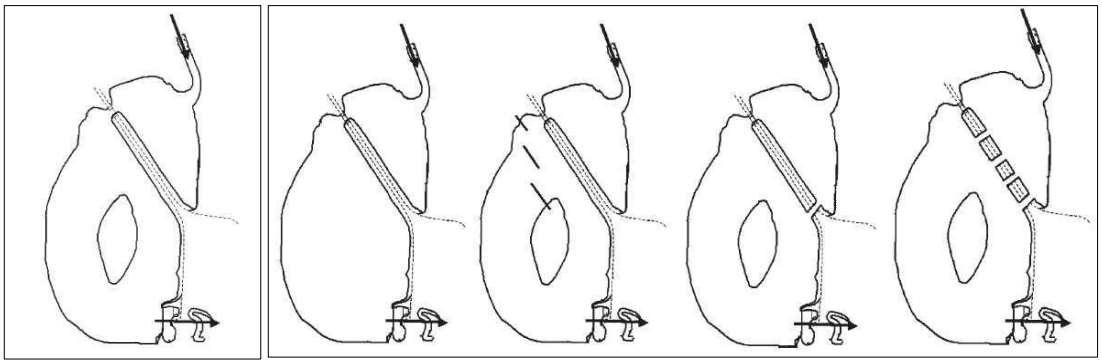

Figure 12: Left: Schematic of the current situation at Backaslov pond. Right: Schematics of modelled cases to enhance removal efficiency. From left to right: i) island removal; ii) baffles setting; iii) one culvert construction under the causeway; iv) four culverts construction under the causeway. (Taken from German et al, 2005).

The results of that study showed that all applied measures, but the removal of the island, enhanced both the hydraulic and treatment efficiency, with the most effective measure being the baffles utilisation. Compared to the base case, the use of baffles improved λ by 57.5%, the use of four culverts by 32%, whilst the use of one culvert only by over 8.5% (German et al, 2005). Results underscore Perrson's (2000) findings that berms enhance significantly λ. In all the investigated cases, treatment efficiency augmented with hydraulic efficiency.

Further on the baffles remediation measure, Chamberlain & Moorhouse (2016) examined baffle curtains installation in a lagoon treating minewater. The study included one lagoon as the control system, and a second lagoon as the baffled system. The settlement lagoons were identically sized and in parallel arrangement. Results demonstrated greater removal efficiency in iron and aluminium in the baffled system by 41% and 34% respectively, compared to the control lagoon. In addition to the removal efficiency enhancement, the retrofitting improved the lagoon's hydraulics, increasing both the HRT and λ approximately by three times.

Based on the findings about λ research, Su et al (2009) attempted to move a step forward, by examining the optimum design strategy of a FWS CW. The authors investigated some of the parameters that influence λ, namely: aspect ratio (A_R), configuration of inlet and outlet and the obstruction designation. Tracer tests were simulated in a numerical model, neglecting tracer decay, adsorption, infiltration, and evaporation effects though. The authors initially examined nine different CWs with varying A_R. They found that λ is analogous to A_R, but not with the same rate. In particular, when A_R is higher than 5, λ=0.9 is achieved, and the influence on λ becomes minor as increasing the A_R further. Concerning the arrangement of in-/outlet locations, Su et al (2009) scrutinised three options, namely midpoint-midpoint, corner-corner, uniform-midpoint, as illustrated in Figure 13. The authors employed a referred case of A_R =1.88, which provides satisfactory efficiency of λ=0.7. Results demonstrated that corner-corner in-/outlet layout decreases the hydraulic efficiency to 0.65, while uniform inflow scenario 2C (Figure 13) accomplishes good hydraulic efficiency of 0.88, and achieves the most uniform flow field in the wetland for the given A_R.

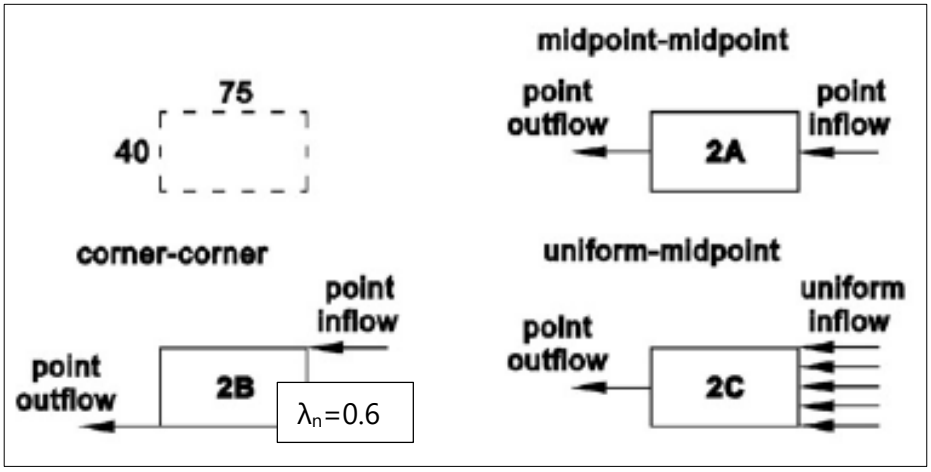

Figure 13: Investigation of 3 hypothetical cases of different inlet and outlet configuration, namely midpoint-midpoint, corner-corner, uniform-midpoint. A referred case of A_R = 1.88 was used (Adapted from Su et al, 2009).

The last examined case by Su et al (2009) was the impact of obstruction designation on λ. The obstructions were simulated as rectangular objects varying in number, width and length, with nine scenarios carried out, as illustrated in Figure 14. The authors used the worst available scenario of in-/outlet layout (see Figure 13, case 2B), which produces λ_n=0.65, and attempted to examine the influence the obstructions would have on λ. They found that

increase in obstruction width had a positive effect on λ, reaching up to λ=0.95. The relationship between the number of obstructions and the λ demonstrated slight difference in λ for 2, 4 or 6 obstruction objects. This infers that more influential role plays the location and the dimensions of the obstructions rather than their number. Eventually, beyond the use of obstructions to improve hydraulic efficacy, attention should also be paid to the effective volume, because obstructions occupy useful water volume, and thus improper obstruction arrangement may result to the reduction of the wetland's effective volume.

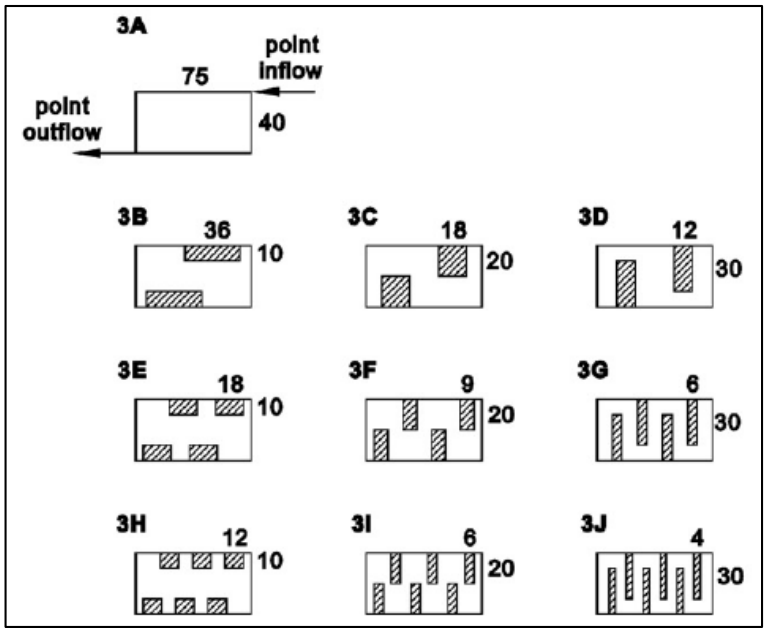

Figure 14: Investigation of 9 hypothetical cases of the influence of obstructions characteristics, referring to the corner-corner inlet & outlet layout scenario (Taken from Su et al, 2009).

2.4.4. Hydraulic indices

This section describes the two major categories of hydraulic indices, i.e. short-circuiting and mixing.

2.4.4.1. Short-circuiting indices

Pollutants removal rate is generally considered to be maximised when the flow velocity is uniform in the system, which entails that all water particles leave the system exactly at the nominal residence time, t_n (Polprasert & Bhattarai, 1985; Lightbody et al, 2009). In a dynamic

system though, non-ideal flow caused by velocity and mixing heterogeneity, leads to different particle travel times, which result in a distribution of residence times, as discussed in Section 2.4.2. Under those conditions, some water particles leave the system earlier, and some others later.

The phenomenon related to the advection of water, promoting part of it to exit the system via preferential flow paths, at a time earlier than the t_n, is called short-circuiting (Thackston et al, 1987; Persson et al, 1999; Lightbody et al, 2008; Lightbody et al, 2009). Short-circuiting is not desirable in a treatment unit, since it causes shorter HRT, and hence reduced treatment efficiency (Lightbody et al, 2008; Lightbody et al, 2009; Min & Wise, 2009). Investigating fast flow paths in a treatment wetland, Lightbody et al (2008) observed that short-circuit paths achieved velocities 10 times greater than the water velocity passing through the vegetation, and found that 20% to 70% of the flow experienced HRT shorter than the one eighth of the t_n (Lightbody et al, 2008). Such results indicate the severe implications of short-circuited flows on HRT and in turn on the treatment capacity of the unit. Apparently, short-circuiting poses a challenge in the design and operation of treatment wetlands, thus scientists try to find ways to understand and minimise its effect and presence.

To date ample research has been conducted to understand the factors connected to short-circuiting in closed pipes and open channels. In open channels, several factors may influence short-circuiting comprising: length to width ratio (or aspect ratio); water level; flow rate; bottom topography; vegetation characteristics (i.e. type and heterogeneity); presence of hydraulic structures; existence of internal structures, i.e. islands, dykes and berms; wind (Min et al, 2009).

Study undertaken by Polprasert & Bhattarai (1985) demonstrated that minimum short-circuiting is achieved in ponds with relatively large A_R underpinning that the actual design of the unit is crucial for reducing short-circuiting. Min & Wise (2009) performed simulations to examine the effects of vegetation and bathymetry on short-circuiting. The authors found that bottom topography variations played greater role in λ deviation, compared to vegetation, and drew the conclusion that short-circuiting has more affinity to bathymetry

than to vegetation resistance. Nevertheless, although modelling flow software represented successfully the CW hydraulic aspects, that study included some significant limitations: i) no seasonal vegetation variation effect was examined; ii) vegetation was assumed homogeneous, which seldom happens in CWs; iii) no field verification of the modelled data on bathymetry and vegetation was carried out. Furthermore, Kjellin et al. (2007) applied a flow transport model to appraise the dependence of vegetation layout, bottom topography, dispersion and flow using field data obtained from tracer tests. The authors found that heterogeneity in vegetation promoted variance in HRT, while changes in bottom topography minimised that variance.

From the above, it is inferred that more research is needed to elucidate the parameters affecting HRT and short-circuiting, as flow transport models use assumptions, e.g. homogeneous vegetation. Field studies are needed to provide empirical data to understand the related phenomena in full-size units. Consequently, the success to understand, predict, and reduce short-circuiting in vegetated systems will contribute to increasing removal rates and to informing wetland designers and modellers.

Evaluation of the degree of short-circuiting in a system, involves analysis of the RTD curves obtained from tracer tests. Short-circuiting indices that have been widely employed are presented in Table 2.5 and discussed in this section.

Table 2.5: Short-circuiting indices (Adapted from Texeira et al, 2008).

Index	Definition	Reference
t_1'	*Initial arrival time* – Indicates the time of the first detection of the tracer at the outlet	Hart et al, 1975; Stamou & Adams, 1988; Laurent et al, 2015
t_{10}	*10% arrival time* – Period of time for 10% of the tracer mass to reach the outlet	Hart et al, 1975; Stamou & Adams, 1988
t_p	*Peak concentration time* – Time at which the maximum concentration was detected at the outlet	Hart et al, 1975; Stamou & Adams, 1988
t_{16}	*16% arrival time* – Period of time for 16% of the tracer mass to reach the outlet	Ta and Brignal, 1998; Persson, 2000
t_{50}	*50% arrival time* – Period of time for 50% of the tracer mass to reach the outlet. This coincides to the median of the RTD	Hart et al, 1975; Stamou & Adams, 1988; Stovin et al, 2008
t_n	*Theoretical (or nominal) retention time* – The average design time necessary for the tracer mass to reach the outlet	Persson, 2000; Stovin et al, 2008; Laurent et al, 2015
t_m	*Mean (or actual) retention time* – The mean time that the tracer needs to reach the outlet. This corresponds to the centroid of the RTD, and is known as HRT.	Agunwamba, 2006

Ta and Brignal (1998) evaluated the results of various modification options in a reservoir on short-circuit, mixing degree and HRT using computer fluid dynamics. The authors observed that uniform velocities throughout the reservoir reduce the short-circuit levels, but noticed that as plug flow state is reached, less mixing occurs in the system, lowering the potential to decrease pollutant peak concentrations. As a result, amongst the various examined cases, the authors compromised for greater short-circuiting amount, which would provide a sufficient degree of mixing. Ta and Brignal (1998) employed Equation 2.11 to calculate short-circuit values, where large S_A-values correspond to zero short-circuiting. As defined in Equation 2.11, S_A is not affected by the tail of the RTD, which is the case discussed in Section 2.4.2, and where low concentrations of tracer exist in the system for prolonged retention times.

$$S_A = \frac{t_{16}}{t_{50}} \qquad \text{Equation 2.11}$$

in which t_{16} and t_{50} are the 16th and 50th percentiles respectively of the RTD at the outlet.

Persson (2000) examined the hydraulic performance and the short-circuiting for different pond designs, and noticed lower short-circuiting effects in ponds with large A_R, as well as in cases where a berm or island was established close to the inlet. Observing the RTDs and other tracer parameters (e.g. σ^2) in each pond case, Persson (2000) remarked that Equation 2.11 of Ta and Brignal (1998) appears to be inadequate and implausible in some cases. For instance, when inlet and outlet are located close to each other, like in case C (see Figure 9), or when t_{16} and t_{50} differ a little from each other, and σ^2 is high, then Equation 2.11 results in high S_A, implying erroneous value of low short-circuiting (Persson, 2000). Another example of erroneous low S_A value would be the case of a pond with large inactive volume and with close to PF conditions; this produces ratio t_{16}/t_{50} close to unity, while in reality the system suffers from significant short-circuiting (Persson, 2000). Therefore, Persson (2000) proposed t_n to be used in lieu of t_{50} at the denominator of Equation 2.11 , thereby calculating short-circuiting as given in Equation 2.12:

$$S_B = \frac{t_{16}}{t_n} \qquad \text{Equation 2.12}$$

Stovin et al (2008) also observed the same phenomenon as Persson (2000) about Equation 2.11, which indicated low short-circuiting and achieved PF, while the storage volume was bypassed. The authors suggested that the S_A may be employed merely as a limited indicator of short-circuiting, as it does not apply in all cases. Stovin et al (2008) used the quotient given in Equation 2.13 to calculate short-circuiting. The authors noted that the t_m (corresponding to the centroid of the RTD) tally with a point on the tail of the distribution curve, while the t_{50} indicates better the peak time concentration.

$$S_C = \frac{t_{50}}{t_n} \qquad \text{Equation 2.13}$$

Agunwamba (2006) conducted laboratory experiments to explore the effect of vertical location variation of the inlets and outlets on short-circuiting in rectangular ponds/reservoirs. The author calculated short-circuiting using Equation 2.14, where the closer α_n is to zero the lower the magnitude of short-circuiting. For all the arrangements of the in-/outlet positions, results showed that α_n decreases with flow velocity. The influence of in-/outlet configuration was found to have greater impact on α_n in smaller tank lengths. In particular, Agunwamba (2006) recommends the inlet to be at the bottom, while the outlet to be structured to outflow at the surface for field ponds design. Regarding mixing, results confirmed that for fixed velocity, the longitudinal mixing effect decreases for longer pond lengths, which supports the perception that PF is achieved at higher A_R.

$$a_n = 1 - \frac{t_m}{t_n} \qquad \text{Equation 2.14}$$

Another measure used to quantify short-circuiting is the ratio of the first arrival time, t'_1, of the plume (which corresponds to the minimum longitudinal distance that the plume traverses in the system), over t_n, practiced by Laurent et al (2015), given in Equation 2.15.

$$S_L = \frac{t'_1}{t_n} \qquad \text{Equation 2.15}$$

It is seen that researchers have employed different indices to measure short-circuiting, using either some percentiles of the RTD curves and/or a combination of RTD parameters. It seems that there is not yet one standard equation for short-circuiting applying in all cases, and that

short-circuit index selection is probably in the discretion of the researcher. Texeira et al (2008), recommend t_{10} as a successful and satisfactory short-circuiting indicator, and underline that t'_1 is also an important short-circuiting indicator. This review showed that high A_R has a minimising effect on the short-circuiting. However, importantly, in all the above-mentioned studies the influence of vegetation on the short-circuiting (either as change in heterogeneity or as ageing) was not examined thoroughly, which poses a gap in research.

2.4.4.2. Mixing Indices

Another hydraulic index involves mixing, which refers to the random spreading of the water in the system, incorporating the joint effects of turbulent diffusion, advection, recirculation and stagnation. Some individual processes of mixing, i.e. longitudinal dispersion, and dead zones, are described in Section 2.4.5. Common mixing indices that have been largely used to-date are presented in Table 2.6.

Table 2.6: Common mixing indices (Adapted from Texeira et al, 2008).

Index	Definition	Reference
S^2	*Dispersion index* – Quotient of temporal variance and the centroid of the RTD	Levenspiel, 1972; Stamou & Adams, 1988
Mo	*Morril index* – Ratio of the 10^{th} and the 90^{th} percentile of tracer mass reaching the outlet, $Mo=t_{90}/t_{10}$.	Hart et al, 1975; Stamou & Adams, 1988

Texeira et al (2008) appraised various mixing indicators and concluded that dispersion index, σ^2, is the most appropriate indicator to evaluate mixing levels, underlining though that when mixing is low, σ^2 becomes less accurate. In such cases, Texeira et al (2008) recommended combination of the σ^2 and *Mo* to evaluate mixing.

2.4.5. Mixing

This section describes hydraulic phenomena, such as dead zones, and mixing, with particular focus on longitudinal dispersion. In this study, the term of *mixing* assembles the aggregated effect of the associated procedures conducive to the spread of a pollutant. Overall, mixing assembles molecular diffusion, turbulent diffusion, differential advection, and mechanical diffusion. In other words, mixing incorporates the joint action of the effects related to the

abovementioned processes that cause spreading, recirculation, or stagnation of the pollutant/tracer. Mixing processes in vegetated flows are described in detail in Section 2.5

2.4.5.1. Dead Zones

While short-circuiting characterises preferential, or fast, flow paths, dead zones describe regions in which velocity moves at a significantly slower pace than the mean velocity, as well as areas of water recirculation (Thackston et al, 1987). Water particles entering zones of stagnation result in prolonged residence times, while longitudinal velocity approaches very low values.

Molecular and turbulent diffusion are the mechanisms that impart the dead zone fluid particles into the main flow (Nepf et al, 1997). The contaminant captured in dead regions is freed again to the main flow when the main tracer cloud has elapsed. Besides producing long residence times, dead zones do not belong (or not actively contribute) into the flowing water system volume, thus decreasing the system's effective volume and potentially its performance (Thackston et al, 1987; Bodin et al, 2012). This entails that the total available water volume might not be completely utilised. This explains one reason that the t_n is larger than t_m (Figure 6).

Dead water flow regions typically occur in the edges and corners of ponds; nevertheless, in vegetated flows, dead water regions may occur anywhere in the system. Thackston et al (1987) introduced a new measure called effective volume ratio, *e*, expressed as the effective system volume, V_{eff}, over the total system volume, V_{tot} (Equation 2.16).

$$e = \frac{V_{eff}}{V_{tot}} \qquad \text{Equation 2.16}$$

Relating the ratio of Equation 2.16 with the t_m and t_n, and multiplying the residence times by the flow rate, Equation 2.17 is produced, as an alternative way to estimate the effective volume of the system (Thackston et al, 1987):

$$e = \frac{V_{eff}}{V_{tot}} = \frac{t_m}{t_n} \qquad \text{Equation 2.17}$$

The active system volume can be estimated by the product of t_m by *Q*, as in Equation 2.18:

$$V_{eff} = t_m \cdot Q$$ Equation 2.18

There is a debate whether volume occupied by dead zones has favourable effects or not on the wetland's treatment efficiency. It is considered that dead zones are part of the total volume that becomes unavailable to the main flow, thereby causing significant decrease to the t_m (German et al, 2005; Thackston et al, 1987; Wörman & Kronnäs, 2005). As a result, when t_n is much greater than t_m, occurrence of dead zones should be expected. On the other hand, dead zones augment longitudinal mixing, producing long trailing edges to the concentration-time tracer profiles, and they also increase the length of the advective zone (Rutherford, 1994).

2.4.5.2. Dispersion

It is frequently observed that discharge of pesticides (or solutes) in natural water bodies may cause severe harm to the wildlife habitat and to human health. As mentioned in Section 2.2, agricultural runoff, significantly contributes to surface and ground water degradation (Hammer, 1992). Understanding the behaviour and effects of soluble matter that is released in natural watercourses is therefore of major importance for the environmental management. Accurate evaluation of the mixing and dispersion of the solutes in an aqueous system contributes to the prediction of the magnitude of the environmental impact. Therefore, mixing coefficients have to be taken into account, as in this case, they constitute essential indicators of a wetland's performance,. The units of the mixing coefficients are normally denoted by squared meters per second, m^2s^{-1}.

Open channel processes conducive to mixing

In open channel flows the key mixing processes taking place are the molecular diffusion, turbulent diffusion and shear dispersion. Molecular diffusion describes the slow spread of the water molecules, i.e. contaminant or tracer, in all three directions (x, y, and z) through a process known as random Brownian motion (Rutherford, 1994). Molecular diffusion is a very slow procedure and obeys to Fick's law when considered in one dimension, as expressed Equation 2.19. Fick's law states that the rate of mass of a solute is analogous to the concentration gradient (Rutherford, 1994).

$$J_x = -e_m \frac{\partial c}{\partial x}$$ Equation 2.19

where J_x is the rate of the molecular conveyance across the unit area; e_m denotes the molecular diffusion coefficient; c is the concentration of the diffused solute; and x is the distance measured perpendicular to the section.

Incorporating the three coordinate directions x, y, z in the diffusion equation, it becomes Equation 2.20 (Rutherford, 1994):

$$\frac{\partial c}{\partial t} = e_m \left(\frac{\partial^2 c}{\partial x^2} + \frac{\partial^2 c}{\partial y^2} + \frac{\partial^2 c}{\partial z^2}\right)$$ Equation 2.20

Molecular diffusion refers to stationary flow, however, when the solute is subjected to laminar flow, where steady velocity exists, the solute or tracer undergoes movement, known as advection. Taking into account the three axial directions x, y, z, the velocity component for each direction will be respectively u, v, w, producing the advection–diffusion equation (Equation 2.21):

$$\frac{\partial c}{\partial t} + u\frac{\partial c}{\partial x} + v\frac{\partial c}{\partial y} + w\frac{\partial c}{\partial z} = e_m \left(\frac{\partial^2 c}{\partial x^2} + \frac{\partial^2 c}{\partial y^2} + \frac{\partial^2 c}{\partial z^2}\right)$$ Equation 2.21

However, in natural flows turbulence occurs. Turbulent diffusion is described as the spreading of random short-term localised particle variations (Rutherford, 1994). Turbulence is generally caused by velocity shear; thus, high turbulence is observed in areas of high shear, such as bed abnormalities and obstacles. The analysis of Taylor is largely used to quantify turbulent diffusion in the solute transport field. Turbulent diffusion is much greater than molecular diffusion, and approximately six orders of magnitude greater than molecular diffusion (Rutherford, 1994). As a result, the effects of molecular diffusion coefficient ($e_m \approx 10^{-9}$ m^2s^{-1}) are considered negligible as opposed to turbulent diffusion coefficient's ($\varepsilon \approx 10^{-3}$ m^2s^{-1}), and thus the three dimension turbulent diffusion equation includes the advection effects by averaging about time, leading to Equation 2.22:

$$\frac{\partial \bar{c}}{\partial t} + \bar{u}\frac{\partial \bar{c}}{\partial x} + \bar{v}\frac{\partial \bar{c}}{\partial y} + \bar{w}\frac{\partial \bar{c}}{\partial z} = \varepsilon_x \frac{\partial \bar{c}}{\partial x^2} + \varepsilon_y \frac{\partial \bar{c}}{\partial y^2} + \varepsilon_z \frac{\partial \bar{c}}{\partial z^2}$$ Equation 2.22

where ε_x, ε_y, ε_z are the turbulent diffusion coefficients corresponding respectively to the x, y, z axial directions.

Dispersion – or shear dispersion – is a basic component of the mixing in a natural stream or wetland. In uniform flow, advection carries a contaminant plume downstream producing zero deformity or spreading (Rutherford, 1994). Nevertheless, velocity is rarely uniform in natural channels due to boundary friction effects. Longitudinal dispersion is the result of differential flow velocity (vertical and lateral velocity shear) also known as differential advection, as the contaminant cloud travels downstream faster in the mid-channel than close to the bed and banks (Rutherford, 1994). The main cause of dispersion is the vertical and lateral changes of the local mean velocity (Thackston et al, 1987).

In the vertical direction, shear velocity and turbulence combined effects are illustrated in Figure 15, considering an instantaneous release of contaminant. Velocity varies vertically, with increasing values towards the water surface, while at the same time turbulent diffusion spreads the plume over. At time zero, t_0, the contaminant profile is represented by a line, while after some time, t_1, the concentration plume has been advected downstream, distorted by differential vertical velocity and spread over by turbulent diffusion (Rutherford, 1994).

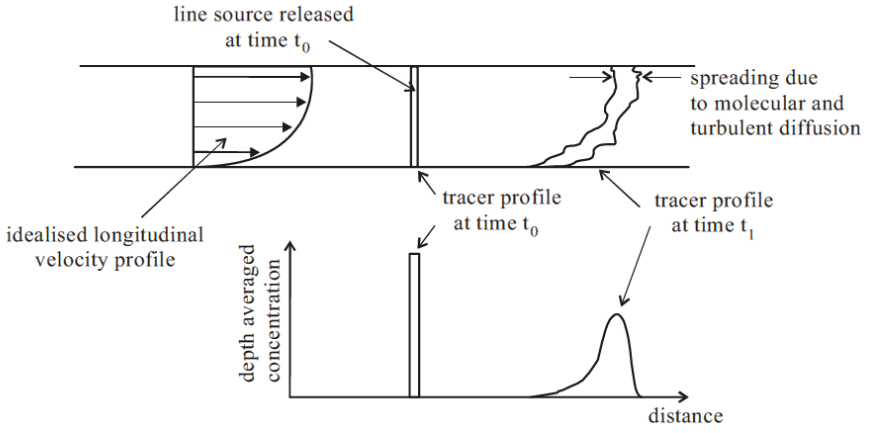

Figure 15: Combined effects of vertical velocity shear and turbulent diffusion on longitudinal dispersion. Differential vertical velocity is lower near the bed and higher near the free water surface. At the same time turbulent diffusion takes place contributing to some degree to the spreading. An slug contaminant injection is made at time t_0 (vertical line) and at time t_1 the plume has been advected downstream, deformed owing to vertical velocity shear and spread over by turbulent diffusion. (Adapted from Rutherford, 1994).

In the transverse direction, considering a slug contaminant release, the concentration plume is carried downstream, slowly close to the banks and bed, and faster towards the mid-channel. The transverse velocity profile resembles a parabolic shape, as illustrated in Figure 16. At the same time turbulent diffusion produces localised dispersion both across and along the channel (see Figure 16). Transverse velocity shear and longitudinal turbulent diffusion induce concentration spreading along the channel, with the major contribution deriving from transverse velocity shear. Longitudinal turbulent diffusion generates very little mixing compared with the transverse velocity shear (Rutherford, 1994).

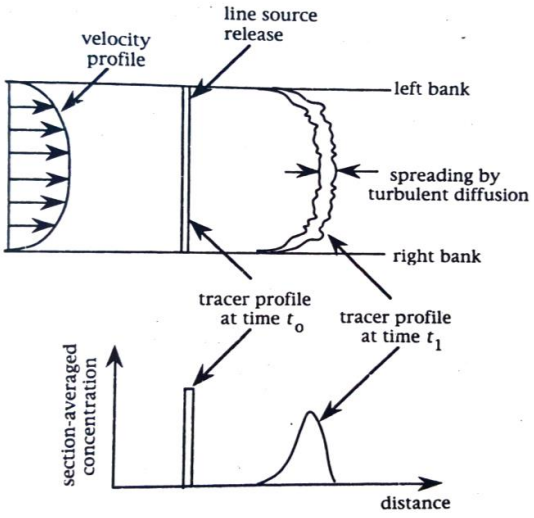

Figure 16: Mixed results of transverse velocity shear and transverse turbulent diffusion on longitudinal dispersion of a contaminant plume. For an instantaneous contaminant release the plume profile is presented as a vertical line at t_0. After some time, t_1, the plume profile is advected downstream, deformed due to transverse velocity shear and spread over due to longitudinal turbulent diffusion. (Taken from Rutherford, 1994).

Shear flow dispersion was initially postulated by Taylor (1953), who manifested that the inter-influence of differential advection and cross-stream diffusion enhances longitudinal dispersion. Differential advection deforms the local flow pattern, stretching the vertical and lateral concentration gradients. On the other side, molecular or turbulent diffusion perform conversely to diminish the generated cross-stream gradients. It is noteworthy that the longitudinal dispersion coefficient, D_x, is inversely analogous to the turbulent diffusion coefficient (Rutherford, 1994). The net result of the above counter-acting processes results in increase of the longitudinal distance of the contaminant plume. The joint action of differential advection and its counteracting diffusion procedure is called shear dispersion.

Taylor (1953) postulated that the results of longitudinal shear flow dispersion become comparable to diffusion after some time, and thus can be expressed by Fick's law (Equation 2.19). Fick's law predicts that the variance of a tracer plume increases linearly with time (Rutherford, 1994). Taylor's analysis demonstrates that the time required to reach the equilibrium zone is comparable to the time required for a tracer cloud originating from a steady source to become cross-sectionally well mixed, hence it can be modelled employing Fick's law. When this condition is valid the three dimensional advection-diffusion equation is valid, given in Equation 2.23.

Shear dispersion describes the net effect of velocity changes about the depth and width. Wind has a direct influence on dispersion, enhancing mixing, rather than decreasing t_m (Thackston et al, 1987). Compared to the turbulent diffusion effects, dispersion coefficient is three orders of magnitude greater than the turbulent diffusion coefficient (Rutherford, 1994); therefore, shear dispersion is the dominant process in river mixing, and its evaluation is major in quantifying mixing characteristics. Fischer et al. (1979) described the Advection-Diffusion Equation (ADE) including the dispersion coefficients for the three axial directions (Equation 2.23):

$$\frac{\partial c}{\partial t} + u\frac{\partial c}{\partial x} + v\frac{\partial c}{\partial y} + w\frac{\partial c}{\partial z} = D_x\frac{\partial^2 c}{\partial x^2} + D_y\frac{\partial^2 c}{\partial y^2} + D_z\frac{\partial^2 c}{\partial z^2} \qquad \text{Equation 2.23}$$

where D_x, D_y and D_z are the dispersion coefficients in the x, y and z directions respectively.

Generally, the ADE model, as initially derived by Taylor (1954), incorporates the effects of advection and dispersion, due to molecular and turbulent diffusion, and due to differential advection. Equation 2.23 is valid only under Fick's law, condition which is met in the equilibrium zone, where the variance of the concentration distribution is linear with distance.

Solution of the ADE Model

The frozen cloud approximation is commonly used as the solution to the ADE model, and suggests that advection dominates dispersion. This method divides the upstream profile into a number of discrete elements of a certain width, Δt. Each element acts as an individual injection source, while each of the individual elements' downstream profile is predicted using

Equation 2.24. The downstream individual distributions are added, producing the downstream concentration profile, as illustrated in Figure 17.

$$c(x_2,t)=\int_{\gamma=-\gamma}^{\gamma}\frac{c(x_1,\gamma)u}{\sqrt{4\pi D_x t_m}}\exp\left[-\frac{u^2(t_m-t+\gamma)^2}{4D_x t_m}\right]d\gamma \qquad \text{Equation 2.24}$$

where D_x is the longitudinal dispersion coefficient, as initially estimated by the method of moments; t_m is the travel time between the centroid of the two distributions; γ is an integration variable.

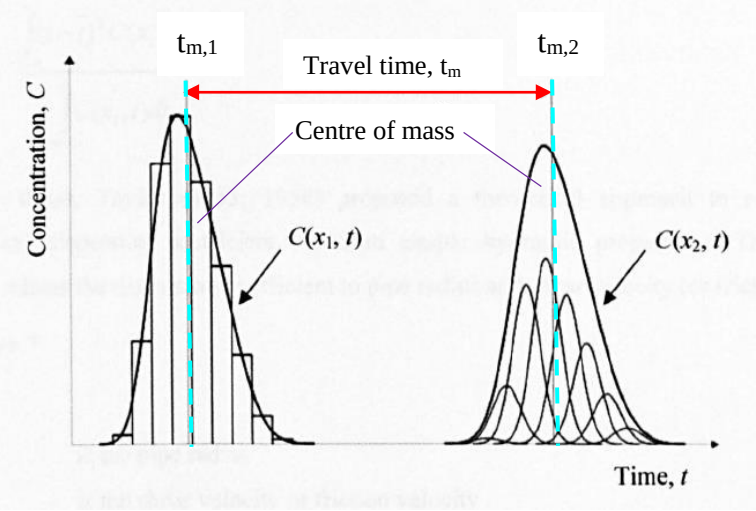

Figure 17: Sketch showing the ADE technique (Adapted from Lau, 2007).

2.4.5.3. Longitudinal Dispersion

According to Rutherford (1994) longitudinal dispersion is defined as the tendency of a solute to disperse along the stream's longitudinal axis. Longitudinal dispersion emerges due to vertical and transverse velocity shear that transfer the tracer/pollutant downstream more slowly close to the bed and banks than in the middle of the channel. Longitudinal mixing can be described as the spreading across an aqueous system of a temporally varying injection of pollutant after it has become cross-sectionally well mixed, and thus for temporally varying sources longitudinal mixing is significant in the far field zone. This applies mainly in sudden pollutants discharge cases. Longitudinal mixing modelling provides a means of accurate prediction of the decay rate of peak concentrations, and of the rate of a pollutant's spread (Rutherford, 1994).

Based on the temporal variance, longitudinal dispersion coefficient, D_x, is expressed by Equation 2.23, and can be calculated through moment analysis (see Section 2.4.1). Employing the concept of Taylor (1953), longitudinal dispersion can be characterised by Equation 2.25. D_x encompasses the effects of velocity shear and turbulent mixing.

$$\mathrm{D_x} = \frac{\mathrm{u}^2}{2}\frac{\mathrm{d}\sigma_t^2(\mathrm{x})}{\mathrm{dt}} \qquad \text{Equation 2.25}$$

The fact that D_x values tend to be high in large rivers (Rutherford, 1994), is mainly attributed to the depth of the river, inferring that in shallower systems D_x should obtain considerably lower values. There are several factors that may influence the D_x value, some of which are discussed in this section. Parameters affecting the degree of D_x in a river stream include flow, cross-sectional shape, plan-form curvature, water depth, bed material and slope, and roughness (Rutherford, 1994). Furthermore, recent research has shown that longitudinal dispersion overall decreases in the presence of vegetation, as discussed in Section 2.5 (Nepf et al, 1997; Shucksmith, 2008).

Firstly, D_x is anticipated to be low in narrow and deep streams, because in such conditions secondary currents are strong, increasing the transverse mixing coefficient, K_y rate. However, in shallow and wide streams velocity varies greatly transversely, hence the large velocity differences produce greater D_x values (Rutherford, 1994). Furthermore, it is reported that transverse velocity shear has a larger impact on D_x in natural channels compared to the vertical velocity shear (Rutherford, 1994).

D_x may vary significantly between purely natural channels (non-uniform shapes) and channels of regular cross-sectional shape (Rutherford, 1994; Guymer, 1998; Kashefipour & Falconer, 2002). An increase in channel curvature is expected to diminish the advective zone length (Rutherford, 1994). Guymer (1998) observed that for the same sinuosity along a river channel, the D_x of a natural channel displayed higher value (over 150%) compared to the corresponding D_x obtained in channels of regular cross-sectional shape. Consequently, D_x is analogous to the channel curvature. Another influencing factor on the D_x are the dead zones,

whose presence increase D_x due to the long trailing edges of the concentration-time distributions of slug injections (Rutherford, 1994).

Finally, the presence of vegetation provides additional resistance, resulting in lower velocities within the canopy, than the velocities over a bare bed. As a consequence, variation in the longitudinal dispersion is observed in vegetated flows, because vegetation alters the flow velocity field across several scales (details are provided in Section 2.5). It has been found that longitudinal dispersion diminishes in emergent vegetation (Nepf et al, 1997; Shucksmith et al, 2010), while in submerged vegetation a different mixing analogy occurs.

Estimation of D_x is key in quantifying the distribution of pollutant concentration for temporally changing pollutant sources. The fact that direct estimation of the D_x via in-situ tracer studies is a laborious, time consuming and fairly expensive procedure brought the need for expressing mathematically the mixing processes. However, the complexity of the various controlling hydraulic and geometric parameters in rivers (i.e. channel width, water stage, bed roughness, bed slope, stream sinuosity, mean velocity, shear velocity, water density and viscosity), and the different conditions prevailing in each stream or river, renders the application of one unique formula unreliable and inaccurate (Etemad-Shahidi & Taghipour, 2012). A historic route of the to-date D_x coefficient predicting formulae follows.

Historic route for longitudinal dispersion coefficient prediction

Over years several investigators have attempted to develop methodologies to predict D_x accounting for some of the easily measurable abovementioned parameters. For steady uniform flow, the 1D advection-dispersion equation (ADE), routing from Equation 2.23, is broadly used to predict the downstream concentration-time distribution profile in channels and rivers, given in Equation 2.26:

$$\frac{dc}{dt} + u\frac{dc}{dx} = D_x\frac{d^2c}{dx^2} + S_S \qquad \text{Equation 2.26}$$

Where: c= concentration; u= longitudinal velocity; D_x= longitudinal dispersion coefficient, x= direction of flow (longitudinal) and S_S= source term.

To obtain accurate results from the application of the 1D advection-dispersion model, proper D_x values need to be selected. When D_x is unknown, it can be evaluated through theoretical or empirical equations. Taylor (1954) set the foundations for estimating the longitudinal dispersion coefficient in a straight circular pipe of turbulent flow regime, and produced Equation 2.27 to predict it:

$$D=10.1*R*u^{*} \qquad \text{Equation 2.27}$$

where: R= pipe radius; u^{*} = bed shear velocity.

Elder (1959) developed Taylor's (1954) methodology for uniform flow in open channels of infinite width, deriving Equation 2.28:

$$D_x=5.93*h*u^{*} \qquad \text{Equation 2.28}$$

where: h= flow depth.

Further exploring Elder's (1959) work, Fischer (1967) demonstrated that Elder's theory is very likely to underestimate D_x, due to the fact that the transverse shear velocity profile is more significant than the vertical velocity profile variation. Therefore, Fischer (1967) used the lateral velocity profile in lieu of vertical velocity variations and produced the integral Equation 2.29:

$$D_x = -\frac{1}{A}\int_0^B h(y)u'(y)\int_0^y \frac{1}{\varepsilon_y h}\int_0^y h(y)u'(y)dydydy \qquad \text{Equation 2.29}$$

where: B= channel breadth; A=cross-sectional area; $h(y)$= local water stage; $u'(y)$= the variations of local average velocity from the cross-sectional average velocity; ε_y= local transverse turbulent diffusion coefficient.

However, the lack of information of a detailed transverse velocity profile and the complexities in the integral form of Equation 2.29, led Fischer (1975) to establish a simplified non-integral approximation of the triple integration, velocity variations and transverse turbulent diffusion coefficient, expressed by Equation 2.30:

$$D_x = 0.011\frac{B^2u^2}{hu^*} \qquad \text{Equation 2.30}$$

Liu (1977) applying Fischer's (1975) expression on river data, and taking into consideration the lateral velocity deviations, derived a longitudinal dispersion coefficient empirical formula, given in Equation 2.31:

$$D_x = \beta \frac{B^2 u^2}{h u^*} \qquad \text{Equation 2.31}$$

where β= function of the channel cross section shape and velocity spread over the stream, represented by Equation 2.32:

$$\beta = 0.18 \left(\frac{u^*}{u}\right)^{1.5} \qquad \text{Equation 2.32}$$

Likewise, Iwasa and Aya (1991) used lateral velocity gradient and implemented Fischer's (1975) equation, using laboratory and previous field records, and produced the empirical Equation 2.33:

$$\frac{D_x}{h u^*} = 2 \left(\frac{B}{h}\right)^2 \qquad \text{Equation 2.33}$$

Seo and Cheong (1998) employed dimensional analysis and regression method, deriving a formula for D_x prediction, as presented in Equation 2.34. The authors used data obtained from rivers in the USA.

$$\frac{D_x}{h u^*} = 5.915 \left(\frac{B}{h}\right)^{0.620} \left(\frac{u}{u^*}\right)^{1.428} \qquad \text{Equation 2.34}$$

Deng et al (2001) used the transverse mixing coefficient, K_y, and formed their formula to predict D_x as presented in Equation 2.35. However, that formula can only be applied in straight uniform streams with *B/h* ratio greater than 10.

$$\frac{D_x}{h u^*} = \frac{0.15}{8 \varepsilon_{r0}} \left(\frac{B}{h}\right)^{\frac{5}{3}} \left(\frac{u}{u^*}\right)^2 \qquad \text{Equation 2.35}$$

where ε_{r0}= transverse mixing coefficient which can be computed as in Equation 2.36:

$$\varepsilon_{r0} = 0.145 + \left(\frac{1}{3520}\right) \left(\frac{u}{u^*}\right) \left(\frac{B}{h}\right)^{1.38} \qquad \text{Equation 2.36}$$

Using field data sets from rivers in the USA, Kashefipour and Falconer (2002) developed Equation 2.37, which predicts D_x:

$$D_x = 10.612hu\left(\frac{u}{u^*}\right) \quad \text{Equation 2.37}$$

A comparison and appraisal of the various aforementioned equations was conducted by Ayyoubzahed (2004) utilising collected river data. The river parameters involved: flow velocity, flow depth, river width and longitudinal dispersion coefficient. The equations were appraised deploying statistical measures, such as discrepancy ratio, λ_d, root mean square, *RMS*, and mean absolute error, *MAE*, as listed in Equation 2.38, Equation 2.39 and Equation 2.40 respectively:

$$\lambda_d = log\frac{D_P}{D_m} \quad \text{Equation 2.38}$$

$$RMS = \frac{1}{N_d}\sqrt{\sum_{i=1}^{N_d}\left(D_p - D_m\right)_i^2} \quad \text{Equation 2.39}$$

$$MAE = \frac{1}{N_d}\sum\left|\left(D_p - D_m\right)_i\right| \quad \text{Equation 2.40}$$

Where D_p and D_m are the predicted and measured longitudinal dispersion coefficients respectively; N_d = number of data.

Overall, that evaluation showed that Equation 2.35 exhibits the greatest regression coefficient value, and the least MAE compared to the other above mentioned equations. This indicates that Deng et al's (2001) method is likely to produce the best results in predicting D_x. Furthermore, it was found that the formulas of Elder (1959), and Kashefipour and Falconer (2002) underestimate the D_x, whereas the equations of Fischer (1975), Seo and Cheong (1998), and Deng et al (2001) overvalue the actual D_x, relying upon the selected values of width to depth ratio (Ayyoubzahed, 2004). Furthermore, Ayyoubzahed (2004) proceeded to sensitivity analysis of the four involved parameters (as mentioned previously), and, interestingly, found that D_x is initially influenced by the flow velocity, with channel width coming second in importance.

Etemad-Shahidi and Taghipour (2012) derived Equation 2.41 and Equation 2.42 relying on the width to depth ratio to predict D_x in streams, as follows:

For B/h<=30.6:

$$\left(\frac{D_x}{hu^*}\right) = 2.75\left(\frac{B}{h}\right)^{0.78}\left(\frac{u}{u^*}\right)^{0.11}(\sigma_s)^{4.04} \qquad \text{Equation 2.41}$$

For B/h>30.6:

$$\left(\frac{D_x}{hu^*}\right) = 8.36\left(\frac{B}{h}\right)^{0.61}\left(\frac{u}{u^*}\right)^{0.85}(\sigma_s)^{1.70} \qquad \text{Equation 2.42}$$

in which σ_s= sinuosity of stream.

However, that method does not have the capacity to account for parameters, such as dead zones, vegetation and hydraulic control structures. Nevertheless, it incorporates a wider range of geometric and hydraulic parameters than the previously mentioned models, including: fluid viscosity and density, channel width and depth, flow velocity and shear velocity, slope, roughness, bed shape and sinuosity. Evaluation of the results of that model was conducted comparing to other formulas, such as Ayyoubzahed's (2004). According to those comparisons, the least satisfactory formulae were Elder's (1959), followed by Fischer's (1975), implying the significance of the transverse variation aspect. It was demonstrated that Liu (1977), Seo and Cheong (1998) and Deng et al (2001) overestimate the predicted D_x. Etemad-Shahidi's and Taghipour's (2012) results are generally in accordance with Ayyoubzahed's (2004) results.

Another model that predicts D_x is the aggregated dead zone model (ADZ). The ADZ model was introduced by Beer & Young (1983) and assumes that within each reach (cell), the solute experiences PF followed by a single mixing tank that represents the total effects of all the dead zones taking place in the system. Therefore, the ADZ model undergoes advection with no dispersion, which is then followed by dispersion without advection. The ADZ model equation describing advection and dispersion derives from the advection diffusion Equation 2.43, and is expressed by a set of conjugated equations as set by Beer and Young (1983):

$$\frac{\partial c}{\partial t} + u\frac{\partial c}{\partial x} = D_x\frac{\partial^2 c}{\partial x^2} + K\Gamma_c(s - c)$$ Equation 2.43

which describes the dispersion within the main flow, and where u is the flow velocity in the longitudinal direction; D_x is the dispersion coefficient; K is a mass exchange coefficient between the main flow and the dead zone; Γ_c is the ratio of the common boundary region between the main flow and the dead zone to the main flow volume; c and s are the tracer concentration entering and departing the dead zone respectively, and Equation 2.44:

$$\frac{\partial s}{\partial t} = K\Gamma_s(c - s)$$ Equation 2.44

which refers to the retention of a tracer within the dead zone and where Γ_s is the ratio of the common boundary region to the dead zone volume.

From the above set of equations, it is apparent that if there were no Fickian dispersion coefficient (D = 0 m/s^2), the process of dispersion would still exist owing to tracer retention within the dead zone.

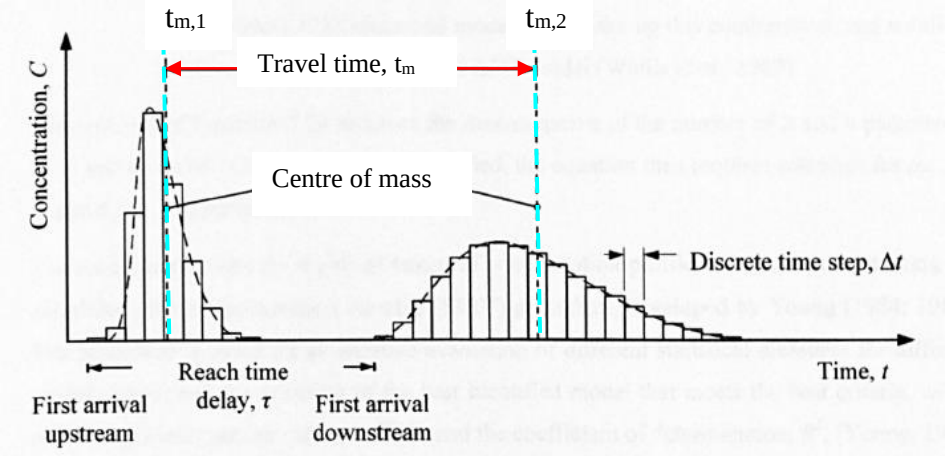

Figure 18: ADZ prediction technique (Adapted from Lau, 2007).

Wallis et al (1989) produced a discrete-time equation to predict the temporal concentration distribution at a downstream location for a single mixing reach/cell, given in Equation 2.45:

$$c(x_2, t) = -a_p c(x_2, t-1) + (1 + a_p)c(x_1, t - \delta)$$ Equation 2.45

where:

$c(x_i,t)$	is the tracer concentration at the longitudinal location x_i at time t, for i equal to 1 or 2 referring to up-/downstream sites respectively
α_p	equals $-e^{\frac{-\Delta t}{T}}$
T	equals $t_m - \tau$, and refers to the residence time
τ	equals $t_2' - t_1'$, and refers to the time delay
$t_m = t_{m,2} - t_{m,1}$	refers to the travel time
Δt	is the time step
δ	is the discrete-time corresponding to the time delay $\tau/\Delta t$

Young and Wallis (1986) determined the dispersive factor as the ratio of the dead zone volume to the total reach volume, described by Equation 2.46:

$$D_f = \frac{T}{t} \qquad \text{Equation 2.46}$$

D_f varies for different channels, but receives invariably lower values in smooth engineered channels compared to irregular natural channels (Rutherford, 1994).

2.5. Role of Vegetation in Hydraulics

Fundamental mixing and hydraulic principles and processes in open channels were described in the previous section. However, discussion about the hydrodynamics of a system will not be comprehensive, unless vegetation, as a physical flow obstruction, is involved. As discussed in Section 2.3.3, wetland vegetation rules the associated interchanges of sediments and contaminants via plant uptake and transformation processes, and influences the hydrodynamics (Kadlec, 1995; Nepf, 1999).

The non-ideal flow regime, described in sub-section 2.4.2, is partially influenced by the presence of vegetation. Vegetated flows affect the flow velocity and mixing in all three dimensions (Kadlec, 1990; Nepf, 1999) and produce stem drag forces (Jadhav & Buchberger, 1995). Firstly, water entering a canopy is forced to transport around each stem, thereby

generating spatially heterogeneous velocity field at the stem scale (Nepf et al, 2007). Vegetation drag has a proportional effect on the water stage, and thus on the HRT, which in turn influences the overall hydraulic and treatment efficiency of the system (Kadlec, 1990; Jadhav & Buchberger, 1995). Stem drag forces promote flow resistance and tend to reduce the mean water velocity (Kadlec, 1990). Stem drag implications are mainly pronounced in shallow planted channels, such as wetlands. Shaffranek et al (2003) monitored the implications of the rapid plant change on the surface water flow conditions in a wetland that was burnt in fire. The authors remarked increased flow velocities at the upper water layer due to reduced shear plant effects, and observed that resistance force was exerted at the lower water layer where stems remained. Therefore, stem drag force profoundly alters the physical flow characteristics within the water column.

Kadlec (1995) reported the inadequacy of Manning's equation to fully describe the wetland internal flow processes. The reason is that Manning's equation was formed for completely turbulent flow regimes in open channels, adapting for bed roughness. However, turbulent flow is not frequently the case in wetlands, due to insufficient slopes and low water depths to generate such velocities. Therefore, Manning's coefficient varies in wetlands and does not receive a unique value, as it depends on the local water depth and on vegetation density (Kadlec, 1990). Kadlec (1990) concluded in a more suitable friction rule that accounts for water depth and friction slope, underpinning the insufficiency of Manning's formula application in vegetated flows. This is explained by the fact that in open channel flows the bottom (bed) drag dominates, while in vegetated flows vegetation drag rules. This is further supported by Nepf (1999), stating that bed shear becomes less important in vegetated regions, where even sparse emergent vegetation presence produces stem wake turbulence that is often greater than the bed shear.

It is seen that vegetated flows introduce greater friction factors and different rules from those in non-vegetated open channel flows (Kadlec, 1990). Furthermore, the natural plant development (growth and dormant) plays an important role in altering the resistance, even by an order of magnitude, providing maximum values at the maturity of growing cycle, as reported by Shih and Rahi (1982). As being the main research question of this thesis, it is

noteworthy that natural seasonal plant variation is also expected to play an important role in altering the flow resistance, flow characteristics, and mixing in vegetated flows.

Jadhav & Buchberger (1995) scrutinised the effects that the aspect ratio, A_R, and plant population density, N_t, of a wetland may have on the HRT, an unaddressed subject until that time. The authors included stem drag force and observed volumetric displacement effects of the dense emergent vegetation case. Conclusions drawn included: i) increased N_t increases the HRT for fixed flow rate, Q; ii) increase in Q reduces the HRT for fixed N_t; iii) as stem density increases HRT comes to be less sensitive to Q; iv) HRT increases with A_R for constant Q, surface area and N_t; v) HRT becomes more sensitive to the A_R with N_t. The above findings provide useful initial insights to understand the basic flow and mixing processes in vegetated flows.

The mixing processes taking place in aquatic systems include diffusion (either molecular or turbulent) and shear dispersion (see Sections 2.4.5). In vegetated flows, an additional process emerges, known as mechanical dispersion, due to the physical obstruction that the plant stems involve (Nepf et al, 1997). To conceptualise this, a schematic is shown in Figure 19, where two fluid particles, A and B, starting concurrently, may journey different tortuous trails through the pore medium spaces, and traverse the same longitudinal distance, L_x, but ultimately evacuate the unit at different times and at different longitudinal locations.

The net diffusion within emergent vegetation is expressed by two components; the turbulent and the mechanical diffusion (Nepf, 1999). These two processes are independent and contribute additively to the final total net diffusion. According to Nepf (1999), turbulent diffusion decreases within a vegetated region, because eddies tend to decrease within emergent plants. Compared to non-vegetated channels, total diffusion is reduced in emergent vegetated flows. Nepf et al (1997) investigated the effects of vegetation on the longitudinal dispersion process and found that: i) as flow speed and stem population density, N_t, rise, mechanical dispersion is enhanced; ii) turbulence intensity grows with N_t, entailing elevated vertical diffusion; iii) elevated vertical diffusion diminishes shear-flow dispersion. Therefore, reduced longitudinal dispersion is anticipated in densely planted systems

compared to open water estuaries. Nepf (1999) observed that the diffusion values obtained were greater than those calculated through turbulent diffusion itself; consequently, the author attributed the increase in total diffusion, by introducing the term of mechanical diffusion.

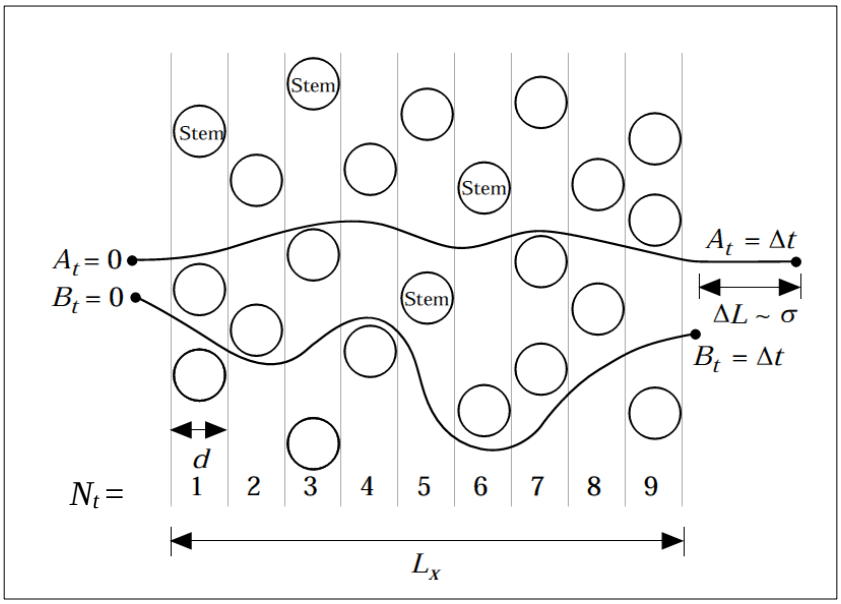

Figure 19: Mechanical dispersion process. Fluid particles A and B start concurrently, but due to plant stems obstacles they take different routes through the pore medium and terminate in different locations longitudinally, spending different times to traverse the stand (Adapted from Nepf et al, 1997).

The longitudinal dispersion amount is directly related to the canopy morphology (Lightbody & Nepf, 2006). Longitudinal dispersion coefficient, D_x, is a function of different factors in emergent and in submerged plant conditions. Furthermore, the particular morphology and physical characteristics of each macrophyte species influence differently the D_x. Lightbody & Nepf (2006) compared the levels of dispersion for three different emergent plants, and observed that different plant morphologies and physical characteristics (e.g. plant frontal area and drag coefficient) induce different shear dispersion levels.

Beyond the canopy morphology, furthermore, the flow field and the levels of turbulence are different in submerged and in emergent canopies. Within emergent macrophytes flow is controlled by the distribution of the canopy frontal area, and turbulence is affected by the stem diameter and spacing, while in submerged macrophytes the stem density rules the

mixing and turbulence (Nepf, 2012). Shucksmith (2008) investigated the influence of emergent and submerged macrophytes on mixing taking into consideration the seasonal plant variation. The author found that for emergent macrophytes longitudinal dispersion was a function of plant age and water depth, while in submerged conditions longitudinal dispersion was dependent upon the degree of submergence, where the depth of submergence is defined as the ratio of water flow depth, *h*, to macrophyte height, *H*.

To date, the majority of the experimental studies investigating the impact of macrophytes have employed artificial (dowel or synthetic) plants instead of natural plants, which overall omits the contribution of the flexibility and development of natural plants in the wetland hydrodynamics. Shucksmith (2008) noticed that in emergent conditions, plant development retarded the flow, and that longitudinal dispersion decreased with plant age, thus with increase in stem density. Additionally, the author observed that a decrease in the water flow depth, caused a reduction in the longitudinal dispersion in all plant ages.

In submerged dense macrophyte conditions, flow is segregated into distinct zones, as depicted in Figure 20. Discontinuity in drag creates differential vertical velocities, and the creation of a shear layer at the top of the canopy. In a free shear layer, coherent eddies are generated continuously downstream, but in a canopy shear layer the vortices reach a constant scale and a steady penetration length, δ_e, into the canopy (Nepf et al, 2007). δ_e separates the submerged canopy into a top layer of fast renewal action and into a lower layer of slow renewal. δ_e is independent of the flow speed, and is a function of the canopy morphology. The top layer of the submerged canopy is denoted as *exchange zone*, because in that region shear scale turbulence creates rapid exchange with the overflow layer, and substantially controls the transport between the two adjacent layers. The bottom layer is called the *wake zone*, and experiences only small-scale turbulence in the stem wakes, involving thereby diminished solute transport. Laboratory and field studies have shown that turbulent diffusion in the wake zone is a function of the local velocity and of the stem density, N_t (Nepf et al, 2007).

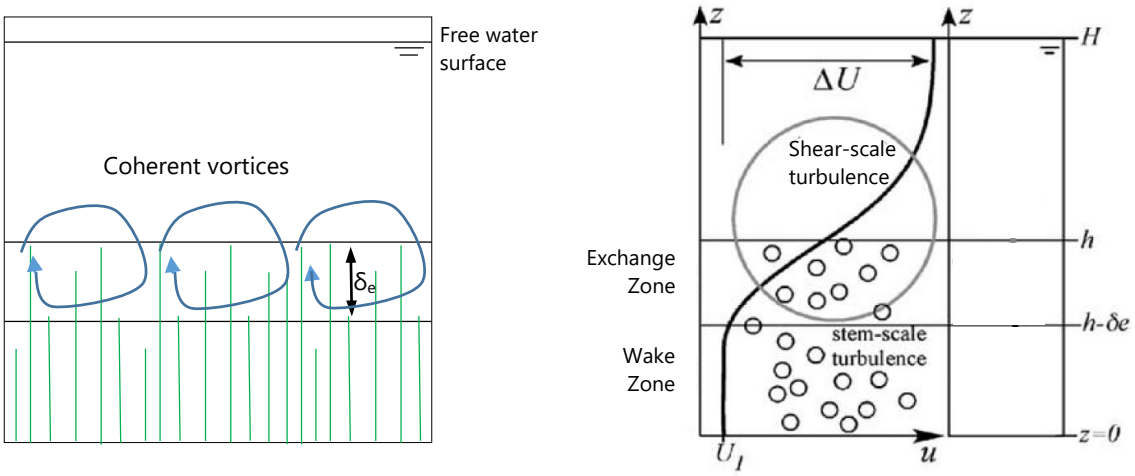

Figure 20: (Left) Flow structure in densely submerged vegetated flow showing shear layer generation and coherent vortices due to the drag discontinuity at the canopy top (z=h), and the penetration length, δ_e, of the shear-scale turbulence. (Right) Velocity profile in and above the submerged canopy. Length of δ_e segregates the canopy into two regions. The exchange zone occurring at the upper layer of the submerged canopy facilitates swift exchange with the overflow layer and produces shear scale turbulence. The wake zone at the bottom layer is governed by stem scale turbulence (Adapted from Nepf et al, 1997).

Concerning the exchange zone, it was found that as the canopy drag increases, δ_e decreases. Therefore, the canopy drag governs the penetration length of the canopy scale eddies. The canopy drag, C_DHa, consists of the canopy drag coefficient, C_D; the height of the canopy-macrophyte, H; and the frontal area per canopy volume, namely the canopy density, α, expressed as $\alpha = d_m/\Delta S^2 = N_t d_m$, where d_m is the stem diameter and ΔS is the average spacing between the elements, i.e. stems (Nepf, 2012). The drag coefficient, C_D, is a function of the canopy density, α; the stem Reynolds number, $NR^* = ud_m/v$ (where u is the mean velocity and v is the kinematic viscosity); and the canopy morphology. Tanino & Nepf (2008) observed that C_D is largest at lower NR^* and at high stem population densities.

Reynolds number, *Re*, expresses the turbulence degree in the water. Due to the turbulence generation at stem wake scale, Nepf & Vivoni (2000) proposed that NR^* is a more appropriate way to determine Reynolds number in vegetated flows. Very sparse submerged canopies (i.e. $Ha << 0.1$) do not produce shear layer eddies, because the canopy drag is small compared to the bed drag, while in denser submerged canopies discontinuity in drag produces shear and coherent vortices, and thus δ_e varies according to the stem density, as illustrated in Figure 21. For very dense stems ($Ha > 0.1$) eddies are created at the upper layer

of the canopy, whereas for stem density close to the transitional region (Hα≈0.1), the vortices occur for a longer penetration length due to the lower canopy drag (Nepf, 2012).

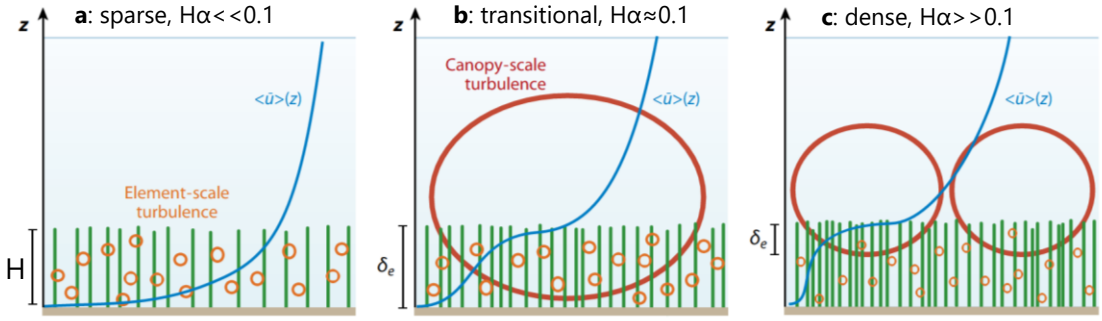

Figure 21: (a) Sparse canopy. Vegetation drag is small against bed drag and stem turbulence prevails; (b) Transitional canopy. Vegetation drag is large enough to create shear layer at the canopy top. Stem density allows longer penetration length and canopy eddies; (c) Dense canopy. Vegetation density is quite high decreasing thereby the penetration length and identifying distinct scales of turbulence, canopy scale (top zone) and stem scale (bottom zone). H is the submerged canopy height. (Adapted from Nepf, 2012).

Another dispersive process in vegetated flows is the regions of dead zones generated by the back flow area within the plant stem wake (Nepf et al, 1997). Dead zones exhibit substantially low longitudinal velocities and produce ineffective utilisation of the entire water volume. Particularly, in the case of vegetated dead zones, it has been observed that the capture and lag of some fraction of the solute, promotes longitudinal dispersion and generates long tails on the concentration-time curves of impulse injections (Rutherford, 1994), as already discussed in Section 2.4.5.

From the above, it is understood that in vegetated flows there is drag creation, which retards velocity, thus pollutant advection, and which ultimately enhances the biochemical degradation process by extending contact time on biofilm surfaces. In addition to this, plant porosity, η, heterogeneities in the canopy morphology and wetland boundaries, affect the mixing processes, especially by introducing turbulence. Assuming that the stem diameter, d_m, is constant with height, the solid volume fraction, Φ, of the plants can be estimated as $\Phi=N_t\pi d_m^2/4$, and thus porosity is estimated as $\eta=1-\Phi$. It has to be noted that so far vegetated flows have been addressed as two-dimensional problems (Nepf, 2004; Nepf & Vivoni, 2004).

A relationship between the stem Reynolds number, *NR**, and vegetative drag is observed. Nepf et al (1997) advised that the size of the stem turbulent wakes produced/formed behind the stems, hinges upon the *NR** of the flow. As such, if mechanical dispersion has a great effect on the longitudinal dispersion, then a relationship between the D_x and the *NR** should be anticipated. Furthermore, Chyan et al (2014) found that the actual hydraulic efficiency, $\lambda_m = t_p/t_m$, is highly correlated to the *NR**.

2.6. Conclusions

Hydraulic residence time (HRT), dispersion and short-circuiting in constructed wetlands (CWs) have been under investigation by many researchers. Nevertheless, to-date research has mostly focused on wastewater pollutant treatment capacity of CWs and ponds, and thus there is need of further studies documenting the potential of CWs to remove satisfactorily a wider range of pollutants, deriving from agricultural runoff, i.e. agrochemicals. Furthermore, regarding CW hydraulics, there is only few information about the investigation and evaluation of hydraulic performance in full-scale wetlands, since previous work concentrated mainly on computer simulations of hypothetical cases of ideal shapes, or laboratory small-scale units of idealised conditions. Therefore, investigating empirical data for various irregular pond/wetland shapes and evaluating their physical flow characteristics and hydraulic performance parameters (fast flow paths, dead water regions, hydraulic efficiency, effective volume) will provide vital information to ecologists and engineers for improvement and remedial actions that can be implemented in the current natural and constructed wetlands.

In addition to this, to-date research on wetland hydrodynamics presents several gaps in understanding the seasonal plant variation effects on flow field, on hydraulic performance parameters and on mixing characteristics. The majority of to-date research on understanding and improving the hydrodynamics of aqueous systems has been mainly conducted in non-vegetated or marginal vegetated ponds, while there are few studies investigating hydrodynamics in the presence of vegetation, in non-ideal shapes, and in full-size units.

Furthermore, particularly in emergent plant conditions, the impact of seasonal vegetation variation on HRT and on mixing characteristics has not been fully investigated. Beyond some indoors laboratory research, there is little knowledge and data acquired about the seasonal effects of emergent vegetation on longitudinal mixing, flow field, and hydraulic performance, while there is no long-term monitoring research published. This will be of potential use for the relevant stakeholders, because there is lack of information about the variation of D_x in different seasons, and will provide an understanding of the impact of flow variations and ageing of emergent plants on the seasonal hydraulic and treatment performance of CWs.

2.7. Research Proposal

The importance of investigating the hydraulic performance and physical flow properties of CWs raises from their interrelation with treatment performance. Sole water or soil sampling to examine the pollutant concentration at in-/outlet does not suffice, unless the hydrodynamics (physics of flow, mixing processes and hydraulics) are viewed. Proper hydraulic design nurtures appropriate conditions to achieve longer HRT, and thus better treatment, greater pollutant concentration mitigation (i.e. through dilution), and enhancement of other transport and removal processes.

Investigation of physical flow characteristics and of various hydraulic parameters of open channel aqueous systems, such as ponds and wetlands, has been conducted by several researchers. Among other factors, aquatic vegetation plays a great role in the hydrodynamics of open channels and of vegetated flows. Despite the amount of research conducted on this subject, there is little information about the seasonal effects of vegetation on the mixing characteristics in emergent vegetated flows, on the physical flow characteristics, and on various hydraulic performance parameters, in full-scale non-ideal shaped wetlands, planted with real emergent vegetation.

Leading studies conducted by Min & Wise (2009), Kjellin et al (2007), Persson et al (1999), Somes et al (1998), Nepf (1999), Stovin et al (2008), German et al (2005), Su et al (2009) and

Shucksmith (2008), draw several suggestions and shortfalls for future research in the field of pollution mixing and transport in emergent vegetated aquatic habitats:

1. Hydraulic residence time (HRT) is intrinsically connected with the treatment efficiency of a unit, and is influenced by the aspect ratio, the flow rate and the stem population density (Jadhav & Buchberger, 1995). It is reported that seasonal plant variations play significant roles in altering the stem resistance and drag even by an order of magnitude upwards during the maturity of growth cycle (Shih & Rahi, 1982). However, the seasonal plant variation effect has not been fully assessed on the impact it has on the HRT and mixing characteristics over a range of flow rates and over different seasons in full-scale units planted with emergent plants. It is also reported that vegetation heterogeneity (uneven stem spacing, different plant species) induces variance in the water detention time (Wörman & Kronnäs, 2005). Therefore, variation in vegetation is anticipated to affect the residence time due to the stem and overall canopy seasonal variations. Thus, monitoring of the seasonal plant variation, including the full dormant season, would elucidate transport and mixing processes essential to be known for the operational stage of treatment units.

2. Hydraulic efficiency, λ, provides a comparable measure among different systems. Effects of vegetation hydrodynamics on the system's λ, measured on the actual site, in full-size ponds and wetlands, have not yet been fully investigated. Somes et al (1998) examined a case of a pond with marginal vegetation, followed by simulated cases; Koskiaho (2003) examined the flow pattern and retention time in two engineered partly vegetated wetlands-ponds; while the majority of researchers (reviewed in this literature) have examined the main factors affecting λ omitting vegetation, and mainly via computer simulations, with fewer studies conducted in the laboratory, mainly in ideal system shapes, i.e. rectangular wetlands, (Persson, 2000; German et al, 2005; Su et al, 2009; Aguwamba, 2006). Furthermore, Su et al (2009) provided a useful guidance on constructed wetland design, prioritizing the factors affecting hydraulic efficiency, albeit overlooking vegetation as well. Koskiaho (2003) quantified λ for two constructed wetlands-ponds of contrasting shapes and deduced that the impact of location and

breadth of inlet is milder in rectangular-wise aquatic systems than in more squared layouts. From the above review, it is inferred that there remains little information about the effects of vegetation (including ageing) on the mixing and flow characteristics and on the hydraulic performance, also combined with the effects of flow rate variation. Evidently, there are few field, full-scale cases investigating the hydraulic efficiency and hydrodynamics in non-idealised conditions, such as irregular system shape, non-uniform bed topography, plant age and heterogeneity.

3. Short-circuiting is a feature that significantly reduces the water quality capacity in wetlands. Factors that affect short-circuiting have been scrutinized both in closed pipes and open channels. The main factors influencing short-circuiting include: length to width ratio (shape of system); flow rate (or water depth); bottom topography; internal structures/baffles, such as islands and berms; hydraulic structures; plant type and heterogeneity (Min & Wise, 2009). Nevertheless, the vast majority of the researchers have examined the short-circuiting phenomenon in the absence of vegetation (Ta & Brignal, 1998; Persson, 2000; Stovin et al, 2008; Aguwamba, 2006). Min & Wise (2009) simulated the impact of vegetation and bed topography on the short-circuiting and found that bed topography has larger effects on short-circuiting than vegetation. However, in a dynamic system, vegetation characteristics (stem diameter, density, resistance, and frontal area) vary with time and vegetation is frequently heterogeneous, aspects that were not considered in the simulations conducted by Min & Wise (2009). As mitigation and reduction of the short-circuiting is chief to enhancing wetland performance, field research on full-size units will shed light in understanding which parameters have more influential role into the short-circuiting, and will provide useful insights about how to moderate it, and how to achieve an optimal CW design.

4. Constructed wetlands constitute a means of dissipating storm water events and attenuating floods; thus, they are able to reduce the peak concentration of sudden pollutant releases. Although ample research has been conducted on the effects of emergent vegetation on various mixing scales, the majority of research has employed artificial vegetation. Shucksmith (2008) investigated the effects of seasonal vegetation

variation on the longitudinal mixing in controlled laboratory conditions between velocities of 5 and 20 cm/s. The author produced correlations between longitudinal dispersion and plant age, and between longitudinal dispersion coefficient and water depth, however, that study managed to monitor only the growth stages of planted reeds, failing to examine the dormant season. Other researchers have investigated plant features and characterized conditions in natural planted environments on the actual site (Nepf, 1999; Lightbody & Nepf, 2006; Nepf et al, 2007; Nepf, 2012a; Nepf, 2012b), but seasonal plant variation was neglected.

Consequently, the aims of this project will address the deficits mentioned above, conducting experiments in full-scale constructed wetlands with fully emergent macrophytes, where:

a) Varied flow rate range from dry weather to storm flow conditions in different seasons, thus different plant ages will be monitored.

b) Mixing characteristics and physics of flow will be investigated conducting pulse and repeatable tracer tests. The potential of storm water peak concentration attenuation will be observed.

c) Various full-scale aqueous systems will be monitored for their physics and hydraulic behaviour. A relative evaluation between the systems will attempt to add knowledge to the current good practices to improve internal hydraulics and treatment efficiency.

The proposed research intends to improve the understanding of wetland treatment units and storm water reservoirs by highlighting the effects of seasonal plant variation and flow rate influence on hydraulic performance, mixing characteristics and physics of flow, and thus on treatment performance. Moreover, poorly understood processes will be explained using the obtained data sets of HRT time, hydraulic performance and mixing regarding natural vegetation in non-uniform (non-ideal) wetland geometries. Furthermore, investigation of the effects of various design parameters (e.g. outlet configuration, internal features, inflow conditions) of various different shape and size full-scale treatment units on hydrodynamics and mixing characteristics, will provide vital information about the current knowledge of design guides' optimisation. Results of this research are going to inform water quality

modellers, environmentalists, regulators, farming community, environmental engineers, designers and constructors of wetlands about the design and optimisation of wetlands, about the size of wetlands to achieve sufficient peak concentration mitigation, and will provide a mixing coefficients database for future use.

3. Methodology

3.1. Introduction

This chapter describes the techniques employed to collect and process the data in two full-scale wetlands, in order to quantify the mixing in emergent vegetation and to monitor the seasonal vegetation variation effect on mixing characteristics and flow pattern. Section 3.1 provides an overview of the experimental set-up, Section 3.2 details the vegetation characteristics, while Section 3.3 the experimental operations to measure the flow in the constructed wetlands (CWs). Sections 3.4 to 3.7 describe the solute tracing experimental methodology, the automated tracer injection system developed, the longitudinal mixing measurements at the in-/outlet and data analysis, and the internal measurements within the CW respectively. Finally, Section 3.8 summarises the experimental test conditions.

The activities and field experiments were conducted outdoors in two full-scale CWs between November 2015 and June 2016. The scope of this study was to investigate the effects of flow rate variation and the effects of seasonal vegetation variation on mixing characteristics and on flow structure in full-size CWs. Furthermore, the work intended to show the potential influence of discharge variation and seasonal plant variation on hydraulic performance parameters. In order to achieve continuous tracing tests on the actual site, and to monitor the natural growth and ageing of vegetation in different seasons, an intelligent automated tracer injection system was developed and installed on site. As such, repeatable tracer tests were achieved in dry weather and in storm conditions during different plant seasons.

The two study sites were two CWs in-series, connected via a stream. The CWs belong into a farm, which receives agricultural runoff pollutants. The two CWs, named as south wetland 1 (SW1) and south wetland 2 (SW2), are of similar size and design by construction. The hydrological regime is common in both wetlands. Flow derives from the surrounding fields' drainage system, and is seasonal, depending on the rainfall. Flow is continuous during rainy and winter months, and flow rate varies. During drier months, and particularly in summer

months, flow nearly ceases, as the phreatic layer drops in the water table. SW1 and SW2 are connected through a 115 m stream.

Quantification of the spatial variations in longitudinal and transverse directions were achieved employing Rhodamine WT dye tracing. As discussed in Chapter 2, dye tracing is commonly implemented to characterise the hydrodynamic characteristics in aqueous systems and in vegetated flows. One plant type, i.e. Phragmites australis, was investigated under the natural evolution between the live (growth) and withered plant months, contrasting the real vegetation at the extremes of the annual plant cycle in this UK micro-climate. Furthermore, a range of flow rates were tested, as far as rainfall profile permitted, in order to cover the maximum span between extreme flow conditions, namely dry weather flow (DWF) and storm flow conditions. The current methodology and findings can apply to any CW or pond, treating any effluent type.

3.2. Experimental Setup for Field Study

The experimental test programme was conducted on two on-line and in-series, free-water surface (FWS) CWs, in Knapwell, Cambridgeshire, UK (National Grid Reference: TL 333625 62549). This is a protected farmland by the RSPB (Royal Society for the Protection of Birds) in Knapwell, shown in Figure 22. The initial purpose of the CWs construction in 2005 was to provide open water throughout the year for birds' habitat and activities. This is still one of the pivotal purposes, but, additionally, water preservation has become a driver because surface agricultural runoff poses a means of diffuse pollution (detailed in Chapter 2). Hence, the potential of the current CWs to treat agricultural runoff from the surrounding fields, has become an additional goal for the RSPB organisation. The relative locations of the two in-series south wetlands (SW1 and SW2) are indicated in Figure 23. Furthermore, Figure 23 shows a third CW, the north wetland (NW), located at the north part of the RSPB Farm, results of which are presented in Chapter 6. NW is on a separate hydrological regime.

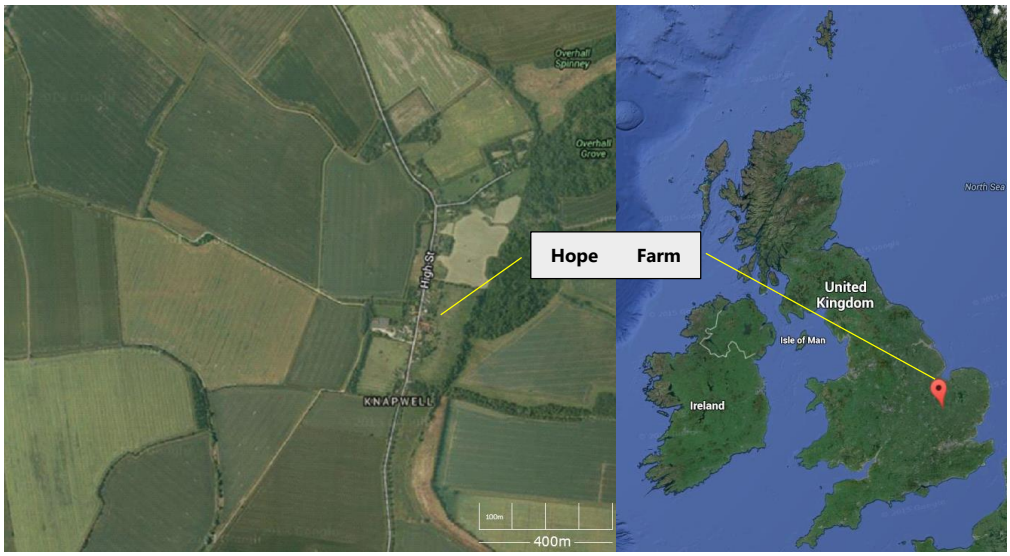

Figure 22: Location of Hope Farm, Knapwell, Cambridgeshire (Source: Google Maps).

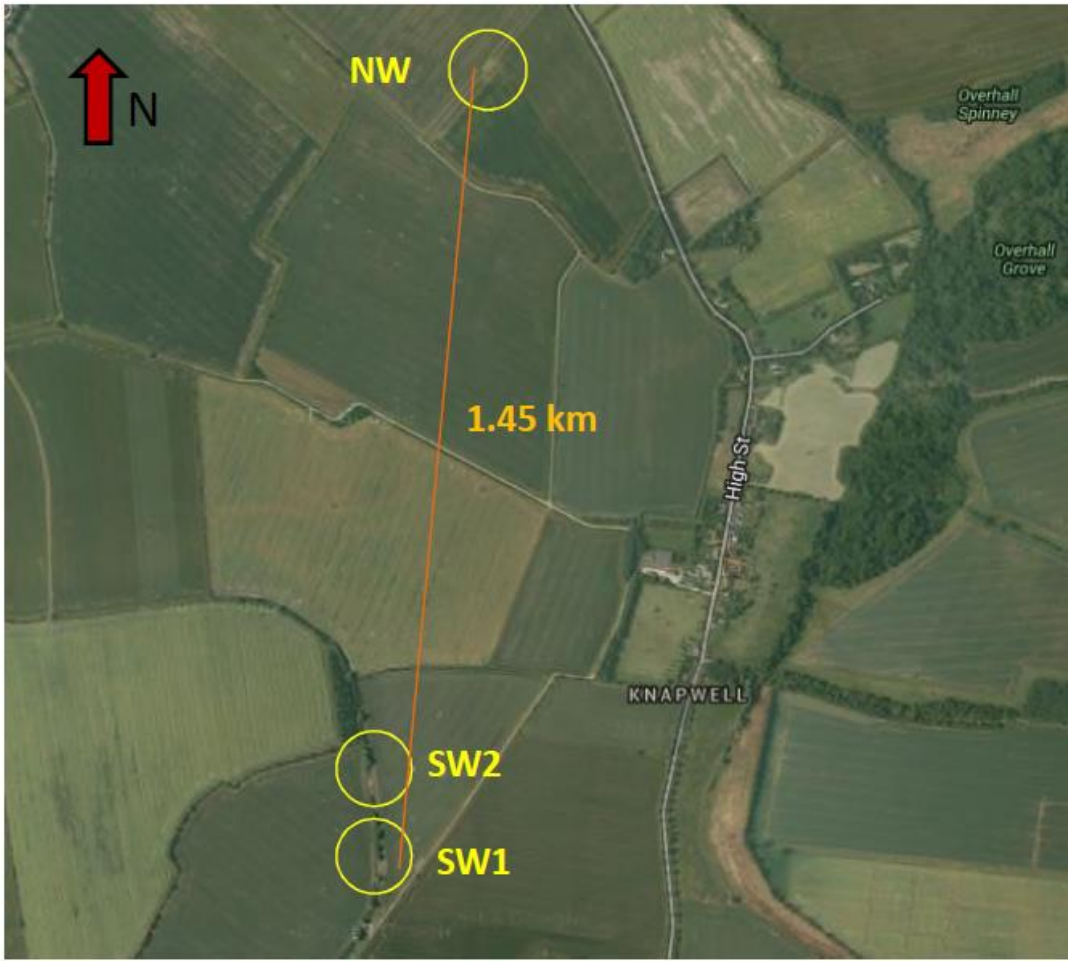

Figure 23: Relative location of the CWs in the Hope Farm. SW1 and SW2 are located at the southern part of the farm, whilst NW at the northern part of the farm (Source: Google Maps).

3.2.1. Overview of Experimental Facility

A schematic overview of the south wetlands (SWs) is shown in Figure 24, indicating the key monitoring points, hydraulic structures and vegetation boundaries. SWs are in-series and connected through a stream of approximately 115 m length, thus creating three individual systems: SW1, Stream, and SW2. SWs are of irregular shape, and are unbunded (non-walled) at the outlet. By construction, SWs were dammed at the outlet, however, during heavy storm flows, the dams were damaged and removed. The lack of a bunded outlet results in shallow, flow-through, and short retention systems, especially during high storm flow conditions. Moreover, Figure 24 indicates the special points, i.e. hydraulic control structures, and tracer injection points. Figure 24 illustrates the average (cyan coloured area), and maximum (blue colour line) water levels. Furthermore, Figure 25 shows the bathymetry in each wetland, indicating the cross-section locations, presented in Section 3.2.1.1 (see Figure 26 and Figure 27).

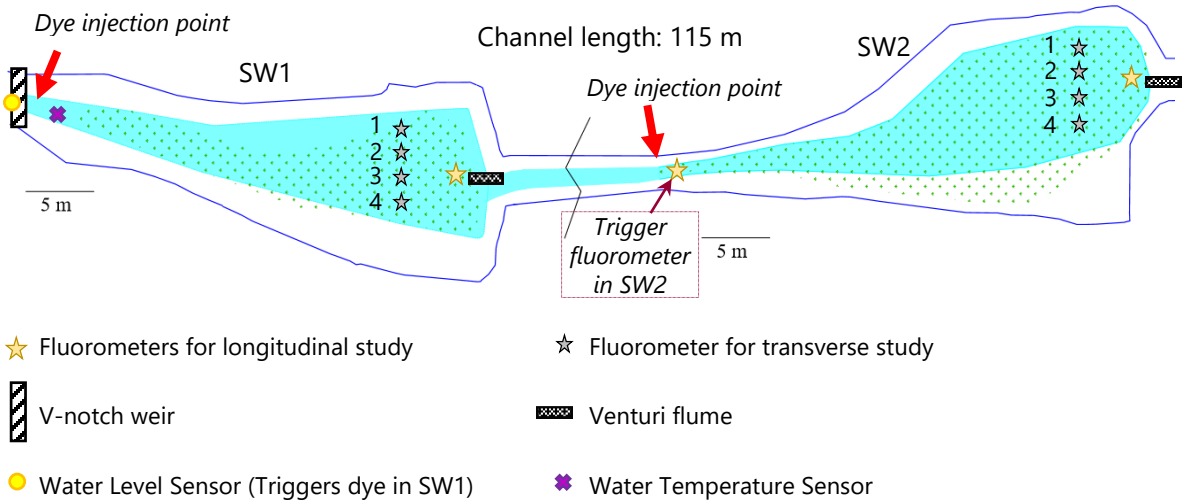

Figure 24: Schematic overview of the south wetlands indicating bathymetry, vegetated area (i.e. Phragmites boundaries), and monitoring locations for the tracing study (i.e. locations of dye injection, of fluorometers for the longitudinal and transverse mixing studies, of V-notch weir and Venturi flumes, of water level and water temperature sensors.

D E F G

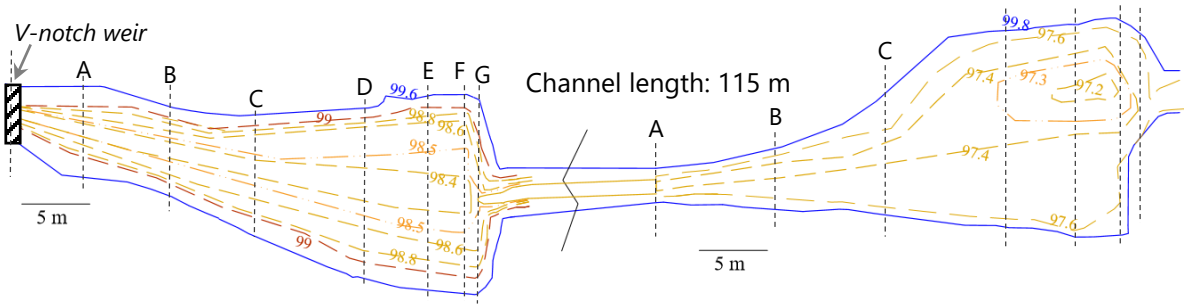

Figure 25: Schematic overview of SWs, indicating the bathymetry (i.e. contour lines) in SW1 and SW2, and various cross-sections.

SWs were designed to have a silty clay material on the bed as an insulation layer to prevent infiltration losses. Evaporation was presumed zero due to the short hydraulic residence times (HRTs) and based on simultaneous flow measurements undertaken at the hydraulic control structures of each CW (inlet and outlet). These results showed that there is no time lag between the inlet and outlet of each wetland at the time of the tracer test. Details of those measurements and results are presented in Appendix I. The total mean travel time of the whole system is in the order of 40 min to 5 h, for the minimum and maximum flow conditions tested. Thus, it has been assumed that the temporal variation of flow at any given time is the same at any location. The total volume of water stored in SWs was calculated based on the surveying works. Details of the site surveying and methodology followed are included in Appendix I. Phragmites australis is the dominant plant species in SWs (details are given in Section 3.3). The vegetation boundaries defined based on the surveying are illustrated in Figure 24.

3.2.1.1. Geometric Characteristics & Dimensions

The general shape of both SWs could be approximated as a trapezium from a plan view (Figure 24), and it is irregular in all three dimensions. Longitudinally, SWs channel is initially narrow, and becomes significantly wider at the outlet. The average bed slope is 0.007 in SW1 and 0.001 in SW2. From a cross-sectional view, the CW channel could be approximated as a trapezium, being deeper at the centre of the wetland, and shallower towards the banks. SW1 is 34 m long, while SW2 is 32 m. The stream is 115 m long, and could be approximated as a rectangular from a plan view, and as a trapezium from a cross-sectional view. It ought to be

noted that the stream has been used as a base case of no vegetation, and is included in the analysis, where applicable (results are presented in Chapter 4).

Although both wetlands were similarly designed, it should be remarked that SW2 has developed an irregular bottom shape with time due to sediments transport, and thus has created a preferential flow path. In particular, bed channel is deeper in the middle-left part of the wetland (toward the flow direction), while the right side is shallower (see Figure 25 and Figure 27). The associated fast flow and slow flow velocity water zones in SW2 are thoroughly discussed in Chapters 4 and 5. Various cross-sections along SW1 and SW2 are shown in Figure 26 and Figure 27 respectively.

SW1 Cross-sections

V-notch weir

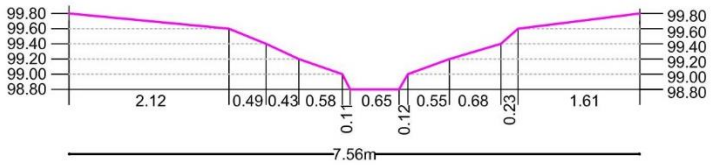

A

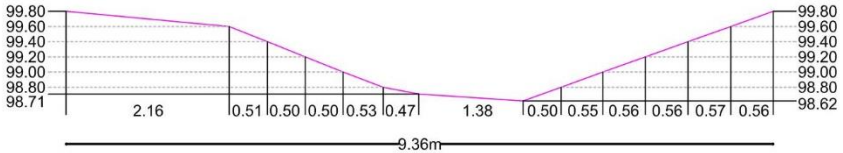

B

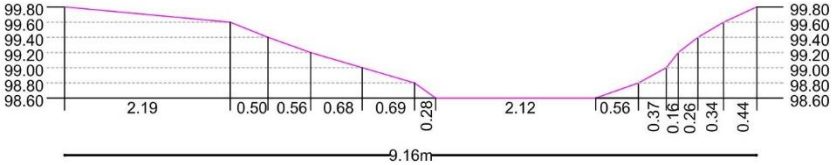

C

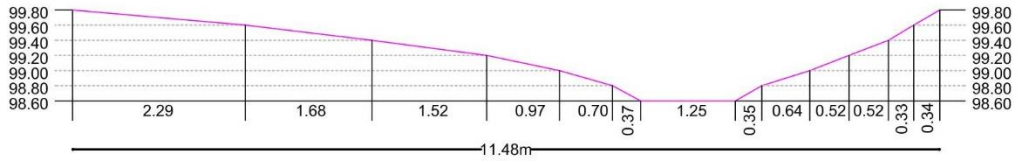
99.80
99.60
99.40
99.20
99.00
98.80
98.60
2.29
1.68
1.52
0.97
0.70
0.37
1.25
0.35
0.64
0.52
0.52
0.33
0.34
11.48m

D

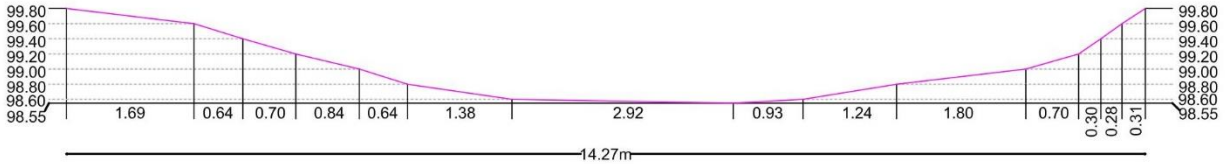
99.80
99.60
99.40
99.20
99.00
98.80
98.60
98.55
1.69
0.64
0.70
0.84
0.64
1.38
2.92
0.93
1.24
1.80
0.70
0.30
0.28
0.31
14.27m

E

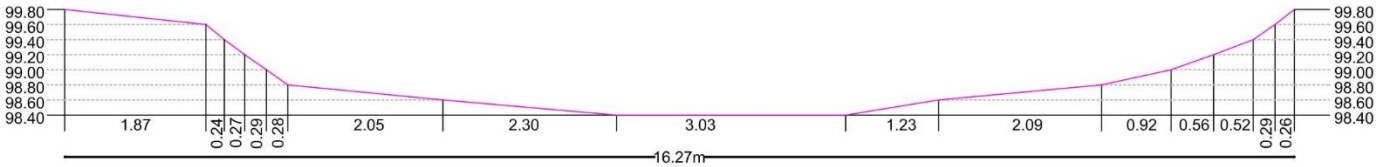
99.80
99.60
99.40
99.20
99.00
98.80
98.60
98.40
1.87
0.24
0.27
0.29
0.28
2.05
2.30
3.03
1.23
2.09
0.92
0.56
0.52
0.29
0.26
16.27m

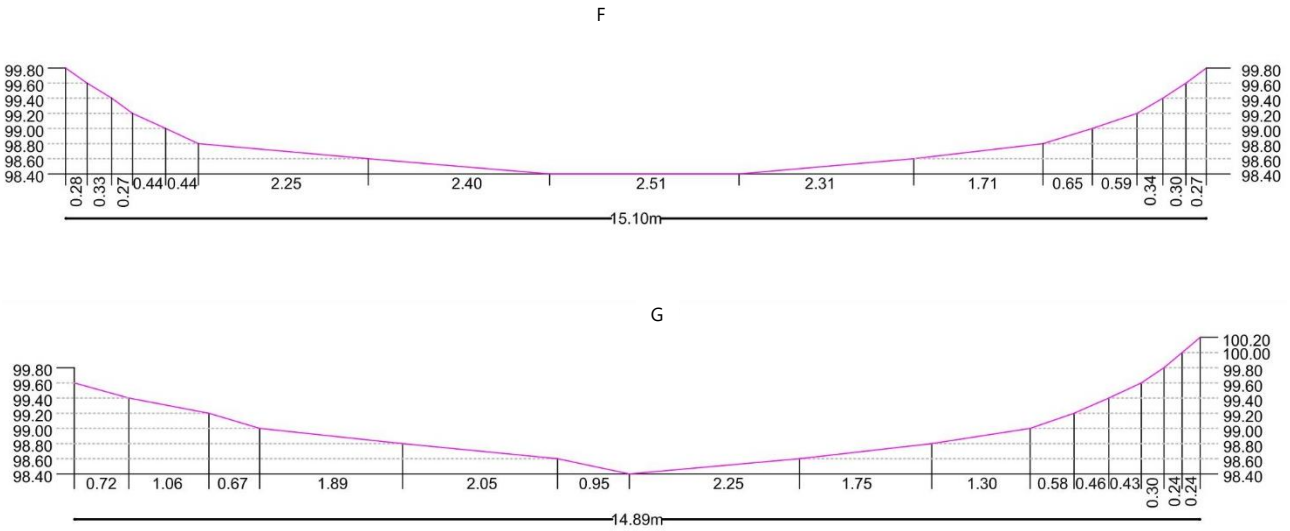

Figure 26: Cross-sectional shape along SW1, from A to G cross-sections.

SW2 Cross-sections

A

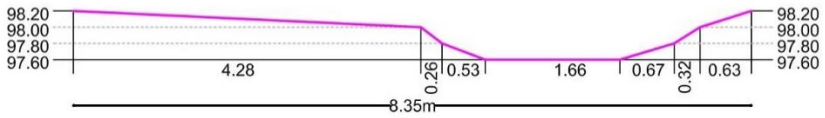

B

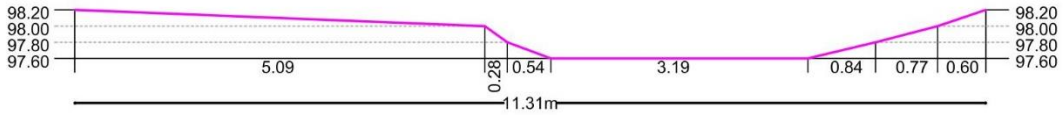

C

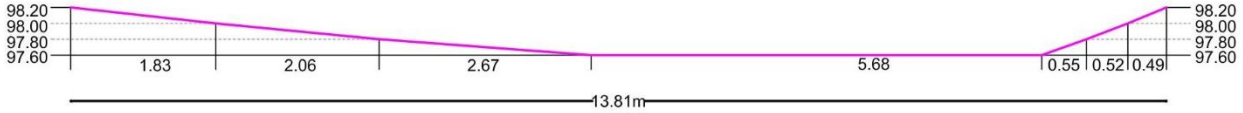

D

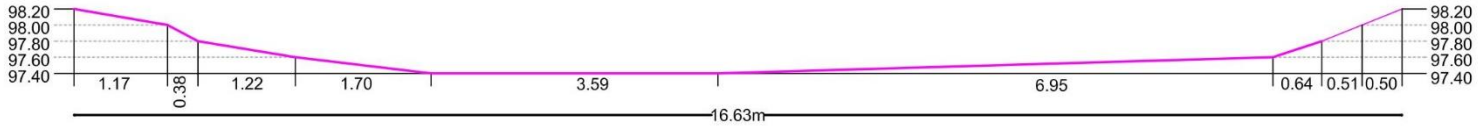

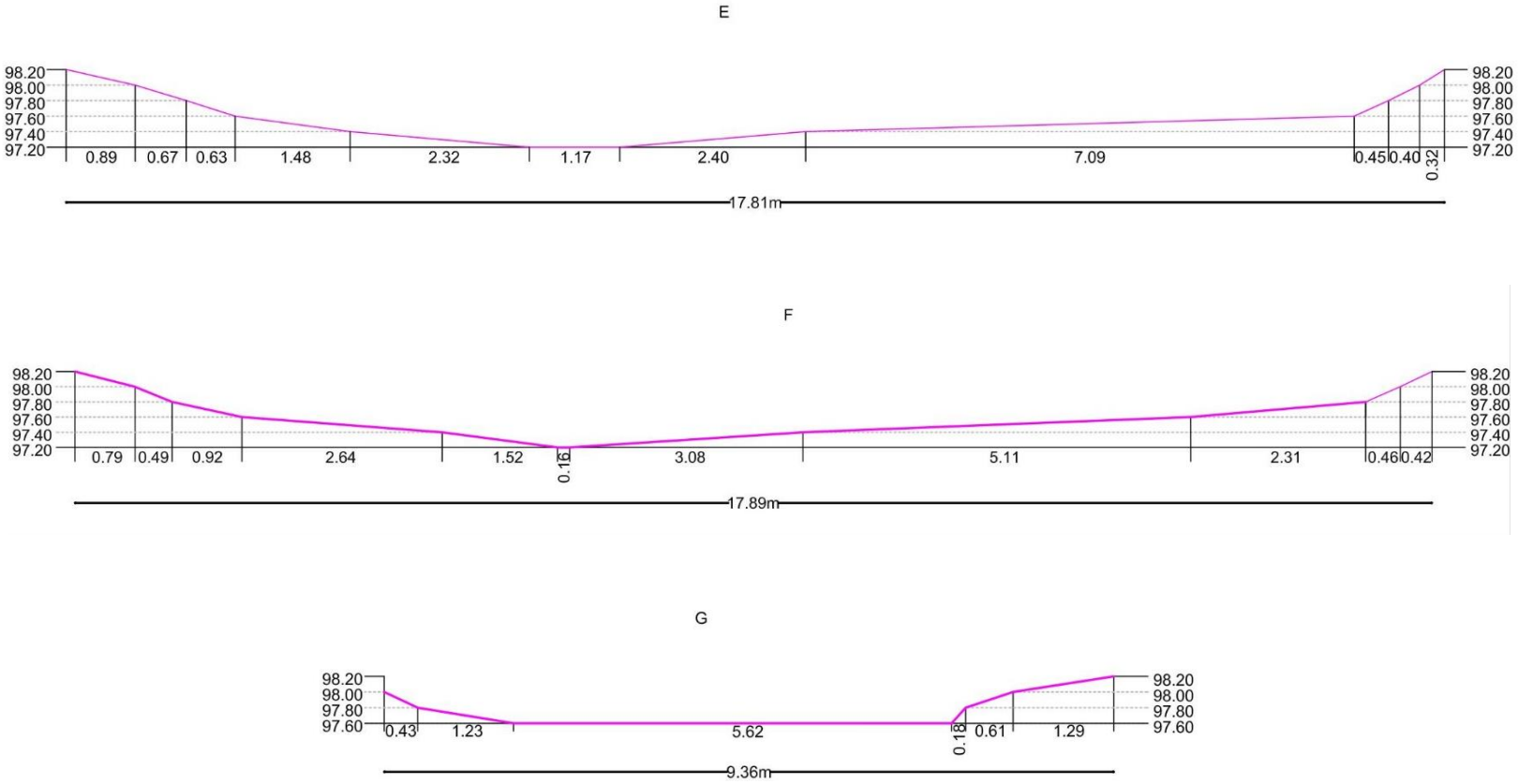

Figure 27: Cross-sectional shape along SW2, from A to G cross-sections.

3.2.1.2. Flow conditions

It should be noted that the flow depth in the wetlands and stream varies depending on the discharge, as a result of water drained from the drainage system due to precipitation, and as there is no regulation of the inflow. The minimum and maximum discharges recorded in SW1 during the testing period were 0.4 l/s and 68.2 l/s respectively. The minimum and maximum discharge values recorded in SW2 are of narrower range, because of the shorter tracer testing period (i.e. unplanned termination of the monitoring period in March 2016 due to equipment malfunction). The corresponding minimum and maximum discharge, Re number, aspect ratio, water depth, volume, and surface area for each wetland is listed in Table 3.1. Overall, for the flow conditions tested, the average water depth did not go above 0.2 m within the wetlands. Table 3.1 presents an average water depth and width, because both values vary across the wetlands due to their irregular shape.

Table 3.1: Geometric and hydraulic characteristics in SW1 and SW2.

	SW1		**SW2**	
Flow condition	min	max	min	max
Flow Rate, Q (l/s)	0.4	68.2	2.8	34.8
Re (-)	384	11577	1591	6756
Length, L (m)	34		32	
Mean Width, W (m)	2.1	5.5	3.3	6.0
Aspect Ratio, A_R (-)	16.5	6.2	10.5	5.7
Mean water depth, h (m)	0.03	0.24	0.07	0.19
Surface area, A (m^2)	70	187	104	192
Total Volume, V_{tot} (m^3)	10.5	39.1	8.1	29.6
Vegetation	Phragmites			

3.2.1.3. Hydrological conditions

There is no irrigation scheme in the RSPB farm fields, thus flow conditions and flow rate is a function of rain intensity, duration, and frequency, as well as percentage runoff. Agricultural runoff water discharges into ditches via the drainage system, and ends up in the CWs, before being discharged into the downstream watercourses. Flow is seasonal, and dependent on the weather. The flow regime is continuous usually between October and until April, unless a prolonged dry period intervenes. During summer months, the phreatic layer drops, resulting in intermittent flow periods occurring from surface water runoff, following a period of precipitation. Flow patterns may vary from year to year though. During the testing period

2015-2016, in particular, weather was overall dry. Due to the dry weather, tracer tests could not start until November 2015, whilst the majority of the tests were achieved during winter and early spring months, when most rainfall events normally happened. The rainfall–runoff record for the monitoring period November 2015 to June 2016 is shown in Figure 28.

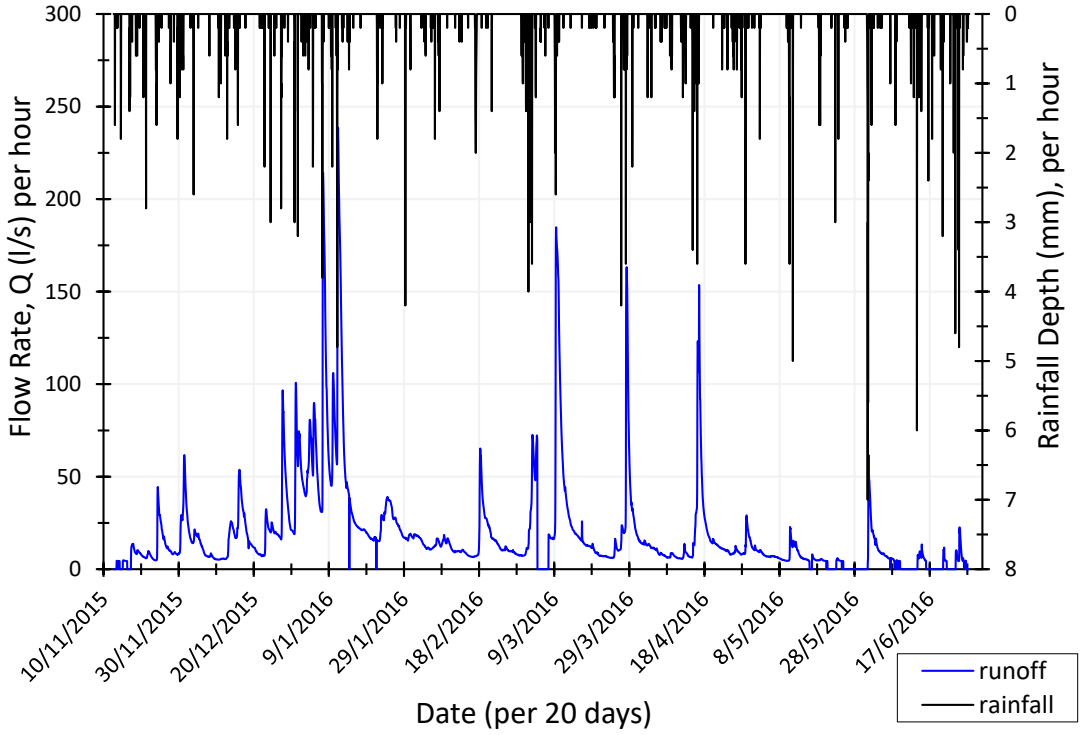

Figure 28: Rainfall – Runoff plot during the monitoring period November 2015 – June 2016.

3.3. Vegetation Characteristics

This section describes the methods for quantifying the vegetation characteristics. One of the main aims of this study was to quantify the mixing characteristics of vegetated flows in full-sized CWs. To achieve this, quantification of vegetation was necessary to associate the potential changes in flow resistance, and mixing characteristics with the changing plant nature. The natural geometric and morphological variation of stems (i.e. deflection), and their natural development and dormant, was monitored in full-scale outdoor conditions of this UK micro-climate. Phragmites australis was monitored in SWs during the entire dormant season (October 2015 to March 2016), and during the new cycle growth season (April to

August 2016). No tracer measurements were undertaken during July, August and September 2016 due to no or extremely low flow conditions.

3.3.1. Description of Vegetation and Seasons

A patch of Phragmites australis (common reed) has been initially planted at the construction stage of the wetlands, and has naturally evolved to the current vegetative state. Vegetation is fully emergent and monoculture. Plant cycle is annual and is distinguished between spring-summer as the growth season (new macrophytes grow and evolve), and autumn-winter as the dormant season (plant growth ceases and wither occurs progressively until the end of annual cycle). In this micro-climate, stems develop and grow up from April to September (live season), while they wither and decompose progressively from October until the end of March (dormant season). The start of plant cycle is in April, whilst its end is in March. During the dormant season, lower flexibility but greater resistance against the flowing water occurs, due to the gradual stems deflection. Typical vegetation conditions in two contrasting seasons are depicted in Figure 29. Vegetation proliferates freely and naturally. Over two years of plants observation, it was observed that in 2015 plants proliferated notably more in number and extent compared to 2014 in both SWs.

(a) Live plant season, June. (b) Dormant plant season, December.

Figure 29: (a) Live plant season with ongoing stem growth in June, in SW1. (b) Dormant plant season under ongoing stems' wither in December, in SW1.

3.3.1.1. Vegetation growth and testing conditions in SW1

As stated earlier in this chapter, the stem diameter and density did not vary significantly with age. Nevertheless, Phragmites stems increased in height quickly, within the first 10 weeks after the start of the new plant cycle in April. Between April and June, the stem population density progressively increased in number, until the proliferation stage ceased, typically in June for this UK micro-climate. The evolution of the stem population in time in SW1 is given through a series of images in Figure 30 (a)-(d), starting with low population in April (Figure 30 (a)), and reaching the peak stem population in June (Figure 30 (c)).

(a) April 2016

(b) May 2016

(c) June 2016

(d) August 2016

Figure 30: Stems in April (Week 1), May (Week 6), June (Week 12), and August (Week 18) in SW1.

However, the channel porosity changed because stems experienced noticeable deflection due to seasonal plant variation at the latest stage of the dormant season (i.e. February – March). Stems displayed their maximum deflection particularly in February and March; this maximum deflection was the worst case applied in this study. However, depending on the flow, the deflected stems were sometimes within and sometimes above the flow depth

(Figure 31 (a)-(b)). Nonetheless, the direction of the deflected stems was random, depending both on the wind activity, and on the magnitude of the discharge. Generally high discharges are expected to induce a more streamlined position of the stems and their foliage. The difference in Phragmites foliage between winter and summer is shown in Figure 32 (a)-(b).

(a) Low flow depth, Feb 2016 (b) High flow depth, Feb 2016

Figure 31: Low and high flow depth during fully deflected stems period, i.e. February-March, creating emergent and submerged flow conditions respectively in SW1.

(a) December 2015 (b) June 2016

Figure 32: Foliage difference between winter (i.e. December 2015) and summer (i.e. June 2016) stems in SW1.

Since the average flow depth was not particularly high during the testing period, it is considered that wind action was the pivotal factor determining the random stems' deflection direction (Figure 31). The transition between the old and new plant cycle is presented with the aid of a photographic record in Figure 33 (a)-(d), for the testing conditions between March and August 2016. In particular, starting from March (Figure 33 (a)), which is the end of plant cycle in this micro-climate, and continuing until August (Figure 33 (d)), when the new plant cycle stems are fully grown, Figure 33 indicates the natural decomposition that

the old stems undergo during the new plant cycle (Figure 33 (b)), and the growth of the new stems (Figure 33 (c)-(d)).

(a) Mar 2016 (b) April 2016

(c) June 2016 (d) August 2016

Figure 33: Natural transition between the old (i.e. March 2016) and the new plant cycle (i.e. April onward) in SW1.

3.3.1.2. Vegetation growth and testing conditions in SW2

As already stated previously, stem diameter and density did not vary with age. For this testing period, stems were already bare in December, as foliage has been already dropping from stems since November in SW2. Noticeable difference occurred naturally in terms of deflection due to seasonal plant variation from December to February, and particularly in February (Figure 34 (a)-(b)). Depending on the flow, deflected stems in SW2 were sometimes under and sometimes above the flow depth (Figure 34 (a)-(b)). Nonetheless, the direction of the deflected stems was random, depending both on the wind action, and on the discharge intensity, where high discharges are expected to induce a more streamlined position of the stems and their foliage. However, because the average flow depth was essentially low (i.e.

approximately 0.15-0.2 m) during the testing period, it is considered that wind action was the pivotal factor determining the random deflected stems direction (Figure 34 (b)).

(a) Jan 2016 (b) Feb 2016

Figure 34: Natural stem deflection due to seasonal plant variation as reaching the highest plant ages, i.e. February in SW2.

3.3.2. *Quantification of vegetation*

Vegetation characteristics (geometry, morphology, and biomass) were quantified in different seasons to allow comparison, and to associate the potential changes in flow resistance and in mixing characteristics with the changing plant nature. Plant biomass measurements in the two extreme seasons (i.e. winter and summer) aimed at giving information to scientists, who deal with pollutant reductions in wetlands planted by Phragmites australis. Vegetation-related quantified features included:

- Average stem diameter, d_m
- Stem population density (Number of plants per meter squared), N_t
- Plant biomass, B_p
- Canopy morphology (expressed by deflection in 2 cases: upright and fully deflected stems).

A record of the measured plant-related characteristics is presented in Table 3.2. The table includes results about mean stem diameter, stem population density, and plant biomass. In addition to this, Table 3.3 lists information about the morphological characteristics, and

particularly about stem deflection estimations for the two extreme cases (i.e. upright stems, and fully deflected stems).

Table 3.2: Record of vegetation characteristics measurements.

	SW1	**SW2**
Mean stem diameter, d_m (mm)	5.80	5.90
Population density, N_t (no./m^2)	174	149
Plant biomass, B_p (gr/m^2)	633 (280)	639 (281)

Note that values in brackets refer to the dry weight of the plant biomass.

Table 3.3: Phragmites stems morphological testing characteristics for each constructed wetland.

	Plant porosity, η	
Stem deflection	**SW1**	**SW2**
Upright, η_g	0.995	0.996
Fully-deflected, η_{dc}	0.959	0.963

Measurements of stem diameter and density were taken from fixed locations in the wetlands in different seasons. Stem diameters were obtained using a digital calliper. An average of 5-6 plants randomly spaced in each wetland were identified and monitored for their stem diameter variation, at a vertical height of 20 cm above their rhizome-bed surface. No variation was found in stem diameters between the live and dormant seasons (Table 3.2), thus stem diameter was considered fixed.

Stem population density was measured as the number of stems per m^2, using a 0.25 m^2 mold. Table 3.2 indicates that SW1 is slightly denser than SW2. The plant biomass process involved removal of a 0.25 m^2 section of stems, cut 15 cm above the soil. The removed stems were counted in the laboratory, and measured for their wet weight. Thereafter, stems were oven baked for 24 hours at 100°C, and, subsequently, dry plant biomass weight was taken. Plant biomass values were very close to each other in SWs, measured for the two extreme seasons (Table 3.2).

Canopy morphology is expressed as stem deflection for the scope of this study. Stem deflection was monitored using a photographic record. The two extremes of plant deflection, i.e. 0% and 100%, are shown in Figure 35. It was observed that two main extreme conditions

occurred throughout the year, namely upright stems (0% deflection) from April to January, and fully deflected stems (100% deflection) between February and March. The random nature of natural vegetation characteristics and ageing (i.e. variation in stem diameter, spatial distribution, spatial population density, natural deflection degree) is an apparent experimental limitation of an outdoors, full-sized system, to quantify those parameters in high mathematical accuracy. Furthermore, there were associated difficulties in measuring intermediate stages of deflection. Therefore, it was presumed that all stems were fully deflected close to the end of plant cycle, i.e. February and March.

(a) Upright stems, April to January (0% deflection) (b) Fully deflected stems, February-March

Figure 35: Comparison between the two extremes of stem deflection, i.e. June (a) and February (b).

The plant solid volume fraction, Φ, has been used to present the rate of growth between the two extremes of stem deflection. To measure the vegetation porosity, η, stem diameter, d_m, of Phragmites was assumed to be constant with depth, since the cylindrical nature of stems allows this approximation. In this way, plant porosity was calculated as $\eta = 1 - \Phi$. This equation is characterised by the stem population density, N_t, per unit area, and by the plant solid volume fraction, $\Phi\ (= N_t \pi d_m^2 / 4)$. Plant porosity was measured for zero stem deflection, η_g, and for total stem deflection, η_{dc}, where g stands for growing and dc stands for dormant case respectively. Plant porosity characteristics for each wetland are listed in Table 3.3, while stem solid volume fraction calculations for the two extreme porosities investigated are detailed in Appendix I.

It is observed that for both wetlands Φ for the upright stems is very low (approximately 0.004-0.005), which entails that in the upright stem case, vegetation occupies 0.5% of the

wetland volume. This indicates that vegetation plays negligible role in the calculation of the wetland volume, and infers that stems density is sparse. However, during the fully deflected scenario, Φ increases approximately by 10 times in both wetlands, suggesting that fully deflected stems account for 4% of the wetland volume. Therefore, it is deduced that vegetation still occupies a minor fraction of the total wetland volume for the deflected stems case.

3.4. Flow Measurements

This section details the discharge and overflow measurements in the monitoring wetlands.

3.4.1. Flow Rate Measurement Structures

Flow rate was constantly monitored at the inlet of SW1 over the full duration of the testing period. A pressure transducer (Panasonic PS-A) was attached on the plate of the V-notch weir, and the transducer's datum coincided with the bottom of the V-notch weir (zero head). The transducer was the primary instrument used to measure flow rate in the wetlands. Additionally, flow rate was measured through the dilution gauging technique.

The transducer had the dual aim to calculate the flow rate, and to trigger the dye injection in SW1, as detailed later in Section 3.5.2. The calibration relationship obtained between the water level at the V-notch weir (in mm) and the pressure transducer (in mV) is given in Figure 37 and in Equation 3.1. The calibration was achieved by taking in-situ measurements in every site visit and by checking measurements with the pressure transducer's logs. From Figure 37 it is also noted that temperature does not affect the results. Logging rate of water level was every 5 min. The readings obtained from the pressure transducer were converted into flow rate through the standard Kindvater & Carter free water surface equation (BS3680–4A, 1981) (equation and conversion details are provided in Appendix I).

$$W.L._{V\text{-}notch.weir} = 0.154 \times \left(W.L._{press.transducer} \right) - 119 \qquad \text{Equation 3.1}$$

Besides the V-notch weir, one Venturi flume was installed at the outlet of each wetland. Water depth measurements were taken on, and prior to, the Venturi flume in every site visit. This allowed a calibration relationship between the water depth at SW1 inlet, and water depth in SW1 and SW2 outlet to be determined, as given in Equation 3.2 and Equation 3.3 respectively, where the water level (W.L.) was in mm.

$$W.L._{Venturi\_SW1} = 0.6346 \times \left(W.L._{V\text{-}notch}\right) - 2 \qquad \text{Equation 3.2}$$

$$W.L._{Venturi\_SW2} = 0.6413 \times \left(W.L._{V\text{-}notch}\right) + 4 \qquad \text{Equation 3.3}$$

Figure 36: Pressure transducer monitoring the water level at the SW1 inlet. The transducer measured the water level and triggered dye in SW1.

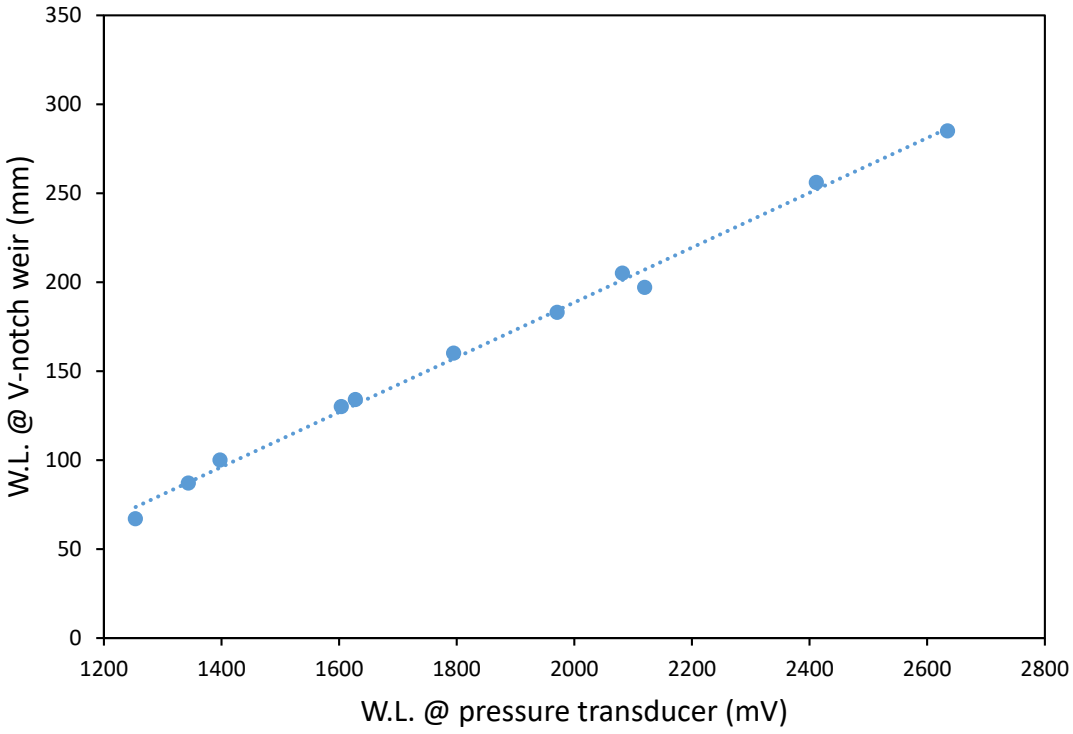

Figure 37: Water Level (W.L.) calibration relationship between the V-notch weir & the pressure transducer at SW1 inlet.

Within porous media, like vegetation, turbulence is generated at the scale of stem wakes. This may make the traditional use of flow depth, *h*, inappropriate to scale the turbulence through the Reynolds number, *Re* (given in Equation 3.4) (Nepf & Vivoni, 2000). Therefore, in vegetated flows, stem Reynolds number, *NR**, may be considered a more proper method for determining Reynolds number. Calculation of *NR** is given in Equation 3.5.

In Newtonian fluids, like water, kinematic viscosity, ν, varies with temperature. There were selected two mean ν values, i.e. $\nu_{winter} = 1.446 \cdot 10^{-6}$ m^2/s, referring to winter season (November to March), and $\nu_{summer} = 1.167 \cdot 10\text{-}6$ m^2/s, referring to summer season (April to October). The seasonal ν values and the mean monthly water temperatures are provided in Table 3.4.

$$Re = u^*h/\nu \qquad \text{Equation 3.4}$$

where u = longitudinal velocity (m/s), and h = mean water depth in open channel flow (m).

$$NR^* = u^* d_m / \nu \qquad \text{Equation 3.5}$$

where d_m = mean stem diameter (m).

Table 3.4: *Kinematic viscosity for water (Adapted from IAPWS, 2008).*

(1)	(2)	(3)	(4)	(5)
Month	Mean monthly T (°C)	ν ($m^2/s * 10^{-6}$)	Season	ν_{mean} ($m^2/s * 10^{-6}$)
NOVEMBER	7.4	1.406	WINTER	1.446
DECEMBER	6.5	1.495		
JANUARY	6.2	1.463		
FEBRUARY	6.1	1.467		
MARCH	7.7	1.398		
APRIL	10.6	1.284	SUMMER	1.167
MAY	13.1	1.198		
JUNE	15.7	1.118		
JULY	17.2	1.076		
AUGUST	15.7	1.118		
SEPTEMBER	14.3	1.16		
OCTOBER	12.5	1.218		

A secondary way to determine discharge was through a dilution gauging measurement technique (BS: 3680–3C). Figure 38 presents the mass balance of the dye in SW2, and the relationship between Q obtained from the pressure transducer, Q_{trans}, and Q obtained from the dilution gauging, $Q_{d.g.}$. Figure 38 suggests good tracer recovery during the normal monitoring period (i.e. till March). At this point, it should be noted that during March the experimental testing programme paused for a few days, and dye concentration was reduced by 10 times (i.e. $C=10^7$ ppb) in all monitoring sites. This was applied after discussion with the Environment Agency, because equipment malfunction occurring in the SW2 automated tracer injection system, caused introduction of larger amounts of dye in the wetland.

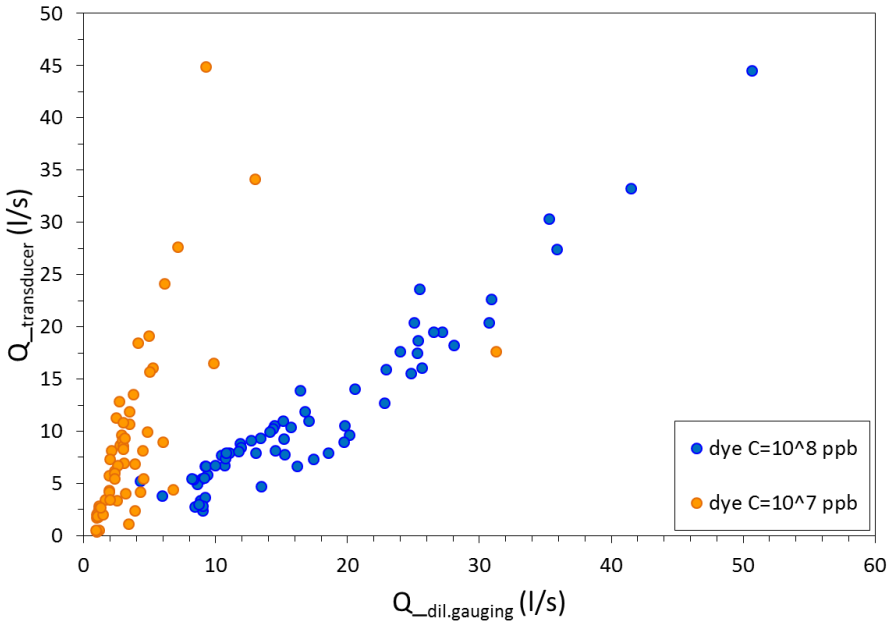

Figure 38: Mass balance of dye between discharges measured from the pressure transducer and from the dilution gauging in SW1. The figure highlights the different dye concentrations, i.e. prior to March ($C=10^8$ppb) and post-March ($C=10^7$ppb).

The post-March dye concentration $Q_{d.g}$ results are shown in Figure 38 in different colour. It is observed that there is some divergence of the post-March tests from the main trend line. This is attributed to glitches in the automated injection system, and particularly to the amount of dye pumped into the system. Although raingauge data suggests various intense storm events in March and April (Figure 28), those are not reflected through the $Q_{d.g}$ in the post-March tests. As a consequence, it is inferred that dilution gauging did not work robustly enough through the automated tracer injection system (SW2 dilution gauging plot is in Appendix I), i.e. not enough dye was injected via the automated injection system, thus all discharge measurements relied upon the pressure transducer.

3.4.2. Overflow Measurements

The maximum flow within the confines of the V-notch weir was 139 l/s, for which the Kindvater & Carter free water surface equation (introduced in Section 3.3.1 and Appendix I) is valid. Above this flow rate, a simple weir equation was applied to estimate the

''overtopped'' flow. Two contrasting flow regimes are shown in Figure 39, displaying near overtopping flow and DWF conditions at the V-notch weir.

Figure 39: (Left) Nearly overtopping flow conditions at the V-notch weir; (Right) DWF conditions.

3.5. Fluorometry Measurements – Rhodamine Dye Tracing

Fluorometric tracing techniques were used to measure the longitudinal mixing, and to study the wetland internal hydraulics through differential advection, within the confines of the CWs. For all the experiments, Rhodamine WT (RWT) dye was employed as the tracer. RWT was chosen because: i) it is detectable in low concentrations; ii) it has a slow rate of decay (Lin et al, 2003), thus it can be assumed conservative, iii) and due to prior experience in the Department. The downside that RWT presents is the photochemical decay it undergoes, especially in tests that exceed a week's time (Lin et al, 2003). However, that was not the case for the current tests, as the maximum tests duration was in the order of hours.

The fluorometers deployed during the testing period were Cyclops-7 by Turner Designs. The fluorometers are sensitive to light brightness or direct sunlight, hence a perforated filter was applied on them, as seen in Figure 40, where and when necessary. This filter also protects the optics from leaves and debris sticking on them, as well as from building less silt or algal bloom, when used for long periods, which was the case mainly for the longitudinal mixing study.

Figure 40: Perforated filter attached on Cyclops-7 to prevent sunlight interference and debris on the optics.

3.5.1. Fluorometer Calibration

All concentration readings were acquired with Cyclops-7 submersible fluorometers. For the longitudinal mixing study, three instruments were normally available. Occasional availability of additional four devices provided the opportunity to conduct internal measurements in the SWs, i.e. study differential advection.

Cyclops-7 fluorometers' function is based on the emission of a certain wavelength of light. When RWT is exposed to that wavelength, it becomes excited and emits light of different wavelength. The Cyclops-7 fluorometer measures the emitted light intensity, which is a function of the dye concentration. The fluorometer gives a voltage output corresponding to the light intensity recorded, as far as the recorded levels are within the linear range values that the instrument can measure. Fluorometers' calibration is conducted in different, and known, concentration solutions. Such results provide a relationship for each fluorometer, which allows the measured concentration, according to the voltage output, to be determined. Figure 41 shows an example of the linear relationship between concentration and voltage output for the two permanently located instruments in SW2 for the longitudinal mixing study, for gain 1 sensitivity. Calibration values for all fluorometers and all gain settings for the longitudinal mixing and differential advection studies are compiled in Appendix I.

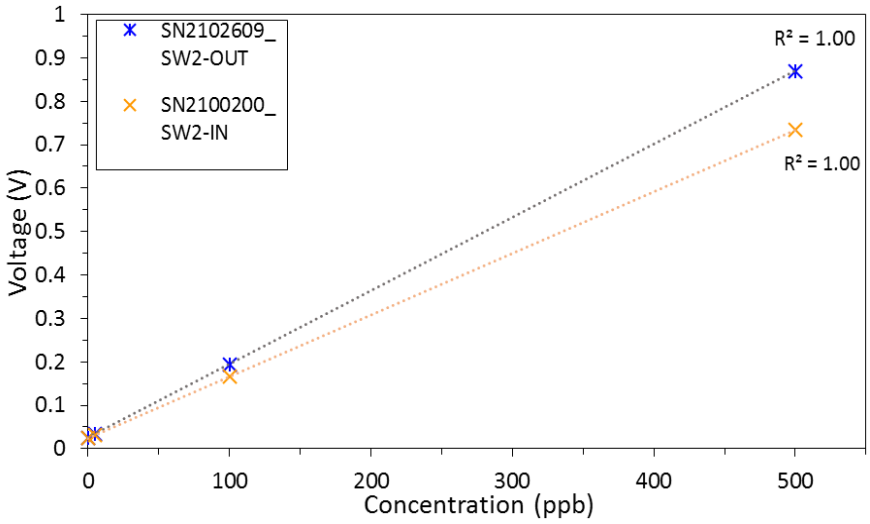

Figure 41: Example of the two fluorometers calibration used for the longitudinal mixing study in SW2.

Fluorescence dye is temperature sensitive and changes approximately inversely with temperature (Smart & Laidlaw, 1977). Fluorometers were calibrated at stream temperatures, and the perforated filter was attached during the calibration, where required. After calibration, Cyclopses-7 were placed directly into the stream flow at the required measurement location (Figure 42).

Figure 42: Cyclops-7 instrument installed in the flow channel, at the outlet before the Venturi flume for the longitudinal mixing study.

3.6. Longitudinal Mixing Study

Longitudinal mixing is considered as the rate of the longitudinal spread of a slug tracer injection over time or distance. In order to achieve the main aim of this study related to the seasonal vegetation variation effect on mixing characteristics and flow profile in full-size CWs, an automated tracer injection system was installed in each CW. For a continuous 8-month period (November 2015 – June 2016), repeatable tracer injections were conducted at various flow rates, depending on the seasonal precipitation, and in different plant seasons. Recall that equipment malfunctions disrupted the long-term testing programme in SW2, achieving three complete months of tracer tests, namely between December 2015 and February 2016.

Three Turner Designs Cyclops-7 fluorometers were set up permanently on site to measure tracer concentration for the longitudinal mixing study. One fluorometer was installed permanently at the outlet of each CW to record the RTD of each system. The extra fluorometer was installed at the inlet of SW2, in order to trigger tracer injection on the dye concentration arriving from SW1 (detailed in Section 3.5.2). Each fluorometer was incorporated into a multi-parameter system to provide power to the system and to distribute a constant output voltage (5V) to the system data logger.

3.6.1. Dye concentration and injection

RWT was injected directly at the inlet of each CW. A peristaltic pump was used to inject a fixed amount of dye. The concentrations of the tracer experiments were dependent on the seasonal flow rate, i.e. from October to March dye concertation was 10^8 ppb, whereas from March to June it was 10^7 ppb. The Cyclops-7 logging sensitivity range was adjusted accordingly to the tracer concentration injected. Each peristaltic pump was calibrated in the laboratory to define the exact amount of dye concentration to be injected, and the particular pumping duration time was adjusted via Arduino microcontroller board (Arduino UNO 3).

3.6.2. Dye Injection System

An initial monitoring period during 2014-2015, included site visits for tracer tests on a weekly basis, and transfer and removal of fluorometer equipment in every visit. That scheme, albeit regular, proved inadequate to build a sufficient tracer data record to describe the systems both over dry and storm flow conditions. Consequently, the site proximity and the seasonal flow regime led to the development of an automated dye injection system. Detailed description of this system is provided for each of the SWs as follows.

In SW1, tracer injection was triggered by the water level at the V-notch weir, as seen in Figure 43. The pressure transducer (described in Section 3.3.1) recorded the head of the water on the V-notch weir. A threshold was established through an Arduino controller, above which an impulse of tracer was injected. This threshold was set to prevent from tracer injection at insufficient or no flows. The Arduino controller programming was used to set the tracer injection intervals, and the data logging duration of the tracer tests. A Cyclops-7 fluorometer was installed permanently underwater at the outlet of SW1, accompanied by a battery supplier and by a LogBox data bank (located on the land and covered in a weatherproof box). Because the data bank capacity of the Logbox memory would fill up more quickly in a continuous logging mode, a digital signal was sent from the pressure transducer to the Logbox to activate logging at the Logbox once threshold condition was met. The logging rate was averaged over 60 s. Data collection duration was set through the Arduino controller, and was set to 8 h during storm months and 24 h during dry months.

After completing the data collection duration for each tracer test, the Arduino controller was programmed to check the water level before repeating the next tracer injection. Provided that the water head on the V-notch weir was above the threshold value set, a new injection would follow; otherwise, the controller would wait until the next scheduled injection to recheck the water depth. During wet months, tracer tests were set to repeat every 8 h, while during drier months, one test per day was performed to allow tracer residual to remove completely from the wetland, so that concentration in the wetland reaches the background levels.

Figure 43: SW1 inlet tracer injection system. A floating material is used to follow water level fluctuations.

SW2 automated tracer injection system was triggered by the concentration of the plume reaching SW2 inlet, as arriving from SW1 through the stream. Due to the in-series arrangement of SW1 and SW2, the dye from SW1 eventually traverses SW2. Therefore, triggering on dye concentration in SW2 inlet managed to prevent dye mixture in SW2 from two different impulses. As such, a Cyclops-7 was installed permanently underwater at the inlet of SW2, logging fluorescence values on permanent mode, while Arduino controller in SW2 was set to trigger dye injection as long as a certain dye concentration threshold (as arriving from SW1) was detected. This entailed that when there was no dye injection in SW1, no dye injection would occur in SW2. As such, once dye concentration detected in SW2 inlet was above the threshold set, Arduino controller was set to inject dye in SW2 after a fixed time. This was done to allow sufficient time for the tracer plume originating from SW1 to traverse and leave SW2, until the SW2 injection system introduces dye. That time lag was 4 h during wet months, and 12 h during dry months. At the time of trigger, a digital input signal was transmitted to the LogBox to prompt logging at the outlet, after the fixed amount of hours has passed. The logging rate and duration was similar to SW1 for the storm and dry flow conditions. In this way, dye mixture in SW2 originating from SW1 was avoided.

3.6.3. Longitudinal Mixing Data Analysis & Processing

Quantifying the longitudinal mixing involves measurements of the temporal concentration profiles from each test, followed by basic analysis procedures, which include:

a. Conversion from voltage values to concentration values using the calibration curves
b. Removal of the background concentration
c. Identification of the start and end of the tracer data
d. Evaluation of the longitudinal dispersion coefficient using the method of moments.

The above procedures are described in detail in the following subsections.

3.6.3.1. Pre-processing of data

The pre-processing steps applied on all the acquired data to specify the real tracer data are explained as follows. The same analysis methodology was applied for each tracer test.

3.6.3.1.1. Voltage to concentration conversion

Raw voltage readings logged by Cyclopses-7 in mV were converted into concentration values in parts per billion (ppb).

3.6.3.1.2. Background concentration removal

It is possible that background fluorescent readings are present in the water flowing in the system due to dye remaining from previous tests, when the flow rate is very low. However, some initial fluorescence readings might frequently originate from the water in the system (i.e. suspended sediments). This fluorescent background is assumed to be constant during the presence of dye. To identify the background, the logged values before the dye arrival and after the dye has passed are examined.

Test logging duration for the SWs tests was given in Section 3.5.2. The background concentration was determined taking the average of the readings in a consistent manner, and particularly between the last 10 minutes of each test (where possible and applicable). A linear horizontal function was estimated for the initial profile (Figure 44 (a)), and background concentration was removed from every test, as seen in Figure 44 (b).

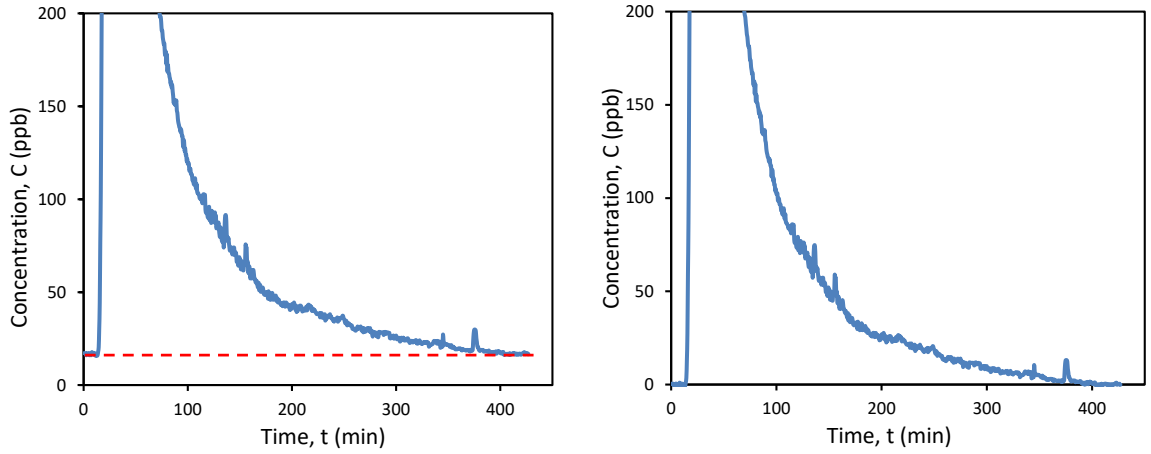

(a) Background level identification. (b) Background level removed.

Figure 44: Typical procedure followed for: (a) Background level identification, using a linear horizontal function; (b) Background level removal.

3.6.3.1.3. Start and end point Identification

After background concentration removal, the tracer data still needs identification of the start and end point of the RTD, because the instrument displays small fluctuations. The methodology applied to achieve this, uses a threshold point, which is defined as the point at which the signal drops below a certain percentage of the RTD's peak concentration. The approach used to define the start/end points was the point at which four successive concentration values drop below a particular percentage of the peak concentration. Figure 45 shows a compilation of concentration profiles for various cut-off percentage values (i.e. 5, 2, 1, 0.5, 0.2 and 0.1 %) in different months and flow rates in SW1. The selection of the peak's percentage is defined as the value that includes the whole RTD profile, whilst minimising the amount of background scatter included. Figure 45 indicates the sensitivity of D_x related to the selection of the cut-off value. In particular, it is shown that when the cut-off value is 2%, a non-negligible part of the distribution is removed, while when the cut-off value is below 1.0%, a great amount of background scatter is included in the distribution profile, which involves significant increase and variation in the D_x coefficients. For this experiment, cut-off value of 1.0% of the peak concentration was used to determine the start/end points of the RTDs in the wetlands.

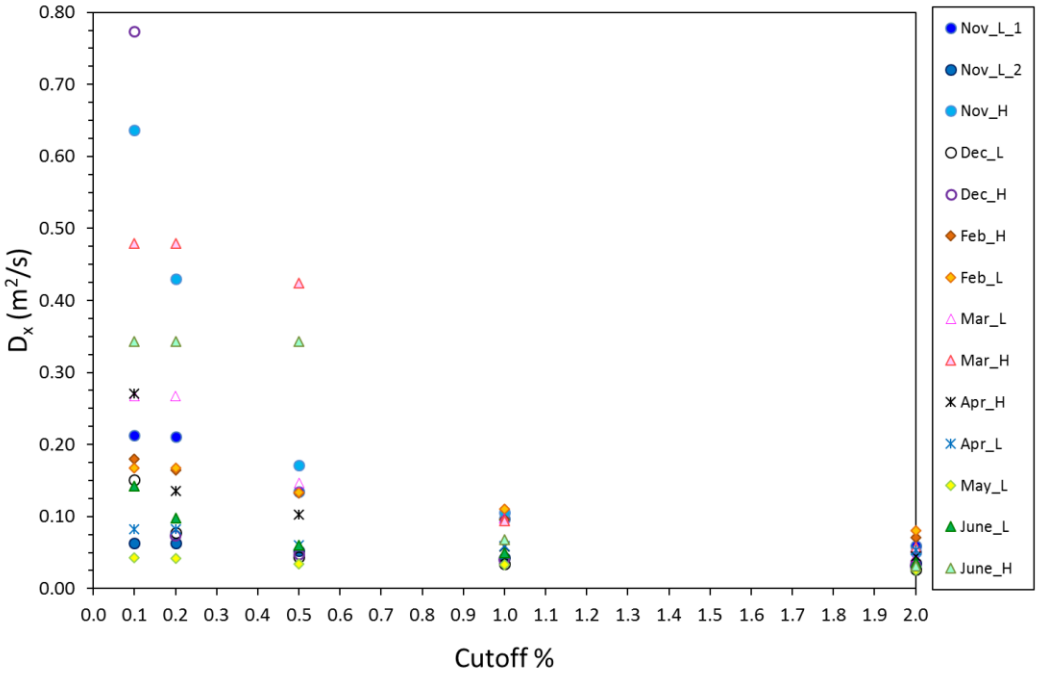

Figure 45: Sensitivity relationship between the cut-off value and the D_x coefficient for a compilation of tracer tests in different months (growth and dormant seasons) and flow rates (i.e. low (L) and high (H)) in SW1.

3.6.3.1.4. Elimination of noisy background data

During the process of identifying the start/end points of the RTDs, there may be noisy data which create spikes or outliers. This data may have occurred due to sunlight interference directly on the instrument's wavelength, or by any other kind of interference. This data has been eliminated using linear interpolation between the outlier values stepping constantly upwards or downwards accordingly.

3.7. Differential Advection Study

The main aim of the differential advection study was to understand and further elucidate the internal wetland processes. Such information can provide insights into the fast paths or dead zones in the wetlands. As such, a cross-sectional profile was measured in each CW, i.e. 10 m prior to the SW1 outlet, and 13 m prior the SW2 outlet respectively. The longitudinal concentration profiles from a slug injection at the inlet, were measured at several points transversely, the locations of which are seen in Figure 24. Four Cyclopses-7 were used to

monitor the concentration profiles, which logged on a continuous mode, every 30 s for a duration of one week in each wetland separately. The analysis methodology and procedures applied were the same as described in Section 3.6.3. Calibration values of the fluorometers are presented in Appendix I.

3.8. Test procedures & Schedule

A range of flow rates were investigated in different plant seasons, i.e. dormant and live, using tracer tests in SW1 and SW2, in order to characterise the wetlands hydraulically and to investigate seasonal variation effects on mixing characteristics. Discharges were random and dependent on rainfall. Tracer tests were achieved through the development of an automated tracer injection system at the inlet of each wetland. Testing duration varied in each system; SW1 testing programme lasted for 8 months (November 2015 to June 2016), whilst SW2 for 3 months (December 2015 to February 2016), due to equipment malfunctions. The frequency of tracer tests depended on the flow conditions. As such, in storm conditions three tracer tests per day were conducted, while in dry weather conditions one test per day was performed.

It should be noted that because autumn 2015 was dry, tests commenced in November 2015, when flow appeared in the systems. Furthermore, rodents' attacks on cables, along with the site proximity, suspended fluorometric measurements in the SW1 during January 2016.

The minimum and maximum discharges observed in both wetlands overall were 0.4 and 68.2 l/s. The mean longitudinal velocity was obtained from the tracer analysis, and was observed in the range of 0.010 m/s and 0.076 m/s for SW1, and 0.032 m/s and 0.055 m/s for SW2.

The age of the plants was expressed in months, from the start of the new plant growth cycle, approximated in the first week of April for this micro-climate. Plant characteristics and quantification procedures were detailed in Section 3.2.

4. Experimental Results

This chapter presents the results of the tracer measurements conducted in the two main monitoring sites, namely South Wetland 1 (SW1) and South Wetland 2 (SW2). The work is developed to investigate the effects of seasonal vegetation variation, and the effects of the flow rate on mixing characteristics and flow profile. Along with the two south wetlands (SWs), data from the connecting stream is presented, as a base case of no vegetation. The results are divided into three sections, where each section refers to each individual system, to allow ease of comprehension. As such, Section 4.1 presents the stream (base case), Section 4.2 the SW1 and Section 4.3 the SW2.

4.1 Stream (Base Case)

This section presents and discusses the results for the Stream, as a basic non-vegetated case, using the parameters derived from the tracer tests.

4.1.1 Fluorescent tracing results

4.1.1.1 Tests collected

The fluorescent tracing tests conducted in the stream were collected by monitoring the SW1 outlet tracer concentration and the SW2 inlet concentration. Details of monitoring concentrations are provided in Chapter 3, and fluorometer locations are seen in Figure 24.

4.1.1.2 Analysis of measured concentration profiles

The stream tracing data was synthesised using the concentration-time profiles obtained at the outlet of SW1 and at the inlet of SW2. In that way, D_x and hydraulic residence time (HRT) were obtained. As described in Chapter 2, Section 2.4.1, a residence time distribution (RTD) is obtained from the impulse of a tracer at the inlet and by monitoring the concentration at the outlet of the system. The derivation of the stream RTD was beyond the scope of this study, but the concentration-time profiles were recorded at the two ends of the stream, upstream (SW1 outlet) and downstream (SW2 inlet). Two contrasting discharges occurring

in February are presented for a low Q_{low}= 5.3 l/s, and a high discharge Q_{high}= 33.3 l/s case. The relevant concentration time profiles are shown in Figure 46 and Figure 47. It is observed that the decrease in discharge results in reduction of the D_x, and increase of the HRT, while it also achieves lower peak concentration levels, allowing for better spread and dilution of the tracer. This happens because as the water spreads out, flow speed is reduced, abating downstream concentration through the processes of dilution and biochemical degradation (Koskiaho, 2003).

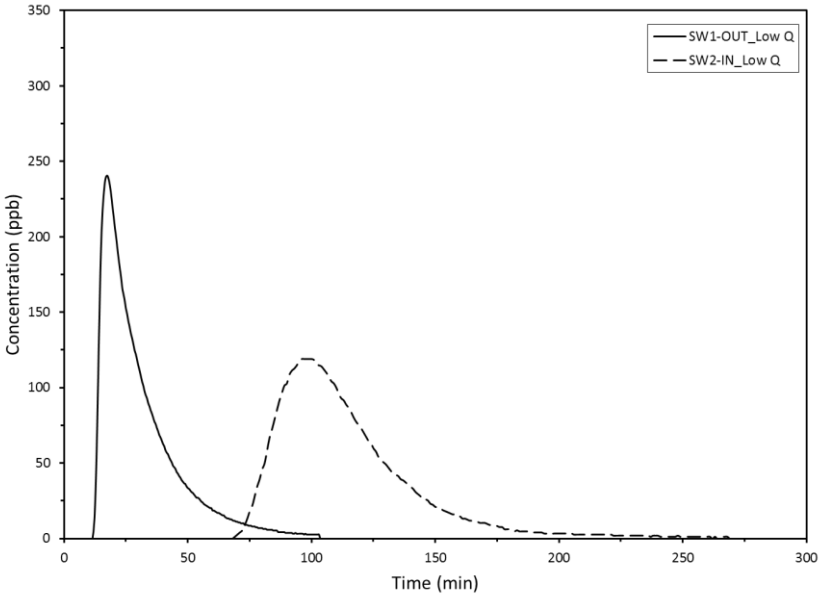

Figure 46: Low discharge case in the stream, Q=5.3 l/s, D_x=0.110 m^2/s.

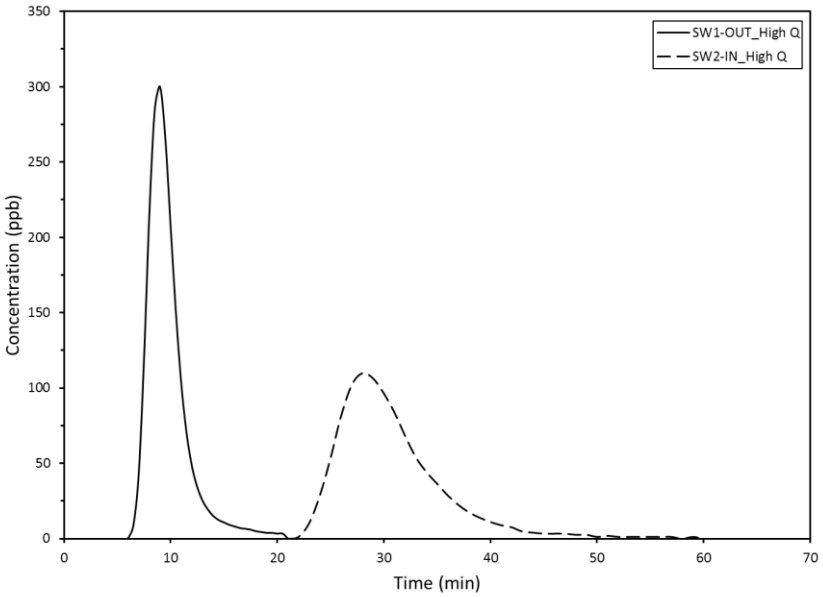

Figure 47: High discharge case in the stream, Q=33.3 l/s, D_x=0.277 m^2/s.

4.1.1.3 HRT

HRT determines the contact time of a pollutant in a system. As obtained from the analysis of the concentration-time profiles (typical profiles were presented in Figure 46 and Figure 47), HRT corresponds to t_m. The HRT in the stream is shown in Figure 48, and follows a typical inverse relationship with time. It is observed that in high discharges, e.g. above 30 l/s, tracer spends approximately 0.5 h in the stream, while in low discharges, e.g. 5 l/s, tracer spends approximately 1.5 h in the system.

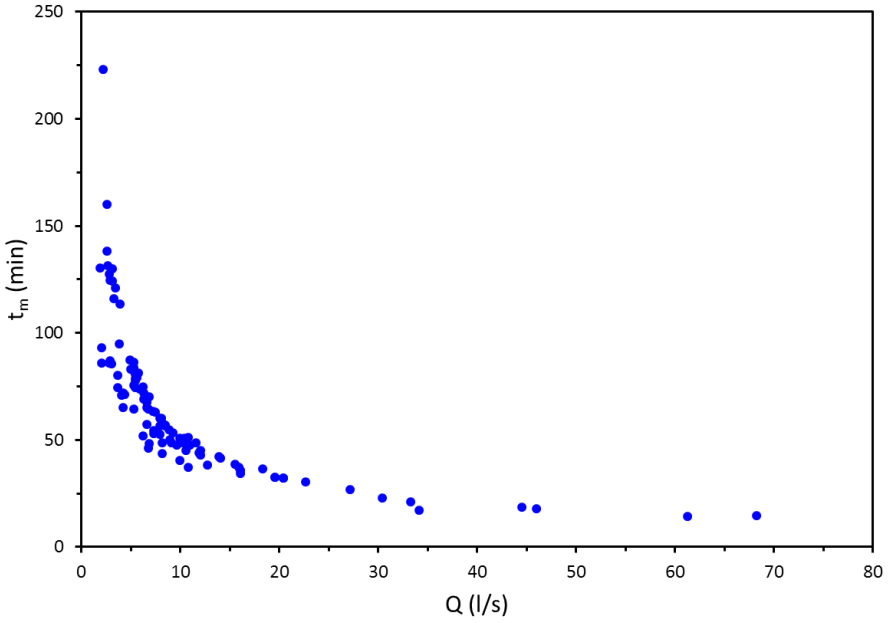

Figure 48: HRT, t_m, against discharge in the Stream, following a typical inverse relationship with time.

4.1.1.4 Mean velocity profiles

This section presents the results of the flow resistance in the stream (base case) with no vegetation. Figure 49 presents the average velocity against discharge in the base case. The u_{mean} is calculated as the ratio of longitudinal distance over time, where the longitudinal distance is fixed (i.e. the distance between the outlet of the SW1 and the inlet of SW2), and time is the HRT (or t_m) obtained through the tracer test. The average velocity increases with flow rate, and follows a good proportional trend, indicating that cross-sectional area does not have much influence on the discharge. This trend was expected by the continuity

equation, as discharge derives from Equation 4.1, where u= longitudinal flow velocity (m/s), and A= cross-sectional area of the channel (m^2).

$$Q = u \cdot A \qquad \text{Equation 4.1}$$

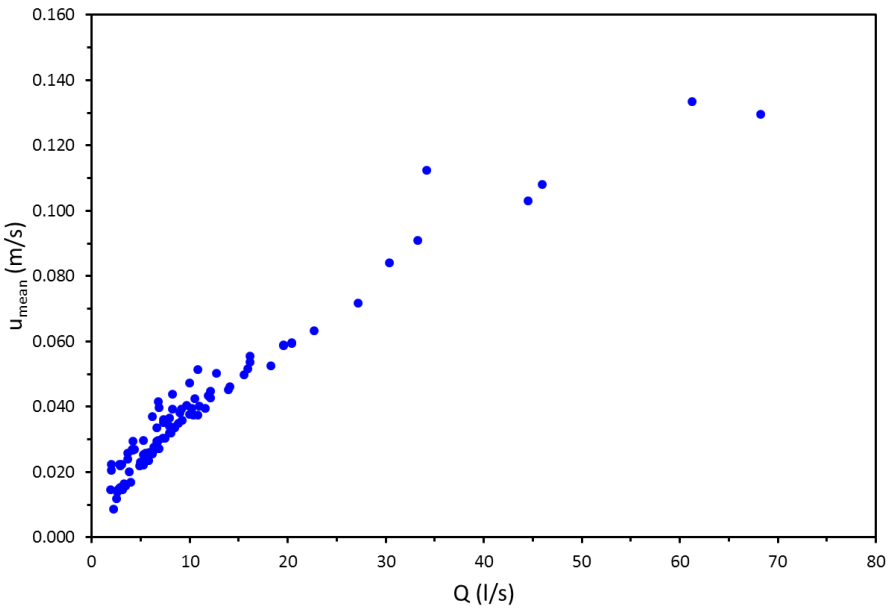

Figure 49: Mean velocity against discharge in the Stream.

4.1.1.5 Longitudinal dispersion measurement

The relationship between D_x and discharge in the stream is plotted in Figure 50 to show the variation of the longitudinal dispersion coefficient with flow rate. The overall trend indicates increase in D_x with discharge. In order to compare the empirical data of the stream with other formulae which estimate the D_x, the Environment Agency (EA) equation (given in Equation 4.2) used in rivers (Guymer, 2002), and the Fischer's (1975) formula (Equation 2.30), have been applied. The estimated D_x coefficients are presented on the same plot (Figure 50). The EA and Fischer's (1975) estimates are overall in agreement with each other and with the D_x data of the stream. From the plot it is apparent that there is some scatter in the stream's tracer tests dataset. However, overall results are in accordance with the EA and Fischer's (1975) formulae.

$$D_x = 2.3014 \cdot Q^{0.6919} \qquad \text{Equation 4.2}$$

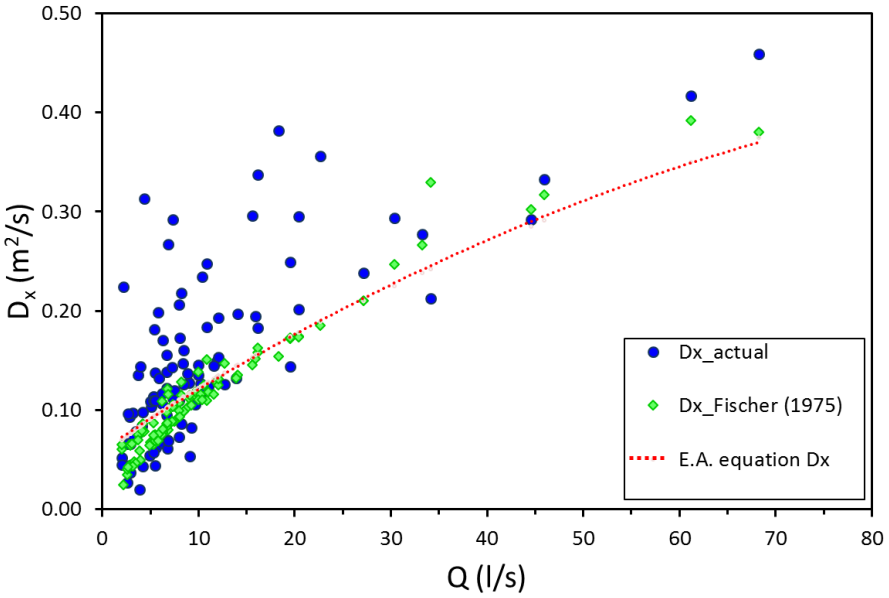

Figure 50: D_x against Q in the stream. The plot also shows the Fischer's (1975) formula and the EA database equation to estimate D_x in rivers.

Similarly, other empirical formulae that predict the D_x coefficient were also applied for the stream dataset, and in particular the formulae of Seo & Cheong (1998), and Kashefipour & Falconer (2002) (Chapter 2, Section 2.4.4.3). Nevertheless, both of those formulae overestimated considerably the predicted D_x coefficients for the stream of this study, results of which are depicted in Figure 51. In particular, those formulae produced twice to ten times larger D_x coefficients, with divergence increasing with Q (Figure 51). However, given that this study site has discharges many orders of magnitude lower than those studies, the difference is expected. This is because those empirical formulae derive from large river datasets obtained in the USA, in which greater secondary circulations and eddies occur due to the larger scale.

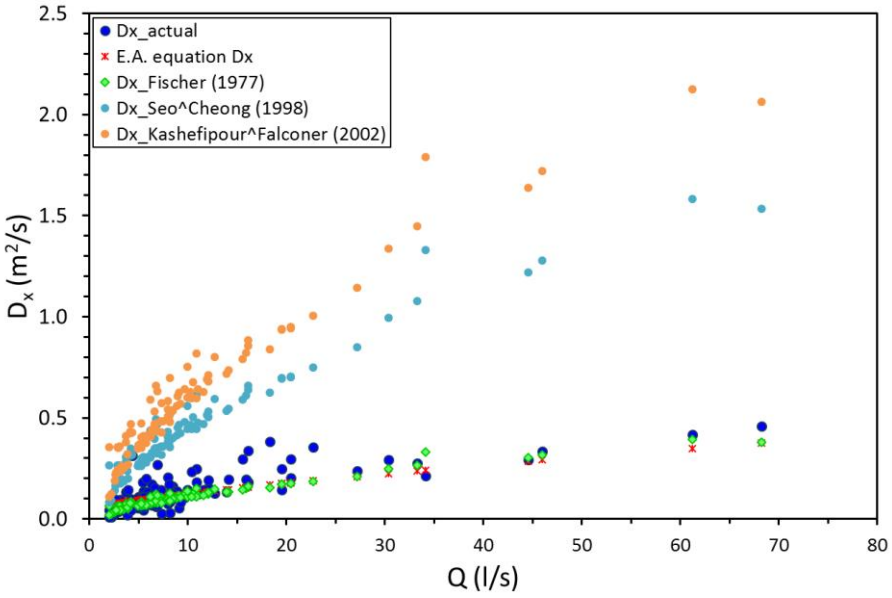

Figure 51: D_x against Q in the stream, incorporating other the D_x predicting formulae, i.e. EA database, Fisher's (1977), Seo & Cheong's (1998), Kashefipour & Falconer's (2002).

4.2SW1 _ South Wetland 1

This section presents and discusses the results for SW1, using the parameters derived from the tracer tests, and associating them with the vegetation characteristics, i.e. seasonal stem deflection. Tracer tests were continuous and covered a period of eight months, from November 2015 to June 2016. To assist the reader about the natural seasonal vegetation variation, a photographic record is provided in Section 3.3.1.1. Section 4.2.1 assembles results and discussion of the fluorescent tracing tests, and Section 4.2.2 compiles a summary of the main conclusions drawn in SW1.

4.2.1 Fluorescent tracing results

4.2.1.1 All tests collected

A total of 125 tracing tests were collected for this study site. The summary of these tests is presented in Table 4.1, assembling essential hydraulic parameters. First column of Table 4.1 determines the unique tracer test code, which consists of: a capital letter, determining the discharge classification (details are listed in bullet points as follows); an integer, which refers

to the month; a second integer, which refers to the test number in ascending order. The rest columns in Table 4.1 indicate the month, discharge, first arrival time of the tracer, HRT, nominal residence time, longitudinal dispersion coefficient, number of CSTR, hydraulic efficiency, and effective volume ratio respectively. For ease of presentation and comparison, the tracer tests were classified into discharge bands, as follows:

- Low Q: 0-5.0 l/s
- Moderate Q: 5.1-9.0 l/s
- High Q: 9.1-15.0 l/s
- Extreme Q: 15.1-45.0 l/s

Table 4.1: Summary of test series & transport parameters from the RTD analysis of the 125 tests in SW1.

Test unique code	*Month*	*Flow Rate regime*	*Flow rate, Q* (l/s)	*First arrival time,* t_1' (min)	*Travel time,* t_m (min)	*Nominal residence time,* t_n (min)	*Longitudinal Dispersion coefficient,* D_x (m^2/s)	*Number of CSTR, N*	*Hydraulic efficiency* λ (t_p/t_m)	*Effective volume ratio, e* (t_m/t_n)
L,11,1	Nov	Low	3.4	9.8	20.1	45.5	0.211	2	0.7	0.4
L,11,2	Nov		2.4	13.5	29.8	55.6	0.063	5	0.7	0.5
L,11,3	Nov		4.7	10.0	17.5	37.5	0.054	10	0.8	0.5
L,12,1	Dec		3.7	12.5	21.5	43.6	0.029	14	0.9	0.5
L,12,2	Dec		2.8	13.5	25.8	51.1	0.059	6	0.8	0.5
L,12,3	Dec		2.9	12.5	24.5	51.1	0.056	7	0.8	0.5
L,12,4	Dec		3.0	12.5	23.4	48.9	0.052	7	0.8	0.5
L,02,1	Feb		5.0	11.0	34.9	36.3	0.109	2	0.5	1.0
L,03,1	Mar		3.9	12.5	31.3	42.1	0.105	3	0.7	0.7
L,03,2	Mar		2.9	11.0	41.4	51.1	0.267	1	0.5	0.8
L,03,3	Mar		2.6	12.0	34.9	53.3	0.147	2	0.7	0.7
L,03,4	Mar		2.2	13.0	35.5	59.1	0.070	4	0.7	0.6
L,03,5	Mar		2.0	13.0	34.7	62.5	0.047	6	0.8	0.6
L,03,6	Mar		1.8	13.5	32.6	66.0	0.027	10	0.8	0.5
L,03,7	Mar		1.8	13.5	42.3	67.8	0.129	2	0.6	0.6
L,04,1	Apr		3.5	7.5	24.3	62.3	0.078	5	0.7	0.4
L,04,2	Apr		4.4	9.5	21.4	51.6	0.082	5	0.7	0.4
L,04,3	Apr		1.9	13.5	30.9	64.3	0.039	8	0.8	0.5
L,04,4	Apr		4.2	11.0	20.7	39.8	0.052	8	0.8	0.5
L,04,5	Apr		2.0	12.5	26.8	62.5	0.047	7	0.8	0.4
L,04,6	Apr		4.1	11.0	24.8	41.3	0.093	4	0.7	0.6
L,05,1	May		3.4	13.5	33.2	45.5	0.043	6	0.8	0.7
L,05,2	May		2.7	16.0	53.9	55.6	0.084	2	0.4	1.0
L,05,3	May		0.6	19.0	45.9	144.6	0.061	3	0.6	0.3
L,05,4	May		3.5	12.5	22.2	45.5	0.042	10	0.8	0.5
L,05,5	May		0.4	15.0	38.1	156.6	0.040	6	0.7	0.2
L,05,6	May		0.6	22.0	53.5	150.6	0.032	5	0.8	0.4
L,06,1	June		4.2	8.5	15.4	40.5	0.091	6	0.8	0.4
L,06,2	June		2.4	9.5	17.3	55.6	0.042	12	0.8	0.3
L,06,3	June		1.2	10.5	20.9	90.9	0.043	10	0.8	0.2
L,06,4	June		4.4	8.0	13.9	50.0	0.065	10	0.8	0.3
M,11,1	Nov	Moderate	5.9	9.3	18.5	33.7	0.200	2.5	0.7	0.5
M,11,2	Nov		6.8	9.0	17.2	31.7	0.187	2.8	0.7	0.5
M,11,3	Nov		8.9	8.7	17.0	28.4	0.208	2.6	0.7	0.6
M,11,4	Nov		7.8	7.8	17.4	30.0	0.391	1.3	0.6	0.6
M,11,5	Nov		8.2	8.5	18.5	29.3	0.300	1.6	0.6	0.6
M,11,6	Nov		7.7	9.0	15.7	30.0	0.096	6.0	0.8	0.5
M,11,7	Nov		8.0	8.8	14.4	29.7	0.068	9.2	0.8	0.5
M,12,1	Dec		9.0	9.0	14.4	28.2	0.065	9.7	0.9	0.5
M,12,2	Dec		8.0	9.5	15.8	29.7	0.080	7.2	0.8	0.5
M,12,3	Dec		7.3	9.5	16.1	30.7	0.074	7.6	0.8	0.5

M.12.4	Dec		6.6	10.0	16.7	32.0	0.078	7.0	0.8	0.5
M,02,1	Feb		6.6	9.5	24.2	32.0	0.163	2.3	0.6	0.8
M,02,2	Feb		7.5	7.5	23.1	30.7	0.152	2.6	0.6	0.8
M.02.3	Feb		6.6	9.0	23.6	32.0	0.180	2.1	0.6	0.7
M,02,4	Feb		8.0	8.5	19.9	29.7	0.164	2.8	0.7	0.7
M,02,5	Feb		8.5	8.5	19.4	29.0	0.154	3.0	0.7	0.7
M.02.6	Feb		5.3	11.0	32.3	35.4	0.110	2.6	0.5	0.9
M,02,7	Feb		5.5	10.5	31.7	35.0	0.109	2.6	0.5	0.9
M,02,8	Feb		5.6	11.0	37.3	34.5	0.091	2.7	0.5	1.1
M.02.9	Feb		8.0	9.5	19.1	29.7	0.101	4.7	0.7	0.6
M,02,1	Feb		8.1	9.0	21.4	29.3	0.140	3.0	0.7	0.7
M,02,1	Feb		6.8	10.0	23.9	31.7	0.129	2.9	0.6	0.8
M.02.1	Feb		5.4	11.5	35.2	35.4	0.167	1.5	0.5	1.0
M,02,1	Feb		5.5	9.5	34.0	35.0	0.113	2.4	0.6	1.0
M.03.1	Mar		5.3	10.0	25.5	35.4	0.108	3.3	0.7	0.7
M.03.2	Mar		8.2	8.0	18.6	29.0	0.123	3.9	0.8	0.6
M,03,3	Mar		7.3	8.5	22.6	30.7	0.212	1.9	0.7	0.7
M,03,4	Mar		8.7	7.5	14.8	30.1	0.052	11.9	0.9	0.5
M.03.5	Mar		6.2	8.5	21.0	38.9	0.174	2.5	0.8	0.5
M.03.6	Mar		5.8	9.0	23.7	41.0	0.334	1.1	0.7	0.6
M.04.1	Apr		8.6	6.5	15.9	30.4	0.313	1.8	0.7	0.5
M.04.2	Apr		8.3	7.5	13.9	31.1	0.088	7.4	0.8	0.4
M,04,3	Apr		7.0	7.5	13.7	35.4	0.080	8.3	0.8	0.4
M,04,4	Apr		6.8	8.5	18.4	36.4	0.121	4.1	0.7	0.5
M.04.5	Apr		6.0	8.5	18.2	39.9	0.119	4.2	0.7	0.5
M,04,6	Apr		5.5	9.0	18.4	42.9	0.066	7.5	0.7	0.4
M,04,7	Apr		8.2	8.0	15.8	29.3	0.156	3.7	0.8	0.5
M.04.8	Apr		6.9	8.5	17.3	31.7	0.118	4.4	0.8	0.5
M,06,1	June		9.0	6.5	11.3	28.2	0.155	5.2	0.8	0.4
M,06,2	June		5.5	7.5	12.8	35.0	0.098	7.3	0.8	0.4
H,11,1	Nov		10.5	8.0	13.3	26.3	0.092	7.4	0.8	0.5
H,11,2	Nov		9.4	8.3	15.9	27.6	0.241	2.4	0.7	0.6
H,11,3	Nov		11.0	7.2	14.5	25.8	0.378	1.7	0.7	0.6
H,12,1	Dec		10.5	8.0	13.2	26.3	0.059	11.5	0.9	0.5
H,12,2	Dec		9.7	8.5	14.2	27.3	0.071	9.0	0.8	0.5
H,12,3	Dec		9.1	10.5	16.9	27.9	0.036	15.0	0.9	0.6
H,02,1	Feb		11.9	7.5	15.2	24.9	0.151	4.0	0.8	0.6
H,02,2	Feb		10.2	8.0	17.6	26.5	0.198	2.6	0.7	0.7
H,02,3	Feb		11.0	7.5	16.8	25.8	0.222	2.4	0.7	0.7
H,02,4	Feb		14.1	7.0	15.4	23.3	0.206	2.9	0.7	0.7
H,02,5	Feb		10.0	8.0	18.7	27.1	0.151	3.2	0.6	0.7
H,02,6	Feb		10.4	8.0	20.5	26.5	0.180	2.5	0.6	0.8
H,02,7	Feb	High	12.7	8.0	19.3	24.3	0.211	2.2	0.6	0.8
H,02,8	Feb		9.3	9.0	17.4	27.9	0.065	8.0	0.8	0.6
H,03,1	Mar		13.9	8.5	15.9	23.3	0.142	4.0	0.8	0.7
H,03,2	Mar		12.9	6.5	18.8	24.0	0.429	1.1	0.5	0.8
H,03,3	Mar		11.3	7.0	17.6	25.4	0.277	1.9	0.7	0.7
H,03,4	Mar		13.6	6.0	10.0	21.7	0.111	8.1	0.8	0.5
H,03,5	Mar		11.9	6.0	10.8	23.9	0.117	7.2	0.8	0.5
H,03,6	Mar		10.7	6.5	11.1	25.8	0.092	8.8	0.9	0.4
H,04,1	Apr		9.7	6.5	11.6	27.8	0.085	9.2	0.8	0.4
H,04,2	Apr		10.8	6.5	12.2	25.5	0.136	5.5	0.8	0.5
H,04,3	Apr		9.1	6.5	12.9	29.1	0.157	4.5	0.8	0.4
H,04,4	Apr		9.4	7.0	14.3	28.4	0.148	4.3	0.7	0.5
H,04,5	Apr		10.0	7.0	13.2	27.1	0.087	7.9	0.8	0.5
E,11,1	Nov		23.6	6.3	12.0	18.9	0.366	2.1	0.7	0.6
E,11,2	Nov		17.7	6.3	12.7	21.2	0.430	1.7	0.7	0.6
E.12.1	Dec		20.4	7.0	11.7	20.1	0.073	10.6	0.9	0.6
E,12,2	Dec		17.5	7.5	12.6	21.4	0.063	11.3	0.8	0.6
E,12,3	Dec		16.1	7.5	13.1	22.0	0.091	7.7	0.8	0.6
E.12.4	Dec		20.4	7.0	12.1	20.1	0.057	13.1	0.8	0.6
E,12,5	Dec		18.7	7.0	12.7	20.8	0.094	7.6	0.8	0.6
E,12,6	Dec		15.9	7.5	14.0	22.2	0.101	6.4	0.8	0.6
E.02.1	Feb		33.3	5.5	10.8	16.5	0.232	3.6	0.8	0.7
E,02,2	Feb		27.4	5.5	12.3	17.8	0.395	1.9	0.8	0.7
E,02,3	Feb		22.7	6.5	13.6	19.1	0.159	4.2	0.8	0.7
E.02.4	Feb		19.6	6.5	14.9	20.3	0.151	4.0	0.7	0.7
E,02,5	Feb	Extreme	18.3	7.0	16.4	20.9	0.299	1.8	0.7	0.8
E,02,6	Feb		15.6	7.5	18.4	22.4	0.237	2.1	0.6	0.8
E.03.1	Mar		19.6	7.0	12.4	20.3	0.100	7.3	0.8	0.6
E,03,2	Mar		30.4	6.0	10.6	17.0	0.124	6.9	0.8	0.6
E,03,3	Mar		68.2	4.5	8.5	13.7	0.279	3.8	0.8	0.6
E,03,4	Mar		44.6	5.0	9.2	15.2	0.129	7.6	0.9	0.6
E.03.5	Mar		62.1	4.5	8.5	14.0	0.153	7.0	0.9	0.6
E,03,6	Mar		18.5	7.0	13.3	17.4	0.119	5.7	0.8	0.8
E,03,7	Mar		16.1	6.0	12.3	19.2	0.188	3.9	0.7	0.6

E.03.8	Mar		44.9	4.0	7.5	9.8	0.115	10.5	0.9	0.8
E,03,9	Mar		27.7	5.0	8.6	13.3	0.114	9.3	0.8	0.6
E,03,10	Mar		24.1	5.0	8.8	14.5	0.134	7.7	0.9	0.6
E.03.11	Mar		19.1	5.0	11.4	17.0	0.479	1.7	0.7	0.7
E,03,12	Mar		15.7	5.5	9.5	19.5	0.075	12.8	0.8	0.5
E,04,1	Apr		34.2	5.0	7.7	16.3	0.054	22.0	0.9	0.5
E,06,1	June		16.5	5.5	9.0	21.9	0.094	10.7	0.9	0.4
E,06,2	June		17.7	4.0	8.1	21.2	0.343	3.3	0.9	0.4

4.2.1.2 Analysis of measured concentration profiles RTDs

This section presents the effects of seasonal plant variation and discharge on flow structure and mixing. RTDs of similar discharge categories were selected from the database of the available tests (see Table 4.1), and are presented in Figure 52. The tests are selected for a range of flow conditions, from low to extreme. Figure 52 evidences a consistent effect of plant age on all flow conditions, where, based on the month, stem morphology (i.e. deflection), and plant friction, seasonal plant variation influences the HRT, the flow pattern and the mixing characteristics (details are presented in Figure 52 (a)-(d)). Note that detailed plots assembling the aggregate of the tracer tests are presented in Appendix II. Difficulties and shortcomings were encountered during the data collection over the 8-month monitoring period, pertaining to lack of data acquisition in January due to attack by rodents on cables.

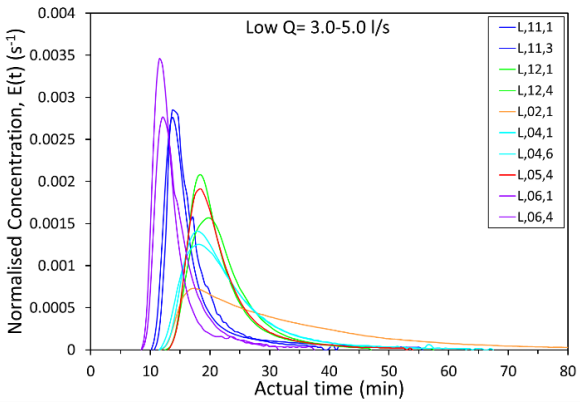

(a) Low Discharge Band, i.e. 3.0-5.0 l/s.

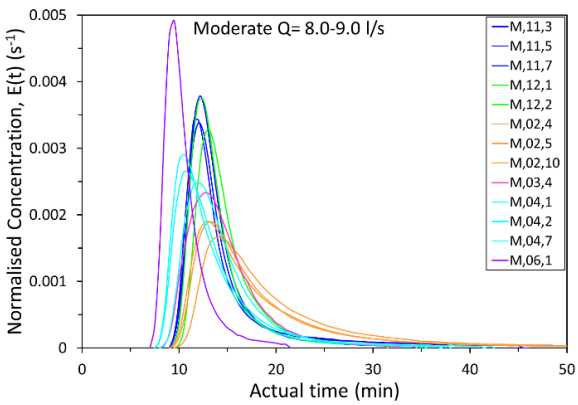

(b) Moderate Discharge Band, i.e. 8.0-9.0 l/s.

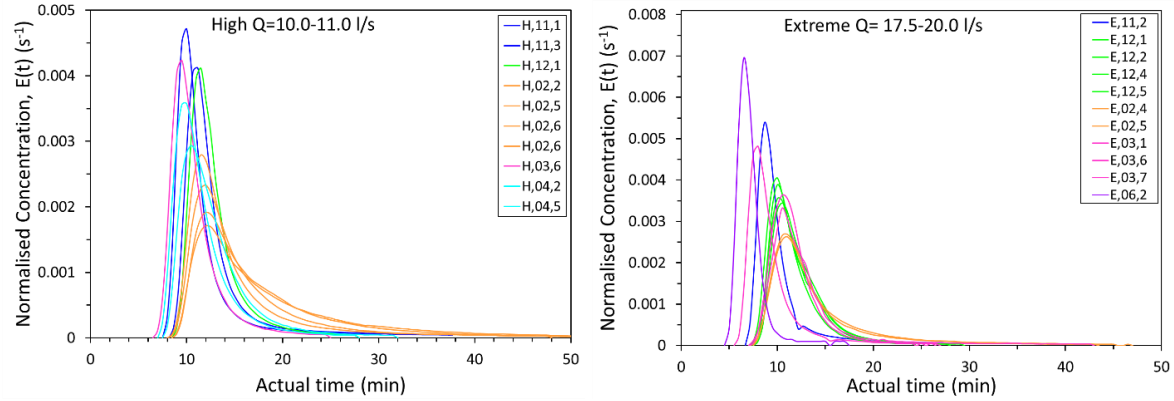

(c) High Discharge Band, i.e. 10.0-11.0 l/s.

(d) Extreme Discharge Band, i.e. 17.5-20.0 l/s.

Figure 52: RTDs for similar discharge in different months. Different flow bands expand from Low (a) to Extreme (d), showing the seasonal plant variation effect. Concentration on y axis is normalised by the M_0. RTDs demonstrated strong affinity of late dormant season on the flow and mixing regime compared to the growth season, at all discharges. Furthermore, there is a consistent effect of discharge on the RTD shape.

Concerning the seasonal plant variation effects on flow structure, low plant age (i.e. June) exhibits shorter travel times and promotes plug flow with minimal longitudinal dispersion, whilst high plant ages (i.e. February, March) present flow retardation and longer distribution tails. Seasonal plant variation affects the mixing pattern, which combines plug flow and backmixing (dead zones), where predominantly in high plant ages (i.e. February and March), flow structure experiences a large quantity of dead regions. This is because beyond November stems decay progressively, and bend over, deflect and nest in clusters, thus altering the channel porosity, flow velocity, and mixing characteristics.

The general mixing pattern shown in Figure 52, suggests that advection process dominates the flow in November and in June, while in February flow profile tends toward stagnant backwater flow conditions. As a result, regardless the discharge variation, dispersion levels and contaminant spread are lower in June, followed by November and December, whereas greater dispersion and pollutant dilution is achieved in February. This happens because of the smaller channel porosity caused by deflected stems, which in turn induces more obstructed flow and complexity of transit paths. As such, the tracer/pollutant passing through the wetland in February requires more time to be released back to the main flow, due to being trapped in zones of lower flow velocity, compared to June or November.

Figure 53 demonstrates the effect of discharge variation on the flow structure and on dispersion levels, spanning between low and extreme flows. Furthermore, Figure 53 incorporates the effect of season, contrasting the two extremes of plant age, namely June (i.e. growth season) and February (i.e. dormant season). It is noticed that larger discharge entails lower spread and dispersion, and shorter distribution tails. For either plant season, increase in discharge affects the flow pattern, which changes from plug flow with stagnant backwaters into plug flow. Therefore, elevated discharges promote more advective flow in the system, minimising the occurrence of dead zones occurrence, due to the shorter distribution tails.

Overall, variation in plant porosity between the growth and the dormant season is a result of the variation of stem deflection, which ultimately affects both the flow pattern and the potential of reducing pollutant peak concentrations in FWS CWs. Looking at Figure 53 for a similar discharge, i.e. 18 l/s, the mixing characteristics differ in the late dormant season (i.e. February), when the wetland experiences greater pollutant spreading, and greater attenuation of pollutant peak concentration. It is evident that in the late dormant season, i.e. February, achieve reduction of the peak concentration by up to three times, compared to the growth season, i.e. June, as seen in Figure 53, e.g. C_{peak} for same flow rates (i.e. 18 l/s or 5.5 l/s) in different seasons.

Summarising, in all flow cases, the governing flow pattern is plug flow with dead zones (as expressed by the long trailing edges); however, the degree of dead zones is a combined effect both of discharge, but mainly of plant season. Noticeably, lower discharges, result in more dead zones. This is explained by the fact that in laminar flows (i.e. low discharge band), diffusion (which is a slow process) is the dominant process for solute spreading, and allows for more interaction and longer contact times within the system due to differential advection (see Figure 67). In addition to this, during the late dormant season, i.e. February, there are additional effects of the tracer moving through the clumps of vegetation, allowing the chemical to be trapped in the clusters of vegetation requiring longer time to be released back to the main flow at lower discharges. However, as flow rate increases, more turbulence

is caused, which seems to outweigh the seasonal vegetation variation influence on flow profile and mixing processes.

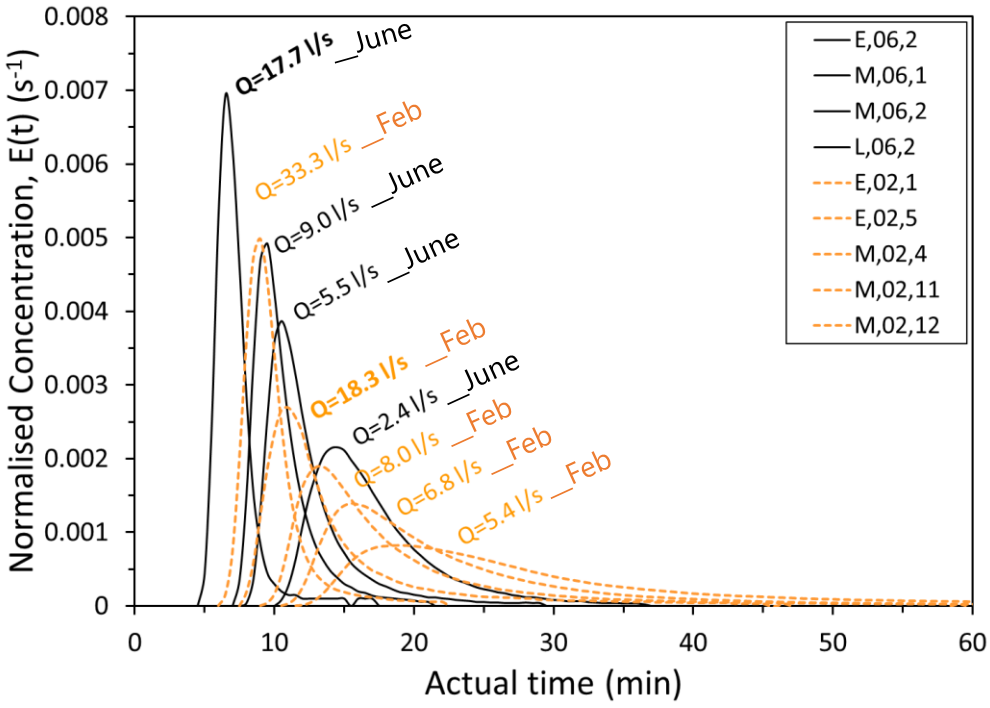

Figure 53: Effect of discharge on flow structure and dispersion between two contrasting plant ages, February (i.e. late dormant season) and June (i.e. growth season). reduction of the peak concentration is achieved by up to three times in the late dormant season, i.e. February, compared to the growth season, i.e. June, for fixed discharge (e.g. 5.5 l/s or 18 l/s).

Comparing the changes between t_m and C_{peak}, it is demonstrated that seasonal vegetation variation (i.e. upright versus deflected stems) plays a significant role in altering the flow pattern from plug flow towards CSTR. This conclusion can also be drawn from Figure 54, where the N represents the degree of mixing of the tracer or pollutant. Values of N close to 1 entail CSTR flow, thus greater dispersion, whilst N values closer to ∞, entail plug flow. Although there is some scatter in the data presented in Figure 54, it is seen that increase in Q promotes increase in N. In addition to this, Figure 54 suggests clear seasonal trends between the two extremes of plant porosities (i.e. between June and February). Thus, there is some dependence of N with season. It is inferred that variation in plant porosity (as a change in stems position due to seasonal growth and decay) plays a more important role in changing the flow pattern in FWS CWs than variation in discharge (or flow velocity). Similar

observation was reported by Chyan et al (2014), conducting a small-scale laboratory model test.

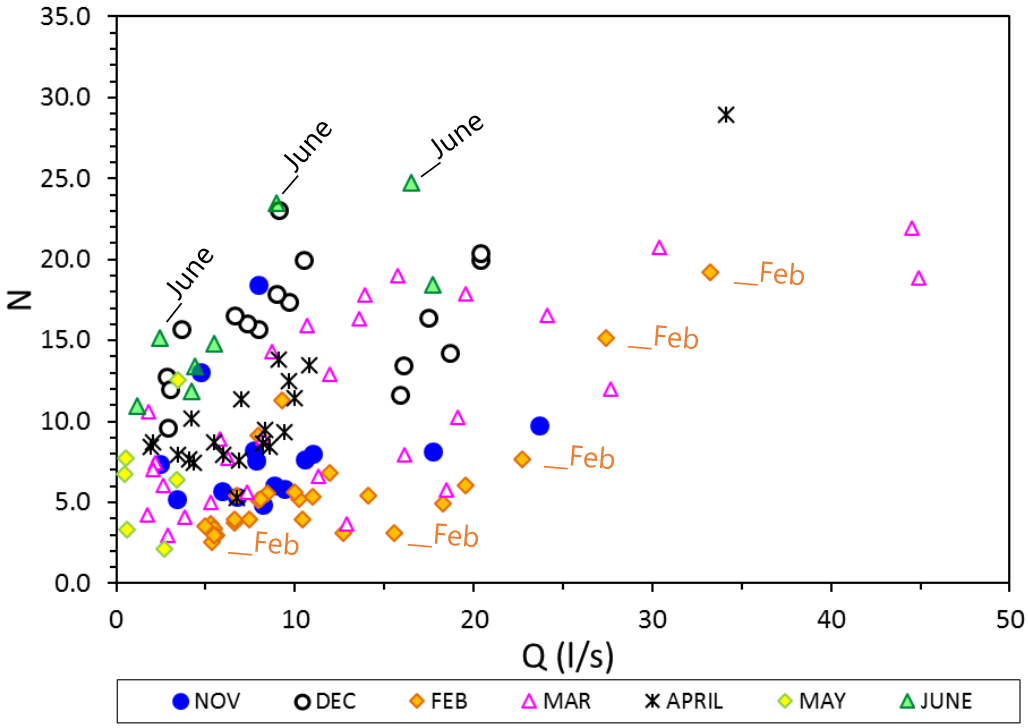

Figure 54: Variations in the number of CSTRs being affected by different flow velocities, and referring to various seasons/plant porosities. Plant season (i.e. growth versus dormant) plays a significant role in altering the flow pattern from plug flow towards CSTR. It is inferred that seasonal plant variation between the two extremes plays a more important role in changing the flow pattern in FWS CWs than discharge.

In summary, the effects of discharge and seasonal plant variation on the mixing pattern and hydraulics were presented and discussed in this section. It was demonstrated that seasonal plant variation retards the flow mainly in higher plant ages, and influences the mixing pattern especially at lower discharges. In particular, gradual increase in discharge, alters the mixing pattern from plug flow with stagnant regions, into plug with some longitudinal dispersion. Considering seasonal plant variation, late dormant stage, i.e. February, achieves more reduction in peak concentration.

4.2.1.3 Cumulative Residence Time Distribution (CRTDs)

This section presents the effects of seasonal plant variation and discharge variation on flow structure using CRTD curves. The corresponding CRTDs of the previously illustrated RTDs in

Figure 52, are now presented in Figure 55 for similar discharges, ranging from low to extreme flow bands. The CRTDs are plotted against actual time and against normalised time side by side for different flow classifications (Figure 55 (a)-(d)).

In order to create a general level of comparison for the obtained data and existing studies, time was normalised by t_n. An assortment of the summation of the individual CRTDs at actual and normalised time can be found in Appendix II.

Discharge has a direct effect on the HRT, short-circuiting and mixing (see left side Figure 55). As the discharge increases, the CRTDs obtain gradually shorter tails and rise more steeply. Considering the seasonal effect, at normalised time, CRTD curves collapse into two main bands, i.e. February (high plant age) and the rest months, whilst June exhibits a third individual trend itself (Figure 55 right side). February's CRTD is distinctly different, indicating large quantities of dead water in the wetland. This effect is directly associated with the clusters of deflected stems, reducing the channel porosity. At the other extreme plant condition in June (i.e. zero stem deflection), flow pattern behaves like pipe flow with some longitudinal mixing, as a result of larger channel porosity. Furthermore, as the flow rate increases, the influence of plant age is lesser, with all the CRTDs ranging into a narrower band, except for June CRTD, which remains individual, entailing promotion of higher levels of short-circuited flows (Figure 55 right side).

Concerning the CRTDs plotted at actual time, the effect of plant season exhibits a distinct change in shape, especially ranging between the two plant age extremes (June and February). Furthermore, CRTDs show evidence of variation in mixing characteristics both due to seasonal plant variation and due to flow rate variation (left side Figure 55).

In all discharge classifications, CRTD curves suggest a system where water passes fast through a main channel and allows for some longitudinal mixing during moderate plant ages (i.e. November – December), and during early plant ages (i.e. April, May). Interestingly, the mixing pattern alters as reaching the highest plant age (i.e. February, March), suggesting plug flow with large quantities of dead zones. This is attributed to the fully deflected stems (see Figure 31) occurring at the end of the annual plant cycle, involving nesting, resistance

add-on, and creation of more pockets for mixing and dilution. Furthermore, it is noticed that regardless of the flow rate variation, CRTDs in February project invariably longer tails. The same mixing mechanism is also observed in November and March, albeit of shorter trailing edges.

However, CRTDs in December, and post-March months exhibit comparable distribution tails independently of the discharge band, while their flow regime resembles pipe flow with some longitudinal mixing. The degree of longitudinal mixing gradually decreases closer to June for all flow conditions, and advection levels (i.e. pipe flow) outweigh. This behaviour is attributed to lower stem resistance, due to the upright stem morphology occurring in June.

In what follows, the affinity of plant cycle growth with the flow resistance is described in more detail. March is the end of the annual plant cycle for the Phragmites in this micro-climate, and involves deflected withered stems that are subject to continuous decomposition. April is the typical start of the new plant growth season; however, as there are remaining old stems, April can be described as a transition stage between the ongoing decomposition of the dead plant material, and the gradual growth of new stems (Figure 30). Stem population density shows gradual increase in May, as new budding stems appear. Newly grown stems are well-established in June, when wetland bed is almost clear from the recently decomposed plant material. The results of this process are directly related to the properties of the newly developed stems. Each stem resembles a bare cylinder of small diameter, while stem density per unit area is sparse; thus, none of these components promotes high vegetation drag. This explains why first arrival times shorten gradually from April to June, and why fast flow paths (short-circuiting) are essentially promoted during those months (low plant ages). The above results support the main hypothesis that seasonal plant variation influences the mixing characteristics, due to variation in stem morphology (in terms of deflection).

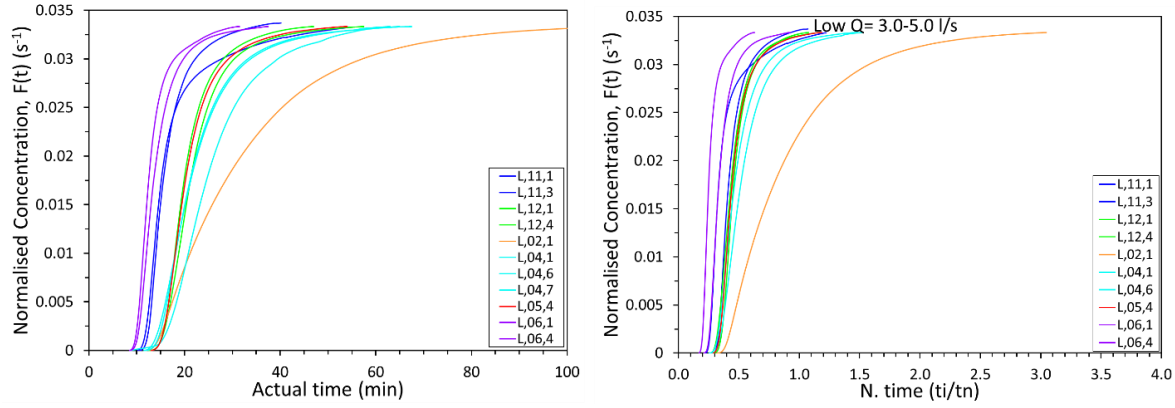

(a) Low Q = 3.0-5.0 l/s

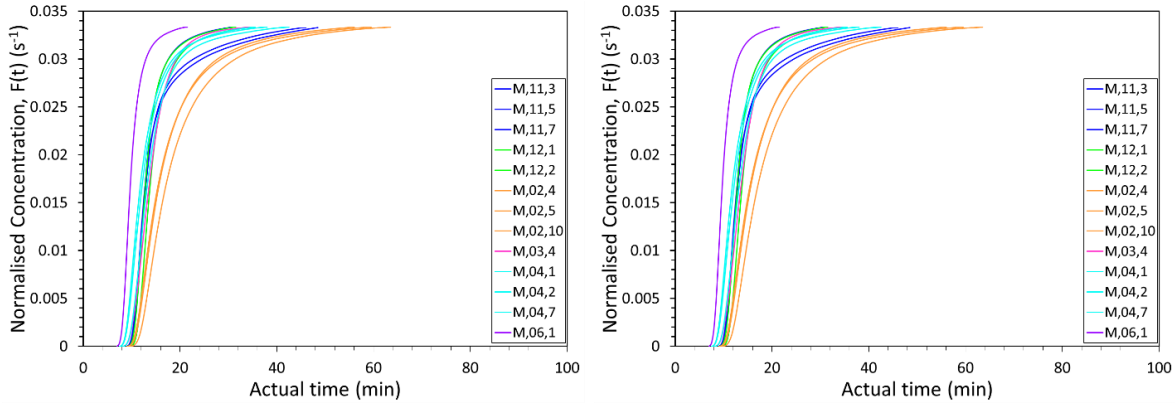

(b) Moderate Q = 8.0-9.0 l/s

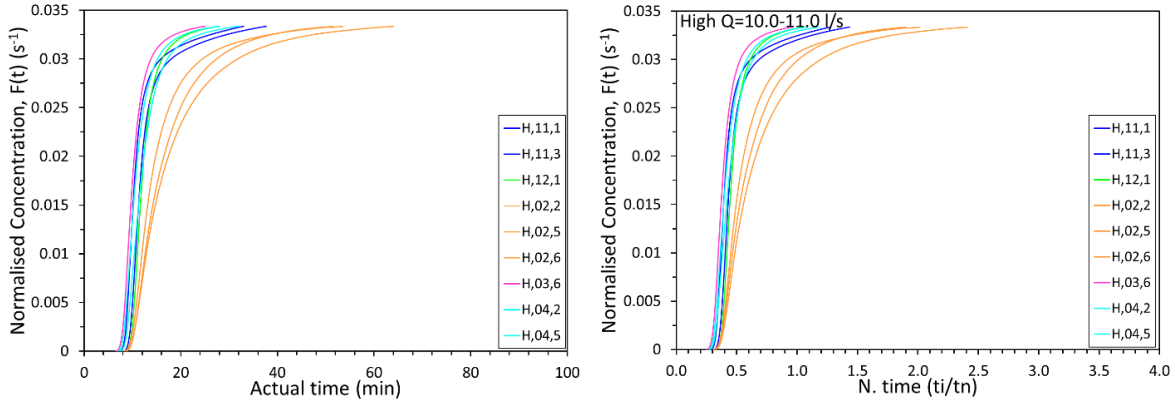

(c) High Q = 10.0-11.0 l/s

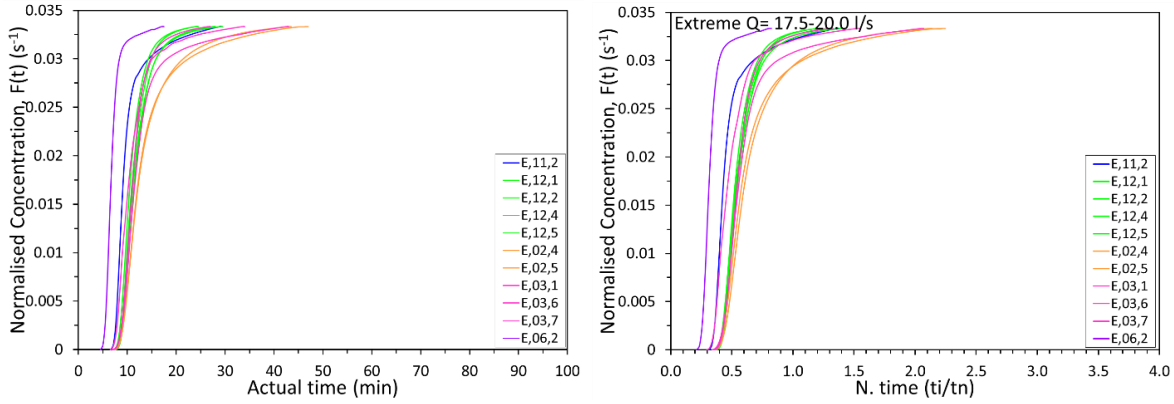

(d) Extreme Q = 17.5-20.0 l/s

Figure 55: Dimensionless CRTD curves for the different flow rate classifications, presented side by side as actual time (on the left side) and normalised time by t_m (on the right side). The flow regime follows the order from Low to Extreme, for certain discharge classifications to allow ease of comparison. CRTD curves demonstrate a strong affinity of plant season with HRT and mixing regime, most prevalent in the dormant season, and at low discharges. Furthermore, CRTDs demonstrate the consistent effect of discharge on mixing regime and HRT.

Furthermore, the CRTD curves give an indication of the short-circuiting degree in the system. This can be inferred from the CRTD plots looking at the point where the steep inclination stops. The short-circuiting increases with increase in discharge, as seen in Figure 55, although the flow is generally highly short-circuited even at low discharges. However, it is important to note that short-circuiting shows a clear dependence on the plant age. At moderate and low plant ages, i.e. December, March-June respectively, the CRTDs curves rise steeply initially, and then change their direction projecting short tails, whose length is predominantly dependent on the flow rate. At those plant ages, flow is short-circuited at values almost always greater than 0.03 (s^{-1}) of the F(t) function. This suggests that more than 85% of the concentration mass of the tracer is short-circuited through the wetland as a straight jet, whereas a small amount of dispersion occurs, as inferred from the short remaining trailing edges. The greatest short-circuited flow is observed particularly in June, when the CRTD curves follow essentially a steep line with a slight short tail. This advocates that in June, tracer passes by the wetland, independently of the discharge, allowing only for minimal dispersion to take place.

Interestingly, at high plant age, i.e. February, the CRTD curves display milder incline, more pronouncedly though at lower discharges. Depending on the discharge, flow in February is

short-circuited at values between 0.015 and 0.025 (s^{-1}) of the F(t) function. Therefore, it is inferred that 40% to 70% of the tracer mass passes by the wetland at low and at extreme flows respectively, whereas the remainder of the tails contribute to longitudinal mixing. Such prolonged tails suggest tracer capture in the clusters of the withered and nested stems, and evidence flow retardation, and tracer trapping in dead zones. In particular, at the low Q band (Figure 55 (a)), flow experiences a big quantity of dead zones. As discharge increases though, flow in the system continues experiencing stagnant backwaters, albeit of lower degree.

It should be noted, that although there were no tests recorded in January due to technical equipment issues (rodents damaged some cables of data transmission-collection), the available results (listed in Table 4.1) describe the overall effects of flow and seasonal plant variation on the mixing and flow, and support the main hypothesis of this thesis (presented in Chapter 1) about seasonal plant variation effect.

At normalised time, CRTDs are divided into two distinct groups, with most months collapsing into one band, and with the extremes of plant age (i.e. February and June) displaying more variation. A comparison of the CRTDs among different discharges proposes that there is less dependence on flow rate compared to plant age (Figure 55 (a)–(d)). February demonstrates an apparent difference which is reflected on the mixing characteristics (i.e. stagnant regions, longer trailing edges, thus more longitudinal mixing), and on the flow properties (i.e. retardation of first arrival time, longer HRTs). As mentioned previously, June exhibits a consistent distinct mixing pattern compared to the other months.

Summarising, this wetland displays a significant variation in the mixing regime and flow pattern at the highest plant age, with more intense signs at low flows. Seasonal plant variation, explained through the stem deflection, alters the flow pattern from plug flow with some longitudinal mixing, into stagnant backwaters. Comparing this finding with similar or larger size systems, analogous effects should be anticipated on mixing and flow characteristics. In addition to this, HRT and reduction in C_{peak} should be expected to be much greater in CWs operating under laminar flow conditions. Overall, the corresponding effects in other wetlands might be escalated, because the majority of the controlled CW systems

operate at laminar flows, and frequently at flow rates much lower than the lowest discharges of this study.

4.2.1.4 HRT

The effects of seasonal vegetation variation and discharge on the HRT are shown in Figure 56, which illustrates the mean residence time, t_m, against flow rate. On the same plot, the theoretical (or nominal) residence time curve, t_n, is presented for the non-deflected stems, based on the plant porosity, estimated in Chapter 3. It is observed that the upright stem conditions, albeit incorporated in the volume calculation, has a negligible impact on the channel porosity.

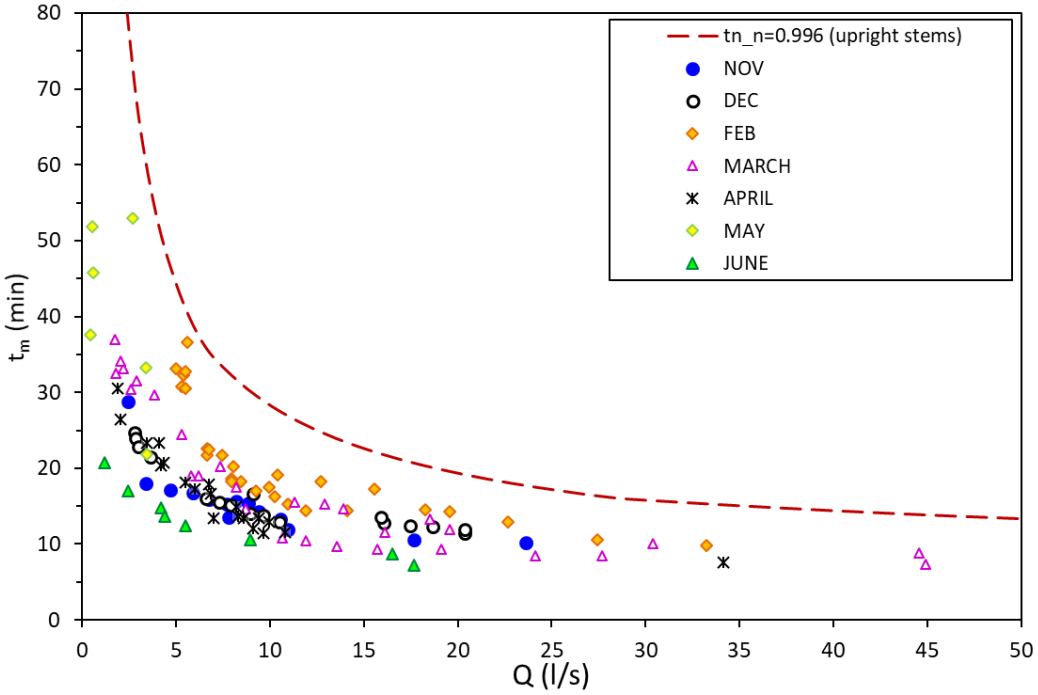

Figure 56: Mean residence time against discharge for the total monitoring period. The plot also shows the nominal residence time curve. Effects of seasonal variations in vegetation are overt on the HRTs and the flow resistance, especially between the late dormant season (i.e. February) and the growth season.

The effect of discharge on the HRT has a typical inverse relationship. Results suggest that seasonal plant variation affects the HRT and the short-circuiting. Late plant dormant stages (i.e. February, March) result in larger HRTs, compared with growth plant stages (i.e. November, June). Stem resistance in the wetland increases with the deflection of plants as a

result of their ageing. Furthermore, it is observed that short-circuiting is greater in the growth season (i.e. November, June). Typically, larger deviation of the measured t_m values from the theoretical retention time curve, t_n, entails shorter retention time of the tracer in the wetland, hence flow through preferential paths.

Deflected stems toward the end of plant cycle (i.e. February, March) are expected to undergo two distinct flow conditions: emergent flow for low discharges, and particularly submerged flow for greater discharges. In the emergent flow, vegetation resistance is larger, retarding the flow. This is observed in Figure 56, where the February and March tracer tests for Q<7 l/s show a distinct difference in t_m, which is over 30 min. However, increase in discharge, increases the flow depth, and flow condition becomes progressively submerged (see Figure 31 (b)). Observing February and March for similar discharges, March presents shorter HRTs, although stems are still deflected. The fact that stems gradually further decompose in March, may decrease their total area, allowing the flow to move more easily through them. Furthermore, the more intense seasonal plant variation effect on flow structure in dormant season, combined with the local boundary effects, promote differential velocity in the lateral direction, where adjacent layers have slow speed due to plant resistance, while other adjacent layers much faster speed. This explains further results in Figure 56, between the two extremes of vegetation age.

4.2.1.5 Mean velocity profiles

This section presents the results of the flow resistance under the seasonal vegetation variation and natural ageing. As detailed in Chapter 3, Section 3.2.2, two main porosities were investigated: one accounting for upright stems (from April to January), thus emergent flow conditions, and one accounting for fully deflected stems (from February to March), where depending on the flow depth, flow condition varies between emergent and submerged (see Figure 31 (a)-(b)). Figure 57 displays the measurements of the average velocity, u_{mean}, in different reeds ages, namely middle (i.e. November), high (i.e. March), and low (i.e. June). The u_{mean} is calculated as the ratio of longitudinal distance over time, where

the longitudinal distance is fixed (i.e. between injection point and outlet fluorometer point), and time is the HRT (or t_m) obtained through the tracer test.

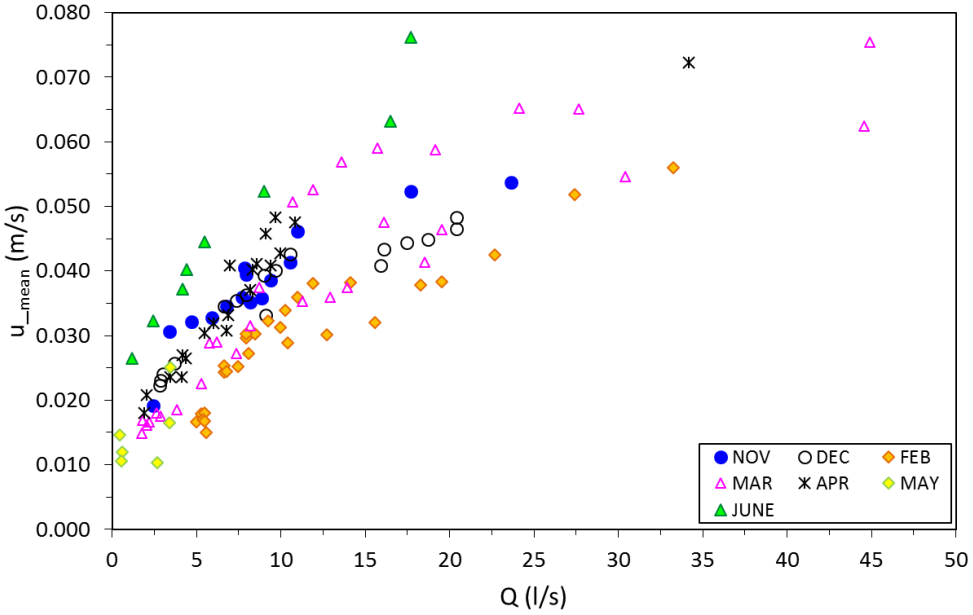

Figure 57: Mean water velocity against discharge in SW1 in different reeds ages. There is a distinct effect of the late dormant season on the flow velocity compared to the growth season (i.e. June).

Flow velocity increases with flow rate, although at a different slope in each month. Flow velocity increases at a lower rate in dormant season (i.e. February, March) and demonstrates retardation when channel resistance is larger, because of the clusters of deflected stems due to natural ageing. As opposed to this phenomenon, flow speed accelerates in June (i.e. growth season), finding less resistance because of the upright stems' morphology. Overall, Figure 57 demonstrates that flow velocity is more flow dominated in growth season (i.e. June – November), whilst flow velocity becomes more vegetation dominated at highest ages, as pinpointed by the curved shape obtained in February.

4.2.1.6 Longitudinal dispersion measurement

This section presents the effects of discharge and seasonal plant variation on the longitudinal dispersion coefficient, D_x and on the dispersive fraction, D_f. Moreover, further relationships between the mixing characteristics, i.e. D_x, D_f, N, and other hydrodynamic parameters, i.e.

stem Reynolds number, NR^*, effective volume ratio, e, hydraulic efficiency, λ, are presented and discussed.

Effect of Flow Depth and Discharge on Mixing

In order to observe any total trends of the water depth and discharge on mixing, Figure 58 to Figure 62 present the aggregate of dispersion coefficients, D_x, and dispersive fractions, D_f, against discharge and flow depth.

The influence of discharge on the longitudinal dispersion is shown in Figure 58 for all seasons, and in Figure 59 indicating each month (thus plant age). Figure 58 also presents the predicted D_x values using Equation 2.42 by Etemad-Shahidi & Taghipour (2012), irrespective of the B/h condition recommended. The stream sinuosity factor included in Equation 2.42 was assumed unity for the wetland (thus zero sinuosity). This adapted formula, showed the closest match as applied to the current dataset, and compared to the other formulae presented in Section 2.4.5.3 (i.e. Equation 2.31-Equation 2.35, and Equation 2.38). The adapted Etemad-Shahidi & Taghipour (2012) formula provides predicted D_x values much lower for the low discharges compared to the actual D_x obtained; however, this is reasonable because that formula does not account for dead zones and vegetation effects.

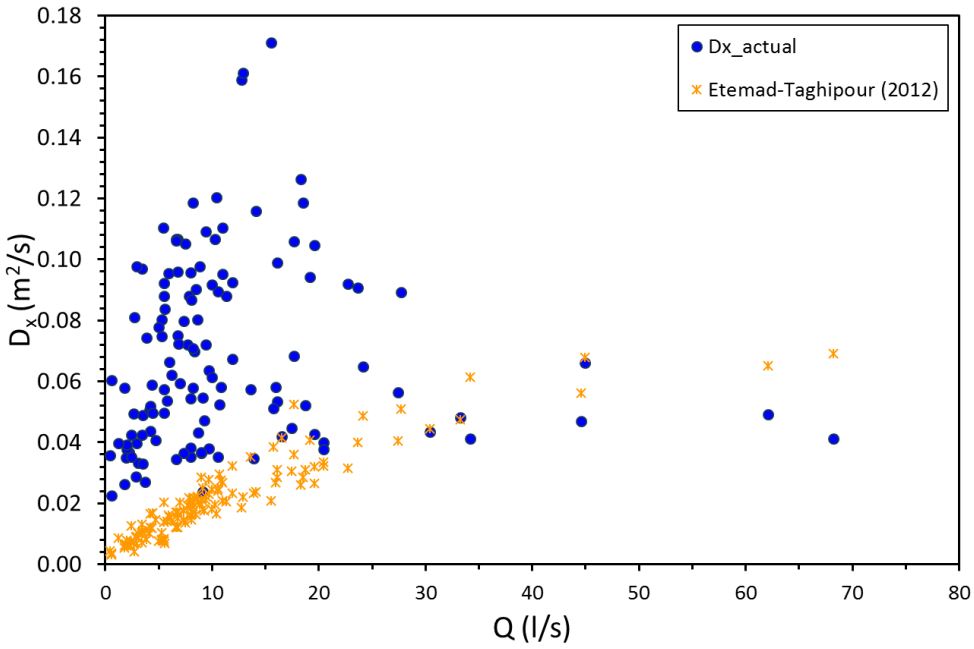

Figure 58: Measured D_x against Q in SW1 in all seasons. Predicted D_x is presented using Etemad-Shahidi & Taghipour (2012) formula. The adapted Etemad-Shahidi & Taghipour (2012) formula provides predicted D_x values much lower for the low discharges compared to the actual D_x obtained, which is attributed to the fact this formula does not account for dead zones and vegetation effects.

Results in Figure 59 show an overall increase in D_x with flow rate, in an approximately linear relationship, almost for each individual monthly dataset. The approximate proportional relationship between D_x and Q varies with month. For instance, the proportional gradient is steepest in February and November, experiencing highest D_x values compared with similar discharges of other months.

Recalling the plant cycle and natural stems ageing processes, described in Section 4.2.1 to assist explaining the results, November experiences stem foliage drop, which might create clusters of mixed foliage travelling in the wetland. In this case, the tracer may encounter some dead regions, as demonstrated by the relatively long trailing edges in Figure 52 and Figure 55. Interestingly, December presents the mildest incline and lowest D_x values. December D_x values remain low and follow a consistent analogy with flow rate. This result is related to the bare cylindrical stems (i.e. no foliage on stems), and infers that foliage resistance is trivial during this month. The large D_x values obtained in February are attributed to the dead zones promoted due to the clusters of the deflected stems (i.e. reduced channel

porosity). Furthermore, large D_x values in February are a result of the long trailing edges of the RTDs, which are reported to increase the D_x (Rutherford, 1994).

March D_x values present a wider scatter compared to other months, albeit they overall follow a mild inclination, and they stay generally lower than February D_x values. However, as described in section 4.2.2.5, the ongoing decomposition of deflected stems taking place in March (as the last month of the annual plant cycle), as well as other random natural factors, including wind action which promotes deposition of the whole or parts of the reed stems, and stem debris deposition, may drastically contribute to the variation in the D_x levels, altering the local flow paths and dead water areas. A combination of those uncontrolled outdoor factors, possibly promotes the tracer to follow different paths within the wetland, as relocation and deposition of the decomposing deflected plant material takes place.

Referring to the new plant cycle, low plant ages, namely April, May and June, display overall lower D_x values. Nevertheless, April experiences higher D_x coefficients compared to June, as a result of the fraction of the remaining stems, ongoing decomposition. As time passes though, decomposition of remaining old stems is completed, and thus the stem population density reduces and the channel porosity increases. Such decrease in D_x is sensible and is reported by Nepf et al (1997), who observed a reduction of D_x with stem population density.

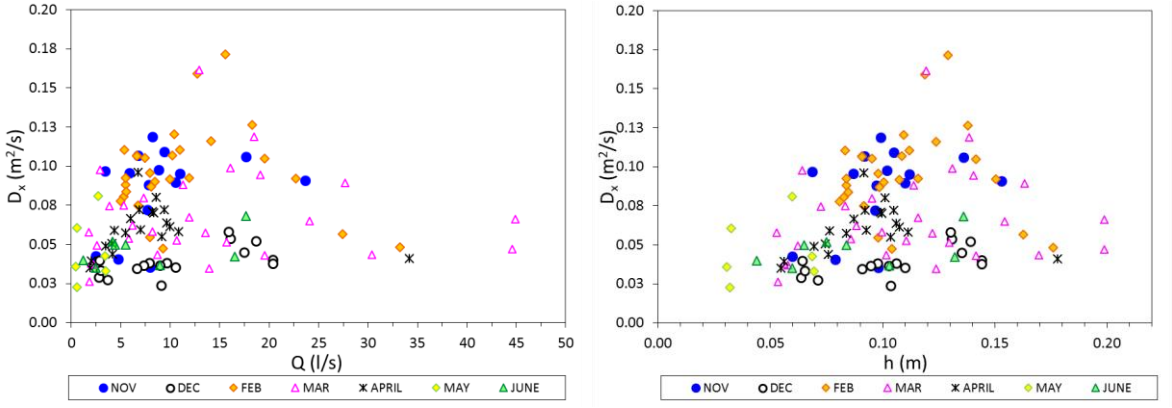

(a) D_x against Q in different plant seasons.

(a) D_x against h in different plant seasons.

Figure 59: (a) Relationship between longitudinal dispersion coefficient, D_x, and flow rate, Q, for different plant ages. Flow regime is plant dominated toward the late dormant season, whilst it becomes discharge dominated during the growth season. (b) Longitudinal dispersion coefficient against flow depth, h, in different seasons. There

is a distinct change in the D_x-h correlation beyond a certain h value (i.e. 0.13-0.14m), beyond which correlation becomes negative.

Figure 59 (a) suggests that D_x increases with flow rate and depth. Furthermore, it is noticed that there is a relationship between D_x and Q for each month, which is initially increasing, and which turns into descending beyond a certain Q value. Similar observations are observed for the flow depth in Figure 59 (b), where the correlation becomes negative between h=0.13 and 0.14 m (depending on the month). This phenomenon is attributed to the resistance of stems on the flow; in particular, in low flow velocity (and depths), internal hydraulics are vegetation dominated, whilst in high flow velocities/depths, internal hydraulics are flow dominated.

Figure 60 illustrates the normalised D_x coefficients obtained in different seasons. The effect of seasonal plant variation is apparent, particularly between the two extremes of plant ages (or deflection). Furthermore, the effect of discharge is apparent, where lower Q entails greater longitudinal mixing. This is most possibly attributed to the larger differential advection occurring at lower discharges. Another way to non-dimensionalise the dispersion coefficient is by using the mean channel width, W, instead of the flow depth, h, as illustrated in Figure 61. This is considered a reasonable approach, because transverse velocity shear has larger influence on D_x in natural channels compared to vertical velocity shear (Rutherford, 1994).

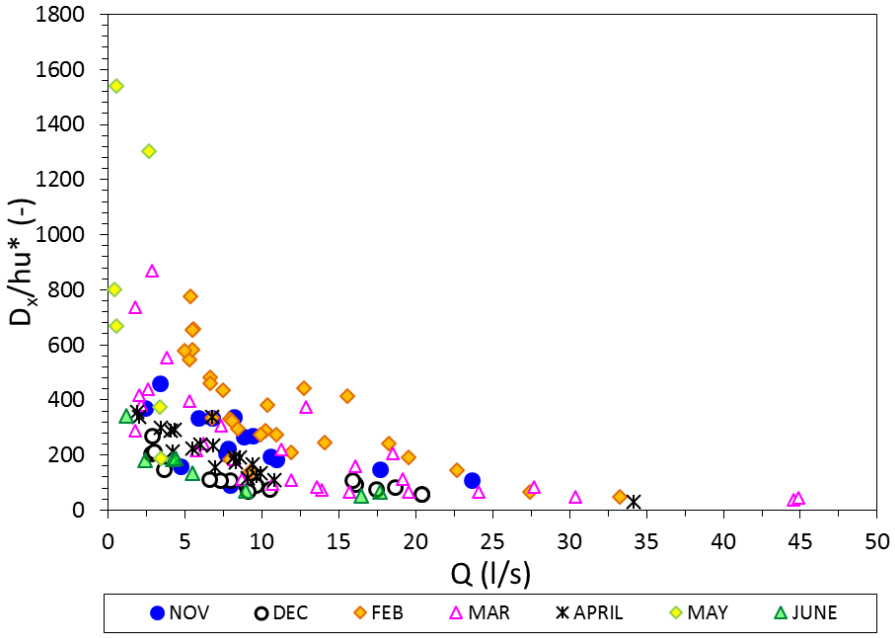

Figure 60: Variation of the non-dimensional longitudinal dispersion coefficient D_x/hu* against discharge in SW1 for each month.

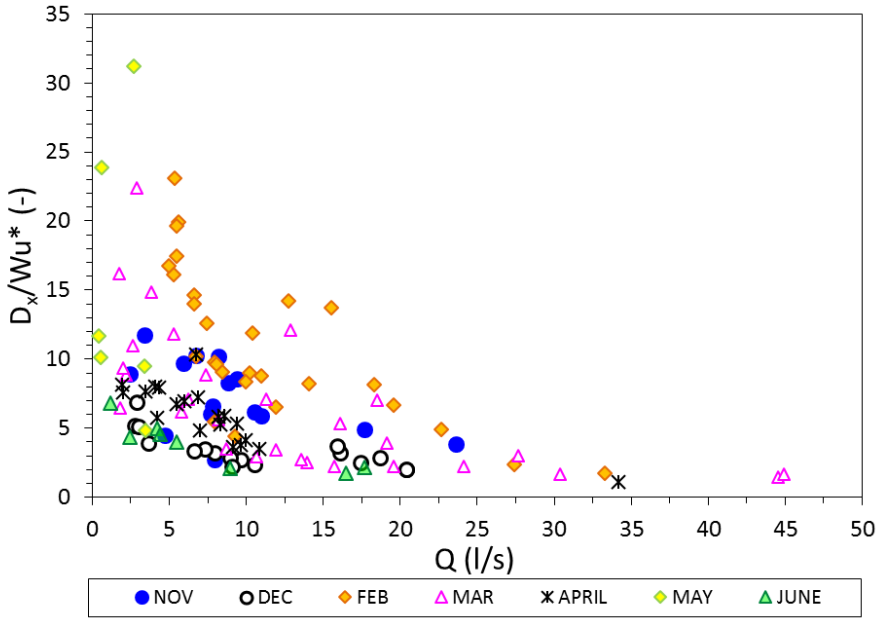

Figure 61: Variation of the non-dimensional longitudinal dispersion coefficient D_x/Wu* against discharge in SW1 for each month.

Figure 61 indicates that non-dimensional D_x/Wu* follows a strong negative correlation with Q, and shows a distinct variation with seasonal plant variation, between the fully-deflected and non-deflected stems. In particular, D_x variation at all discharges is between 3 to 4 times,

with larger scatter at lower discharges. D_x/Wu* falls within the range reported by Rutherford (1994), i.e. $2<D_x/Wu^*<50$. Overall, Figure 60 and Figure 61 suggest that longitudinal mixing in emergent flow reduces with flow rate and depth, and varies by a factor of four between months of deflected (i.e. February) and non-deflected (i.e. June) stems. Nepf (1997) and Shucksmith (2008) also found an inverse relationship between flow velocity (thus discharge) and D_x.

Figure 62 suggests an inverse relationship between D_f and discharge (or flow depth). It is observed that there is some trend in D_f with plant porosity due to ageing (especially between the two extremes of stem deflection), whereas the overall trend is inverse. It is reminded that D_f is based on the ADZ model, where values close to unity denote high number of dead zones.

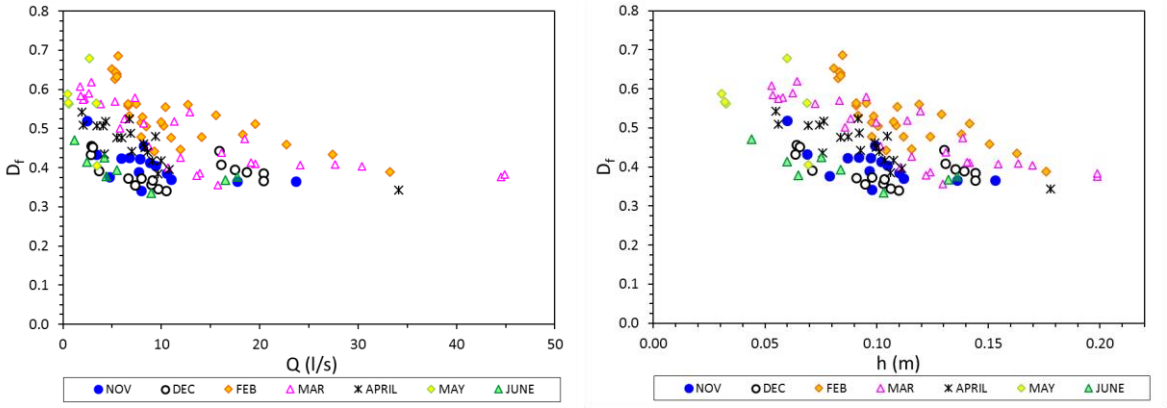

(a) D_f against Q in different plant seasons.

(b) D_f against h in different plant seasons

Figure 62: (a) Dispersive fraction against discharge in different plant seasons. (b) Dispersive fraction against flow depth in different plant seasons.

Summarising the results from Figure 59 to Figure 62, an overall decrease of D_x with increase in flow rate appears, with variations based on the seasonal datasets. Furthermore, there appears some influence of depth and flow rate on the D_x in each month. The influence of plant age is overt on the magnitude of D_x, where February's longitudinal dispersion coefficient is approximately four times larger than June's. The natural processes occurring in the wetland, i.e. stem withering and deflection of the decaying reed patches, combined with external natural factors, i.e. stem deflection due to high flows, and mainly due to wind action, result in different D_x values seasonally. Larger D_x values obtained in February are attributed

to the clusters of deflected reed stems, which reduce channel porosity, and promote long tails due to dead water regions. Overall, it is inferred that vegetation growth and decay has an impact on mixing properties and flow profile. Moreover, the scattered nature of the data collected might also be attributed to field effects, and to outdoor unforeseen factors, i.e. wind action which promotes deposition of whole decaying reed patches, randomness of the spatial seasonal plant variation processes in the wetland. D_f fraction provides an extra indicator of the large proportion of dead zones in the system at lower Q, and more predominantly in high plant ages.

Effect of Seasonal plant variation on Mixing

Although Figure 59 to Figure 62 show the monthly plant variation trends, they are still affected by variations in discharge. In order to eliminate the effect of flow on D_x, similar flow rates were plotted, to allow investigation of any potential seasonal trend of D_x with plant age. As such, Figure 63 (a)–(d) show the D_x against month (thus seasonal plant variation) for various discharges.

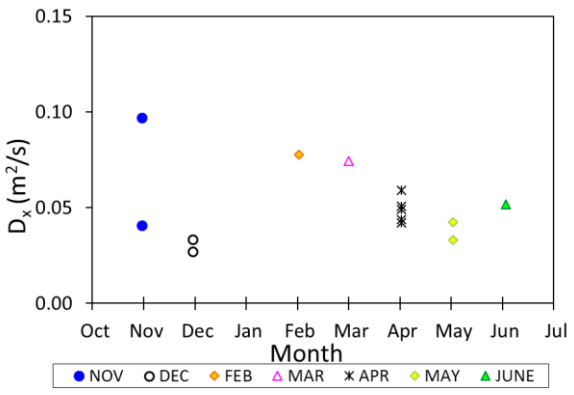

(a) Low Q = 3.0-5.0 l/s

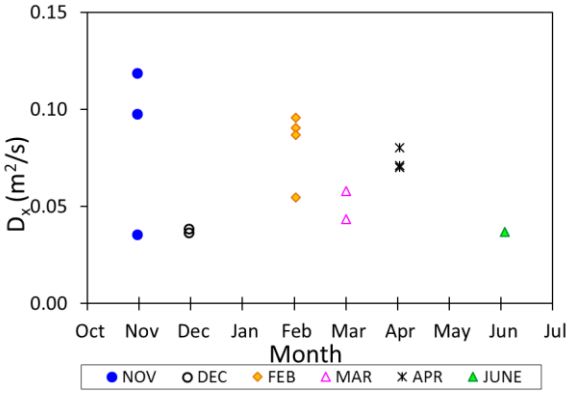

(b) Moderate Q = 8.0-9.0 l/s

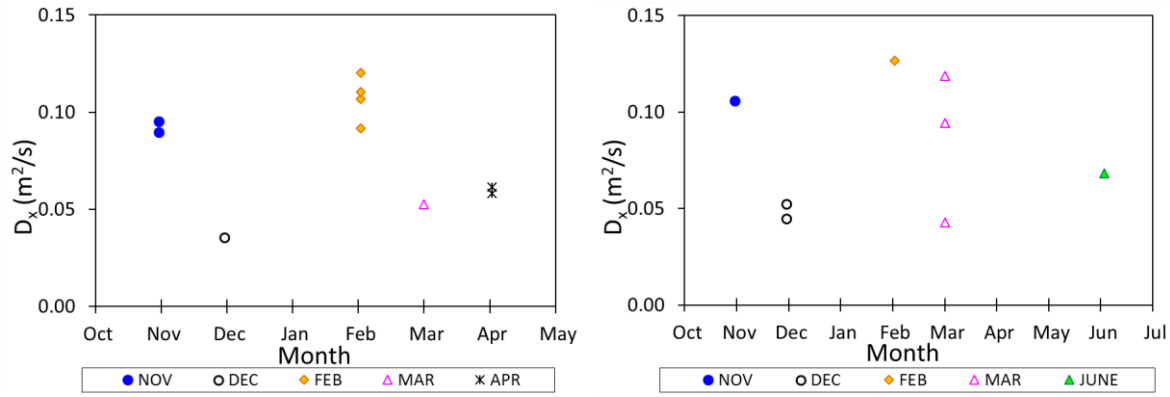

(c) High Q = 10.0-11.0 l/s (d) Extreme Q = 17.5-20.0 l/s

Figure 63: Seasonal D_x against month for different flow bands (i.e. low to extreme).

The profile of the monthly D_x against plant age, presented in Figure 63, shows some consistency for each discharge classification, and suggests that variation in water velocity does not affect the overall trend. This advocates that seasonal plant variation is the primary influence that causes variation in D_x. Figure 63 also indicates some scatter on D_x in November and March (i.e. difference of approximately an order of magnitude), which is explained by seasonal plant variation due to foliage drop in November, and ongoing decomposition in March (as discussed earlier in this section). Although there were only few tests in May, due to the dry weather, it is assumed that D_x in May follows similar trends (thus low values) as April and June.

Despite the lack of data in-between some months, the overall picture suggests a general, albeit weak, monthly trend of D_x with season, which gives insights of the expected annual tendency of D_x with seasonal plant variation in full-scale systems of similar micro-climate. In particular, longitudinal dispersion coefficient is large in November, followed by a consistent recession in December, and a recurrence increase in February. Then, D_x reduces between March and May. D_x in June appears to recur at levels greater than December D_x values, a result that is associated to the complete decomposition of the remainder old plant cycle stems, thus to the lower stem population density. It is expected that D_x values between July and October receive similar values as June, because there is no further change in the stem density population, or stem diameter variation. The dominant processes for each month with

regard to D_x were explained earlier in this section (see 'Effect of Flow Depth and Discharge on Mixing').

Development of seasonal dead zones can be considered by plotting D_f against season. Figure 64 suggests a dependence of dispersive fraction on discharge, where increase in Q eliminates the variation in D_f for different seasons. Furthermore, D_f shows some affinity with age (or plant porosity), reaching a peak toward February-March, manifesting large proportions of stagnant backwaters in high plant ages. As the stem density and diameter of Phragmites remain constant, increase in age is expressed by stem deflection, which alters the porosity. Such change is apparent in February and March (Figure 64), and is associated to the clustered deflected stems, which generate extra pockets and paths for the tracer to pass through.

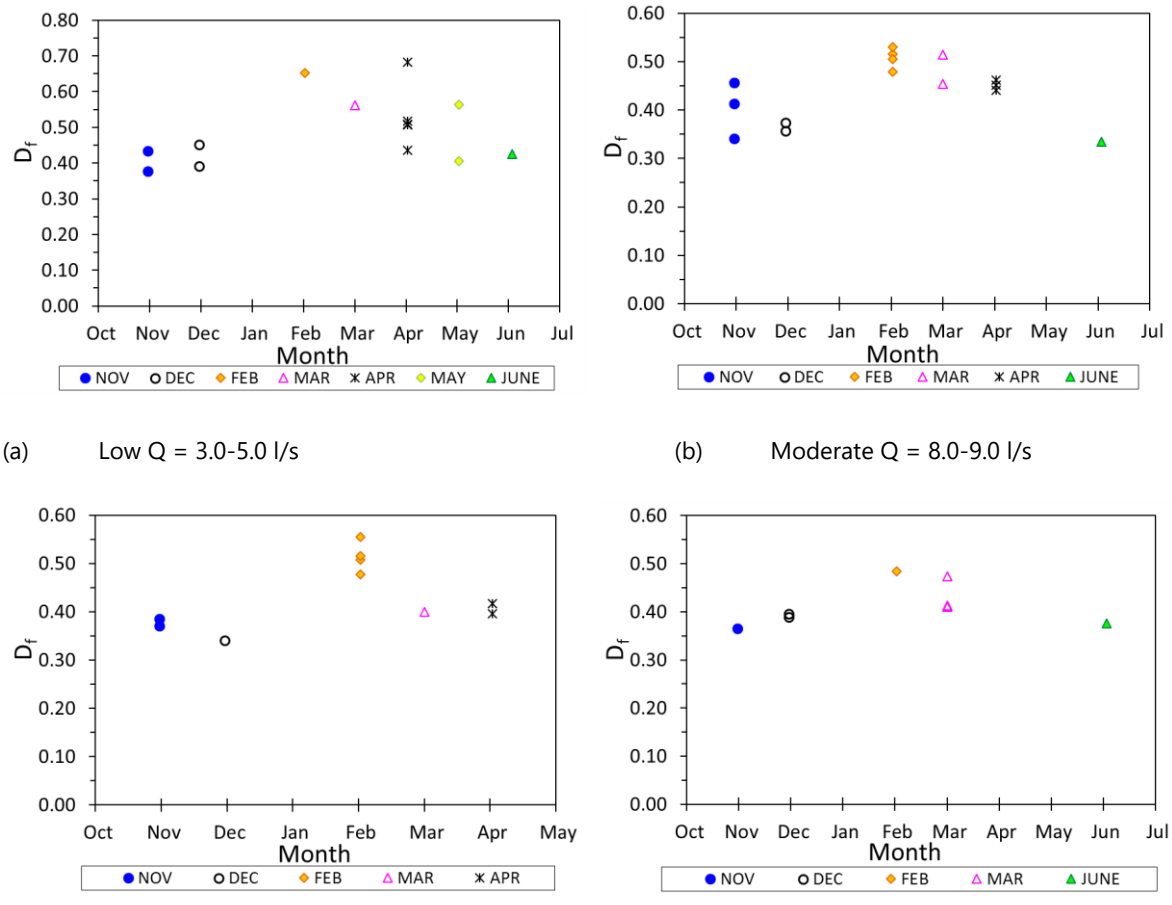

(a) Low Q = 3.0-5.0 l/s

(b) Moderate Q = 8.0-9.0 l/s

(c) High Q = 10.0-11.0 l/s

(d) Extreme Q = 17.5-20.0 l/s

Figure 64: Seasonal D_f against month for different flow bands (i.e. low to extreme).

Effect of longitudinal mixing on stem Reynolds number

Mechanical dispersion might have an effect on mixing in emergent canopies, as introduced and discussed in Chapter 2, Section 2.5. Nepf et al (1997) observed that plant stem wakes can cause mechanical dispersion, by deflecting and retarding some amount of the tracer mass. The potency of mechanical dispersion hinges upon the magnitude and vigour of turbulence that the wakes generate behind the stems, which is expressed by the stem Reynolds number, NR^*. Therefore, should mechanical dispersion have a significant effect, D_x and NR^* should present a relationship.

Figure 65 shows all the D_x coefficients against NR^* for all discharges, while Figure 66 eliminates the effect of discharge. Although there might appear a typical trend in December, April and June, overall Figure 65 does not show any apparent link between D_x and NR^*.

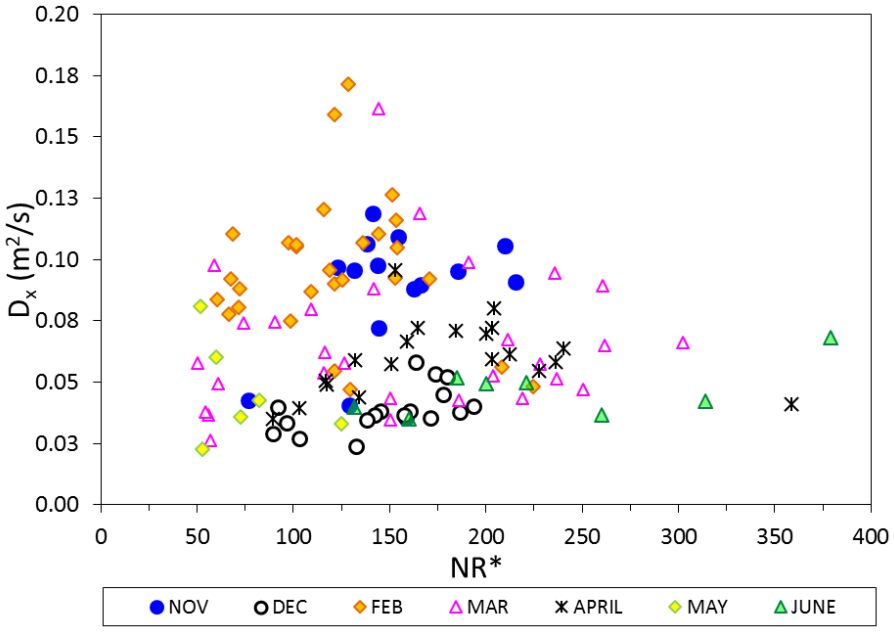

Figure 65: Dispersion coefficient against stem Reynolds number in different seasons.

Isolating the discharge influence, Figure 66 suggests at least twice larger NR^* in June, i.e. growth stage, compared to February, i.e. late dormant stage, which are the two extremes of vegetation growth. Figure 66 also shows a consistent descending trend from February to June. Overall, there is a high dependence of NR^* on discharge, while Figure 66 does not connote any strong link between D_x and NR^*. This might imply that mixing due to trapping

is not the governing source of mixing, or that *NR** might not be a proper measure to describe the efficacy of stem wakes to spread the tracer in the system, especially for deflected reed stems or decayed vegetation.

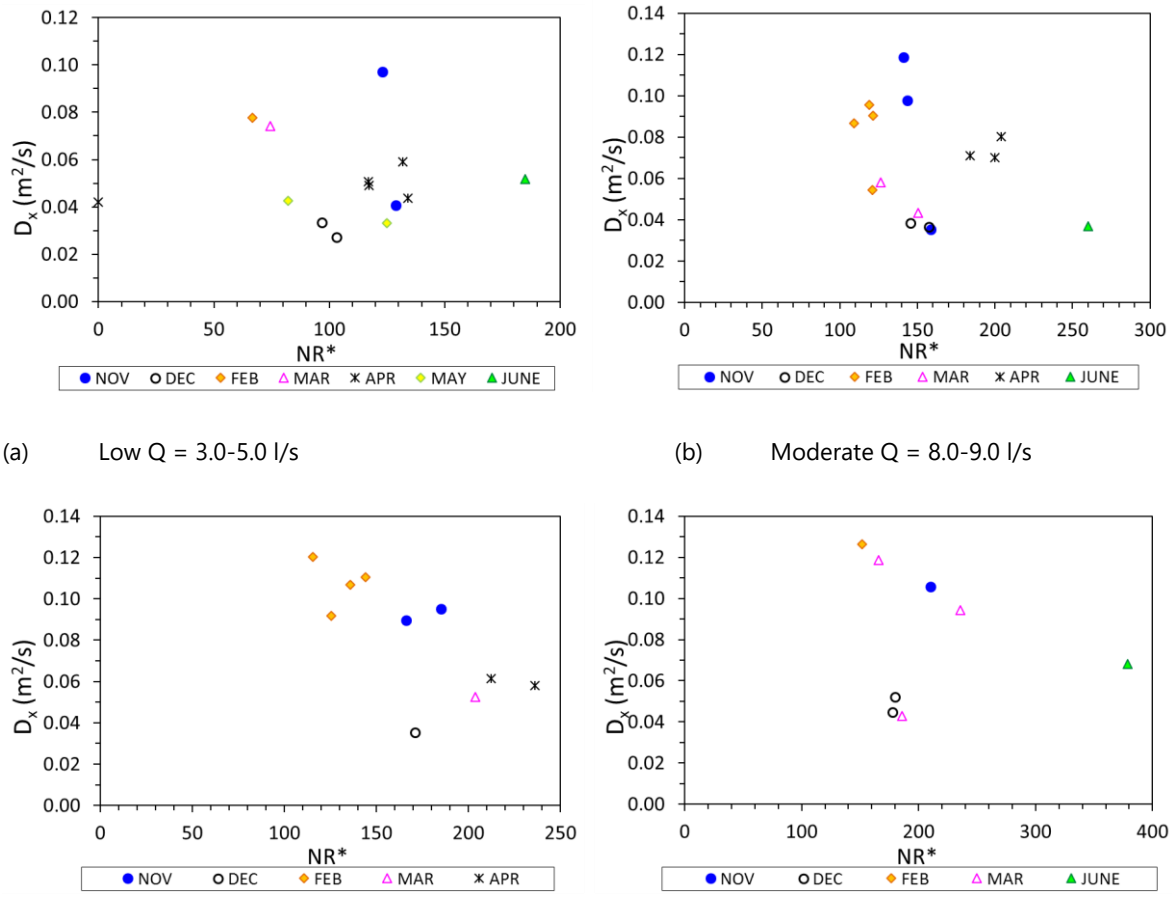

(a) Low Q = 3.0-5.0 l/s

(b) Moderate Q = 8.0-9.0 l/s

(c) High Q = 10.0-11.0 l/s

(d) Extreme Q = 17.5-20.0 l/s

Figure 66: Dispersion coefficient against Stem Reynolds number for different discharges and in different months.

4.2.1.7 Differential advection

Complementary longitudinal mixing tests were conducted for one week in February to elucidate the mixing characteristics and to give insights of differential advection within the wetland. Results are presented in Figure 67 and Figure 68, for two contrasting discharges, namely low Q=10 l/s, and high Q=38 l/s. The plots in Figure 67 and Figure 68 display results on identical axes scale, to allow easy comparison between the two flow conditions investigated. The small image attached on the right top of Figure 67 and Figure 68

respectively illustrates the full extents of the tracer in each transverse location. The locations of the instruments are shown in Figure 24.

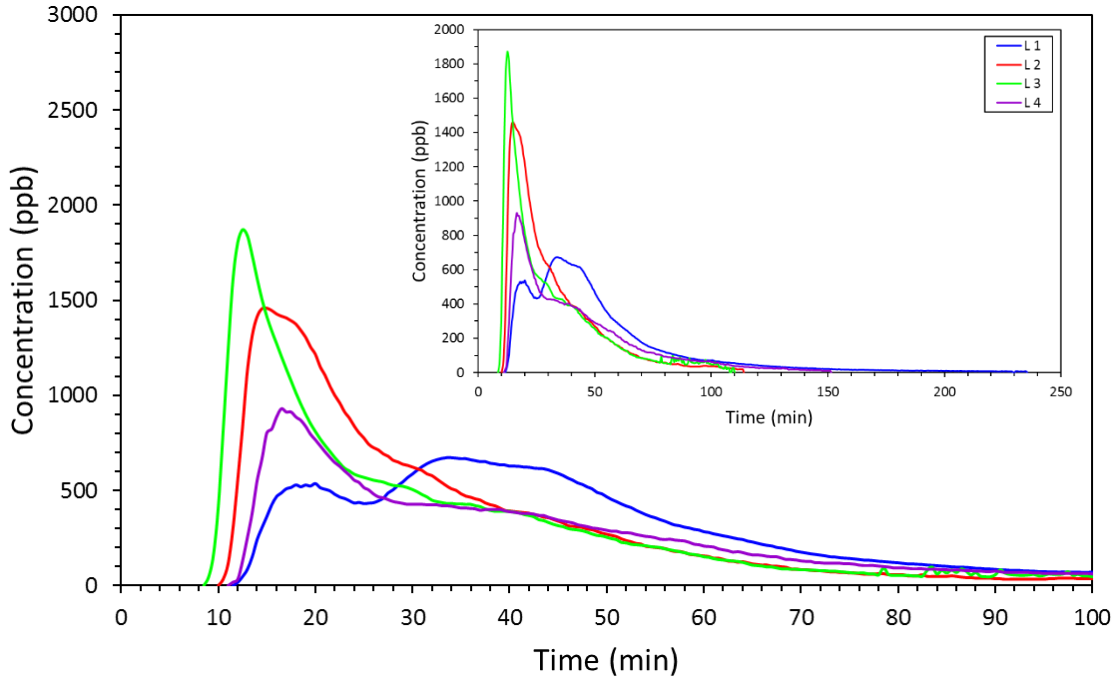

Figure 67: Transverse mixing study on one cross-section of the SW1 for a low flow rate case, Q=10 l/s .

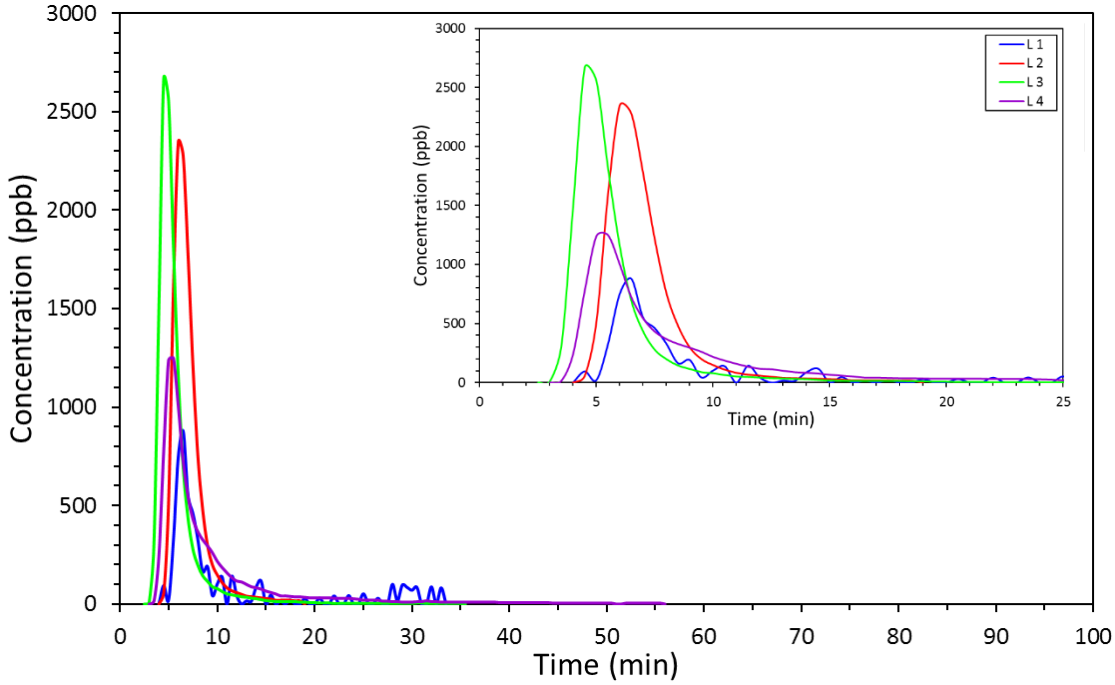

Figure 68: Transverse mixing study on one cross-section of the SW1 for a high flow rate case, Q=38 l/s.

In both flow conditions differential advection was apparent for the instruments recording in locations 1 and 4 travelling in lower flow velocities, while flow velocity closer to the centre (locations 2 and 3) travels more quickly. This is expected though, as locations 1 and 4 are closer to the boundaries of the wetland. Shear stress is generated due to boundary effects and due to secondary velocities developed. As the cross-sectional shape of the wetland is not flat-bottomed, but approximates a trapezoid shape, the shallower locations toward the banks may result in some differential advection. As this complementary study was done at high plant age (i.e. February), an additional factor affecting the differential advection could be the deflected stems. Location 1 is particularly prominent in lower velocities and larger travel times, inferring slower water speed in that side of the wetland, and potential of stagnant zones, where tracer is trapped.

In the low discharge case, mean velocity travels more quickly at the centreline (locations 2 and 3). All RTDs are unimodal, with the typical skewed bell-shape, apart from location 1, which is bimodal. This is a sign of recirculated or trapped tracer in that side of the system. On the other hand, the low flow rate case allows for better cross-sectional mixing, as demonstrated from the mean velocities and travel times (Figure 68). Transverse profiles of mean velocities through SW1 are displayed in Figure 69 for the low and high flow rate cases.

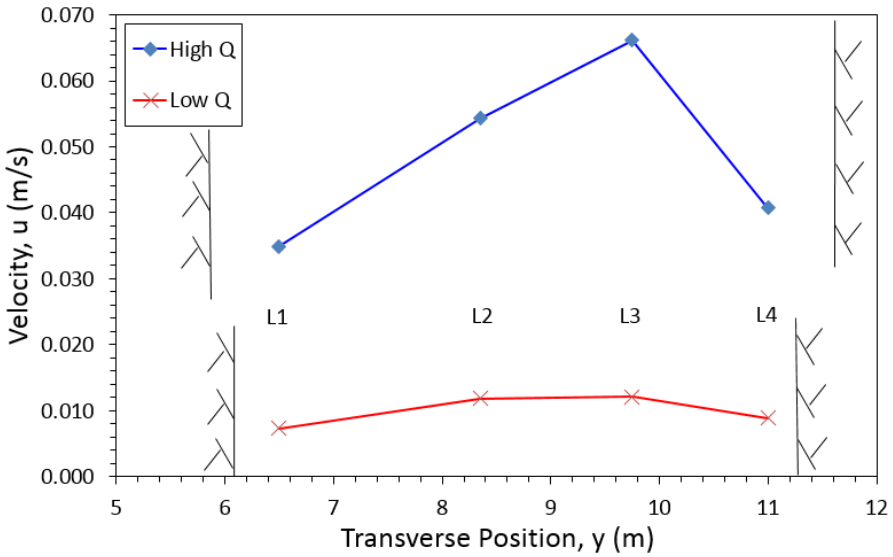

Figure 69: Comparison of the transverse profiles of mean velocities for two contrasting discharges (i.e. 10 l/s and 38 l/s) in SW1.

It can be seen that the increase in Q fosters flow shear velocity, with more differential advection occurring closer to the channel boundaries. The low Q case suggests almost plug flow conditions, whilst in greater flows a preferential path is prevalent through L3 location.

4.2.1.8 Hydraulic performance parameters

This section presents and discusses hydraulic performance related parameters, i.e. hydraulic efficiency, number of CSTRs, effective volume ratio, in relation to the stem Reynolds number, discharge, flow velocity and depth.

Hydraulic efficiency

Hydraulic efficiency, λ, plays a central role in the CW design and investigation. According to Equation 2.10, calculation of λ_n involves the t_n. Although t_n is readily calculated, it fails, however, to describe the actual conditions in the CW, because it diverges from the t_m, which is the actual residence time obtained from the tracer test. Such divergence between t_m and t_n is reported in Table 4.1. As such, attempting to describe a more real situation in the CW, λ is defined as the ratio of t_p over t_m. This measure has been previously used and recommended by Bodin et al (2012), and Chyan et al (2014), in analysing their results.

The presence of vegetation in FWS CWs introduces the use of stem Reynolds number, and is expected to cause some variation in λ. The relationship between the actual hydraulic efficiency, λ, and the stem Reynolds number, *NR**, is presented in Figure 70. It is seen that there is strong relationship between λ and *NR**. Nevertheless, λ does not show any particular variation with flow velocity, apart from February. This is in contrast with Chyan et al (2014) who linked λ and *NR** through an empirical relationship. In this case, there is a minimal variation in λ with *NR**, suggesting that the effectiveness of stem wakes on λ is minimal, except for February. The divergence between the two studies is mainly attributed to the contrasting scale of the systems compared, i.e. Chyan et al (2014) established their relationships employing a small physical model (1m*0.3m*0.3m), testing at laminar flow conditions, i.e. discharges 300 to 9000 times smaller.

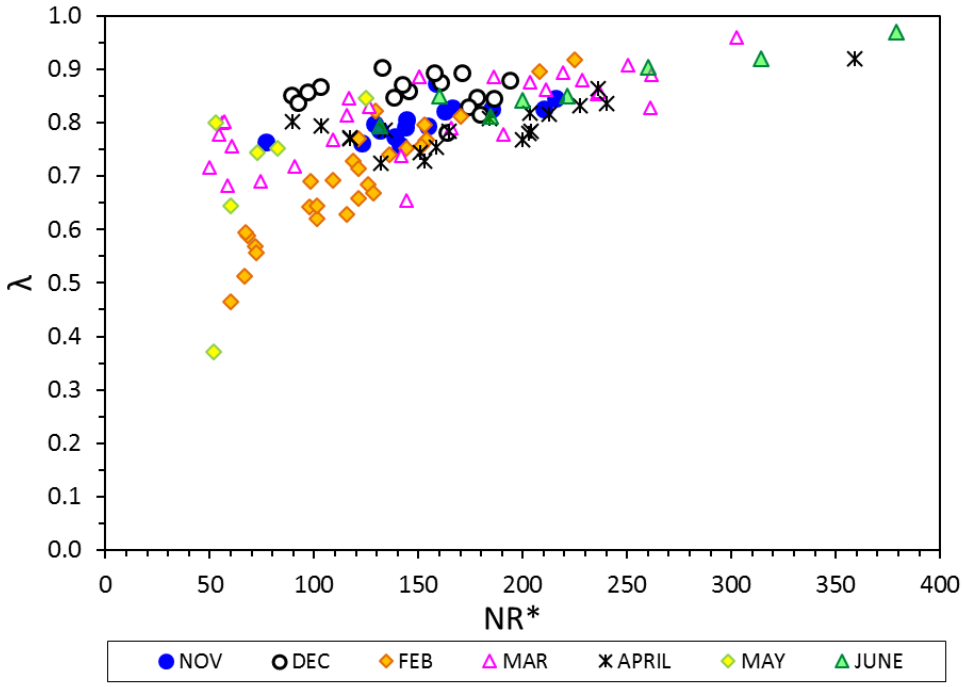

Figure 70: Stem Reynolds number against hydraulic efficiency in different months.

Effect of flow depth on effective volume

A relationship of the effective volume ratio, e, and water depth for different plant ages is shown in Figure 71. Previous research has demonstrated that increase in stem density of emergent plants reduced e in CWs (Bodin & Persson, 2012; Schuetz et al, 2012). However, this is not the case in SW1, as the change in plant porosity results from stem deflection (hence change in morphology due to decay). A distinct increase in e from June to February is observed. It has to be noted that stem population density is sparse, and that the calculated worst case scenario of fully deflected stems occupied only 4% of the wetland volume (see Chapter 3), which has a negligible contribution to the total volume.

Furthermore, Liu et al (2016) underline that there is a certain water depth that maximises the effective volume in a wetland. Nevertheless, no apparent variation between flow depth and e is observed in Figure 71. Although there is a minor enhancement in e with flow depth during the upright stem condition (i.e. June, November), Liu et al's (2016) statement cannot be ratified under the low flow depths tested in SW1 (i.e. the mean water depth did not exceed

0.2 m on average over the monitoring period, as a result of drier weather conditions, and of the non-dammed CW outlet construction).

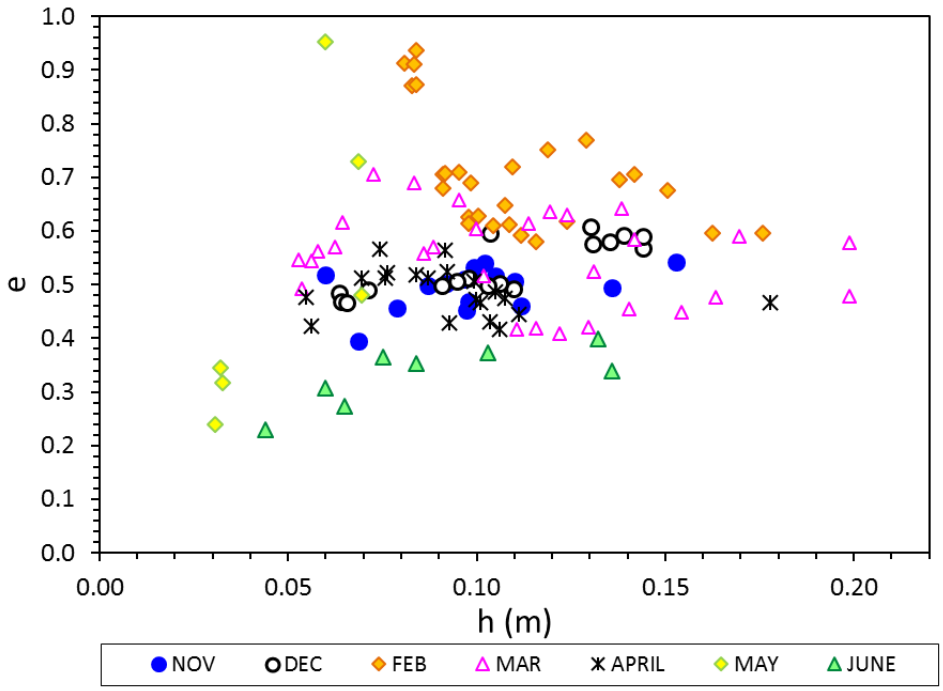

Figure 71: Effective volume ratio against flow depth for different plant ages.

4.2.2 Summary of main findings in SW1

Recall the two variables investigated in this CW were discharge variation and seasonal vegetation variation. The main findings and conclusions to be considered from Section 4.2 are:

- Tests through vegetation growth and ageing demonstrated significant influence on mixing, and on the RTD shape, particularly in high plant ages.
- Flow pattern during upright stem position behaves like plug flow with some longitudinal dispersion, whilst in fully deflected stem conditions, flow pattern promotes large quantities of stagnant backwaters.
- Seasonal vegetation variation increases the flow resistance in the wetland. Flow resistance increases as the stems deflect due to ageing, thus due to stem morphological variation.

- Higher resistance is observed in dormant season, therefore, slower velocities occur, resulting in longer contact times of the tracer within the clusters of deflected stems and the regions of diminished velocities. This results in larger longitudinal dispersion coefficients.
- Increase in flow rate promotes advective flow, and overall decreases the longitudinal dispersion in all plant ages.
- In fully deflected stem conditions, differential advection is apparent in all flow conditions. Due to cluster formation, flow travels faster in the free zone flow, and slower within the canopy, resulting in transverse shear velocities and dead zones.
- Shear dispersion and longitudinal mixing increases under fully deflected stem conditions.
- Longitudinal mixing coefficient demonstrated up to four times difference between February and June.
- A decrease in longitudinal mixing with increase in discharge or flow depth is observed.
- Dilution or spread increases approximately 3 times in February compared to June, and it increases in lower discharges at all plant seasons.

Further discussion of the summary of the SW1 findings is conducted in Chapter 5.

4.3SW2 _ South Wetland 2

This section presents and discusses the results for SW2, using the parameters derived from the tracer tests, and associating them with the vegetation characteristics, i.e. seasonal stem deflection. To assist the reader regarding the natural seasonal vegetation variation, a photographic record is provided in Section 4.3.1, followed by Section 4.3.2 which includes the fluorescent tracing tests results. Section 4.3.3 compiles a summary of the main conclusions drawn in SW2. It has to be noted that the testing period for this wetland was essentially three full months, namely December 2015 to February 2016. Thus, results involve the end of the dormant plant period. Equipment malfunctions, and the associated

complexity of the in-series SWs arrangement, did not allow monitoring of the seasonal vegetation variation effect for a longer period, as initially aimed.

4.3.1 Fluorescent tracing results

4.3.1.1 All tests collected

The original objective for SW2 was to monitor the vegetation variation effect over different seasons. However, malfunctions on the automated tracer injection system in SW2 in March 2016, as well as the complexity of preventing dye injections mixture due to the in-series systems, and the site proximity, led to the decision of removing the automated tracer injection system from SW2, and keep monitoring continuously the tracer concentrations deriving from the SW1 slug injections, at the SW2 inlet and outlet. Thus, the results collected in SW2 include essentially three months, namely December, January, and February, thus including both upright and fully deflected stem conditions.

The collected tests are listed in Table 4.2, where the first column determines the unique tracer test code, which consists of: a capital letter, determining the discharge classification (details are listed in bullet points as follows); an integer, which refers to the month; a second integer, which refers to the test number in ascending order. The rest columns in Table 4.2 indicate the month, discharge, first arrival time of the tracer, HRT, nominal residence time, longitudinal dispersion coefficient, number of CSTR, hydraulic efficiency, and effective volume ratio respectively. For ease of presentation and comparison, the tracer tests were classified into discharge bands, presented as follows:

- Low Q: 0-5.5 l/s
- Moderate Q: 5.6-13.0 l/s
- High Q: 13.1-20.5 l/s
- Extreme Q: 20.6-35.0 l/s

Table 4.2: Summary of test series & transport parameters from the RTD analysis of the 81 tests in SW2.

Test unique code	*Month*	*Flow Rate band*	*Flow rate, Q* (l/s)	*First arrival time,* t_1' (min)	*Travel time,* t_m (min)	*Nominal residence time,* t_n (min)	*Dispersion coefficient,* D_x (m^2/s)	*Number of CSTR, N*	*Hydraulic efficiency* λ (t_p/t_m)	*Effective volume ratio, e* (t_m/t_n)
L,12,1	Dec	Low	4.6	11.0	16	23.0	0.051	11	0.87	0.70
L,12,2	Dec		3.9	11.0	17	24.1	0.061	9	0.88	0.69
L,12,3	Dec		3.5	11.5	17	24.9	0.042	13	0.87	0.67
L,12,4	Dec		3.4	11.5	17	25.1	0.050	11	0.89	0.67
L,12,5	Dec		2.8	11.5	17	26.7	0.046	11	0.89	0.65
L,12,6	Dec		3.3	11.5	17	25.4	0.049	11	0.87	0.68
L,12,7	Dec		3.5	11.5	17	24.9	0.044	12	0.87	0.69
L,02,1	Feb		5.0	10.5	17	22.4	0.036	15	0.85	0.76
L,02,2	Feb		4.8	10.5	17	22.6	0.050	11	0.84	0.76
L,02,3	Feb		4.2	7.5	17	23.6	0.039	13	0.86	0.74
L,02,4	Feb		5.4	10.5	16	21.8	0.061	9	0.86	0.75
L,02,5	Feb		4.8	10.5	16	22.6	0.054	10	0.85	0.73
L.02.6	Feb		4.2	10.5	17	23.6	0.062	9	0.85	0.72
M,12,1	Dec	Moderate	10.1	10.0	14	18.0	0.047	14	0.92	0.79
M,12,2	Dec		9.4	10.0	14	18.5	0.044	14	0.90	0.78
M.12.3	Dec		8.5	10.0	14	19.0	0.027	23	0.91	0.75
M,12,4	Dec		7.6	10.5	15	19.8	0.037	17	0.92	0.75
M,12,5	Dec		7.3	10.5	15	19.9	0.039	15	0.90	0.75
M.12.6	Dec		5.6	10.5	15	21.6	0.044	13	0.90	0.72
M,12,7	Dec		12.1	9.0	13	17.5	0.035	20	0.94	0.76
M,01,1	Jan		12.9	8.00	12	17.5	0.032	24	0.94	0.67
M.01.2	Jan		12.2	8.00	12	17.5	0.039	20	0.92	0.68
M,01,3	Jan		12.1	8.00	12	17.5	0.044	17	0.91	0.69
M,01,4	Jan		11.5	8.00	12	17.5	0.042	18	0.91	0.69
M.01.5	Jan		12.1	8.00	12	17.5	0.045	17	0.91	0.69
M.01.6	Jan		11.8	8.00	12	17.5	0.056	13	0.90	0.70
M,01,7	Jan		12.7	8.0	12	17.5	0.037	21	0.94	0.67
M,02,1	Feb		6.1	10.0	16	21.1	0.046	12	0.85	0.78
M.02.2	Feb		5.7	10.0	16	21.4	0.051	11	0.85	0.77
M,02,3	Feb		12.1	9.0	12	17.5	0.035	21	0.92	0.71
M,02,4	Feb		11.1	9.0	12	17.5	0.025	29	0.93	0.71
M.02.5	Feb		10.7	9.0	13	17.7	0.037	19	0.93	0.72
M,02,6	Feb		9.4	9.0	14	18.5	0.072	9	0.88	0.74
M,02,7	Feb		8.6	9.0	14	18.9	0.066	10	0.87	0.73
M.02.8	Feb		7.1	12.5	14	20.0	0.049	13	0.89	0.70
M,02,9	Feb		6.1	10.0	14	21.1	0.048	13	0.90	0.69
M,03,1	Mar		7.1	10.0	15	19.8	0.048	13	0.89	0.74
H,12,01	Dec	High	18.3	8.5	13	17.1	0.039	18	0.93	0.75
H,12,02	Dec		16.1	9.0	13	17.3	0.016	46	0.94	0.74
H,12,03	Dec		20.4	8.5	13	17.0	0.023	32	0.95	0.74
H,12,04	Dec		17.1	8.5	13	17.2	0.030	23	0.94	0.74
H,12,05	Dec		15.2	9.0	13	17.4	0.022	32	0.93	0.74
H,12,06	Dec		15.6	8.5	13	17.3	0.048	15	0.92	0.75
H,12,07	Dec		14.6	9.0	13	17.4	0.022	33	0.93	0.74
H,12,08	Dec		14.3	9.0	13	17.4	0.068	10	0.89	0.77
H,12,09	Dec		13.2	9.0	13	17.4	0.036	19	0.94	0.76
H,01,01	Jan		19.8	7.5	11	17.0	0.028	30	0.95	0.65
H,01,02	Jan		18.9	7.5	11	17.1	0.046	17	0.93	0.66
H,01,03	Jan		18.3	8.0	11	17.1	0.022	37	0.95	0.64
H,01,04	Jan		17.9	8.0	11	17.2	0.026	32	0.95	0.65
H,01,05	Jan		17.3	8.0	11	17.2	0.031	26	0.93	0.65
H,01,06	Jan		17.1	8.0	11	17.2	0.034	24	0.94	0.65
H,01,07	Jan		17.3	8.0	11	17.2	0.046	17	0.93	0.66
H,01,08	Jan		16.9	8.0	11	17.3	0.031	26	0.94	0.65
H,01,09	Jan		15.9	8.0	11	17.3	0.028	28	0.92	0.66
H,01,10	Jan		15.0	8.0	12	17.4	0.037	21	0.91	0.67
H,01,11	Jan		13.9	8.0	12	17.4	0.048	16	0.93	0.68
H,01,12	Jan		13.1	8.0	12	17.4	0.042	18	0.92	0.68
H,01,13	Jan		20.4	7.5	11	17.0	0.023	37	0.94	0.63
H,01,14	Jan		19.1	7.5	11	17.1	0.028	30	0.93	0.63
H,01,15	Jan		17.3	7.5	11	17.2	0.031	26	0.91	0.64

H,01,16	Jan		16.1	8.0	11	17.3	0.051	16	0.93	0.65
H,01,17	Jan		14.1	8.0	12	17.4	0.058	13	0.90	0.67
H,01,18	Jan		13.1	8.0	11	17.4	0.038	21	0.91	0.66
H,02,01	Feb		18.9	8.5	12	17.1	0.022	34	0.94	0.71
H,02,02	Feb		17.1	8.5	12	17.2	0.026	29	0.95	0.70
H,02,03	Feb		13.1	8.5	12	17.4	0.025	30	0.94	0.70
E,12,01	Dec	Extreme	22.9	8.0	12	16.8	0.023	32	0.94	0.73
E,01,01	Jan		25.6	7.5	11	16.6	0.023	38	0.93	0.65
E,01,02	Jan		22.9	7.5	11	16.8	0.050	16	0.91	0.65
E.01.03	Jan		21.1	7.5	11	16.9	0.086	9	0.88	0.67
E,01,04	Jan		24.4	7.5	11	16.7	0.030	28	0.92	0.65
E,01,05	Jan		25.9	7.5	10	16.5	0.022	40	0.95	0.63
E.01.06	Jan		31.2	7.0	11	16.1	0.028	30	0.97	0.67
E,01,07	Jan		34.8	8.0	11	15.9	0.025	34	0.98	0.67
E,01,08	Jan		33.3	7.0	10	16.0	0.031	28	0.92	0.65
E.01.09	Jan		33.0	7.0	10	16.0	0.029	31	0.93	0.64
E,01,10	Jan		22.2	7.5	11	16.8	0.025	34	0.94	0.63
E,02,01	Feb		30.1	7.0	11	16.2	0.050	16	0.91	0.68
E.02.02	Feb		23.4	8.5	12	16.8	0.025	30	0.94	0.73
E,02,03	Feb		21.3	8.5	12	16.9	0.028	26	0.94	0.72

4.3.1.2 Analysis of measured concentration profiles RTDs

This section presents the effect of plant season on flow structure. The plant age is high and includes data only from the stem dormant period. RTDs of similar discharges selected from each flow category (from low to extreme) (see Table 4.2) are presented in Figure 72 (a)-(f). As expected, larger flow rates result in shorter first arrival times and HRTs (see Figure 72 (a)-(f)). The effect of plant age is minimal on all flow categories. Note that plots assembling the summation of the tracer tests are presented in Appendix II.

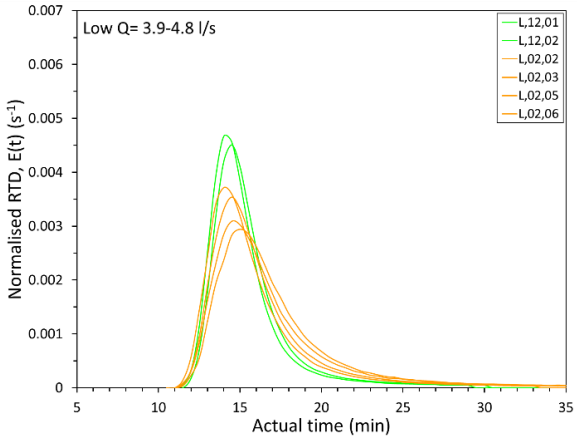

(a) Low Q = 3.9-4.8 l/s

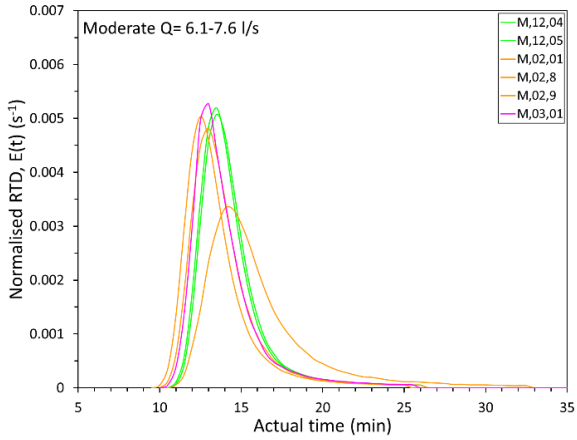

(b) Moderate Q = 6.7-7.6 l/s

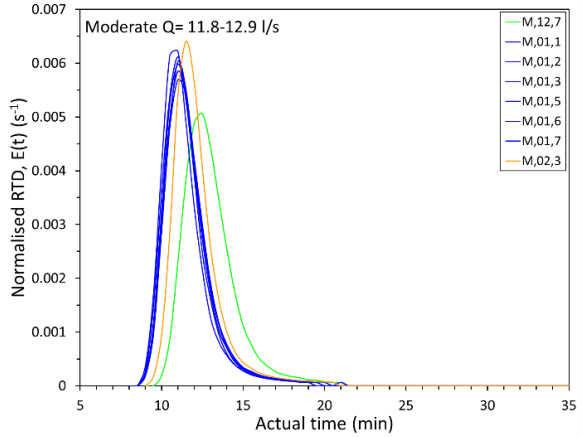

(c) Moderate Q = 11.8-12.9 l/s

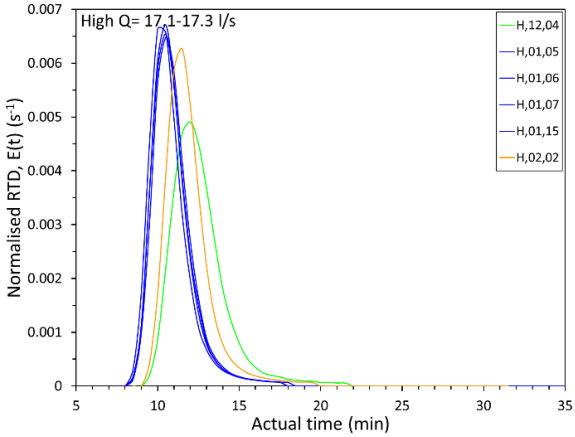

(d) High Q = 17.1-17.3 l/s

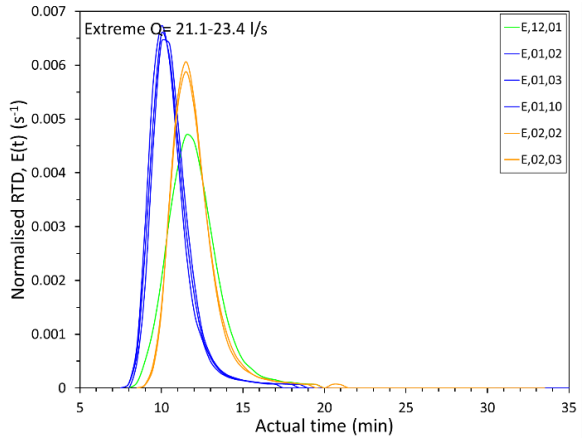

(e) Extreme Q = 21.1-23.4 l/s

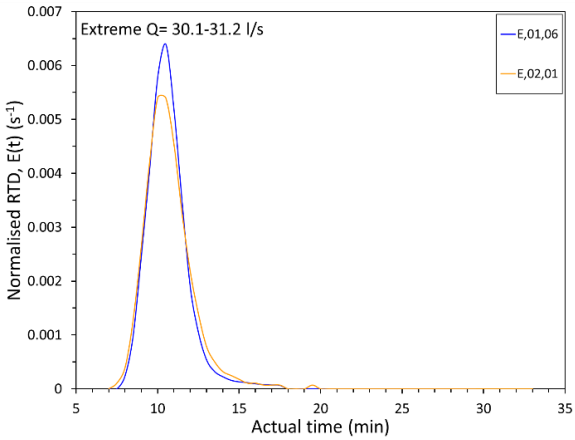

(f) Extreme Q = 30.1-31.2 l/s

Figure 72: Effect of season for same flow classifications in SW2, ranging from low to extreme, (a)–(f). Effect of season is minimal on the shape of the RTD and on the HRT.

It is characteristic that the general mixing pattern in all seasons resembles plug flow with a minimal amount of longitudinal dispersion, due to the short tails (Figure 72 (a)-(f)). No particular seasonal effect is observed, apart from the slightly shorter HRTs, and the greater plug flow amount taking place in January.

There appears to be no apparent variation in the flow retardation or in the vegetation resistance between the monitored months. It appears that discharge overweighs the seasonal plant variation influence in SW2. For example, it is observed that in the low discharge class, pollutant attenuation is slightly larger in February than in December; whereas at larger discharges the opposite effect occurs. This is possibly due to the irregular channel bed, which creates a natural fast flow path in the middle-left side of the wetland,

towards the flow direction. As such, at low discharges, deflected stems possibly induce some degree of resistance, allowing for more dispersion and interaction of solute in the created clusters (see Figure 72 (a)). In the extreme discharge class, further increase in Q, i.e. Q>30 l/s, advocates that this wetland functions as a pipe, where water essentially passes by (see Figure 72 (f)).

In an attempt to understand the effect of discharge variation on the flow structure, Figure 73 (a)-(b) is presented, spanning between all flow categories. Typically, increase in discharge should entail lower solute spread and higher concentration peak in a regular open channel. However, there seems to be a discharge boundary, above which the flow structure slightly alters, both in terms of tracer spread and peak concentration. Nevertheless, the value of this boundary differs between December and February, due to seasonal plant variation (thus stem deflection). In particular, December's Q limit is around 13 l/s, whereas February's Q limit is approximately 20 l/s. Above those Q values, increase in discharge attenuates slightly more the peak concentration. This is noticed in Figure 73 (a)-(b) for December and February respectively. This effect is attributed to the compound bottom topography of the channel, where increase in Q increases the flow depth, thus the shallower side of the wetland becomes progressively wet and active. However, it is overall noticed that increase in Q promotes further plug flow and reduces the longitudinal mixing, as inferred from the gradually shorter trailing edges obtained (Figure 73 (a)-(b)).

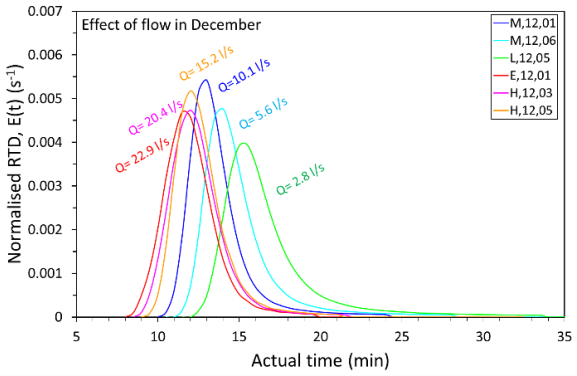

(a) Flow structure in December

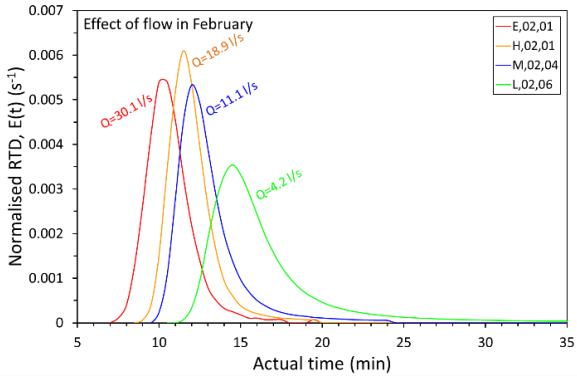

(b) Flow structure in February

Figure 73: Effect of discharge on flow structure, for same month, in December (a) and in February (b). It is observed that above a flow rate the RTD (hence flow structure) slightly alters, i.e. greater tracer spread and peak concentration. This result is attributed to the irregularity of the bed channel.

In summary, the effects of discharge and seasonal plant variation on the mixing pattern and hydraulics in SW2 were presented and discussed in this section. It was demonstrated that seasonal plant variation has less important effect on flow structure and mixing characteristics, and that discharge overwhelms. The compound bed channel topography along with the unbunded outlet in SW2, encourage short-circuiting, and are both considered the governing factors influencing the wetland's hydrodynamics.

4.3.1.3 Cumulative Residence Time Distribution CRTDs

This section presents and discusses the effects of seasonal plant variation and discharge variation on flow structure in the form of CRTDs. The corresponding CRTDs of the already presented RTDs in Figure 72 are plotted for similar discharges, for all flow conditions. The CRTDs are presented in Figure 74 against actual time and against normalised time, side by side, for each flow classification. In order to create a general level of comparison for the obtained data and the existing studies, time was normalised by the t_n. An assortment of the summation of the individual CRTDs at actual and at normalised time are presented in Appendix II.

For the CRTDs plotted at actual time, seasonal plant variation indicates negligible effect during the dormant season. Furthermore, CRTDs show evidence of high short-circuiting, which increases with discharge. This is deduced from the CRTD plots, by identifying the point at which the steep incline stops. At all discharges, the CRTDs display an initial sharp rise, before they change direction, protruding a short trailing edge. The curves suggest that a minimum fixed short-circuiting mass of 70% passes by the system for the lowest Q band (see Figure 74 (a)), with the remaining tracer mass promoting mixing, as tracer is trapped in the lower flow velocity adjacent areas. Nevertheless, increase in discharge, results in higher short-circuited masses passing across the system. The gradual shorter length of the trailing edges as Q increases, entails lower degree of longitudinal mixing. It is apparent that SW2 suffers from high preferential flows.

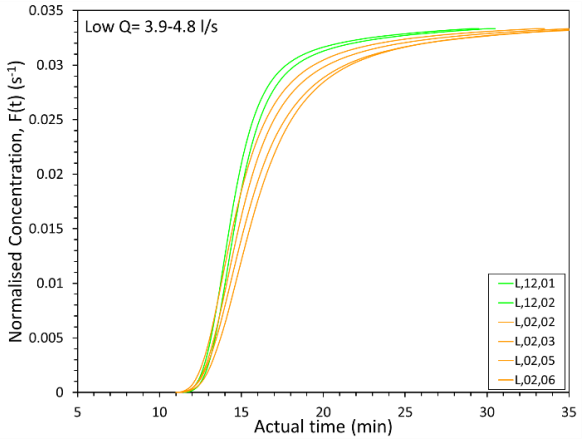

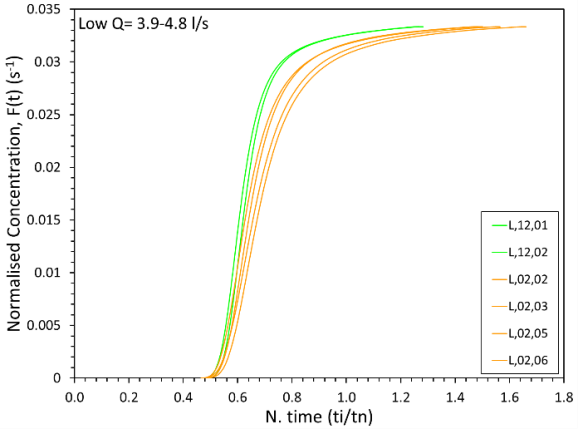

(a) Low Q = 3.9-4.8 l/s

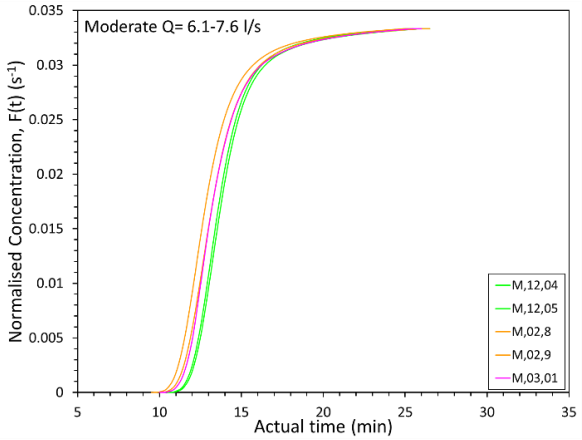

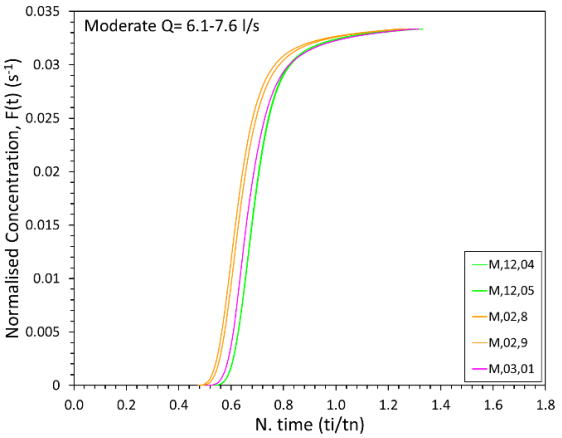

(b) Moderate Q = 6.7-7.6 l/s

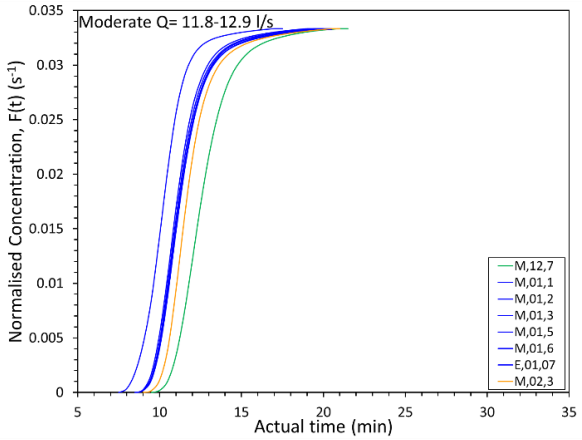

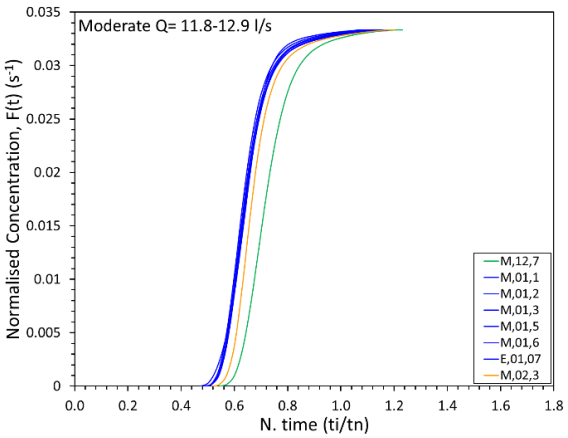

(c) Moderate Q = 11.8-12.9 l/s

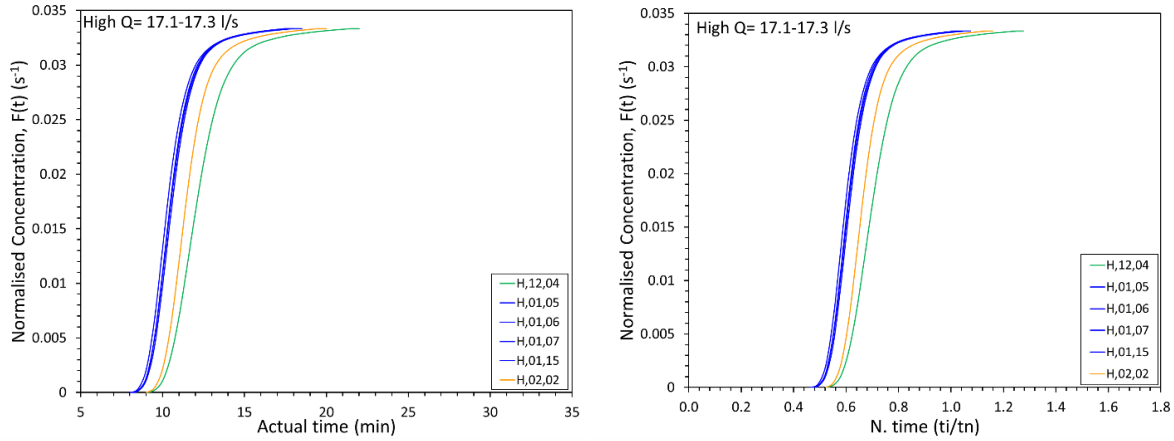

(d) High Q = 17.1-17.3 l/s

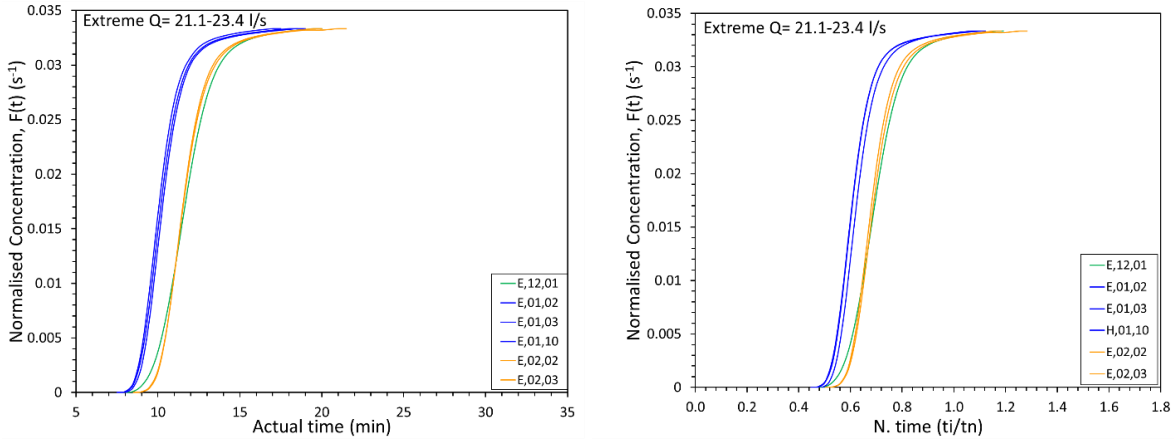

(e) Extreme Q = 21.1-23.4 l/s

Figure 74: Dimensionless CRTD curves for the different flow rate classifications, presented side by side as actual time and normalised time by t_n. The flow regime follows the order from Low (a) to Extreme (e), for certain discharge classifications to allow ease of comparison. CRTDs demonstrate minimal effect of season both on the mixing pattern and on flow structure in SW2 during the dormant season.

At normalised time, the CRTD curves collapse into one main bunch, with some minimal variation between January and the other months (Figure 74 (a)-(e) right side). At all plant stages of the dormant season (i.e. December to February), as well as at all discharges, CRTDs obtain a single prevalent shape, consisting of a steep incline with a relatively short projected tail. A slight difference is noted only in the low discharge class (Figure 74 (a)), where seasonal plant variation between December (i.e. upright stems) and February (i.e. deflected stems) appears to have a small effect on the short-circuiting amount and on the generally longer tails projected. Because lower flow rates result in lesser turbulence, slower movement of the

tracer occurs across the wetland, whereas the additional change in channel porosity due to the clusters of deflected stems in February induces some flow resistance, thus flow retardation, reflected on the minimal change of the CRTD shape. However, this change is trivial, and it is inferred that there is minimal effect of season both on the mixing pattern and on flow structure in SW2.

The effect of discharge variation on mixing pattern is further investigated for two different stem deflection conditions, thus months, i.e. December and February, as seen in Figure 75 (a)-(b). It is observed that there is little dependence of CRTD shape on flow rate, where increase in discharge increases short-circuiting. Low discharges induce overall longer projected tails. However, it is overall seen that short-circuiting levels are constantly very high. This result is due to the non-flat bottomed channel bed, promoting the formation of a preferential path. Furthermore, important role in the short-circuiting plays the non-walled outlet configuration.

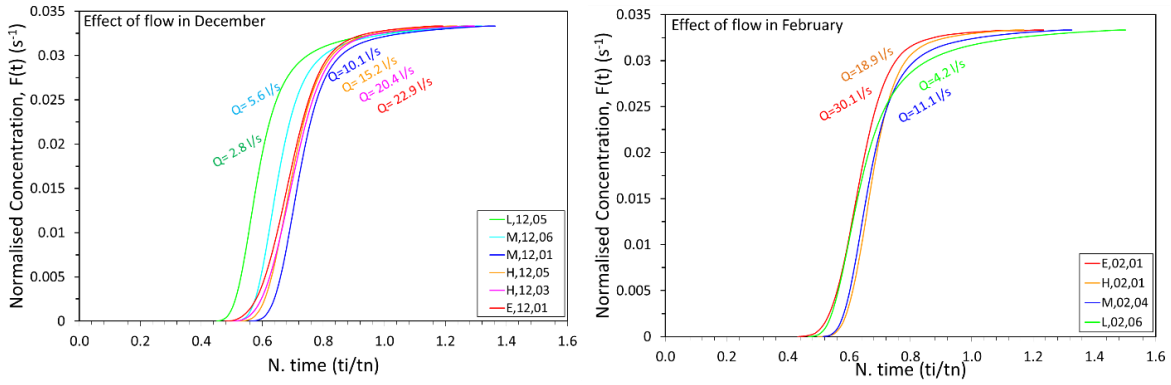

(a) Effect of discharge in December

(b) Effect of discharge in February

Figure 75: Normalised CRTDs for various different flow rates in December (a) and February (b). High short-circuiting is observed in all discharge conditions, whilst the mixing pattern does not show any significant difference with the flow rate variation. Other underlying factors may explain the prevalence of short-circuiting in SW2, such as the compound (or irregular) channel topography.

Summarising, the testing period in SW2 was shorter than the planned due to equipment malfunctions, albeit sufficient to investigate the effects of seasonal plant variation during the dormant season, to draw useful conclusions. Results showed that seasonal plant variation has minimal effect on the hydraulics, i.e. HRT, flow retardation, short-circuiting. Short-

circuiting is high in all discharge conditions. The mixing pattern did not show any significant difference with the flow rate variation. Therefore, it is inferred that there are other underlying factors to explain the prevalence of short-circuiting in this system, such as the compound (or irregular) channel topography, which overwhelm the impact of seasonal plant variation on mixing characteristics and on flow pattern.

4.3.1.4 HRT

The effects of seasonal vegetation variation and discharge on the HRT are shown in Figure 76, which illustrates the mean residence time, t_m, against discharge. The t_n curve is also presented on the same plot, for the upright reed stems condition, where plant porosity is incorporated in the volume calculation. It is observed that upright stem condition (i.e. growth season) has a minimal impact on the channel porosity.

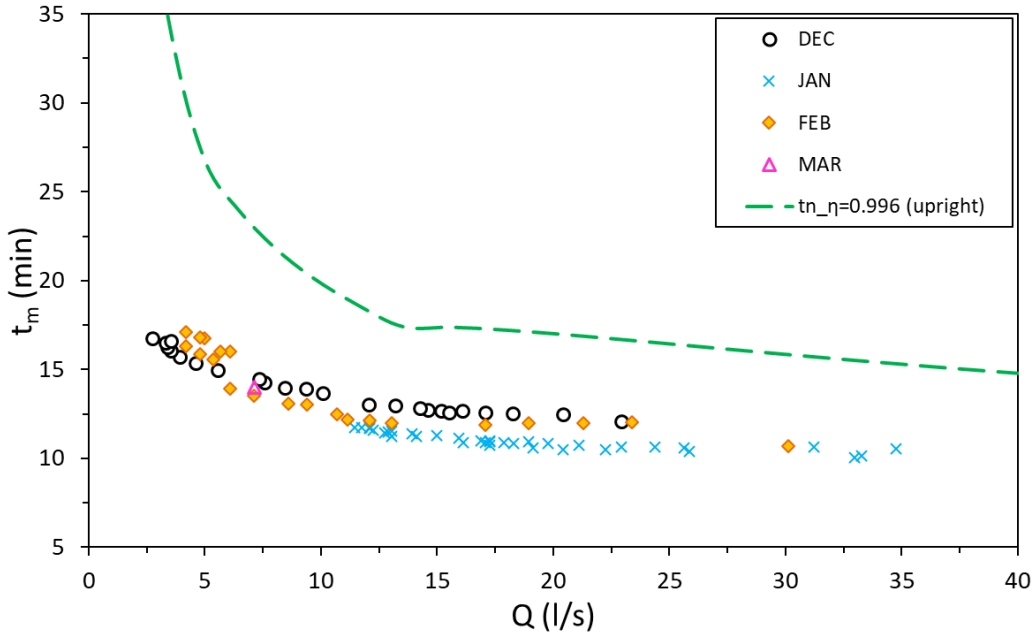

Figure 76: Mean residence time against discharge in SW2. The plot also shows the nominal residence time curve. High short-circuiting is consistently observed during the dormant season at all flow rates tested.

4.3.1.5 Mean velocity profiles

The flow resistance results over the three-month monitoring period are presented and discussed in this section. Although the monitoring period is short, it covers the transition period from upright to deflected position of stems. As such, based on the flow depth, flow

condition during February varies between emergent and submerged. Figure 77 presents the measurements of the average velocity at different plant ages, indicating minimal variation in flow resistance between upright (i.e. December) and fully deflected stems (i.e. February).

It is noticed that higher plant ages, i.e. January and February, demonstrate lower vegetation resistance, albeit variation is minimal. Flow velocity is largest in January, displaying a slight decrease in February. The slight flow retardation is a direct effect of the stems' deflection and nesting nature, during February and March. Furthermore, it is observed that in particularly low discharges, i.e. Q<7 l/s, plant resistance differs slightly between December and February. This minor difference should be generally expected at low discharges, because low Q entails low flow depths. In low flow depths, although stems might be fully deflected, the flow condition is probably still emergent in Q<7 l/s, because the water depth has not yet reached the top of the clusters of the deflected stems. Overall, stem resistance is proved to be negligible in SW2.

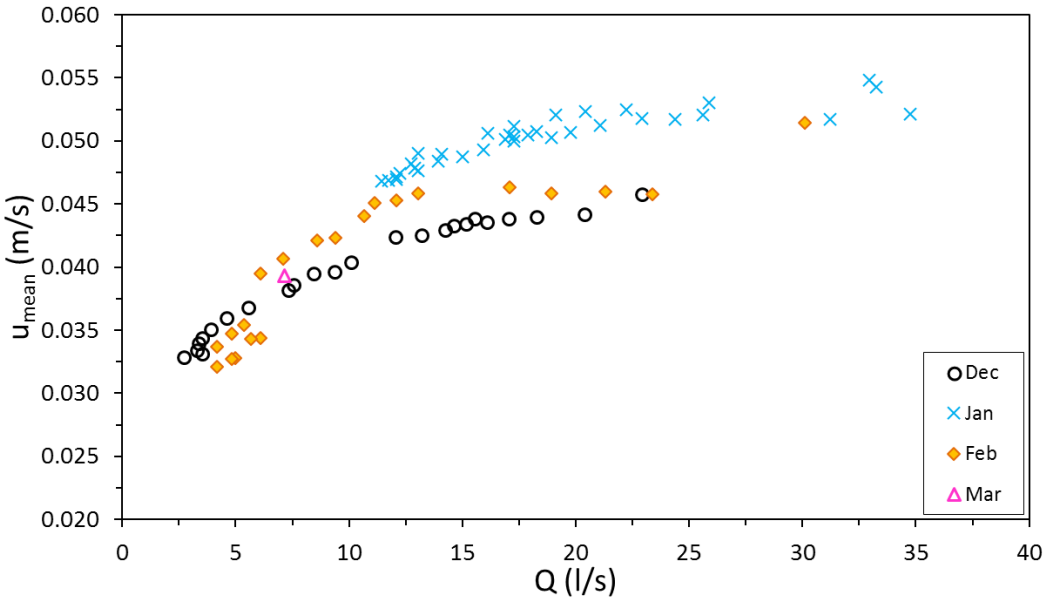

Figure 77: Mean water velocity against discharge per month in SW2. Stem resistance appears to be negligible during the dormant season, between the upright and fully deflected stems.

4.3.1.6 Longitudinal dispersion measurement

This section presents the effects of discharge and seasonal plant variation on the longitudinal dispersion coefficient, D_x and on the dispersive fraction, D_f. Furthermore, relationships

between the mixing characteristics, i.e. D_x, D_f, N, and other hydrodynamic parameters, i.e. stem Reynolds number, effective volume ratio, hydraulic efficiency, are presented and discussed.

Effect of Flow Depth and Discharge on Mixing

To observe any total trends of water depth and discharge on mixing, Figure 78 to Figure 81 present all the dispersion coefficients, D_x, and dispersive fractions, D_f, against discharge and flow depth.

The influence of discharge on the longitudinal dispersion is shown in Figure 78 including all months monitored, and in Figure 79 differentiating for each month (thus plant age). Furthermore, Figure 78 presents the predicted D_x values using Equation 2.42 by Etemad-Shahidi & Taghipour (2012), irrespective of the B/h condition suggested. The stream sinuosity factor included in Equation 2.42 was assumed unity for the wetland (thus zero sinuosity). This adapted formula, showed the closest match applied to the current dataset, and compared to the other formulae presented in Section 2.4.5.3 (i.e. Equation 2.31-Equation 2.35, and Equation 2.38). As the discharge increases, the adapted Etemad-Shahidi & Taghipour (2012) formula provides predicted D_x values larger compared to the actual D_x obtained. Nevertheless, the divergence is attributed to the fact that that formula does not account for dead zones and vegetation.

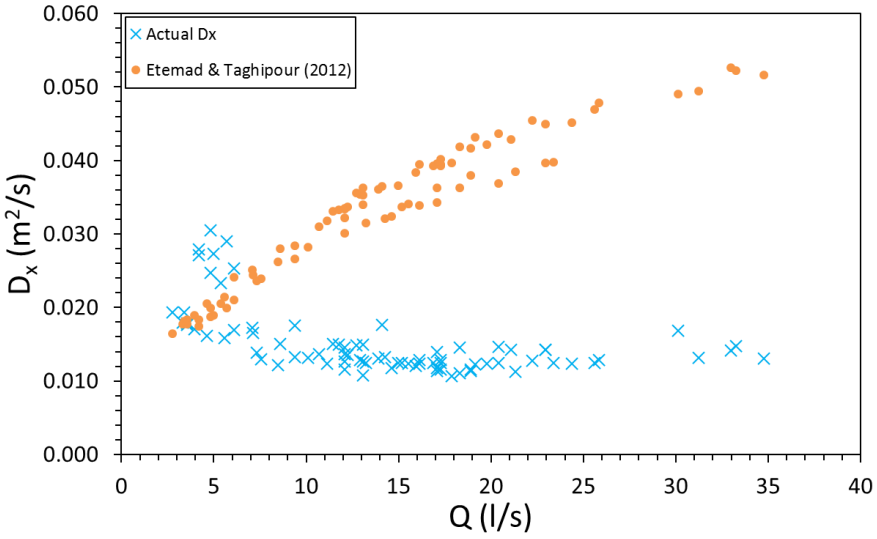

Figure 78: Measured D_x against Q in SW2 for the three months monitored. Predicted D_x is presented using Etemad-Shahidi & Taghipour (2012) formula.

The influence of discharge on the longitudinal dispersion is shown in Figure 79 indicating each month. Results show a slight decrease of D_x with increase in flow rate. D_x seems to have greater dependence at low discharges, i.e. 7 l/s, and particularly in high plant ages, i.e. February. The general trend suggests an inverse relationship between D_x, Q and flow depth, as also reported by other studies to date (Nepf, 1997; Shucksmith, 2008). For similar low discharges, February presents larger D_x coefficients compared to December, which is expected due to the deflected stems in February.

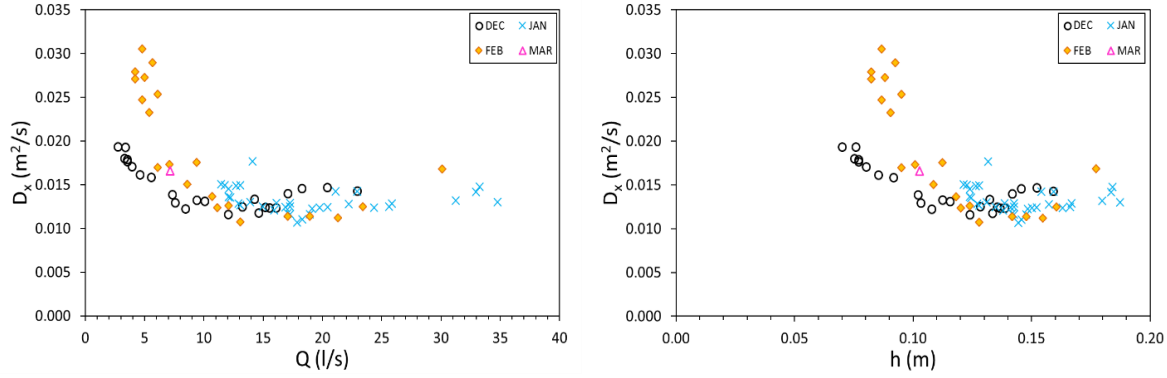

Figure 79: (Left) Relationship between longitudinal dispersion coefficient, D_x, and flow rate, Q, for different stem deflection degree during the dormant season. (Right) Dispersion coefficient against flow depth for different stem deflection degree during the dormant season.

The normalised longitudinal dispersion coefficient (using h) is depicted in Figure 80, which advocates the decrease of D_x with increase in flow rate, and the minor stem resistance existence in February, at the very low flow rates tested. It should be noted that similar characteristics were observed by non-dimensionalising D_x using W instead of h.

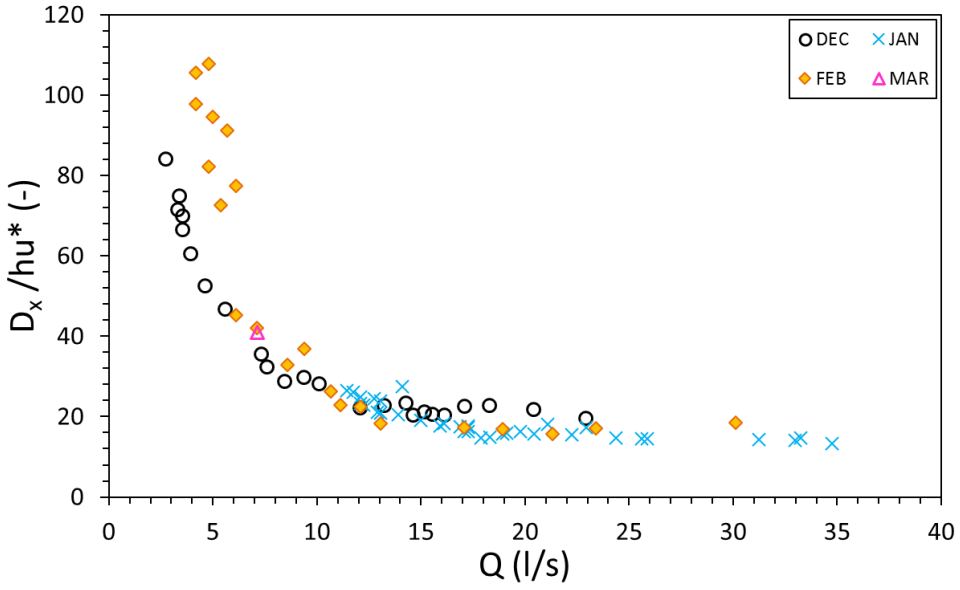

Figure 80: Normalised longitudinal dispersion coefficient against Q in different months in SW2. The trend shows a decrease of D_x with flow rate.

Dispersive fraction suggests a constant trend between D_f and Q (or flow depth) (Figure 81). The tendency appears to segregate into two sections, approximately at Q=12 l/s for December, and at Q=18 l/s for February. In particular, the D_f-Q relationship shows initially a negative correlation, where below the above mentioned Q values, D_f-Q relationship obtains a positive correlation. This interesting result possibly suggests independence of flow velocity and dispersive fraction, and is primarily attributed to the CW construction parameters (unbunded outlet layout, and irregular bed topography). These results manifest that there is a threshold beyond which water increases enough to utilise the shallower side of the wetland, introducing different mixing interactions. D_f suggests moderate and low dead zones in SW2, with slight increase of dead zone proportion in February, thus associated to seasonal plant variation. Furthermore, above a certain flow rate (or depth), D_f increases, entailing that dead regions augment in the system. This is explained due to velocity differences between

the main channel and the shallower area, where solute mixing exchanges at a different rate, requiring more time to reverse back into the main flow. Similar observation was remarked and discussed in section 4.3.2.2 (Figure 73).

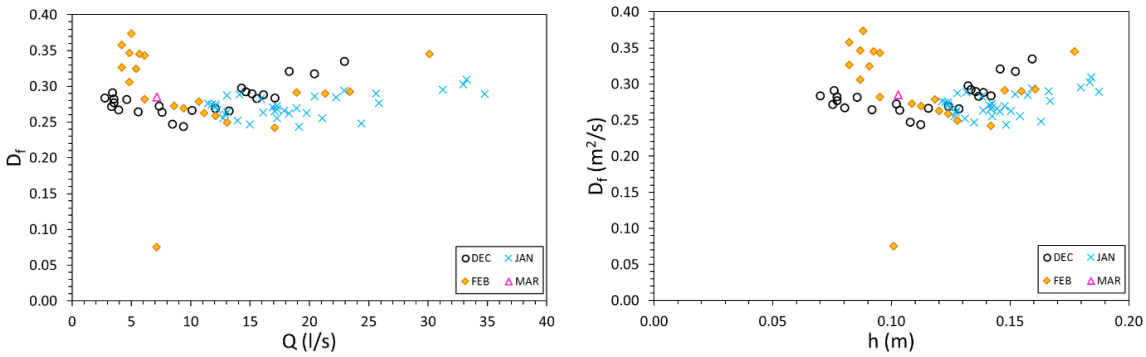

Figure 81: (Left) Dispersive fraction against Discharge. (Right) Dispersive fraction against flow depth. Both plots indicate a change in the relationship between D_f and Q or h above a certain flow rate or depth, which is attributed to the bed channel irregularity.

Effect of Seasonal plant variation on Mixing

Although plant age effect appears minimal in SW2, an investigation of any potential monthly trends of D_x and D_f during the dormant months is attempted in this section. This is achieved by plotting similar flow classifications. As such, Figure 82 (a)–(d) show the D_x and D_f against month (hence seasonal plant variation) for various discharges.

Although tracer tests were conducted only for the late dormant period, the fact that they involve the two extreme stem deflection conditions between December and February, provides confidence to interpret the data. Figure 82 suggests that there is a dependence of D_x on discharge for certain months. In particular, longitudinal mixing is larger in February (i.e. deflected stems) compared to December (i.e. upright stems) in the low flow classification. The gradual increase in discharge induces opposite trends, namely greater longitudinal mixing in December compared to February (Figure 82 (c)-(d)). This suggests that flow is discharge dominated rather than vegetation dominated.

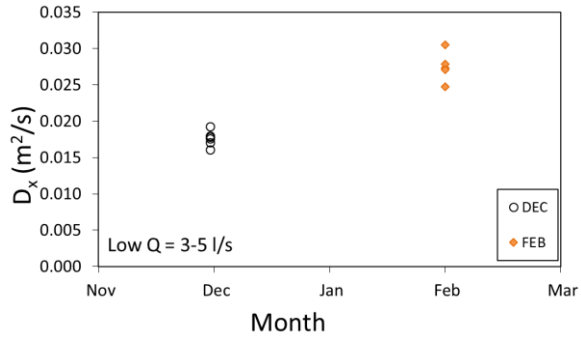

(a) Low Q = 3.0-5.0 l/s

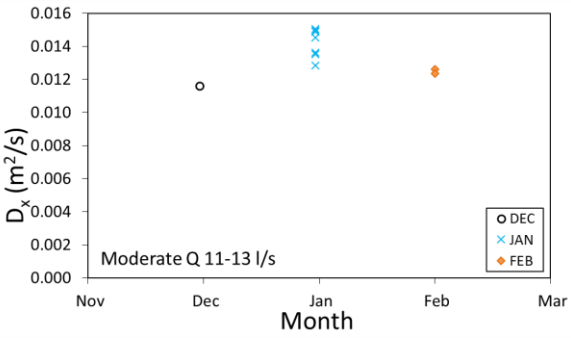

(b) Moderate Q = 11.0-13.0 l/s

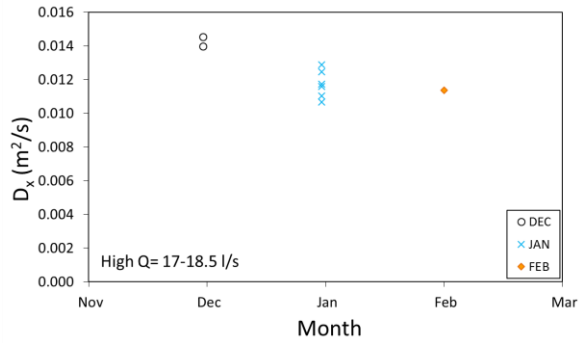

(c) High Q = 17.0-18.5 l/s

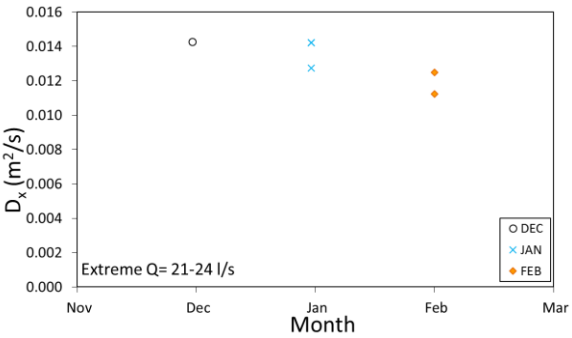

(d) Extreme Q = 21.0-24.0 l/s

Figure 82: Seasonal D_x against month for different flow classes in SW2.

Figure 83 shows D_f against month (hence seasonal plant variation) for various discharge classifications. D_f suggests that increase in discharge leads to more consistent mixing characteristics (i.e. less variation in mixing as Q increases), and evidences minor affinity with plant porosity variation inferred by the deflections of stems.

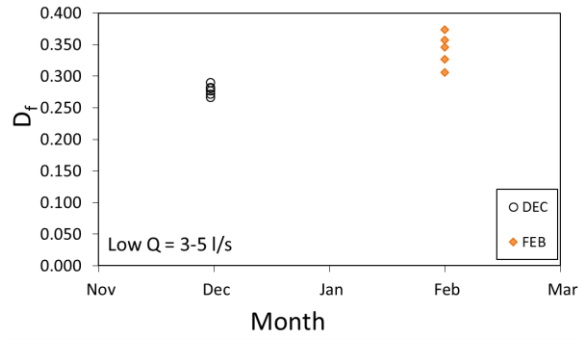

(a) Low Q = 3.0-5.0 l/s

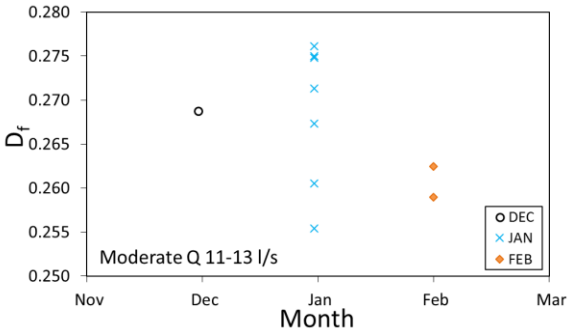

(b) Moderate Q = 11.0-13.0 l/s

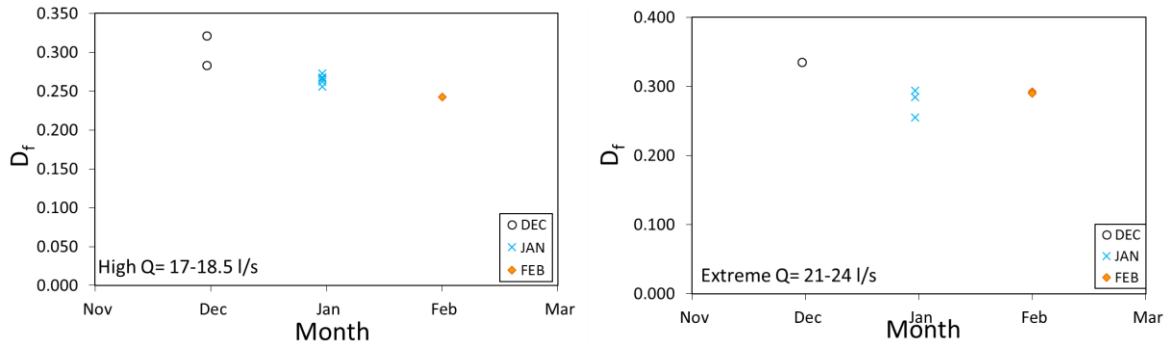

(c) High Q = 17.0-18.5 l/s

(d) Extreme Q = 21.0-24.0 l/s

Figure 83: Seasonal D_f against month for different flow bands in SW2.

Summarizing, the longitudinal mixing coefficient variation in SW2 is minimal in different months and flow rates. Furthermore, results showed that seasonal plant variation has less influence on the residence time and on mixing pattern in SW2 for the testing duration. Overall, a notable dependence on discharge is noticed. The effect of discharge is apparent on both D_x and D_f, in relation to the hypothesis that increase in flow depth (or velocity) promotes utilisation of the shallower part of the wetland. Overall, it is inferred that design parameters, such as bed topography, and unbunded outlet, have greater importance on the physical flow characteristics in the wetland, and overweigh the vegetation growth and ageing.

Effect of longitudinal mixing on stem Reynolds number

Mechanical dispersion might have an effect on mixing in emergent canopies, as discussed in Section 2.5. Nepf et al (1997) observed that plant stem wakes can cause mechanical dispersion, by deflecting and retarding some amount of the tracer mass. The influence of mechanical dispersion depends on the extent and strength of turbulence that the wakes generate behind the stems, which is expressed by the stem Reynolds number, NR^*. Therefore, should mechanical dispersion have a significant effect, D_x and NR^* should present a relationship.

Figure 84 demonstrates some relationship between the D_x and NR^* in different months. This suggests that mechanical dispersion process has some influence on the total mixing. Furthermore, it is observed that beyond a certain flow velocity (or discharge), this

relationship breaks; i.e. for December *NR** values beyond 170, for January and February beyond 190. As the *NR** increases, the flow regime around the stems alters progressively from ideal smooth flow, to entirely turbulent flow, causing a segregation zone behind the stems and generation of wakes.

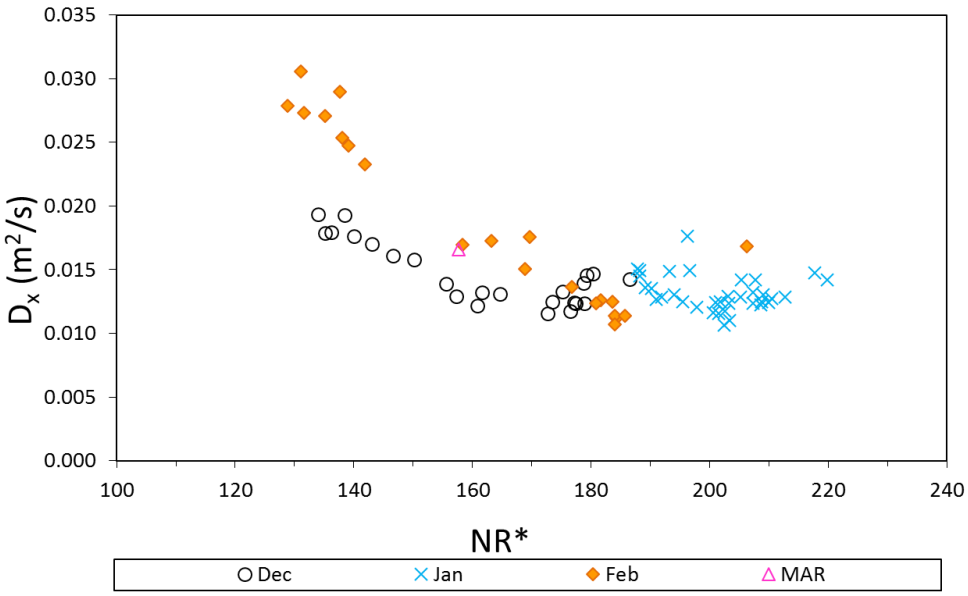

Figure 84: Dispersion coefficient against stem Reynolds number in SW2 during the dormant season.

Figure 85 isolates the effect of discharge on *NR**. It is observed that some weak relationship between D_x and *NR** exists particularly at the low discharges, suggesting that mechanical dispersion might have some influence on the net diffusion especially in laminar flows. However, as Q increases, there is no apparent relationship between D_x and *NR**, which is linked to the generally sparse stem population density. Possibly in denser canopies, mechanical diffusion has a greater impact at larger discharges, as reported by Nepf et al (1997) who found that there is an affinity between the stem population density and mechanical dispersion.

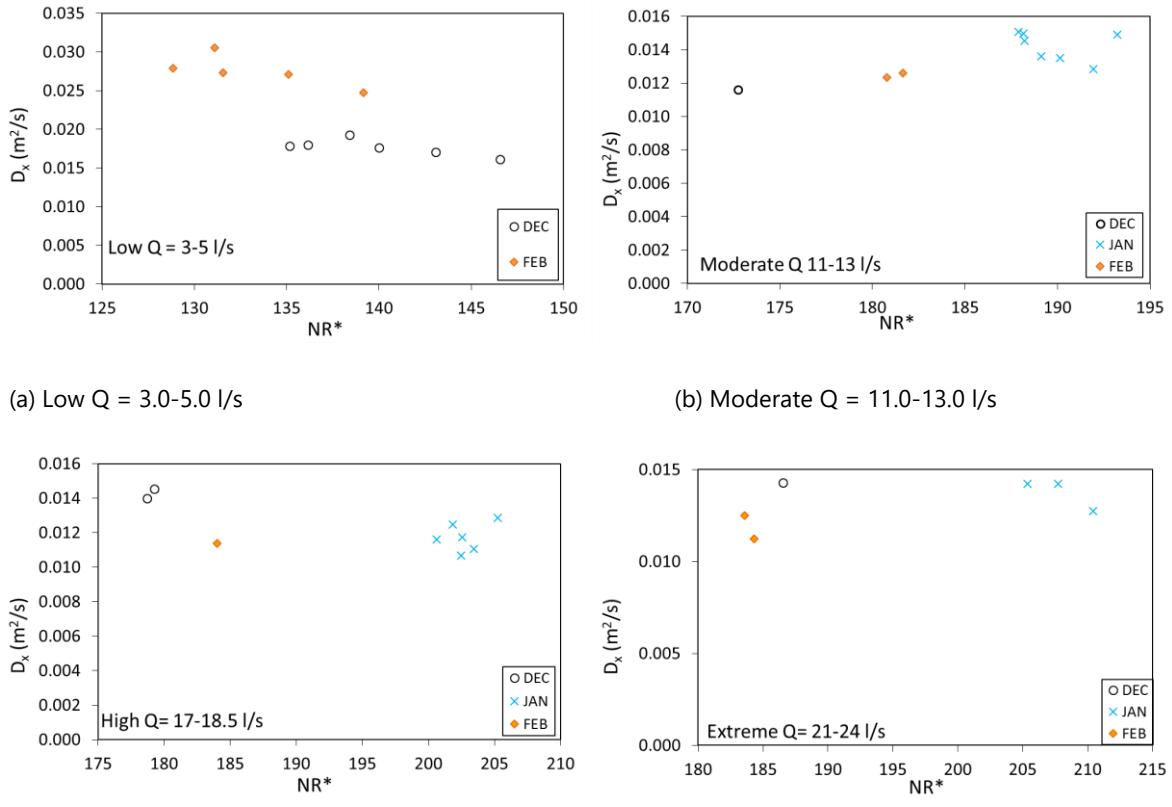

(a) Low Q = 3.0-5.0 l/s

(b) Moderate Q = 11.0-13.0 l/s

(c) High Q = 17.0-18.5 l/s

(d) Extreme Q = 21.0-24.0 l/s

Figure 85: Dispersion coefficient against Stem Reynolds number for different discharges in SW2.

4.3.1.7 Differential advection

Complementary longitudinal mixing tests were conducted for one week in February to elucidate the internal mixing characteristics in SW2. This monitoring duration was due to special availability of four extra fluorometers. Results are presented in Figure 86 for a moderate discharge, i.e. Q= 8.3 l/s. It has to be noted that due to limited variation in rainfall profile during that testing week, all the tracer tests experienced similar flow rates, ranging from 6 to 8 l/s. As a result, the flowing water was passing mainly through the preferential path, whilst the right shallower side of the wetland was overall dry.

For the flow conditions tested, Figure 86 indicates no differential advection in SW2, as the mean velocity in each location was the same. Therefore, it is deduced that plug flow conditions are fostered in SW2 during the high plant age. The overall short trailing edges indicate that tracer trapping is not an important source of mixing in this wetland.

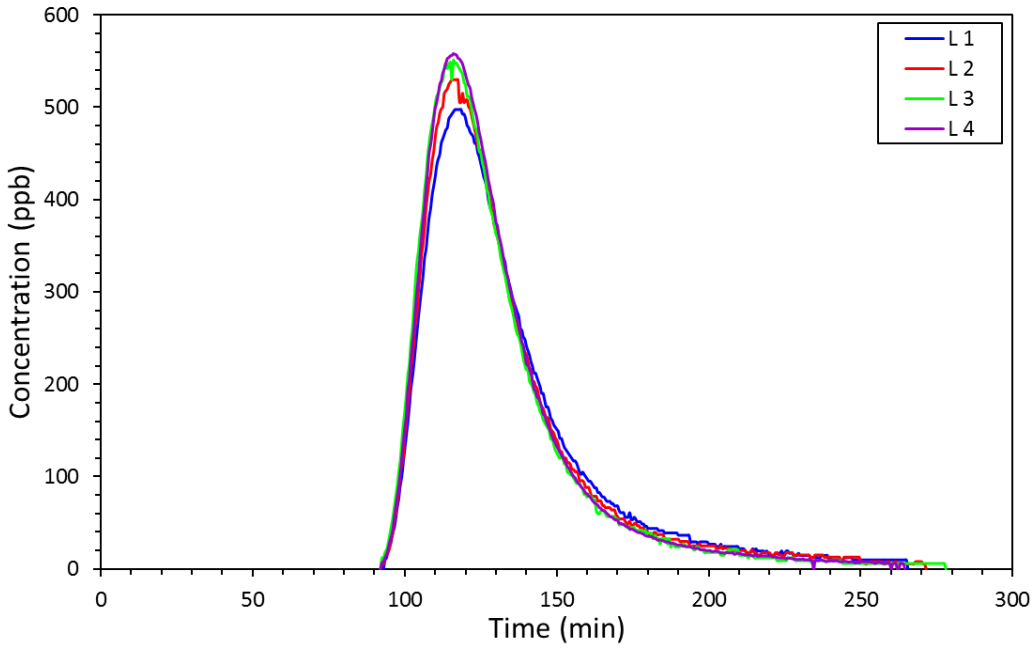

Figure 86: Transverse mixing study on one cross-section of SW2 for a low flow rate case. No differential advection occurs in the main channel.

4.3.1.8 Hydraulic efficiency – performance

This section presents and discusses hydraulic performance related parameters, i.e. hydraulic efficiency, number of CSTRs, effective volume ratio, in relation to the stem Reynolds number, discharge, flow velocity and depth.

Hydraulic efficiency

Hydraulic efficiency, λ, plays pivotal role in the CW design and investigation. As explained in section 4.2.2.8, calculation of λ_n using the t_n, fails to describe the actual conditions in the CW. As such, in order to describe a more real situation in the CW, λ is defined as the ratio of t_p over t_m, as previously used by Bodin et al (2012), and Chyan et al (2014). The presence of vegetation in FWS CWs introduces the use of stem Reynolds number, *NR**, and is expected to cause some variation in λ with Q or with seasonal plant variation. The relationship between the actual hydraulic efficiency λ and *NR** is presented in Figure 87. It is seen that there is no influence and interdependence between λ and *NR**, i.e. λ is constant with *NR** (the smaller plot in Figure 87 provides a zoomed in section of the y axis). This is in contrast with Chyan et al (2014) who linked λ and *NR** through an empirical formula, and found an inverse

relationship. In SW2, the effectiveness of stem wakes on λ is minimal. The divergence between the two studies is mainly attributed to the contrasting scale of discharge and size of the systems, i.e. Chyan et al (2014) established their relationships employing a small physical model (1m*0.3m*0.3m), whilst their tests were conducted in laminar flows with discharges 300 to 9000 times smaller than the current study.

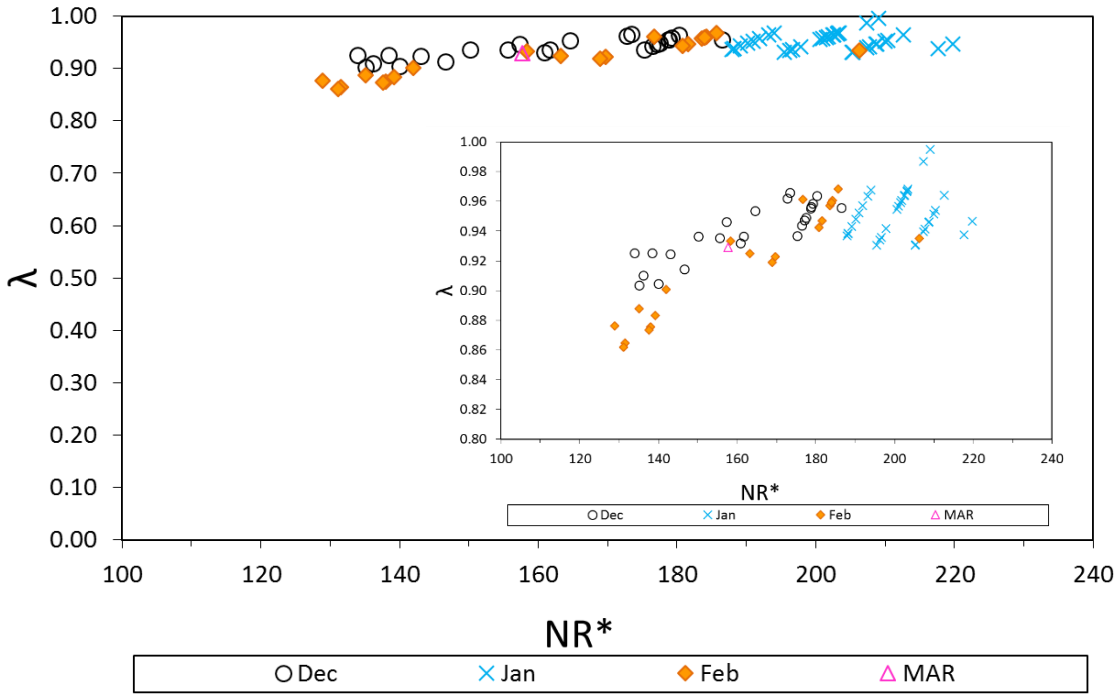

Figure 87: Stem Reynolds number against hydraulic efficiency in SW2.

Furthermore, it is contrasting that SW2 suffers from high short-circuiting, and provides very good hydraulic efficiency, ranging from 0.85 to 1. The plug flow conditions allow for high λ, however, SW2 is not necessarily an effective system in removing pollutants, due to the tube-like function and high the short-circuited flows.

Effect of flow depth on effective volume

The relationship of the effective volume ratio, e, and water depth in different plant ages is shown in Figure 88. Previous research has demonstrated that increase in stem density of emergent plants reduced e in CWs (Bodin & Persson, 2012; Schuetz et al, 2012). However, this is not the case in SW2, as the change in plant porosity results from stem deflection. Furthermore, there is no apparent relationship between e and h, for the limited water depth

conditions tested (h was on average lower than 0.2 m). Nevertheless, a slight increase in e with depth can be seen in Figure 88, until approximately 0.12 m. However, since this variation between flow depth and e is minor, these results cannot support Liu et al's (2016) recommendation, stating that there is a certain water depth that maximises the effective volume in the wetland. Moreover, as already pinpointed in the previous sections, the effect of bed irregularity is also visible in Figure 88, where the correlation of e-h becomes negative above a certain flow depth, i.e. h=0.12 m.

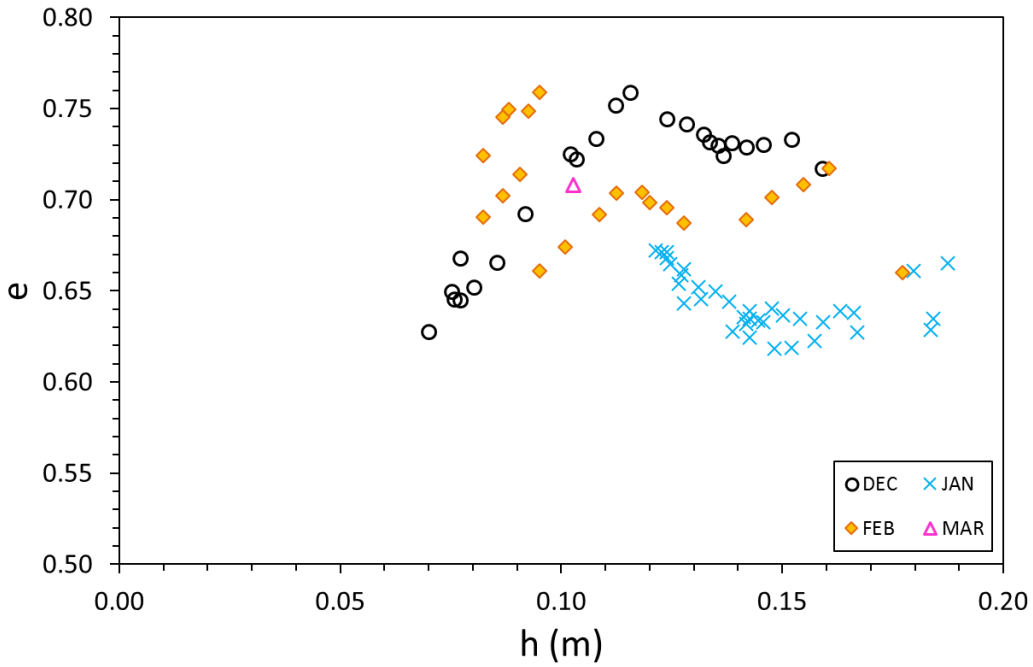

Figure 88: Effective volume ratio against flow depth for different plant ages in SW2. The correlation changes above a certain flow depth in each month, which is characteristic of the irregularity of the bed channel, inducing different mixing interactions.

4.3.2 Summary of the main findings in SW2

Recall the two variables investigated in SW2 were discharge variation and seasonal vegetation variation. The main findings and conclusions to be considered from Section 4.3 are:

- Tests during vegetation decay demonstrated less influence on mixing, and on the RTD shape.

- Flow pattern behaves like plug flow with minimal longitudinal dispersion, both in upright and in fully deflected reed stem positions.
- Seasonal vegetation variation presents minimal flow resistance in SW2. Minor flow resistance is observed only at very low flow rates.
- Discharge and flow depth indicate primary affinity to the bed channel irregularity. Bed channel topography overwhelms the effect of seasonal vegetation variation on mixing and flow characteristics.
- Increase in flow rate promotes significantly advective flow.
- In fully deflected stem conditions, there is zero differential advection at low and moderate discharges. Flow travels uniformly across the main channel.
- A decrease in longitudinal mixing with increase in discharge (or flow depth) is observed.

Further discussion of the summary of the SW2 conclusions is conducted in Chapter 5.

5. Summary of SW1 & SW2 Results & Discussion

This section summarises the results and discussion provided in Chapter 4, regarding how seasonal vegetation variation affects flow and mixing characteristics. The summary comprises values from the stream (base case), SW1 and SW2.

5.1 Summary of Vegetation Ageing Effect

The effect of seasonal vegetation variation and natural decay on hydraulic performance and mixing characteristics was explored and investigated in this study in two similarly sized CWs. It was primarily deduced that seasonal vegetation variation affects the RTD shape, the mixing characteristics and flow structure. Seasonal vegetation variation was especially pronounced between the two extremes of plant cycle, i.e. February and June, and only in SW1. Secondly, the results of this study revealed that seasonal vegetation variation has secondary influence on the hydrodynamics compared to other design factors, such as outlet layout, and bottom topography. In particular, the two in-series CWs, despite having similar construction design features, demonstrated unlike affinity with seasonal vegetation variation. A summary of the discussion and conclusions is provided as follows:

a. Seasonal vegetation variation effect on flow structure and mixing characteristics was overt in SW1, whilst less influential in SW2. Mixing characteristics in SW1 exhibited variation between plug flow with longitudinal dispersion for upright stems, and plug flow with mixing due to dead zones creation, closer to the highest age, i.e. February (i.e. fully deflected stems). Variation in the canopy morphology due to stem deflection changed the channel porosity, inducing resistance and creating more clusters, through which the tracer required more contact time in order to revert back to the main flow. Furthermore, longitudinal dispersion coefficient varied up to four times between the two extremes of seasonal vegetation variation, i.e. February and June in SW1. Taking into consideration the similar construction design and the

random array of stems in both SWs (and also the comparable stem population density numbers between them), the lesser influence of seasonal plant variation on mixing and flow pattern in SW2 is specifically attributed to design elements; for example, the formation of the irregular bed channel promotes preferential flow at the deeper channel part. A regular bed channel topography is anticipated to induce different effects on the transverse water distribution, and to dissipate the short-circuiting levels in SW2.

b. Seasonal plant variation appeared to be a secondary factor in affecting the hydrodynamics of full-scale FWS CWs, when bed irregularities exist and when systems are unbunded. Irregular bed topography was shown to be the dominant factor affecting short-circuiting compared to seasonal vegetation variation. This result is in agreement with Min & Wise (2009), who found more affinity of short-circuiting with bathymetry than with vegetation heterogeneity. Furthermore, design construction of a dam or embankment at the outlet to regulate the outflow and maintain sufficient quantity of operational volume is deemed another important factor. In this way, water hold back, and greater utilisation of the available total volume could be achieved. The effects of an outlet dam are considered beneficial to increase the HRT, and to abate the short-circuiting levels. The fact that the downstream dam in both SWs has not yet been re-installed, after having been washed away (many years previously), is considered the dominant feature for elevated short-circuiting levels in both systems.

5.2 Summary of Longitudinal Mixing

The longitudinal mixing coefficients in the three connected systems, namely stream, SW1, SW2 were shown in Figure 50, Figure 59, and Figure 79 respectively. The range they present in D_x differs per system, where, in particular (Figure 89):

i. Stream D_x coefficients display a wide range, between 0.01 and 0.3 m^2/s.

ii. SW1 D_x coefficients lay within 0.03 and 0.13 m^2/s.

iii. SW2 displays a pretty constant dataset of D_x coefficients spanning between 0.01 and 0.03 m^2/s.

A strong positive correlation between D_x and Q is observed in the Stream, whereas SW1 displays a mild positive correlation (Figure 89). However, relationship between D_x and Q in SW2 is almost constant, whilst slightly negative. Recall that the methodology to process the data, and particularly to identify the boundaries (i.e. start/end point) of the concentration profiles, has been applied consistently in each system. In particular, the selected cut-off value was 1% of the peak concentration (Chapter 3, Section 3.5.3). The reason for maintaining the same methodology for data processing (i.e. using a fixed cut-off value), was to achieve best consistency of D_x results, and less biased results, because SWs form part of the same site, and of an overall in-series system, and have same design characteristics.

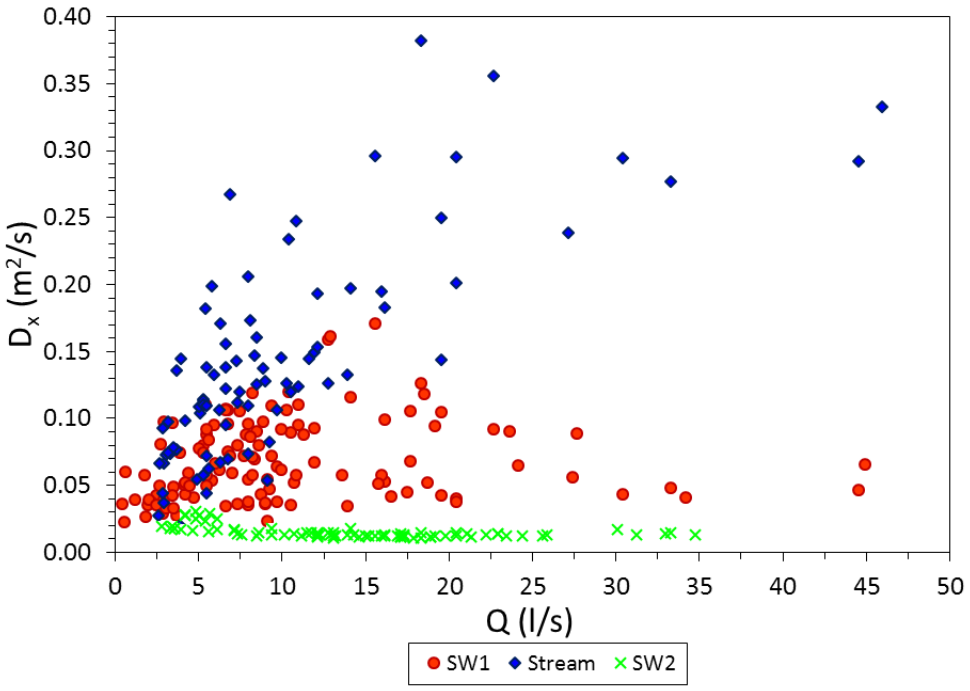

Figure 89: Comparison of D_x coefficients against Q between the in-series South Wetland systems.

However, it is noticed that SW2 D_x coefficients present minimal variation, and an overall ideal trend. Therefore, in order to have a better overview of the SW2 D_x results, analysis was carried out only on the SW2 tracer tests, applying a lower cut-off value of 0.2% of the peak concentration. This analysis was complementary, and is mentioned only for reference

purposes in this section. Results of SW2 D_x coefficients under the lower cut-off value are presented in Figure 90, where the stream and SW1 have been processed by the 1% cut-off value. SW2 D_x coefficients in Figure 90 are slightly increased compared to those in Figure 89, and range between 0.03 and 0.08 m^2/s, whilst they are closer to SW1 D_x coefficients only for the low discharges. More results pertaining the mixed cut-off values processing are included in Appendix III for reference purposes.

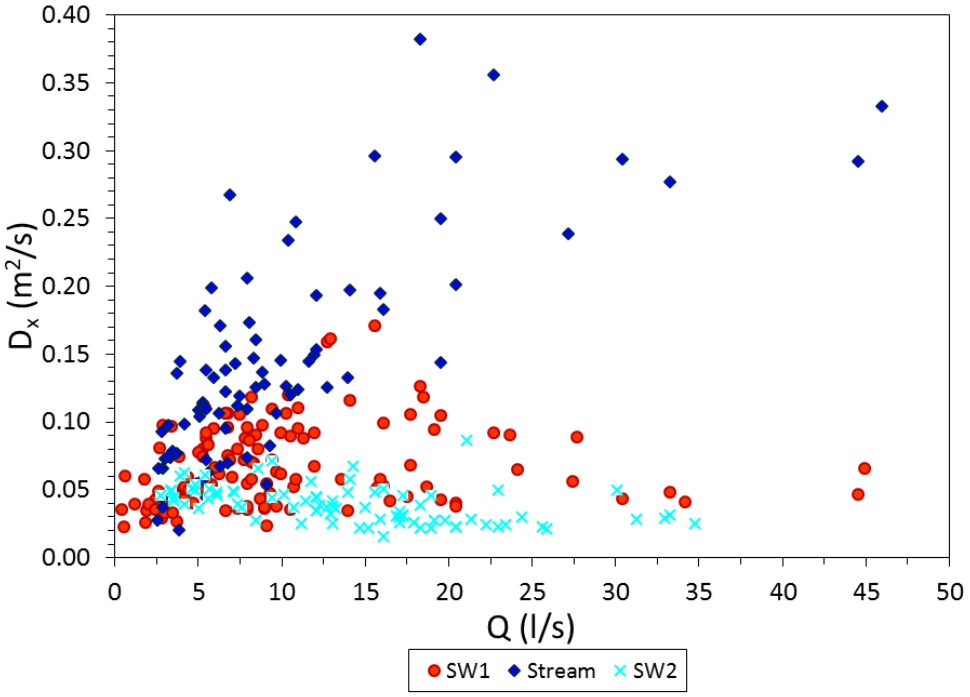

Figure 90: Comparison of Dx coefficients against Q between the in-series South Wetland systems, where SW2 data is analysed with a lower cut-off value, i.e. 0.2%.

The non-dimensional longitudinal dispersion coefficients D_x/hu* against discharge for all the SWs systems are depicted in Figure 91, and generally fall within the range provided by Rutherford (1994), i.e. $30<D_x/hu^*<3000$. SW2 obtains the lowest D_x coefficients, restricted in a very narrow band. This might be characteristic of the pipe (or plug) flow effect that this system experiences. Dimensionless D_x coefficients in SW1 and in the Stream are of similar magnitude though. Nevertheless, the processes liable for the comparatively elevated SW1 and stream D_x coefficients compared to SW2 D_x coefficients, are different in each system; in particular, stagnant backwaters (i.e. prolonged RTD tails) are related to the SW1 D_x coefficients, whereas in the Stream, the different shape and non-vegetated nature may

enhance mixing. Overall, the reduction of D_x/hu* with increasing flow rate, as seen in Figure 91, has been previously reported in other river studies (Rutherford, 1994). This reduction is caused because as the flow increases, differential advection across the channel and bed friction influence are reduced, whilst transverse mixing coefficient augments.

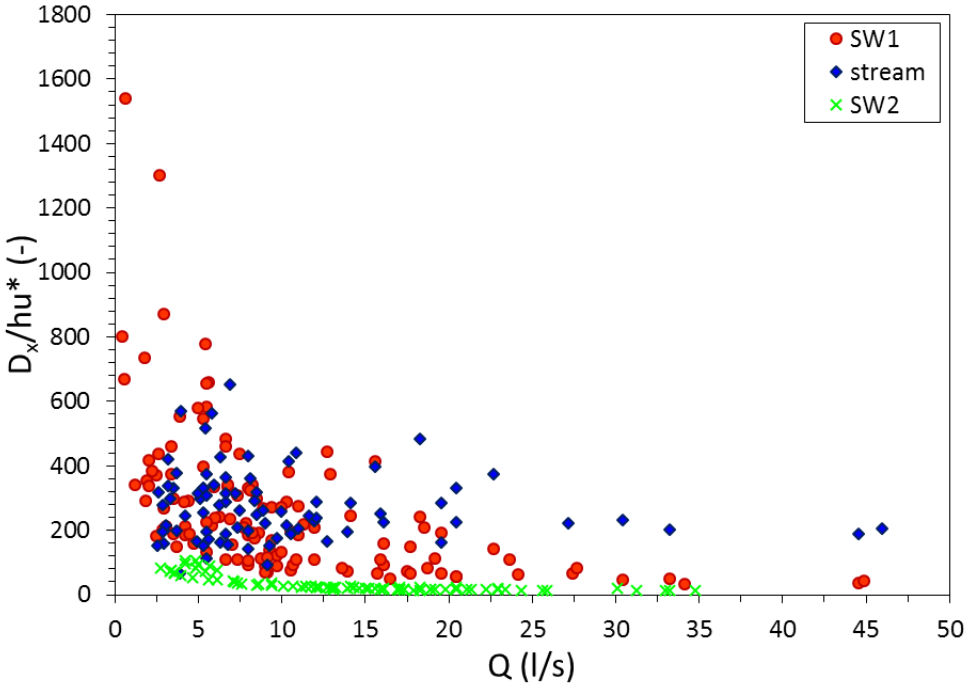

Figure 91: Comparison of normalised longitudinal dispersion coefficients between the three in-series systems at South Wetlands. Normalised D_x reduces with increase in flow rate.

It is generally expected that non-vegetated systems obtain larger D_x values compared with vegetated systems (Kadlec et al, 1994; Nepf et al, 1997). This may explain initially why the stream, as a non-vegetated base case, received a wider range of D_x coefficients, relatively larger than the SW1. The dimensionless form of D_x indicated similar range of D_x coefficients between SW1 and Stream though. The formation of dead zones due to the presence of plants or influence of seasonal plant variation, enhance the longitudinal dispersion due to trapped plume within those regions, thus due to the associated long distribution tails. As presented and discussed in Sections 4.2.2.6 and 4.3.2.6, similar characteristics were observed in SW1 and SW2 irrespective whether W or h was used to non-dimensionalise D_x. Therefore, presentation of the dimensionless D_x in this section was done using h.

Regarding the difference in the D_x coefficients between SW1 and SW2, this might be a result of the differential advection. Longitudinal dispersion is the result of the coupled effects of differential advection and transverse diffusion. SW1 exhibits differential advection, while SW2 experiences uniform velocities and isotropic turbulence (see Sections 4.2.2.7 and 4.3.2.7). The affinity of differential advection with the D_x, possibly explains the much lower D_x coefficients existing in SW2.

The magnitude of D_x coefficients in SW1 is comparable, although slightly greater than Shucksmith's (2008) D_x coefficients (i.e. 0.005-0.018 m^2/s), who conducted tests in reeds and in similar discharges (i.e. 10-30 l/s) for two contrasting plant seasons, albeit in laboratory conditions. Nevertheless, SW2 D_x coefficients are very similar to Shucksmith's (2008) study. Shucksmith (2008) reported that the increase in plant age resulted in D_x reduction, where plant age was mainly expressed as a function of stem population density increase. However, in that study the vegetation was planted in situ and thus could not represent the actual natural growth, which was further affected by the indoors conditions (i.e. less exposure to direct sunlight, and warmer temperatures especially in winter months). The difference of that study with this study, is that this study aimed and achieved to monitor the entire dormant plant season, and the subsequent new plant cycle growth in this UK micro-climate outdoor conditions, incorporating the transition stage due to decomposition between the old and new stems cycles. Therefore, due to the inherent difficulties in monitoring the variation in stem population density, the seasonal plant variation in this study is expressed through the variation of the reeds' stem deflection, due to stem decay.

The slightly larger D_x values obtained in SW1 compared to Shucksmith's (2008) may be either due to the different aspect ratio, A_R, between the two systems, or due to the different bed channel shape, introducing differential advection. Persson (2000) underlined that the CW A_R affects significantly the amount of mixing. In particular, a high A_R = L/W promotes plug flow, diminishing dispersion levels. Shucksmith (2008) conducted tracer tests on real Phragmites in a laboratory flume with A_R =14.5/1.22 =11.9; the SW1 A_R varied between 5 and 13 depending on the tested flow rates. Variation in the A_R (as a function of flow rate) may introduce a greater variation on the D_x of the present study. The second possibility is that

lower differential advection is expected in the laboratory flume, due to the regulated inflow, the zero wind interference, and the rectangular channel shape, all of which might have contributed to lower D_x coefficients achieved. Comparing with the present study, differential advection was found in SW1. The occurrence of differential advection in SW1 is a function of non-ideal shape of the natural channel, and the associated secondary flows which may occur near the banks, as well as the bed friction. In addition to those attributes, the presence of natural deflected vegetation may add on the differential advection magnitude, creating dead zones and eddies in which the tracer plume spends more time until released back. From the above, it is hypothesised that differential advection has a significant impact on the longitudinal dispersion, and that the field effects are primarily liable for the larger D_x coefficients of this study.

Another experimental study that measured D_x coefficients was conducted by Nepf et al (1997), using dowel vegetation (0.6 cm diameter) in a small-scale laboratory flume. For the low plant population density investigated, i.e. 280 stems/m^2, the authors found D_x coefficients ranging between 2.5-3.8 cm^2/s (for mean velocities 2.9-7.4 cm/s). That population density is comparable to the present study. The magnitude of those D_x coefficients obtained is between 10^2 to 10^3 times smaller than the D_x coefficients obtained in SW1, whereas they are of same magnitude with SW2. Among the possible factors conducive to this divergence is importantly the field effects in SW1 (i.e. irregular shape and differential advection) and the different A_R between the systems (namely 5-13 for SW1, and 20/0.38 = 52.6 for Nepf et al's (1997) study).

5.3 Summary of Flow Patterns

The calculated Pe numbers allowed to distinguish different mixing regimes between the two wetlands. Figure 92 depicts the Pe number against some flow and mixing variables, i.e. Q, *Mo* index, λ, and D_x/hu*. Figure 92 (a) indicates increase in Pe with Q in both SWs, albeit SW2 shows greater correlation. Concerning mixing properties, Figure 92 (b) and (d) manifest greater variation in longitudinal and in overall mixing in SW1, maintaining a strong negative

correlation with Pe. This suggests that increase in Q increases Pe, thus advective process prevails. However, SW2 suggests minor variation in mixing processes (i.e. steady mixing conditions), and continuous increase of advection with discharge (Figure 92 (b) and (d)). Similarly with the abovementioned outcomes, hydraulic efficiency, λ, shows minimal dependence on flow rate in SW2, whereas λ demonstrates enhancement with increase in flow rate in SW1 (Figure 92 (c)). From the above, it is deduced that although the two SWs have the same design characteristics and size, they demonstrate completely different mixing characteristics. In SW2 advection dominates, and the main flow regime is plug flow, whilst SW1 experiences less advective flows, greater mixing, and stagnant backwaters which vary with seasonal vegetation. The differences in the mixing and flow properties between the two wetlands are attributed to internal design parameters, i.e. irregular bed channel in SW2 fosters preferential flow.

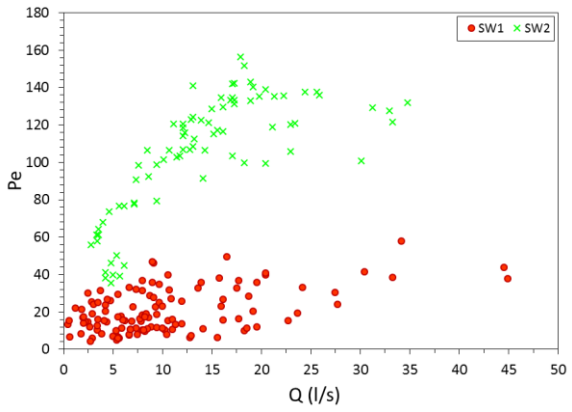

(a) Pe against Q.

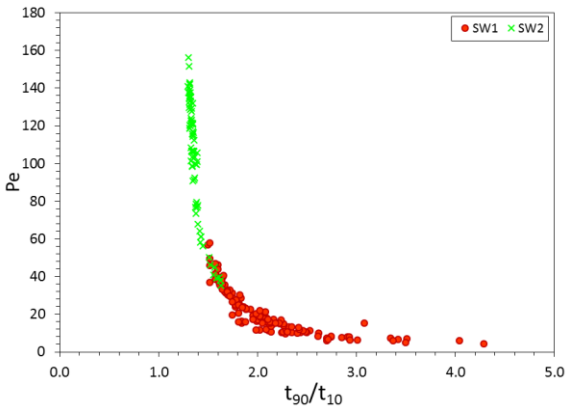

(b) Pe against Mo index.

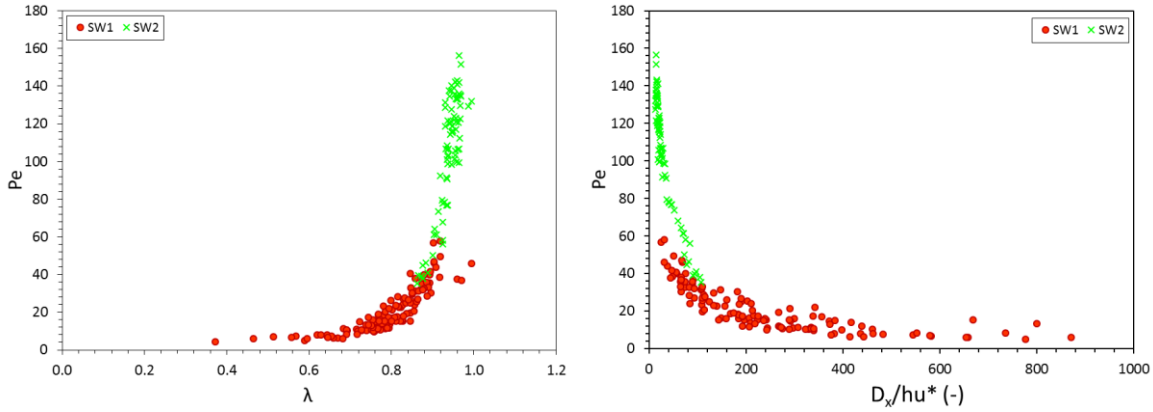

(c) Pe against λ.

(d) Pe against non-dimensionalised D_x.

Figure 92: Comparison of Pe number with discharge, mixing index, and hydraulic efficiency between SW1 & SW2. There is a distinct variation of Dx (and mixing processes) with discharge in SW1, whilst SW2 demonstrates less dependence of mixing characteristics on flow variation.

5.4Summary of Hydraulic Efficiency

The hydraulic efficiency of SW1 and SW2 is presented and discussed in this section. Using parameters of the RTDs that reflect the actual hydraulic efficiency, $\lambda=t_p/t_m$, in each system, it was found that SW2 lies into the excellent classification, whilst SW1 receives lower λ values, albeit they still fall mainly into the good quality classification (Figure 93 (a)). SW2 has minimal dependence on Q, which is characteristically attributed to the pipe flow regime, due to the bed channel irregularity. Although λ is realistically very good in that system, the flow regime (i.e. pipe flow) and the associated very short HRTs, do not correspond to the expected typical CW function in terms of pollutants treatment and hydraulic performance.

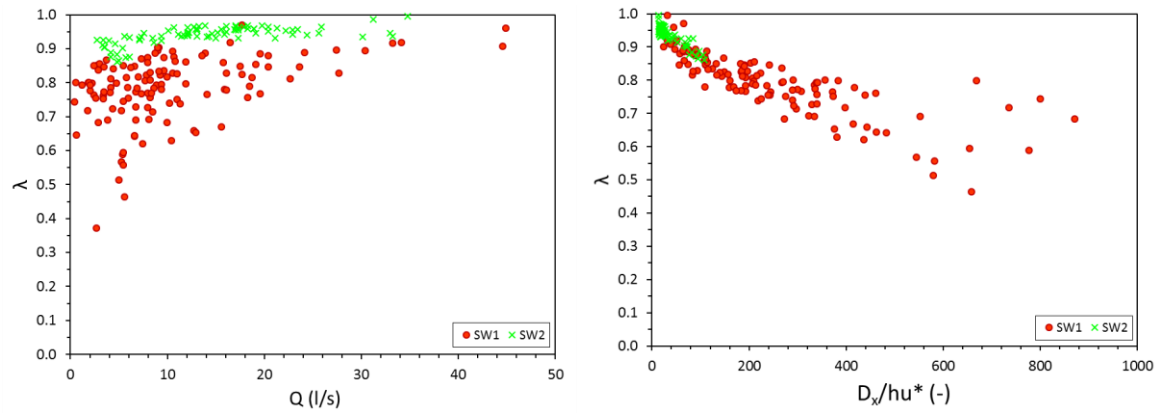

(a) λ against Q.

(b) λ against D_x/hu*.

Figure 93: Comparison of hydraulic efficiency and flow rate (a), and hydraulic efficiency and dimensionless longitudinal dispersion coefficient (b) between SW1 & SW2.

Regarding SW1, λ displays greater variation with flow (Figure 93 (a)) and season (see Section 4.2.2.8, Figure 70). It is seen in Figure 93 (b) that SW1 shows a strong negative correlation between λ and longitudinal dispersion (which is also valid for SW2). The value of λ increases with discharge, and varies with season, and particularly in late dormant season (i.e. February). By definition λ incorporates and reflects the RTD shape (i.e. mixing) and the effective volume utilisation. This explains the reason why λ varies mainly in SW1, reflecting the impact of seasonal vegetation variation on mixing and on flow pattern.

6. Further Applications & Experimental Results

This chapter presents the results of further applications – case studies investigated during this PhD study. The applications comprise four outdoor full-scale systems, and in particular, two CWs and two lagoons, across the UK. The case studies were monitored and assessed for their hydraulic performance and mixing characteristics, using fluorescent tracer tests.

The aims of this chapter are to contribute to the current knowledge regarding mixing characteristics, effect of system size on contaminant dispersion, and assessment of hydrodynamic behaviour of large full-scale treatment units. It has to be noted that the tests were conducted simultaneously with the SWs testing programme (detailed in Chapters 3

and 4), and, therefore, were at times subject to particular challenges, such as time restriction, site proximity, equipment shortage. This chapter initially introduces the testing and design conditions of each system, and provides discussion of the obtained results.

Results are divided into three sections, to facilitate comprehension and comparison between the systems. Section 6.1 presents North Wetland, which is a FWS CW in the RSPB farm in Cambridgeshire; Section 6.2 presents the A-Winning Minewater Treatment Scheme, which is a FWS CW in Derbyshire; Section 6.3 introduces the Clough Foot Lagoons, located in Yorkshire.

6.1 North Wetland (NW)

6.1.1. System Description

North Wetland (NW) is located at the north part of the RSPB farm, Knapwell, Cambridgeshire (farm details are provided in Chapter 3). This is a FWS CW, of fully emergent vegetation, where Phragmites australis is the dominant plant species, covering the full breadth of the channel. The system has dimensions of 32 m length, 6 m average width, and a minimum of 0.4 m mean water depth during discharging conditions. Water depth is regulated from the downstream bunded conditions, where an elevated closed pipe is set in an embankment (Figure 94 and Figure 95 (a)), and discharges the water into the ditch further downstream (Figure 95 (b)). A plan map of the NW is shown in Figure 94, indicating the key monitoring locations for the longitudinal mixing study, and the differential advection study at a cross section 5 m before the outlet pipe. The hydrological regime is intermittent and seasonal, because flow depends on rainfall, and particularly on the water drained via the surrounding lands' drainage system. The influent type treated through this wetland is agricultural runoff.

The rainfall-runoff record for the monitoring period (November 2015-June 2016) is shown in Figure 28.

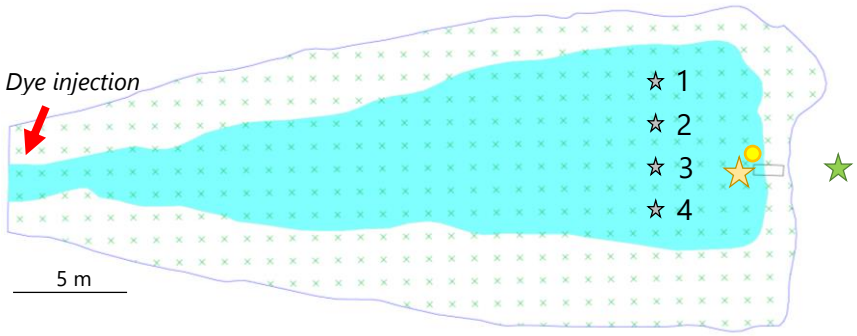

Figure 94: Schematic plan view for NW. Numbers indicate the transverse mixing measurement location names.

(a) Entrance of the exit pipe at the outlet of NW (side view). (b) Pipe exit at downstream ditch.

Figure 95: Outlet pipe location at NW, upstream (a) and downstream (b) of the embankment.

6.1.2. Methodology

It is noteworthy that this system has been being monitored concurrently with the SWs operations, and that data collection was desirable, but not pivotal. The original and central aim was the monitoring of the vegetation seasonal effects on flow pattern and mixing characteristics. The reason that led to the decision of monitoring this system was the

contrasting bunded outlet, which creates a deeper system, compared to SW1 and SW2. NW was instrumented by an automated tracer injection system (Figure 94), and was being monitored during autumn 2015–spring 2016 (Campaign I), aiming at the seasonal vegetation variation.

However, the main testing period proved fruitless in terms of monitoring the seasonal vegetation variation effect on mixing characteristics, due to the dry weather conditions and the intermittent hydrological regime. Both the drought (lack of rainfall) and the large HRTs occurring at low discharges (e.g HRTs varied approximately between one to three days), required a more sophisticated automated tracer injection system, that could be triggered for low-defined and high-defined discharges. Additionally, the quick effect of flushing-through water in the wetland, resulted in changing quickly the flow rate in the NW. Such an effect made part of the collected tracer tests inappropriate for use and analysis, as by definition, discharge is regarded steady in the slug injection method to derive the RTD.

Due to those challenges, the automated tracer injection system managed to collect only a small amount of tracer tests, thus the seasonal vegetation variation effect failed to be monitored. However, a typical record of the vegetation characteristics in NW is provided in Appendix IV.

In order to obtain more robust results and to elucidate further mixing processes in the NW, a complementary tracer test campaign was conducted between December 2016 and January 2017 (Campaign II), as completion of tests in the other monitoring sites allowed for equipment use at that period. This expedition included instrumentation of the NW to monitor flow depth before the outlet pipe, as well as differential advection in one cross-section of the wetland (location name details are illustrated in Figure 94). The key location to monitor longitudinal mixing was before the outlet pipe (Figure 94), however, an extra fluorometer was installed downstream of the exit pipe, in the ditch (shown in Figure 95 (b)), as a secondary measurement of concentration profiles, as a small amount of seepage was evident in the bunded dam section. During Campaign II, a brief series of tracer tests of

manual slug injections was conducted, because of the intermittent flow regime, and lack of rainfall.

In both campaigns, discharge was measured via the dilution gauging, using the tracer. Alternative way to measure the flow rate was not possible at that time (e.g. instrumenting NW with a V-notch weir or Venturi flume). Flow rate results and measurements might be qualitative, but they are representative of the actual flow conditions, as double-checked from the pressure transducer recording the flow depth during Campaign II.

6.1.3. Fluorescent tracing results

6.1.3.1. All tests collected

The summary of the 10 collected tracing tests is presented in Table 6.1, assembling essential hydraulic parameters. A unique test code identifies each test, where first value refers to the test number, and second value states the campaign period (i.e. I or II respectively). The shadowed section in Table 6.1 designates Campaign II tracer tests. The flow conditions were very low during all tests, with Re ranging between laminar and transitional flow.

Table 6.1: Summary of test series & transport parameters from the RTD analysis of the 10 tests in NW for both campaigns.

Test unique code	*Month*	*Date*	*Flow rate, Q* (l/s)	*First arrival time,* t_1' (h)	*Travel time,* t_m (h)	*Nominal residence time,* t_n *(h)*	*Dispersion coefficient* D_x (m^2/s)	*Number of CSTR, N*	*Hydraulic efficiency,* λ (t_p/t_m)	*Effective volume ratio, e* (t_m/t_n)
1,CI	Dec	18/12/2015	0.05	3.3	13.0	(91)	0.008	2.2	0.51	(0.1)
2,CI	Jan	01/01/2016	0.9	0.8	1.7	(6)	0.024	5.5	0.64	(0.3)
3,CI	Jan	14/01/2016	0.1	0.3	4.1	(32)	0.031	1.7	0.55	(0.1)
4,CI	Feb	19/02/2016	1.3	0.5	2.3	(5)	0.046	2.1	0.39	(0.5)
5,CI	Feb	25/02/2016	0.3	5.7	14.3	(16)	0.003	6.0	0.67	(0.9)
6,CI	Mar	11/03/2016	1.0	0.6	1.5	(6)	0.028	5.4	0.72	(0.2)
1,CII	Dec	11/12/2016	5.1	0.7	1.4	2.5	0.009	9.8	0.80	0.6
2,CII	Dec	14/12/2016	0.9	2.5	4.7	9.7	0.003	2.8	0.70	0.5
3,CII	Dec	24/12/2016	0.7	1.7	5.4	8.3	0.002	4.8	0.80	0.7
4,CII	Jan	03/01/2017	3.8	0.9	3.8	2.0	0.005	7.3	0.75	0.9

Due to the ongoing multiple missions in the other monitoring systems, the flow depth was not continuously measured in the wetland during Campaign I due to equipment availability. Therefore, V_{tot}, t_n and e values were approximated, and are shown in brackets in Table 6.1.

6.1.3.2. Analysis of measured concentration profiles RTDs/CRTDs

This section presents the RTDs obtained from the tracer tests during both campaigns, as illustrated in Figure 96. All cases experience similar flow rates, expect for test 1,CII, obtaining the highest discharge for the season, 5 l/s. Figure 96 distinguishes Campaign I tests into two discharge conditions: low, i.e. Q>0.5 l/s, illustrated by thermal coloured continuous lines (i.e. orange, red, magenta), and very low, i.e. Q<0.5 l/s, displayed by dark colours and dashed lines. The need for this differentiation arose because of the characteristic shapes of the obtained RTDs. The nearly stagnant flows (Figure 96, dashed lines) produce distinctly high attenuation of solute concentration, and appreciable delay of the first arrival time. This indicates a high ponding or detention effect, and suggests that flow depths were nearly flowing through the outlet pipe. The compiled CRTDs for the NW tracer tests in both campaigns are shown in Figure 97, where time axis is normalised by the actual residence time, t_m. Overall, the mixing pattern suggests reasonable flow with a large quantity of dead zones, as demonstrated by the exponential decay of the distribution tail, and by the t_m being in the expected place. It is suggested that the flow pattern shows some variation depending on the hydrology (flow depth and discharge).

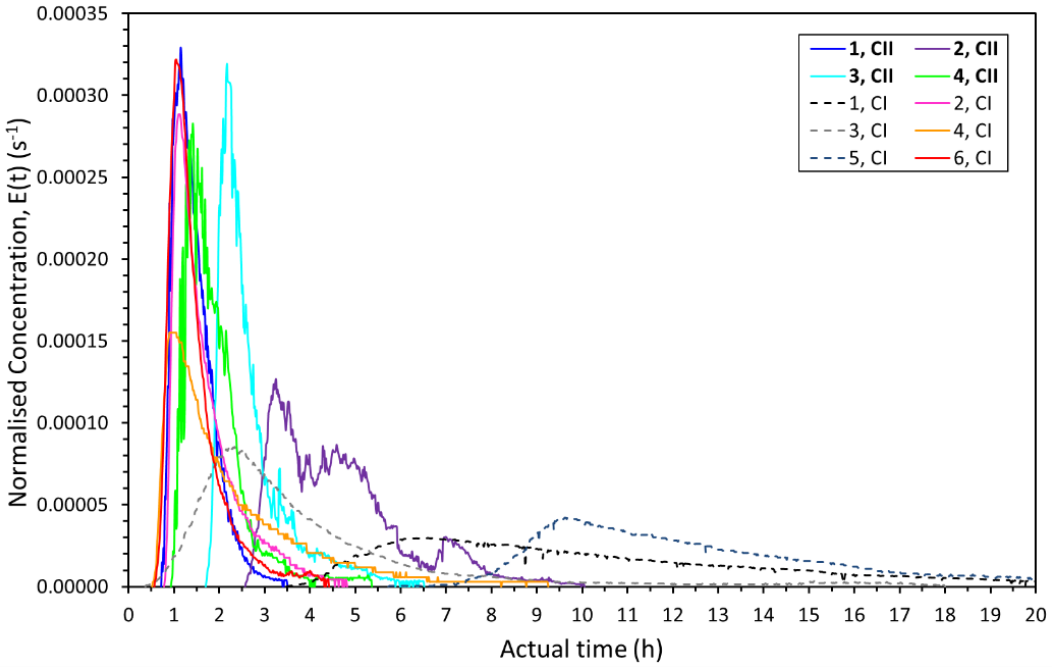

Figure 96: Compilation of RTDs obtained in NW. Concentration on y axis is normalised by the M_0.

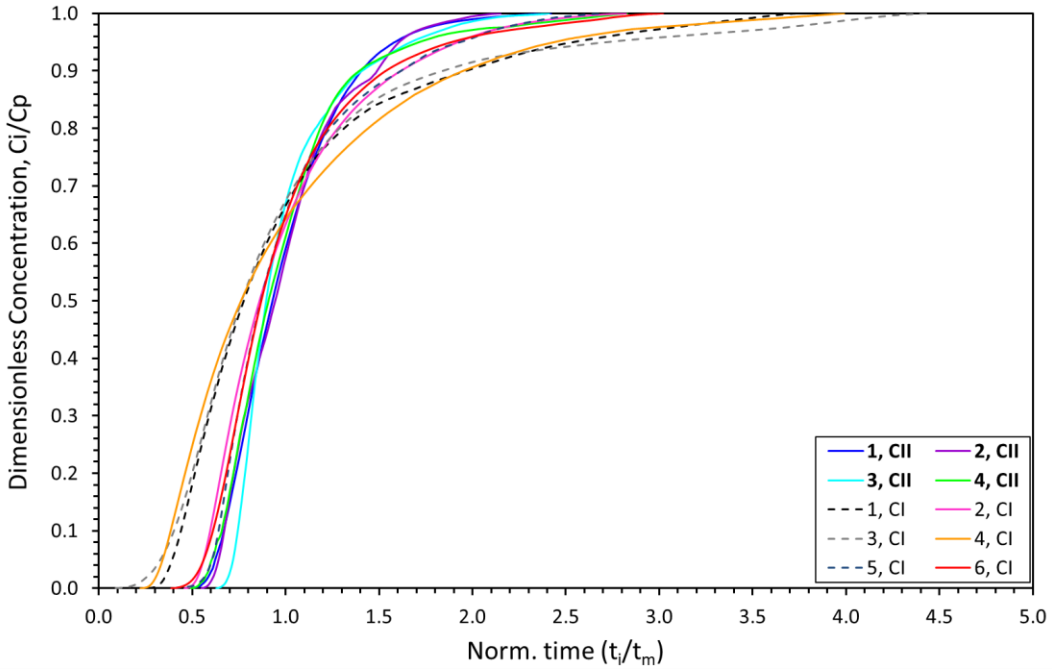

Figure 97: Compilation of CRTDs obtained in NW. Concentration on y axis is normalised by the peak concentration, C_{peak}, and on time axis by t_m.

6.1.3.3. HRT

The effects of discharge on HRT are shown in Figure 98, which illustrates the mean residence time, t_m, against flow rate. On the same plot, the theoretical (or nominal) residence time curve, t_n, is presented, based on Campaign II measurements. The effect of discharge on the HRT follows a typical inverse relationship. No effects of plant seasonal patterns can be identified on the HRT and on short-circuiting, due to the limited number of tests achieved in each month. Overall, short-circuiting levels appear moderate. Typically, the larger the deviation of the measured t_m values from the theoretical time curve, t_n, the shorter the tracer stays in the CW, following preferential paths.

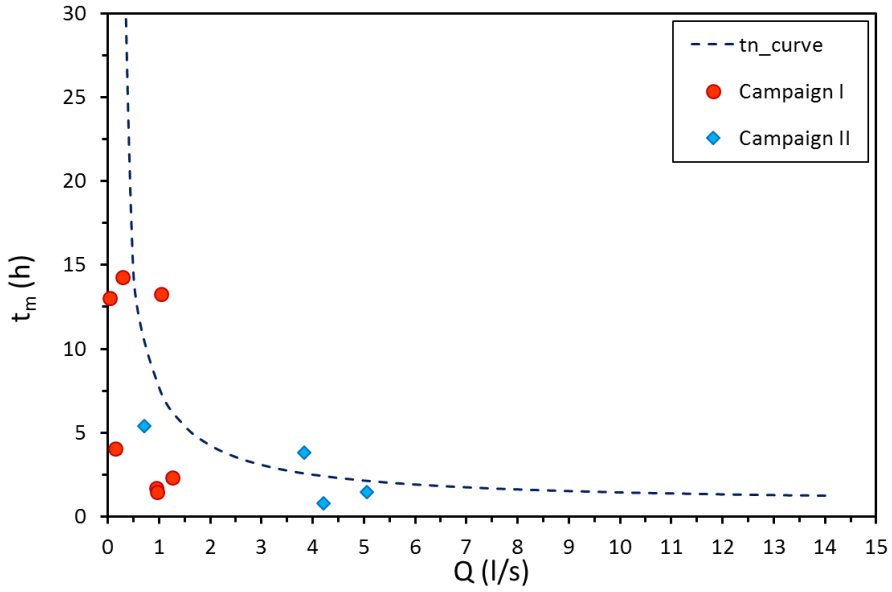

Figure 98: Mean residence time against discharge in NW. HRTs from campaigns I & II are plotted together. The plot also shows the nominal residence time curve.

6.1.3.4. Longitudinal dispersion measurement

This section presents the effects of discharge on the longitudinal dispersion coefficient, D_x and on the dispersive fraction, D_f. Further relationships between the mixing characteristics, i.e. D_x, D_f, λ, and other hydrodynamic parameters, i.e. flow rate, Q, and stem Reynolds number, NR^*, are presented and discussed.

Effect of Discharge on Mixing

In order to observe any total trends of discharge on mixing, Figure 99 presents the aggregate of dispersion coefficients and dispersive fractions against discharge. Each campaign shows a different rate of affinity between D_x and Q. This is attributed to the inadequacy of the dilution gauging method to estimate Q using the tracer. It is hypothesised that during Campaign I, the very low flow depths might not have promoted continuous discharge of effluent through the pipe, thereby resulting in prolonged residence times of the RWT in the system (thus ponding), therefore the tracer mass recovery might not have been complete. Although D_x-Q results from Campaign I are reported, the discharges should be treated with caution. Campaign II discharges are considered more representative of the flow status, albeit qualitative. Based on that, D_x during Campaign II appears to present slight increase with flow

depth and discharge (Figure 99), although results are not conclusive, due to the limited number of tracer tests. Recall that due to equipment availability, tracer concentrations were also monitored within the ditch, after the outlet pipe (Section 6.1.2). As such, the D_x coefficients obtained (where available) are also presented in Figure 99 showing minimal deviation from the D_x obtained before the pipe, and providing confidence of the results obtained.

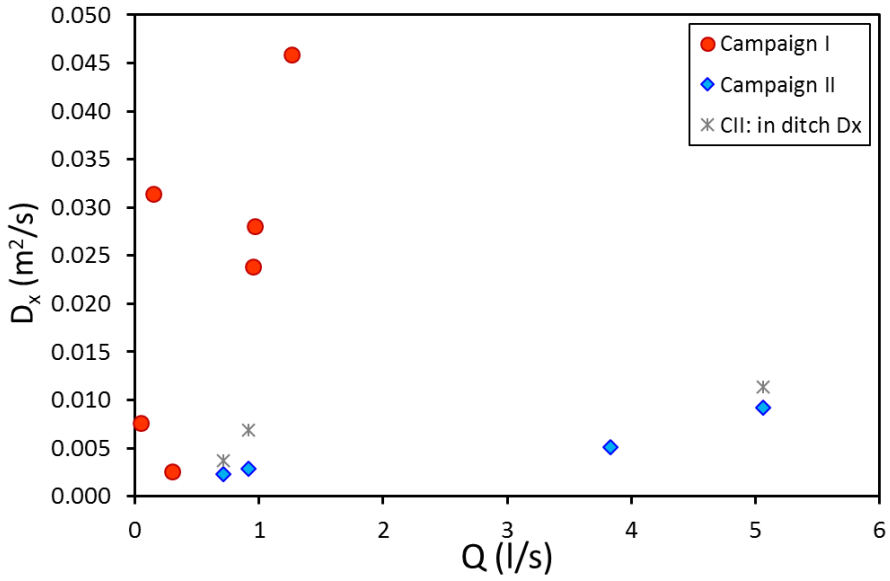

Figure 99: Longitudinal dispersion coefficient against discharge in NW for both campaigns. D_x obtained in ditch during Campaign II is also plotted (where applicable), providing confidence of the results obtained in the wetland and in the ditch.

Figure 100 presents the relationship between D_f and Q. However, there is no apparent relationship between D_f and Q. Figure 100 pinpoints that at least 50% of the total wetland volume functions as dead water. In particular, it is suggested that very low flow rates promote great deals of stagnant backwaters, which are plausible due to the ponding effects, while at slightly higher discharges the quantity of dead zones is slightly reduced. However, the restricted number of tests, the limited Q band tested (i.e. very low flow rates), and the lack of equipment to robustly measure Q, do not allow for more definite conclusions to be deduced.

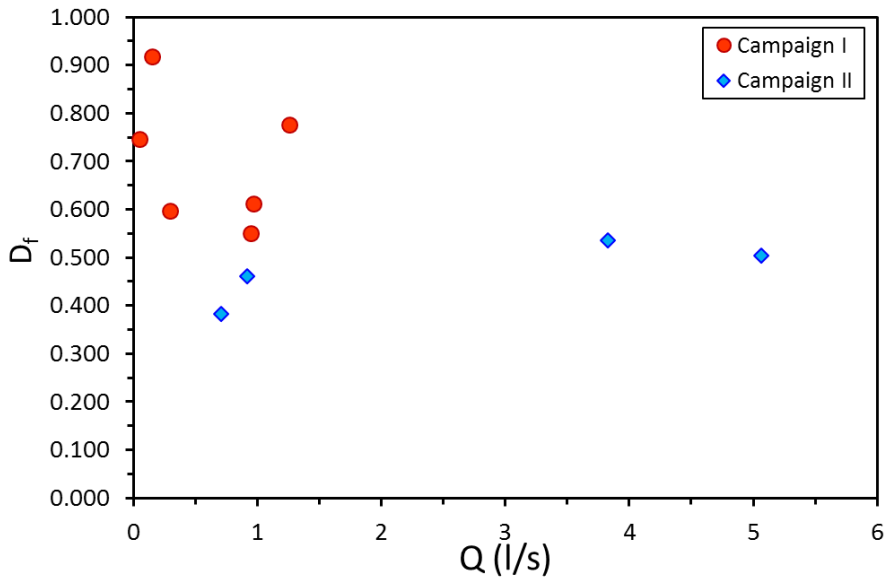

Figure 100: Dispersive fraction against discharge in NW.

Effect of longitudinal mixing on stem Reynolds number

Mechanical dispersion might have an effect on mixing in emergent canopies, as discussed in Section 2.5. Nepf et al (1997) observed that plant stem wakes can cause mechanical dispersion, by deflecting and retarding some amount of the tracer mass. The potency of mechanical dispersion hinges upon the magnitude and vigour of turbulence that the wakes generate behind the stems, which is expressed by the stem Reynolds number, NR^*. Therefore, if mechanical dispersion has a significant effect, D_x and NR^* should present a relationship.

Figure 101 (a) shows the ensemble of D_x coefficients against NR^*. There appears to exist a weak positive correlation between D_x and NR^* in both campaigns, which infers that mechanical dispersion might have an effect on the mixing properties. However, the small number of tests do not allow to draw a conclusive outcome. Moreover, no apparent relationship was found between D_f and NR^* (Figure 101 (b)).

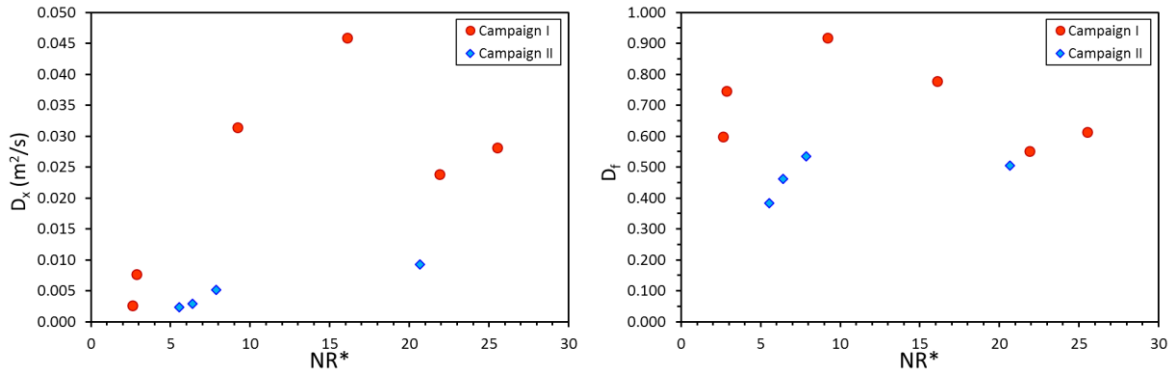

(a) D_x against NR^*. (b) D_f against NR^*

Figure 101: Dispersion coefficient against stem Reynolds number.

6.1.3.5. Differential advection

During Campaign II, differential advection measurements were conducted to provide more information about the mixing characteristics within NW. Results are presented in Figure 102 and Figure 103, for two different discharges, a very low Q=0.7 l/s, and a higher Q=5 l/s. The locations of the instruments are shown in Figure 94.

In both flow rates differential advection was apparent, particularly in the vicinity of the wetland boundaries, i.e. locations 1 and 4. Shear stress is generated due to boundary effects and due to secondary velocities developed. Dye passes easier from location 3 because of in-/outlet layout, while increase in Q promotes better mixing in the centreline of the wetland. The shallower locations toward the banks result in distinct differential advection in both discharges presented, where zones of diminished flow occur.

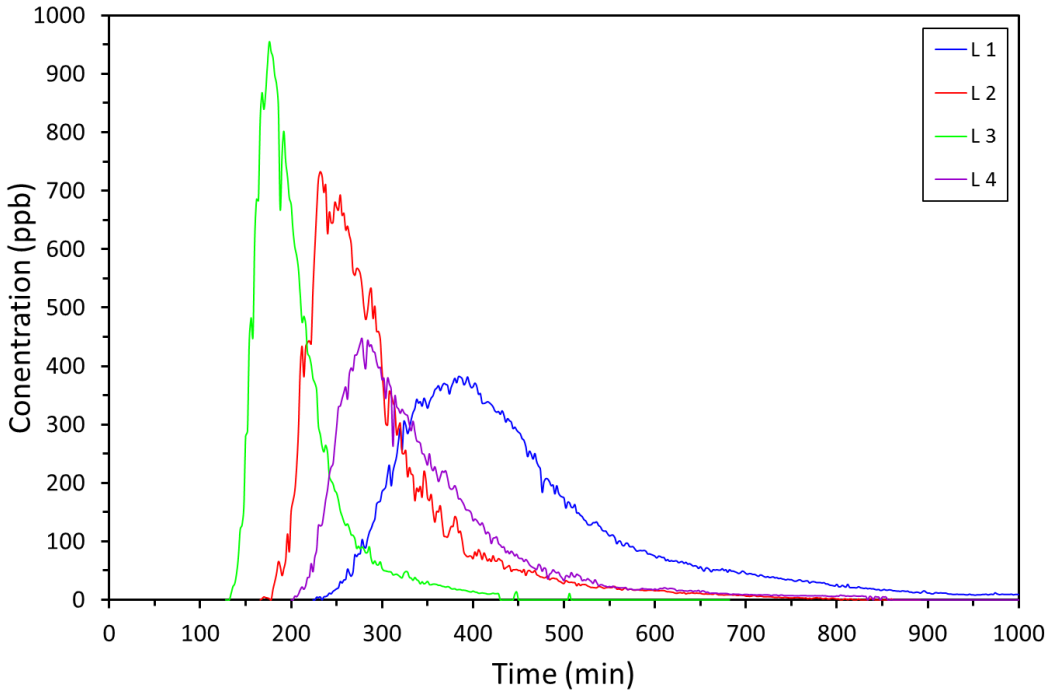

Figure 102: Transverse mixing study on one cross-section of the NW for a low discharge case. Differential advection is overt in the wetland, especially towards the banks.

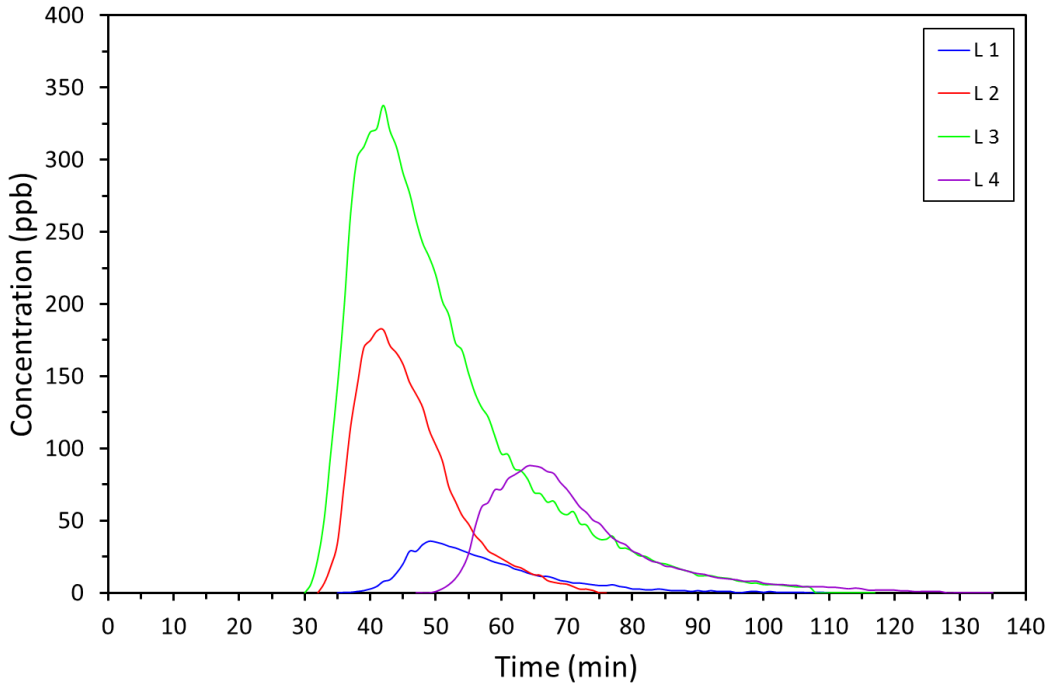

Figure 103: Transverse mixing study on one cross-section of the NW for a higher discharge case. Differential advection is apparent between the centre and the boundaries of the wetland.

6.1.3.6. Hydraulic efficiency

This section presents and discusses hydraulic efficiency in relation to the stem Reynolds number.

Hydraulic efficiency

Hydraulic efficiency, λ, is defined as the ratio of t_p over t_m. The presence of vegetation in FWS CWs introduces the use of stem Reynolds number, *NR**, which is expected to cause some variation in λ. The relationship between λ and *NR** is presented in Figure 104, indicating a weak affinity. This small variation in λ with *NR**, pinpoints some minimal effectiveness of stem wakes on λ. This is in opposition with the strong relationship Chyan et al (2014) found, which is primarily attributed to the different systems size and scale. Overall, the hydraulic efficiency in NW lays between the moderate and very good classifications, according to Persson et al (1999).

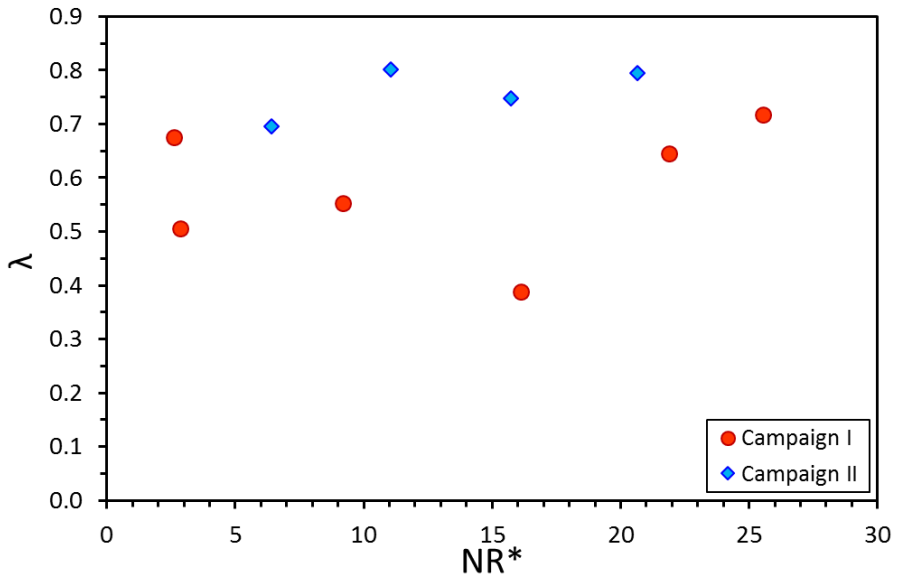

Figure 104: Stem Reynolds number against hydraulic efficiency in NW.

6.2A-WMTS (A Winning Minewater Treatment Scheme)

This section presents and discusses the results obtained from the A-MWTS CW monitoring site, in Derbyshire. Section 6.2.1 presents an overview of the experimental facility, Section 6.2.2 describes the methodology to acquire the data, and Section 6.2.3 presents and discusses the fluorescent tracer results.

It is noteworthy that the initial and central aim of monitoring the CW of this overall large facility, was the seasonal vegetation variation effect on hydraulics and mixing characteristics. The A-WMTS CW provided the ideal opportunity for this aim, because flow conditions are controlled (thus constant flow rate), resulting in a single variable, i.e. the seasonal vegetation variation. Nevertheless, results were disrupted before the completion of a full monitoring season, due to the breakdown of one of the lagoons (details are provided in Section 6.2.3). This shifted the aim into studying the effects of inflow conditions on flow and mixing pattern in large full-scale units.

6.2.1 Overview of the experimental facility

An additional monitoring site of the seasonal vegetation variation was the CW in the A-Winning minewater treatment scheme (A-MWTS), in Derbyshire (Blackwell, Alfreton). The total scheme was constructed in 2012 to prevent pollution of underground water supplies and uncontrolled discharges to surface watercourses. The overall scheme is shown in Figure 105, and is under The Coal Authority management, aiming at protecting a local aquifer, one of the most important sources of drinking water in the Midlands. Based in a strategic location, the scheme protects the aquifer due to its underground connections between the abandoned coal mines. Water is pumped from the shaft at the pump station, across a brook and to the treatment cascade which aerates the water. It then flows into the two lagoons and the wetland (Figure 105).

The CW dimensions are 105m*40m*0.5m (Length*Width*Water Depth), which produces a surface area of approximately 4200 m^2, and a total volume of 2100 m^3.

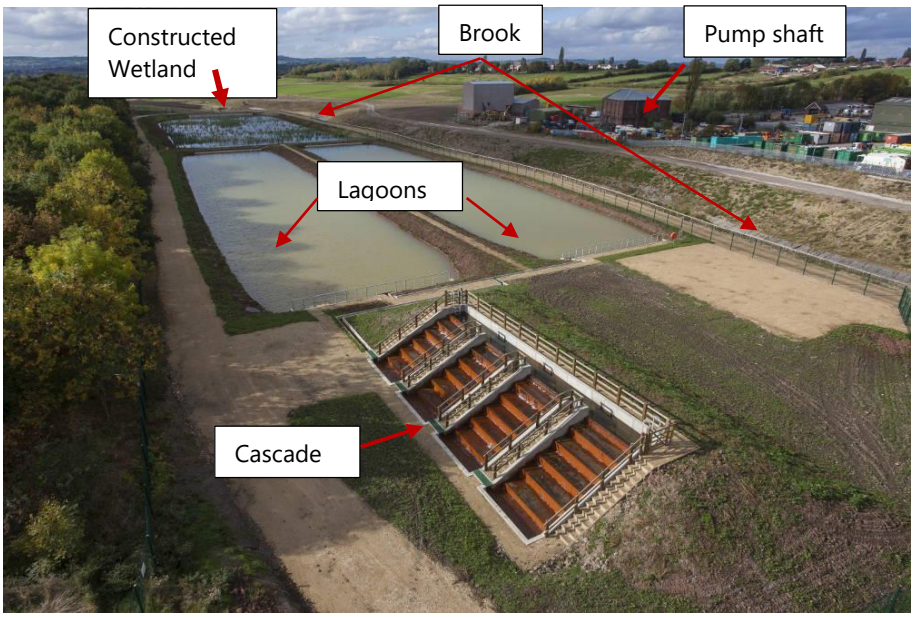

Figure 105: A-WMTS facilities showing the individual compartments of the overall treatment scheme.

There are two lagoons of approximately 3m depth which promote sedimentation. Flow is constantly pumped at a rate of 70 l/s. Water discharges into the CW from two inlet locations, each of which discharges the inflow from the respective upstream lagoon (see Figure 106). The incoming water is distributed evenly over the inlet via a weir, as seen in Figure 107. Water discharges via two outlets at the far end of the CW, and passes through a final pipe where a V-notch weir is installed (see Figure 106). The V-notch weir is located beyond the outlet points, towards the end of the chamber, as indicated by the green arrow in Figure 106.

As a convention, from this point further, A-WMTS refers to the CW (reedbed), and not to the total facility, because all the experiments took place in the CW.

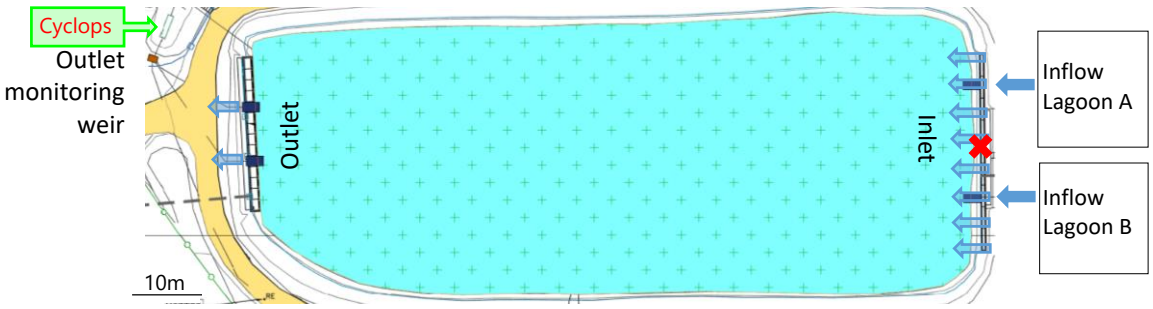

Figure 106: Schematic plan map for A-WMTS reedbed.

✖ = dye injection point

Figure 107: CW inlet point and water distribution across the weir in A-WMTS.

Vegetation is FWS emergent and monoculture consisting of Phragmites australis. The vegetation evolution and ageing is the typical that occurs on Phragmites in the UK micro-climate, as already mentioned in Chapter 3. There is no groundwater infiltration, as a fabric liner geo-membrane was placed on the CW bed during construction.

6.2.2 Methodology

6.2.2.1 Data Collection

To accomplish the aims outlined in the introduction of this section, measurements involved quantification of vegetation characteristics, and longitudinal mixing. The frequency of tests was approximately one tracer test per two to three weeks. This frequency was decided because of the controlled flow rate condition, and because of the main goal of observing the longitudinal mixing at different seasons. The quantification of vegetation included stem density, stem diameter monitoring, stem deflection monitoring, and plant biomass measurement in different seasons. Tracer data collection is detailed in the following section. Nevertheless, breakdown of lagoon A (Figure 106), disrupted the testing programme and shifted the seasonal vegetation variation effect aim. The overall testing period ultimately was between October 2015 and June 2016, and splits into two sub-periods: pre lagoon

breakdown (October 2015 – January 2016), normal inflow conditions; post lagoon breakdown (February 2016 – June 2016), single inlet inflow conditions.

6.2.2.2 Longitudinal Mixing Study

RWT was used for the tracing tests. The dye was introduced manually in the mid-distance between the two inlets across the weir (see Figure 106). The amount of dye and injection methodology was invariably the same for all tests. Tracer concentration was recorded downstream at the weir (Figure 106). This monitoring location was decided because it is the common ending path of the two outlet pipes.

One Cyclops-7 (by Turner Designs) was placed directly before the weir plate (Figure 108), operating at a sensitivity X10 (see details in Chapter 3, Section 3.5.3). Logging interval was set to 60 s average. The data analysis and processing applied is detailed in Chapter 3, Section 3.6. Results of the longitudinal mixing study are presented and discussed in Section 6.2.3.

(a) Preparation of fluorometer underwater installation.

(b) Fluorometer installation before the weir.

(c) Screen protection of weir, and camouflaged fluorometer's cable.

Figure 108: Preparation and installation of the fluorometer at the weir at A-WMTS.

6.2.3 Fluorescent tracing results

6.2.3.1 All tests collected

Although the initial objective for the A-WMTS was the monitoring of the seasonal vegetation variation over different seasons, breakdown of Lagoon A in January 2016 disrupted the testing programme, rendering the initial aim unachievable within the timeframe of this PhD study. Nevertheless, the aim was shifted to observe the potential influence of the inflow conditions on the flow and mixing characteristics. To achieve this objective, a few more tracer tests have been conducted after the breakdown incident. A compilation of the five tracer tests is presented in Table 6.2, providing a unique test code, and transport and mixing parameters obtained from the tracer tests. Tests conducted after the lagoon breakdown (i.e. single-inlet conditions) are distinguished by grey colour in Table 6.2, while their incomplete RTD profiles did not allow to derive the relevant transport parameters from the tracer tests, which explains the n/a values used.

Table 6.2: Summary of test series & transport parameters from the RTD analysis of the 5 tests in A-WMTS.

Test unique code	*Month*	*Date*	*Flow rate, Q* (l/s)	*First arrival time,* t_1' (h)	*Travel time,* t_m (h)	*Nominal residence time,* t_n (min)	*Dispersion coefficient,* D_x (m^2/s)	*Number of CSTR, N*	*Hydraulic efficiency,* λ (t_n/t_m)	*Effective volume ratio, e* (t_m/t_n)
1	Dec	03/12/2015	70	2.07	6.36	8.32	0.1989	2.37	0.55	0.80
2	Dec	11/12/2015		1.95	7.61		0.1526	2.69	0.53	0.91
3	Dec	21/12/2015		2.23	8.16		0.1684	2.51	0.59	0.89
5*	Apr	19/04/2016		n/a	n/a		n/a	n/a	n/a	n/a
6*	May	16/05/2016		n/a	n/a		n/a	n/a	n/a	n/a

*Symbol * refers to the tracer test operating with single inlet conditions.*

It is noted that both lagoons operated normally until January 2016. Furthermore, it should be noted that the total flow rate was maintained at 70 l/s after the breakdown, and was diverted totally through lagoon B. The single-inlet condition entailed different incoming flows compared to the two-inlet operation, as visualised in Figure 109 (a)–(b).

(a) Route of injected dye for normal inflow conditions (Left), and single-inlet conditions (Right), indicating the different flow paths followed during the different inflow conditions.

(b) Side view of injected dye at A-WMTS for normal inflow conditions (Left), and single-inlet conditions (Right).

Figure 109: Route of injected dye (a) and Side view of injected dye (b) at A-WMTS, for normal inflow conditions (Left), and single-inlet conditions (Right).

6.2.3.2 Analysis of measured concentration profiles RTDs/CRTDs

This section presents and discusses the effects of inlet configuration and inflow conditions on flow structure and mixing characteristics. RTDs and CRTDs obtained prior to the Lagoon breakdown are presented in Figure 110 (a)–(b) respectively. Obtained tests before the lagoon breakdown refer to December 2015, while post breakdown tests were undertaken in April and May 2016. Figure 111 ((a)–(c)) evidences a distinct effect of inflow configuration on the flow regime and mixing characteristics in the wetland under the single-inlet operation.

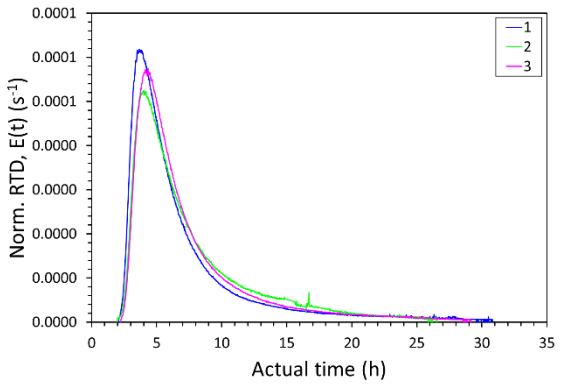

(a) RTDs during normal operation.

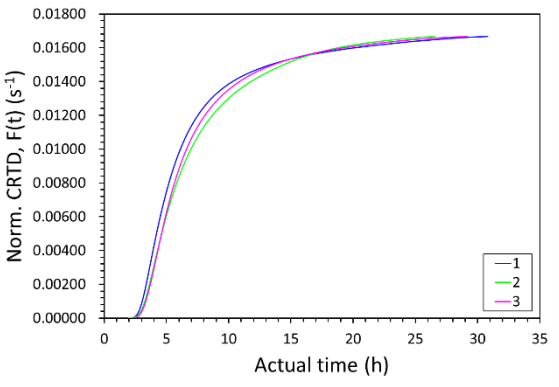

(b) CRTDs during normal operation.

Figure 110: RTD & CRTD curves of December tracer tests obtained in A-WMTS under normal inflow conditions.

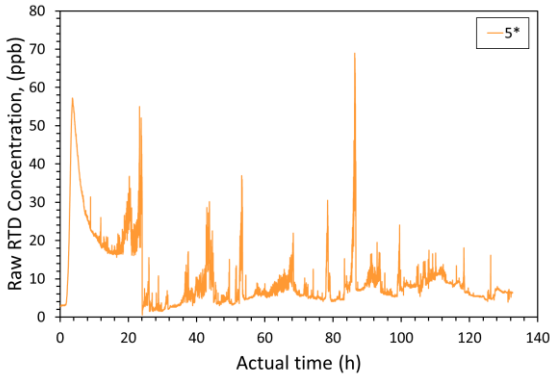

(a) April, recirculated currents.

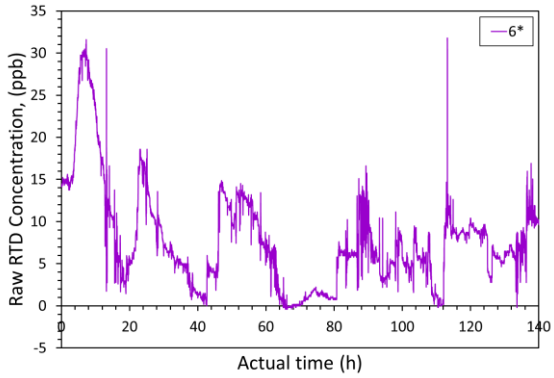

(b) May, promoted recirculation.

Figure 111: RTDs for post lagoon A breakdown period effects in A-WMTS. Fig. (a)-(b) indicate the recirculated currents promoted after the one inlet operation in April (a) and in May (b).

The general mixing pattern under the normal inflow conditions, shown in Figure 110, suggests plug flow with stagnant backwaters. The reasonable good flow is inferred from the fact that t_m is close to t_n, while stagnant backwaters are inferred from the prolonged distribution tail. However, the flow regime alters dramatically under the single-inlet condition. Raw RTD concentration profiles in Figure 111 (a)–(b) demonstrate slow internal recirculation in the wetland. This suggests sluggish turnover of fluid, and inadequate mixing. As such, the tracer (thus pollutant) passing through the wetland under the single inlet operation, requires more time to be released back to the main flow due to recirculation zones, and is mixed insufficiently, compared to the two-inlet operation. Summarising, it is

underlined that when the total of discharge inflows from a single inlet (or side), both the flow and mixing patterns change radically, and show an overall reduction in hydraulic performance. Therefore, it is evidenced that inflow conditions and inlet configuration play a central role in the hydraulic performance of large full-sized systems.

6.2.3.3 Hydraulic performance

The hydraulic performance is a wider concept incorporating many aspects. One indicator of the overall hydraulic performance is the hydraulic efficiency, λ, which ranges between 0.5 and 0.6 in A-WMTS. This implies moderate hydraulic efficiency of the system. Nevertheless, the index of the effective volume, *e*, obtains high values, implying that the majority of the volume is actively used. The moderate λ values are affected by the RTD shape, which suggests stagnant backwaters. A good indicator of the reasonably good flowing conditions of the wetland is the fact that the t_m (actual HRT) is close to the t_n. Unfortunately, no complete tracer tests were obtained during the single-inlet inflow conditions to allow a quantitative comparison, however, the raw concentration of those tracer tests (Figure 111) suggest poor internal hydraulics, and thus hydraulic performance.

6.3 Clough Foot Lagoons

This section presents and discusses the results obtained from the Clough Foot Lagoons monitoring site, in Yorkshire. Section 6.3.1 presents an overview of the experimental facility, Section 6.3.2 describes the methodology of data acquisition, and Section 6.3.3 presents the fluorescent tracer results and produces further discussion.

It is noteworthy that the study of this large lagoon facility emerged during the ongoing collaboration with The Coal Authority on the A-WMTS CW, and their request to assess the hydraulic performance of the Clough Foot lagoons. The lagoons treat mine water and their particular aim is to remove iron, i.e. hydrous ferric oxide. Previous tracer studies on those lagoons have shown that their HRT was very short to treat the pollutants in interest. Therefore, remediation action was taken by installing baffle curtains in one of the lagoons,

aiming at improving the flow regime, increasing the HRT, and ameliorating the treatment efficacy.

The aim of this tracer study project was to assess the two lagoons and compare their HRT, flow and mixing characteristics, and their overall hydraulic performance. Clough Foot includes two identically sized lagoons, the Control and the Baffled, the latter of which was retrofitted in order to achieve greater hydraulic and treatment performance. The Clough Foot application provided a good opportunity to assess in-situ the baffles retrofitting effect on large full-scale facilities. Details of the site are described in Section 6.3.1.

6.3.1 Overview of the experimental facility

Clough Foot minewater treatment scheme (MWTS) is located in Yorkshire, and comprises a single large cascade, two identically sized settlement lagoons, which are operated in a parallel arrangement, and a constructed wetland for polishing effluent, before discharging into the adjacent Brook. The two lagoons consist of a control and a baffled system, with the latter having been retrofitted by curtains as a remediation measure, to enhance lagoon hydraulics. The schematic of the baffled system is shown in Figure 112. The Control Lagoon is of identical size with the Baffled Lagoon, albeit without the baffle curtains (Figure 112).

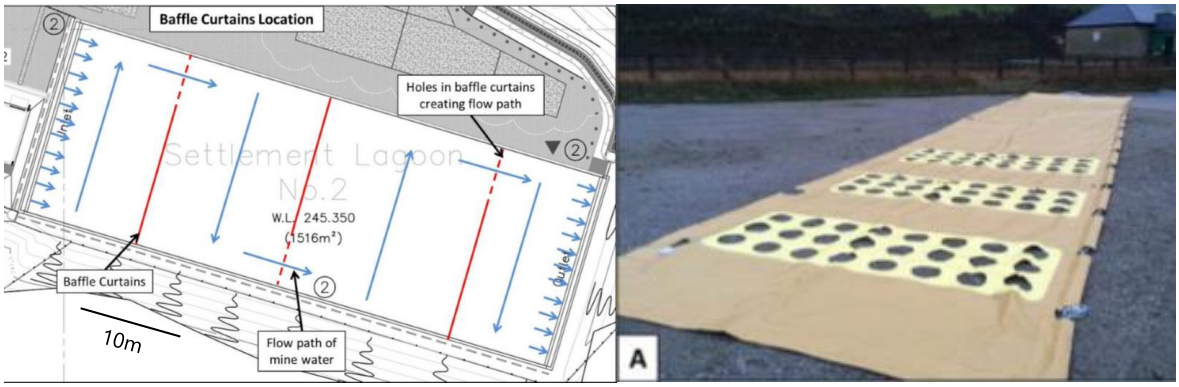

Figure 112: (Left) Clough Foot Baffled Lagoon, indicating curtain locations, orientations and flow path through the lagoon. (Right) Baffle curtains (Taken from Chamberlain & Moorhouse, 2016).

Each lagoon size is 64.5m*23.5m*3.8m (Length*Width*Water Depth), which produces a surface area of 1516 m^2, and a total volume of 5760 m^3.

6.3.2 Methodology

6.3.2.1 Data Collection

To accomplish the aims outlined in the previous section, fluorescent tracing tests were undertaken to quantify hydraulic parameters and the longitudinal mixing. Tests took place on 29th February 2016. Cyclops-7 (by Turner Designs) were used to detect fluorescence dye RWT, at continuous mode for 7 days. An overview of the entire MWTS indicating the key locations is provided in Figure 113.

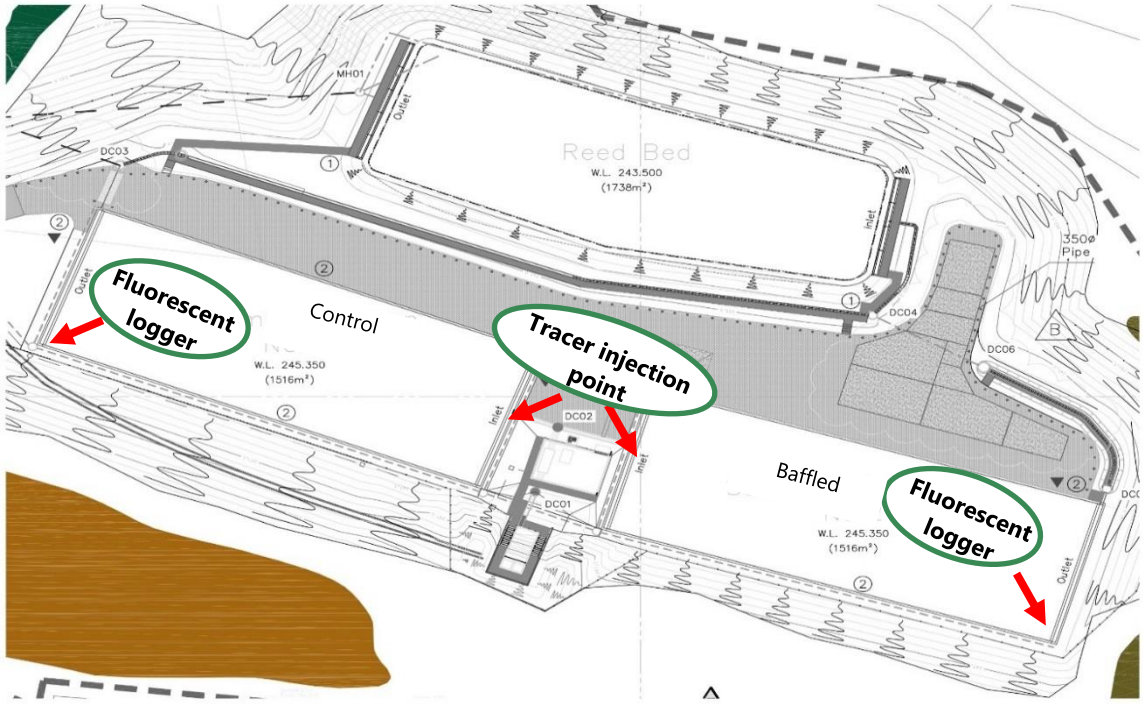

Figure 113: Overview map of Clough Foot indicating injection points and outlet data collection points.

6.3.2.2 Longitudinal Mixing Study

The longitudinal mixing study included dye injection at the inlet of each lagoon, and monitoring of the fluorescent dye concentration at the outlet of each lagoon (see Figure 113 for tracer injection and monitoring points). RWT was injected manually (i.e. slug injection) simultaneously and in the same way, at the inlet of each lagoon (Figure 114). Tracer concentration was recorded at the outlet channel pipe of each lagoon (Figure 115). Each fluorometer was positioned underwater in the outlet pipe of each lagoon (Figure 115) to

prevent from sunlight interference, and was operating at a sensitivity X1 (details are provided in Chapter 3, Section 3.5.3). The logging interval was 1Hz averaged over 60 s. Data analysis and processing details can be found in Chapter 3, Section 3.6. Results of the longitudinal mixing study are presented and discussed in Section 6.3.3.

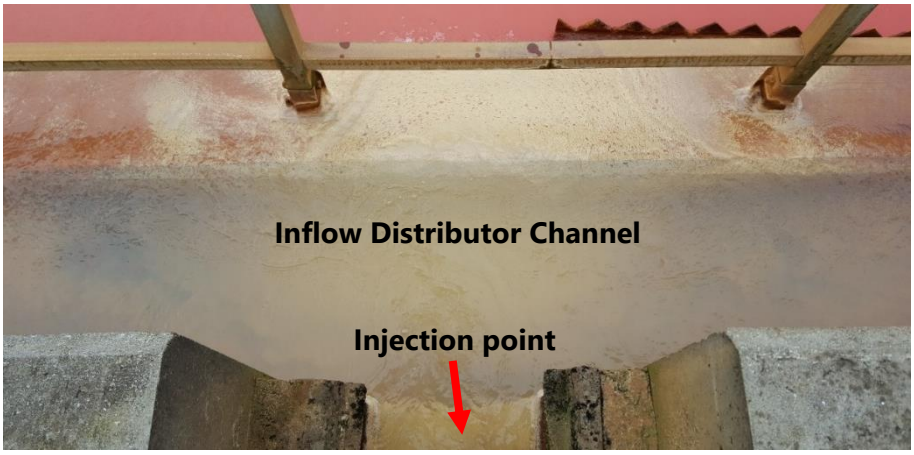

Figure 114: Inlet tracer injection point in the Clough Foot Lagoons.

Figure 115: Outlet channel pipe in which the fluorescent logger was installed underwater to prevent from sunlight, in Clough Foot Lagoons.

6.3.3 Fluorescent tracing results

For the scope of this study one fluorescent tracer test was conducted to determine the hydraulic performance of each lagoon. Results of the fundamental hydraulic parameters are listed in Table 6.3. It is noted that total (combined) discharge is measured by a V-notch weir, and subsequently, flow is directed into each lagoon, and is designed to be equally distributed. The approximate average combined flow rate during the testing period based on the totaliser device was 30 l/s. Therefore, the expected flow rate in each lagoon should be approximately 15 l/s. The flow rate obtained through dilution gauging provided elevated values, and in particular 37 l/s in the Control Lagoon, and 18 l/s in the Baffled Lagoon. The elevated $Q_{d.l.}$ values possibly result from the build-up of mine ochre on the fluorometers.

Table 6.3: Tracer tests & transport parameters of the Clough Foot Lagoons, Control and Baffled.

Lagoon Name	*Expected Flow rate, Q* (l/s)	*First arrival time,* t_1' (h)	*Travel time,* t_m (h)	*Nominal residence time,* t_n (min)	*Dispersion coefficient,* D_x (m^2/s)	*Number of CSTR, N*	*Peclet number Pe*	*Hydraulic efficiency,* λ	*Effective volume ratio, e*	*Dispersive Fraction,* D_f
Control	15	1.6	16.7	106.7	0.024	1.4	2.8	0.13	0.16	0.91
Baffled	15	5.2	52.7	106.7	0.003	3.7	7.4	0.66	0.49	0.90

6.3.3.1 Analysis of measured concentration profiles RTDs/CRTDs

This section presents the effects of baffle curtains on flow structure, HRT and mixing characteristics. Figure 116 evidences a distinct effect of baffles retrofit on the HRT and on the flow regime. In particular, HRT increased by three times, indicating an improvement of approximately 70%. This had a direct positive effect on the active volume utilisation, which enhanced by three times in the baffled system.

The general mixing characteristics in the Control Lagoon, shown in Figure 116 and Figure 117 (a), suggest highly advective flow. This is demonstrated by the very early t_m, and the very short tail, which does not reach the design t_n value. Such an early RTD curve is also a sign of dead zones. The tubular (or plug) flow effect is additionally evidenced by visualisation of the RWT dye, which after injection, traversed the Control Lagoon straight through, and exited the system. This suggests that thermal stratification effect takes place in the lagoon. As such, the solute buoys due to the higher water temperature at the top layer of the lagoon, and

travels through that 'top layer preferential path', as seen in Figure 118. The remaining lagoon depth, of approximately 3 m, remains inactive. This explains further the completely inactive volume in the Control Lagoon at the deeper layers, and the associated large quantities of dead regions, also supported by the high D_f value.

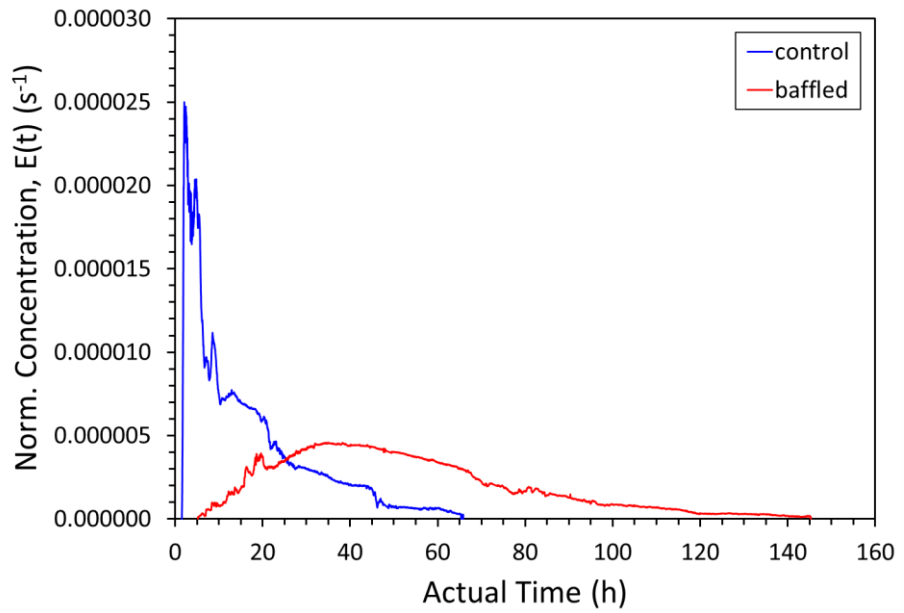

Figure 116: RTD curves against actual time for the control and Baffled Lagoon, in Clough Foot MWTS.

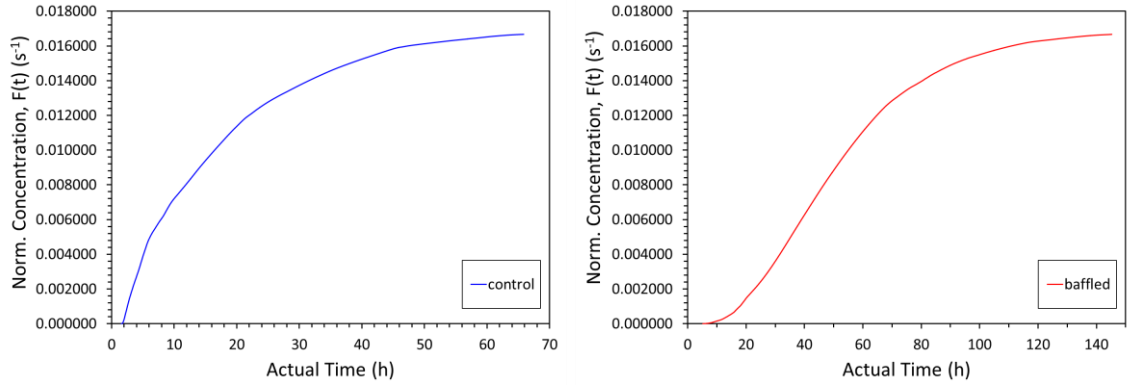

(a) Control Lagoon CRTD curve.

(b) Baffled Lagoon CRTD curve.

Figure 117: CRTDs obtained in the Control Lagoon (Figure (a)) and in the Baffled Lagoon (Figure (b)).

Regarding the mixing characteristics in the Baffled Lagoon, retrofitting has improved the mixing properties, as evidenced by the shorter difference between t_m and t_n; nevertheless, the retrofitting still suggests advective flow and a quantity of remaining stagnant backwaters

(Figure 116, and Figure 117 (b)). Overall, baffle curtains reduced the overall mixing (i.e. achieving lower $Mo=t_{90}/t_{10}$ index and dimensionless variance), and the longitudinal dispersion coefficient, which suggests that the flow pattern has reached plug flow conditions. Nevertheless, the retrofitted lagoon displayed radical improvement of the hydraulic efficiency, λ, raising from poor to moderate classification.

Figure 118: Thermal stratification effect in the Control Lagoon, Clough Foot MWTS.

In summary, the retrofitting using baffle curtains had a distinct impact on the flow and mixing characteristics. The increase of HRT and better utilisation of V_{eff} in the retrofitted system is significant, albeit still moderate, inferring that there is still space for enhancing the internal hydraulics in order to optimise the overall performance. The various hydraulic values obtained, such as e, λ, D_f, indicate that the Baffled Lagoon improved the overall hydraulic performance, thus treatment efficiency, and is ratified as a sufficient internal configuration measurement to improve hydraulic performance in treatment units encountering low HRTs.

7. Comparison of all Applications, Discussion & Summary

This chapter performs a relative comparison and evaluation of the six case studies totally investigated in this thesis, i.e. the SW1 and SW2 (see Chapters 4 and 5), and the further four applications (presented in Chapter 6). Section 7.1 provides a summary of the characteristics of the six case studies addressed. In sections 7.2–7.3, several parameters (i.e. longitudinal mixing, hydraulic performance, short-circuiting) are discussed, through qualitative and quantitative assessment respectively. Section 7.4 comprises a comparative evaluation of the hydraulic performance of the six case studies and summarises the main findings.

7.1 Overview of the Applications

The six full-size studied sites included four CWs and two lagoons. This section presents an overview of the geometric properties of the systems. Detailed information about the materials and methods applied for each site can be found in the relevant chapters, i.e. Chapter 3 for the SW1 and SW2, and Chapter 6 for the extra four applications.

Table 7.1: Geometric characteristics of the six investigated systems, influent type, and location.

	SW1	SW2	NW	A-WMTS	Control Lagoon	Baffled Lagoon
General shape	Trapezium	Trapezium	Trapezium	Rectangular	Rectangular	Rectangular
Length, L (m)	34	32	32	105	64.5	64.5
Width, W (m)	(4.4)	(5.3)	(5.7)	40	23.5	23.5
Aspect Ratio, A_R	7.8	6.0	5.7	2.6	2.7	2.7
Mean water depth, h (m)	0.15	0.16	0.46	0.5	3.8	3.8
Surface area, A_s (m^2)	148	170	181	4,200	1,516	1,516
Total Volume, V_{tot} (m^3)	23.5	23.0	45.0	2,100	5,760	5,760
Vegetation	Phragmites	Phragmites	Phragmites	Phragmites	-	-
Other obstacles	-	-	-	-	-	Baffle Curtains
Influent type	AR	AR	AR	Minewater	Minewater	Minewater
Location	Cambridge	Cambridge	Cambridge	Derbyshire	Yorkshire	Yorkshire

Note that width varies along the RSPB CWs, and is a function of flow depth and rate. The value with brackets ( ) is the average width obtained based on the particular flow depth of the selected tracer test.

A compilation of the schematics (i.e. topographic maps) for each system is provided in Figure 119 (a)-(f). The geometric characteristics, influent type, and location of each system are summarised in Table 7.1. Note that geometric values of the three RSPB monitored systems (i.e. SW1, SW2, and NW) refer to the particular flow conditions (i.e. flow rate and depth) of the selected tracer test.

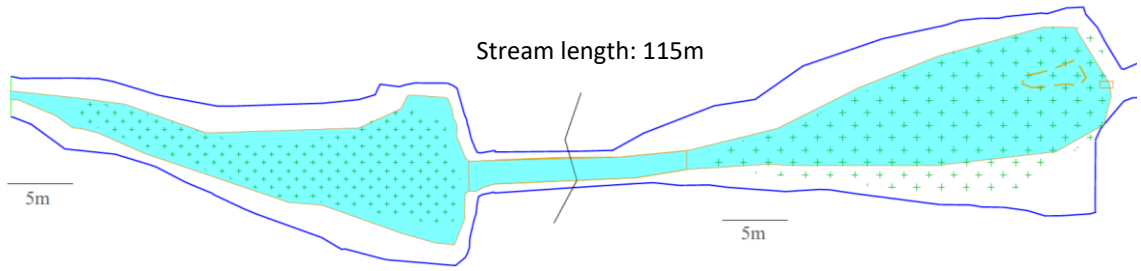

(a) SW1 (b) SW2

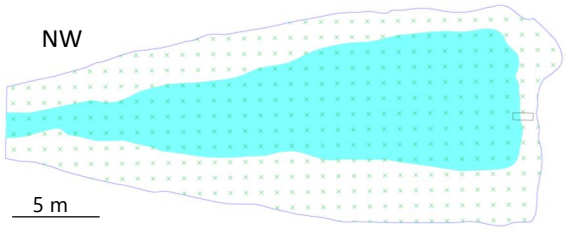

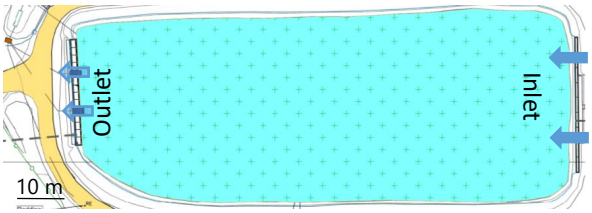

(c) NW (d) A-WMTS

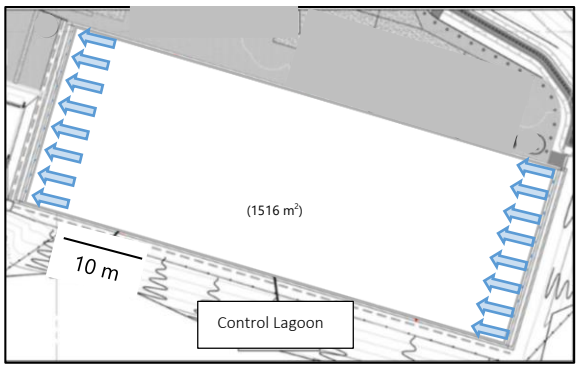

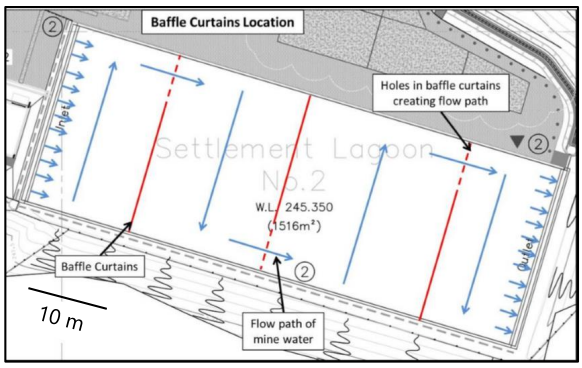

(e) Control Lagoon (f) Baffled Lagoon

Figure 119: Compilation of the schematics of each case study investigated.

7.2 Qualitative Analysis of the RTDs

This section showcases and discusses the RTD and CRTD curves of each system. One test was selected and presented for each case study. The selection of the test was conducted based on the criteria of dimensionless flow rate, and same month, to offer unbiased and easy comparisons between the different sized systems. For the systems where flow rate varies (i.e. SW1 and SW2), the selection of each test from the central database was based on the criterion of producing a dimensionless flow rate value, Q_{norm}, between 0.6 and 0.8, in order to be comparable with the Q_{norm} obtained at the other two vegetated CWs, i.e. NW and A-WMTS. This was done because NW has a limited amount of tests, thus the highest Q available was used, while A-WMTS has a fixed Q. Additional criterion for the test selection was the month, hence plant age. This was done because in vegetated flows, comparison would be unbiased for tracer tests conducted in the same month, i.e. December, thus upright stem position.

A summary of the hydrodynamic transport parameters derived from the RTDs analysis for each selected test are listed in Table 7.2, in which columns refer to each aqueous system and rows present an assortment of parameters related to hydrodynamic, mixing and physical flow characteristics. RTDs were obtained by monitoring the tracer concentration at the outlet of each system, and are presented in Figure 120 (a)–(f), allowing assessment of the global flow trends. In particular, there is a strong correlation between the left side plots in Figure 120 ((a), (c), and (e)), indicating strong short-circuiting. Contrary to that, the right side plots in Figure 120 ((b), (d), (f)) undergo distinctly lower short-circuiting, larger active volume utilisation, and greater dispersion mainly due to prolonged tails.

The left side plots in Figure 120 ((a), (c), and (e)), present a type of RTD that combines plug flow with some longitudinal mixing, according to Danckwerts (1953). Furthermore, the fact that t_m is very early compared to the expected t_n, demonstrates that preferential paths are prevalent in all those systems, while minimal longitudinal mixing takes place, as suggested by the short trailing edges. Those tails occur because the residual of the dye mixed in the main volume takes slightly longer to exit the system. It is remarked that the high short-

circuiting noticed particularly in the Control Lagoon, is attributed to the buoyancy effect from water temperature (thermal stratification). The tracer rapidly traverses the Control Lagoon utilising only the top layer of the water column, eventually leaving intact the majority of the total available volume. However, short-circuited flows in the SWs are attributed primarily to the downstream unbunded (non-dammed) layout. This condition does not support water hold-back in the system, and promotes stream-like rather than wetland function.

Table 7.2: Hydrodynamic transport parameters obtained from RTD analyses.

	SW1	**SW2**	**NW**	**A-WMTS**	**Control Lagoon**	**Baffled Lagoon**
Q (l/s)	20.4	22.9	5.0	70	15	15
$Q_{norm}= Q/(V_{tot}/t_m)$	0.64	0.73	0.56	0.79	0.16	0.50
Vegetation configuration	F. EM. (Dec)	F. EM. (Dec)	F. EM. (Dec)	F. EM. (Dec)	UNPL.	UNPL.
u_{mean} *(m/s)*	0.047	0.046	0.006	0.006	0.0012	0.00034
u_{max} *(m/s)*	0.073	0.069	0.012	0.020	0.012	0.003
t'_1	7.5 (min)	8.0 (min)	0.72 (h)	2.07 (h)	1.6 (h)	5.2 (h)
t_m	11.8 (min)	12.0 (min)	1.4 (h)	6.62 (h)	16.7 (h)	52.7 (h)
t_n	20 (min)	16.8 (min)	2.5 (h)	8.32 (h)	106.7 (h)	106.7 (h)
t_p	10 (min)	11.5 (min)	1.2 (h)	3.7 (h)	2.1	34.6
σ^2 (h^2)	0.00191	0.00076	0.20	18.45	195.94	747.28
σ_ϑ^2 (-)	0.049	0.019	0.094	0.421	0.702	0.269
D_x (m^2/s)	0.038	0.014	0.009	0.199	0.024	0.003
D_x/hu^*	56	20	74	632	60	23
D_x/Wu^*	1.8	0.6	0.6	7.9	9.6	3.7
Re (-)	4640	5033	865	2177	2819	894
NR (-)*	187	187	20	25	n/a	n/a
D_f (-)	0.37	0.34	0.50	0.69	0.91	0.90
V_{eff} (m^3)	14.5	16.6	26.4	1670	902	2845
e (-)	0.59	0.72	0.59	0.80	0.16	0.49
λ (-)	0.85	0.96	0.80	0.55	0.13	0.66
Pe	40.7	105.7	21.3	4.75	2.8	7.4
N (-)	20.4	52.8	10.7	2.37	1.4	3.7
t_{10}	9.0 (min)	9.9 (min)	0.97 (h)	3.3	3.0 (h)	21.2 (h)
t_{16}/t_{50} (-)	0.85	0.88	0.76	0.67	0.31	0.54
t_{16}/t_n (-)	0.46	0.61	0.42	0.43	0.04	0.25
t_{50}/t_n (-)	0.54	0.69	0.55	0.64	0.12	0.45
t'_1/t_n (-)	0.37	0.48	0.29	0.25	0.01	0.05
$Mo = t_{90}/t_{10}$ (-)	1.66	1.39	2.10	4.09	12.6	4.42
Bo = 1/Pe	0.025	0.009	0.05	0.21	0.35	0.13

F. EM. = Fully Emergent; UNPL. = Unplanted. Values denoted as '-' are due to the fact that measurements don't derive from the RTD. n/a means that value is not applicable.

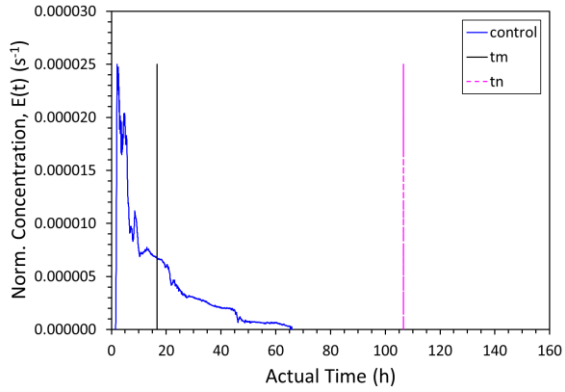

(a) Norm. RTD, Control Lagoon.

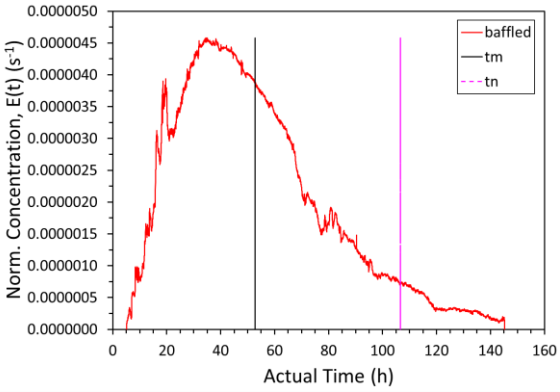

(b) Norm. RTD, Baffled Lagoon.

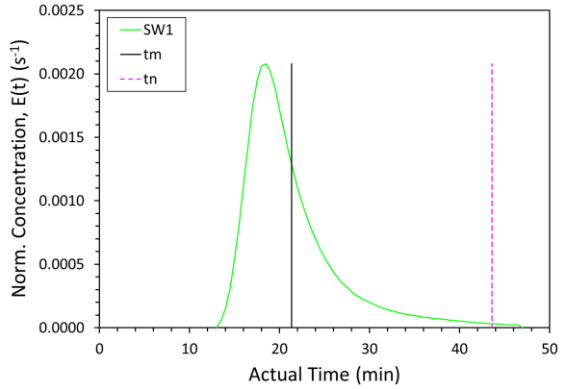

(c) Norm. RTD, SW1.

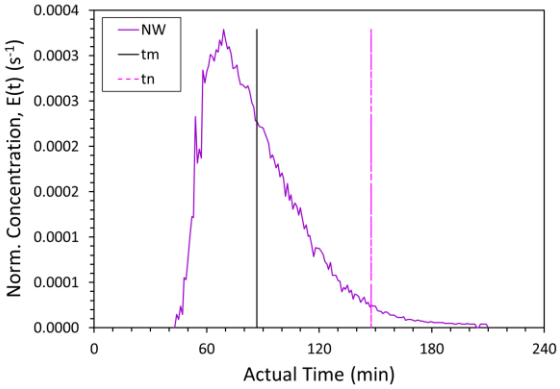

(d) Norm. RTD, NW.

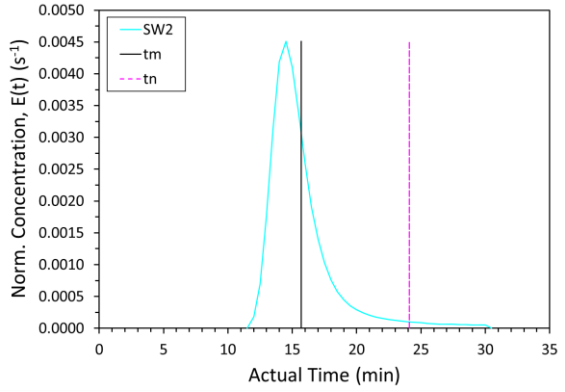

(e) Norm. RTD, SW2.

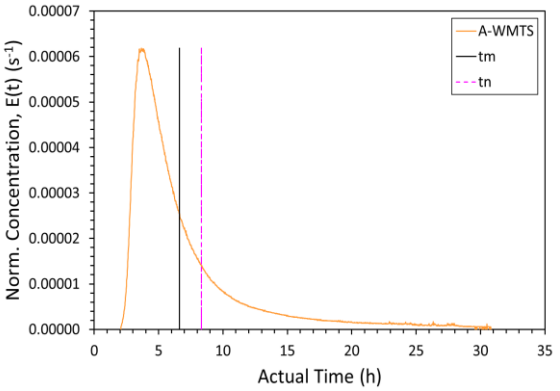

(f) Norm. RTD, A-WMTS.

Figure 120: Compiled RTD curves for each case study.

The right side plots in Figure 120 ((b), (d), (f)) indicate distinctly lower short-circuiting, larger *e* and greater dispersion. The RTDs in the Baffled Lagoon and in the NW suggest plug flow with longitudinal mixing, while the A-WMTS RTD demonstrates high active volume, along with a great quantity of stagnant backwaters.

The compiled normalised and dimensionless form of the six RTD and CRTD curves are presented in Figure 121 (a)-(b), allowing for a comparison of the RTDs and CRTDs among the different aqueous systems. The concentration axis is normalised by the peak concentration, C_{peak}, while the time axis by the volumetric travel time, t_n. The quantitative evaluation of the RTD and CRTD curves is performed in the Section 7.3.

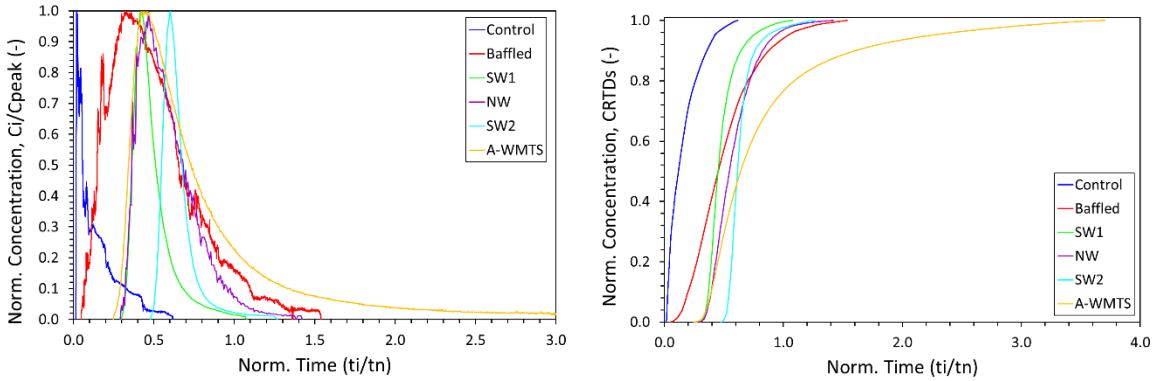

(a) Compiled Normalised RTDs.

(b) Compiled Normalised CRTDs.

Figure 121: Compiled Normalised RTD and CRTD curves for the six investigated aqueous systems.

7.3 Quantitative Assessment of Transport Parameters

In order to evaluate quantitatively the hydrodynamics of the six studied aqueous systems, transport parameters were derived from the individual RTDs (Table 7.2). Comparison, discussion and interpretation of the characteristics of the studied systems takes place in the following sections, in terms of hydraulic performance parameters (Sections 7.3.1 and 7.3.2), flow and mixing characteristics (Section 7.3.3.), and discussion on short-circuiting indices (Section 7.3.4).

7.3.1 Hydraulic Residence Times (HRT), Effective volume (e)

The six investigated systems were of different size (see Table 7.1), and thus, of different nominal residence times, t_n. However, of similar size were the three RSPB CWs, namely SW1, SW2, NW. Based on the system size, the measured HRTs (or t_m) should be in the order: Clough Foot Lagoons > A-WMTS > NW > SW1 > SW2. This assumption is ratified by the t_m values listed in Table 7.2. Nevertheless, HRTs of the Control Lagoon, SW1 and SW2 were too far from their relevant expected t_n value, whereas the Baffled Lagoon and NW displayed less divergence. Consequently, for the Control Lagoon, SW1 and SW2 the effective volume, V_{eff}, was lower compared to the design volume. This stresses the need for appropriate selection of design parameters (particularly to avoid dead zones and to reduce preferential flow paths). In contrast to the above, HRT in A-WMTS was close to the corresponding t_n value, implying large active volumes, i.e. $e \approx 0.8$. According to Thackston et al (1987), based on the e-values, the Control Lagoon encounters big quantities of dead zones, while SW1, NW and Baffled Lagoon undergo moderate amounts of dead zones. It is remarked that the baffled curtains retrofit increased significantly the proportion of the active volume in the lagoon, however, e-value after retrofit still indicates large dead water volumes, inferring the need for further improvement of the internal hydraulics.

Related to the ADZ model (see Chapter 2), dispersive fraction, D_f, is a parameter that quantifies the ratio of the river reach acting as a dead zone to the total reach volume; therefore, it indicates the ratio of the reach responsible for the dispersion of the tracer. As such, variation in D_f might be comparable to the D_x. D_f values closer to unity indicate high proportion of dead zones. Results showed lower, but similar, D_f values in SW1 and SW2, whilst maximum and same, D_f values in the Clough Foot Lagoons (Table 7.2). It is interesting that the baffle curtains retrofit did not contribute to any reduction of the D_f fraction, thus implying high proportion of dead regions, although the flow regime turned into plug flow.

7.3.2 Hydraulic efficiency

There is some differentiation between hydraulic performance and efficiency. Hydraulic performance is set in a wider context, which covers more elements of flow conditions (e.g. short-circuiting), and is overall less value-oriented (Persson, 2000). On the other hand, hydraulic efficiency, λ, indicates firstly how well the incoming water distributes in the system, and secondly the amount of mixing or recirculations (Wong & Somes 1995). By definition, λ incorporates e, and (1-1/N), where the latter term describes the RTD shape. Therefore, high e values do not necessarily entail high λ values, as proved by Persson et al (1999). In several of the hypothetical cases Persson et al (1999) investigated, e value was very high, but the RTD shape (expressed either as mixing, or as recirculation or stagnant backwaters) had a significant influence in reducing the final value of λ. For example, Somes et al (1998) investigated various options of channel bathymetries and of vegetation layouts through simulations, and found that plug flow is not invariably the best case, as compromises may be needed in the N (i.e. selecting lower N, to achieve increased mixing) in order to achieve enhanced λ values. In this study, λ is expressed as the ratio of t_p over t_m, and the reason for choosing to use the t_m is to obtain the actual hydraulic efficiency of the system. Referring in Table 7.2, the use of t_n for the estimation of λ would not be representative of the real conditions, due the overall large divergence between t_m and t_n in most systems.

7.3.3 Flow Patterns (i.e. Longitudinal Mixing)

Figure 120 and Figure 121 demonstrate that Control Lagoon, SW1 and SW2 behave like plug flow reactors, with minimal longitudinal dispersion. The lower N in SW1 compared to SW2 is supported by the larger D_x coefficient. The flow pattern in NW and Baffled Lagoon shows some similarity, and suggests plug flow with some longitudinal dispersion. Mixing is greater in the Baffled Lagoon though, as demonstrated by the lower N value, and the greater *Mo* and D_x/Wu^* values. This indicates that the baffles are more efficient at promoting mixing. RTD obtained from A-WMTS connotes a system with lots of dead water. In that context, the majority of the tracer passes through a restricted channel, while a considerable fraction of the tracer is caught in eddies and stagnant backwaters.

Overall, Pe reveals the degree of advective flow taking place in the order of: SW2 > SW1 > NW, which is consistent with the higher velocities observed (Table 7.2). The N and $Mo=t_{90}/t_{10}$ mixing properties indicators are consistent, following an ascending order as: SW2 > SW1 > NW > Baffled Lagoon > A-WMTS > Control Lagoon. This order connotes more plug flow conditions in SW2 and more mixing in Control Lagoon. The transverse mixing study in SW2 (see Chapter 4) demonstrated no lateral mixing, and no differential advection, which is in accordance with these results. It is noteworthy that the temperature buoyancy effect of the tracer in the Control Lagoon promoted the tracer to advect at the top surface layer straight through the lagoon, and contributed to the high *Mo* value.

The dimensionless longitudinal mixing D_x/hu*, as employed in streams by Rutherford (1994) appears to receive comparable longitudinal mixing values between SW2 and Baffled Lagoon, and between SW1 and Control Lagoon. However, as those systems are totally different in geometries (i.e. dimensions, shapes), flow depth, *h*, might not be the appropriate dimension to normalise D_x in wetlands/ponds. As such, D_x was normalised also by width, *W*, as seen in Table 7.2. The relationship between the inverse of Pe number against normalised D_x/Wu* is presented in Figure 122 (Left), where low 1/Pe values entail more advection. Figure 122 (Left) indicates a positive correlation between mixing (thus Dispersion number) and width, and suggests that width plays an important role in the mixing and that the scale effects between the small and larger systems are minimal. However, given that Pe number depends on *L*, u_{mean} and D_x, there might be an expected relationship with the D_x/Wu*. Figure 122 (Right) presents 1/Pe against longitudinal dispersion coefficient normalised by h (thus D_x/hu*), and indicates that use of the flow depth, h, between systems of different shape and scale does not provide a representative dimension to normalise D_x. The difference is apparent particularly for the larger full-size units run by The Coal Authority (Figure 122 (Right)).

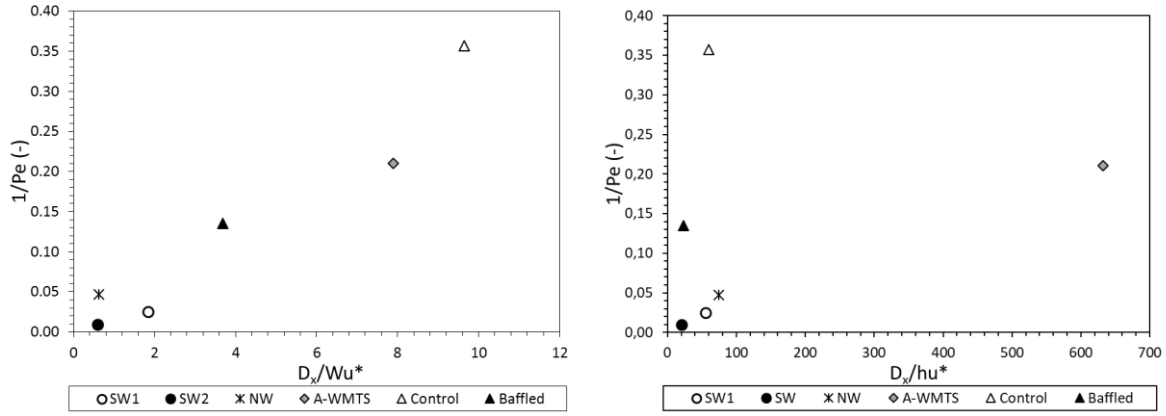

Figure 122: (Left) 1/Pe against D_x/Wu* indicating zero scale effects between the systems. (Right) 1/Pe against D_x/hu* indicating different scale effects between the systems. Width appears to be a more important dimension compared to depth in affecting mixing characteristics in different scale systems.

Another element that influences the mixing degree is the aspect ratio, $A_R = L/W$. Persson (2000) underlines that the CW A_R does not only affect the effective volume ratio, e, but also the amount of dispersion. In particular, high A_R promotes plug flow, and diminishes dispersion levels. Comparison of the A_R with the D_x values for each system, is not possible because of the different processes causing the dispersion in each system, and the different inflow and outflow conditions. However, a typical comparison between the Control and Baffled lagoons evidences that increase in A_R (as happened after the retrofit) increased e and HRT, whilst it decreased D_x, promoting plug flow.

7.3.4 Short-circuiting & Mixing Indices Assessment

The flow pattern inside each system frequently deviates from the ideal, lowering the hydraulic and treatment performance. Evaluation of the hydraulic performance of a system is important to understand the expected treatment efficacy. One aspect of the hydraulic performance relates to the short-circuiting phenomenon, while another aspect to the mixing. There are various short-circuiting indices suggested in the literature to appraise a system's performance, albeit drawing in different conclusions. This section discusses the application of various short-circuiting and mixing indices on the six treatment units of this study.

Overall, greatest short-circuiting is observed in SW1, SW2 and in the Control Lagoon. This is instantly observed in Table 7.2, where the t_n is substantially far from t_m, demonstrating the

advective flow dominant pattern. Both SW1 and SW2 experience high short-circuiting levels, mainly due to the unbunded outlet layout. On the other hand, in spite of the similar shape and dimensions, NW manages to retain the tracer six times longer than the SWs, and to mitigate maximum and mean velocities considerably better (i.e. at least by five times), while t_1' is six-fold lower. This result is particularly attributed to the deeper and controlled outlet layout, providing a good reference for CW design construction. Investigating the short-circuiting in the two identical lagoons, results suggest that the baffle curtains retrofitting attenuates instantly the short-circuiting. Therefore, it is attested that simple system modifications, either using berms or baffles of long width, or designing proper outlet configuration, can improve radically short-circuiting, and thus treatment efficacy.

t_{16}/t_n index appears to be the most plausible short-circuiting ratio for the systems investigated, and is regarded the most representative for the six systems overall. It was found that t_{16}/t_{50} is high for each aqueous system, implying low short-circuited flows, which is unrealistic. The inadequacy of the ratio t_{16}/t_{50} in some cases, has been previously reported by Persson (2000). Ratio t_{50}/t_n suggests moderate short-circuiting levels for SW1, SW2 and NW (group 1), which is unrealistic especially for SW2, while it suggests credible values for A-WMTS, and Clough Foot Lagoons (group 2). Therefore, t_{50}/t_n might need further consideration before applied in CWs.

It is inferred that there is no standard rule for the selection of a unique short-circuiting index, and that selection varies, based on the shape of the RTD. Therefore, it is advisable to observe the RTD shape, and then to decide about the appropriate indicator. Overall, for the assembly of the case studies examined, t_{16}/t_n appears to fit best. Finally, Texeira et al (2008) recommend t_{10} as a safe and credible indicator of short-circuiting, because it is not affected by other phenomena, such as stagnant backwaters or recirculation, as the t_{50} value does.

Regarding the mixing characteristics, it is noted that the term mixing incorporates the random spread of the tracer/solute due to the joined action of diverse phenomena, such as recirculation, stagnant backwaters, and turbulent diffusion. Two mixing indicators were employed to evaluate the mixing properties in this study, namely the dimensionless variance,

σ_θ^2, and the Morril index, *Mo*. Texeira et al (2008) recommend a combined investigation of the dispersion index, which corresponds to the spatial variance of the RTD, σ^2, and the *Mo*, to interpret the mixing conditions. Both σ_θ^2, and *Mo* are overall consistent, indicating greater mixing levels in the descending order: Control Lagoon > Baffled Lagoon – A-WMTS > NW > SW1 > SW2. However, the associated processes liable for the mixing level in each system are different, as already discussed earlier in this section.

7.4Comparative evaluation of the six Applications for their Hydraulic Performance

This section assembles and discusses various hydraulic performance related parameters for the aggregation of the six aqueous systems, and attempts to make a comparative evaluation of the hydraulic and treatment performance among the systems. Furthermore, this section provides recommendations to ameliorate the current hydraulics in each system, and provides general good practices when designing and constructing a treatment unit.

7.4.1 Effect of Obstacles and Baffles on the HRT & Hydraulic Performance

7.4.1.1 HRT

HRT is an indication of the hydraulic and treatment performance, in such a way that longer HRT entails enhanced treatment (Dierberg et al, 2002; Lee et al, 2015; Stern et al, 2001; Pappalardo et al, 2016; Tournebize et al, 2016). HRT depends on the hydrology (i.e. water depth, flow rate), and hydraulics (i.e. obstructions, vegetation, and system shape, i.e. A_R) (Johannesson et al, 2015; Kadlec, 1990; Jadhav & Buchberger, 1995). Given the highest HRT in the Baffled Lagoon in comparison with the other five applications, this system would probably exhibit the best efficiency for a variety of treatment effluents, i.e. municipal and industrial wastewater, agricultural and urban runoff. Concerning the SW1 and SW2, their HRT is very short; thus, their size, internal hydraulics and outlet configuration pose these wetlands inadequate to achieve good treatment levels for agricultural runoff pollutants.

Possible retrofitting could enhance the detention volume, hydraulic and treatment efficiency in SW1 and SW2. For example, replacing the outlet dam, would initially increase the flow depth, detention volume and HRT. Secondly, in order to augment the treatment performance, given the current opposite in-/outlet layout, and the relatively small size of the wetlands, retrofitting using baffles or rectangular obstacles of sufficient width would create a meandering flow path increasing the HRT, enhancing the overall mixing, reducing stagnant backwaters, and mitigating velocities. This practice has been suggested in the literature as an appropriate retrofit to ameliorate hydraulic and treatment efficiencies (Persson, 2000; Su et al, 2009). Although preliminary results presented in the ERAR CRD annual technical meeting (Whelan, 2016) suggested that SWs present minimal peak attenuation and low removal efficacy of certain pesticides due to their small size compared to the catchment area, the recommended retrofitting is considered useful for the mitigation and removal of a variety of agrochemicals applied in the surrounding catchment area. Furthermore, given that SWs are an on-line and in-series system, further mitigation and reduction efficiency of agrochemical compounds is anticipated to be achieved through discharging from SW2, into the downstream watercourses.

7.4.1.2 HRT & Obstacles / Baffles

Baffled Lagoon

In the case of baffles, it is observed that for the same system shape, i.e. Clough Foot lagoons, the baffle curtains retrofit increased significantly various hydraulic parameters, and in particular λ by 5 times (by 67%), e by 3 times (by 80%), and HRT by 3 times (by 68%), and increased the treatment efficacy. In particular, iron and aluminium removal increased by 41% and 34% respectively, after the retrofitting (Chamberlain & Moorhouse, 2016). However, Chamberlain & Moorhouse (2016) stated that although the HRT and hydraulic efficiency enhanced, the corresponding improvement in removing metals was merely 10%. This underlines the link between hydraulic and treatment performance, and stresses the need to study both fields of sciences closely, and underpins that internal hydraulics and physics of flow should not be overlooked. The difference between the hydraulic and treatment

efficiency, possibly results from the yet existing large dead regions proportion in the Baffled Lagoon, which most likely occurs either due to the thermal stratification or due to the need of further retrofitting practices to reduce the stagnant backwaters. Another reason could be the different season that the tracer (i.e. February) and the metal monitoring data (May-October) was undertaken, entailing less thermal stratification effect over summer months. Further investigation is required to reveal this, and a recommended methodology would be tracer tests to assess the vertical mixing over the Baffled Lagoon depth.

SW1 & SW2 – Vegetated Flows

In the case of vegetated flows, where plants act as obstacles to the flow, SW1 and SW2 results (see Chapter 4) indicated that Phragmites australis' stem morphology (i.e. small diameter), along with the sparse population density, did not show particular resistance with flow rate variation during the growth season (0% stem deflection). However, monitoring of vegetated obstructed flows in relation to seasonal plant variation due to stem deflection for the certain plant species, demonstrated some influence on the flow structure, on mixing characteristics, and on some hydraulic performance parameters, particularly during the highest plant age. It was found that in SW1 during the highest plant age, i.e. February (thus fully deflected stems), there was resistance added on the flow, inducing flow retardation and longer HRTs. Furthermore, there was a change in the RTD shape, promoting dead zones and attenuating better the peak concentrations.

Unlike SW1 results, seasonal vegetation variation effect on flow structure and hydrodynamics showed less influence in SW2. In particular, flow resistance and retardation was minimal during the fully deflected stems period, i.e. February, and most prevalent only in the very low flow rates. The determining element influencing the flow and mixing properties in SW2 was found to be the wetland design, and particularly the combined effect of the outlet layout (i.e. lack of an outlet dam) and of the irregular bed channel topography (i.e. promotion of a preferential path).

As an overall evaluation of the impact of seasonal plant variation on hydrodynamics in SW1 and SW2, it is considered that should there have been an outlet dam in each wetland, affinity between the seasonal plant variation and hydrodynamics would have been greater.

7.4.1.3 Short-Circuiting & Hydraulic Optimisation

In terms of the hydraulic optimisation of the available volume, SW2 appears to combine very good λ and e values, implying that impact of stagnant backwaters is minimal on the pollutants mitigation mechanisms. However, SW2 functions as a well-mixed pipe or stream, as proved from the RTD profiles and from the high short-circuiting levels, thus is deemed poor in terms of treating pollutants as is. Therefore, taking into consideration the HRT, λ and e values, both NW and A-WMTS systems would be considered the best ones to mitigate treatment effluents more efficiently, compared to the other systems.

As an internal configuration improvement measure, baffle curtains retrofit managed to reduce notably the short-circuiting levels. Su et al (2009) recommended implementation of obstructions to enhance the hydraulic efficiency of an aqueous system, if that is poor by construction. Furthermore, the authors found that the number of obstructions is not so important, as is their width, to enhance λ and to reduce internal recirculations. It is recommended that A_R must be at least larger than 1.88 to allow for λ >0.7 (Su et al, 2009). However, despite fulfilling the A_R criterion in all the six examined studied cases, it did not necessarily entail λ or e close to, or larger than 0.7. Furthermore, Su et al (2009) recommended A_R>5 to achieve λ>0.9, case that is observed to apply merely for the SW2. The divergence of Su et al's (2009) design recommendations indicate that they should be dealt only as indicators, mainly because their results were produced through numerical simulations, and refer to ideal shapes, which is rarely the case in reality (thus they omit the field effects). Nevertheless, a combination of a bunded outlet (thus proper outlet configuration) in conjunction with rectangular obstacles (thus better internal configuration) in SW1 and SW2 is expected to improve significantly the current performance.

7.4.2 Effect of Inflow Condition on Hydraulic Performance

The inflow configuration has an effect on the short-circuiting and effective volume of the treatment unit. Persson (2000) demonstrated that having an inlet along the whole base reduces short-circuiting, enhances significantly the active volume and hydraulic efficiency, and decreases the amount of mixing. Su et al (2009) investigated various ways to improve the hydraulic performance in CWs, demonstrating that uniform inflow spreading is the best inflow configuration at the inlet. In the systems operated by The Coal Authority, i.e. A-MWTS, Control and Baffled Lagoons, the inlet configuration approximates the recommended uniform inflow spread.

In A-WMTS in particular, during the normal inflow conditions (i.e. operation of both lagoons), inflow occurs across a large weir, and is considered to be uniform. The active volume achieved is 80%, although the RTD profile indicated stagnant backwaters. In addition to this, tracer tests showed that RWT was not instantly spread uniformly across the inlet, but followed initially a specific preferential path (Figure 123), and afterwards it became well mixed.

Figure 123: Tracer route during the normal inflow operational condition. Tracer takes an initial preferential path (Photo taken 3/12/15).

The single-inlet configuration (i.e. single lagoon operation) promoted a different flow regime, where inflow was forced toward the low flow velocity zone, at the right side of the inlet weir (Figure 124 (a)), and influent spread more slowly, following a different route, which

used the right side of the wetland (Figure 124 (b)). At the single-inlet condition, tracer/pollutant takes a different path as entering the CW, experiencing lower initial velocity as entering the system, because the tracer is stuck at the corner of the inlet weir and reverses slowly back into the main flow. This inlet condition supports internal recirculation and inadequate mixing of the solute in the wetland (Figure 111 (a) – (b)). This actual case study evidences the central role of inlet configuration in the flow regime, mixing characteristics, and thus pollutant treatment efficacy of large full-scale units.

(a) Tracer forced at the low flow velocity area of the inlet weir.

(b) Tracer follows a slow spread using the right side of the CW.

Figure 124: Tracer route during the single-lagoon inflow condition. Tracer is forced at the low flow velocity zone and spreads more slowly, following a different route (Photos taken 21/01/16).

7.4.3 Effect of Outlet Layout on Hydraulic & Mixing Properties

The three RSPB CWs are by construction of similar size and shape, however, they differ mainly because of their outlet configuration. The main differentiation between NW and SWs is that NW is controlled downstream by an elevated pipe, established in an embankment, while SWs are unbunded. This outlet layout results in two contrasting flow conditions,

namely shallow for the SWs, which lead to a flow-through regime, and deep for the NW, which lead to dissipated flows in NW (and frequently to detention or ponding). It has to be recalled that the initial construction of SWs included a dam at the outlet, which, however, in future storm events failed and was removed.

Nowadays, as shallow systems, SWs operate normally between 0.1 and 0.2 m average flow depths. On the other hand, NW allows for 0.3 m as a mean detention or ponding flow depth, before it flushes through the pipe, while as discharging through the pipe, water depth may reach 0.4 to 0.5 m, depending on the flow rate. Furthermore, it needs to be reminded that flow regime in SWs is normally continuous during wet months, whilst NW displays intermittent flows. Instantly, it is clear that NW allows for two operations: i) detention or ponding of effluent, occurring when flow depth is below the exit pipe; and ii) approximately twice deeper operational depths, and dissipated velocities. As a consequence, HRT in NW is in the order of hours, whilst in SWs it is in the order of minutes. Furthermore, N is significantly decreased in NW, indicating more complete mixing conditions, while the lower Pe number implies less advection, and more longitudinal dispersion as suggested by the *Mo* index. In addition to this, better spread and mixing in NW is advocated by the dimensionless variance, σ_θ^2 (see Table 7.2). Furthermore, it is worth noting that although NW experiences more intense winds than the SWs, stems didn't evidence significant deflection during the highest age. This, in conjunction with the nearly laminar flow regime in NW, resulted in exertion of lower pressure on stems, preventing streamline stems deflection. Thus, the downstream outlet construction promoted dissipated flow velocities.

Biochemical data collected in the three RSPB CWs for the potential of mitigating some pesticides, were presented in the ERAR CRD Annual Meeting in 2016 (Whelan, 2016), and showed that SWs, as continuous flow-through systems, presented no significant difference in some pesticides (i.e. metaldehyde and carbetamine), while the mitigation capacity of the intermittent flow regime existing in NW was underlined. In particular, NW managed to abate significantly some pesticides (i.e. quinmerac, metazachlor, metaldehyde) particularly because of the detention capacity of this system, which allows for treatment time between two storm-

flushing through the pipe events. This sheds some light to previous research conducted by Diaz et al (2012), who hypothesised that continuous flow-through CWs seem more effective in removing a variety of agricultural NPS pollutants, compared to flood-pulse hydrologic regime, which resembles the NW intermittent flow regime.

In summary, this section underlined the importance of outlet configuration (i.e. retaining and controlling water downstream at the outlet) in order to achieve better treatment efficiency. It is inferred that detention systems and intermittent flows are not necessarily a negative aspect in the hydraulic and treatment performance of aqueous systems, but have the potential of functioning both as storage or detention basins and as areas of enhanced treatment processes.

Summary of the main conclusions

A comparative evaluation and discussion of the main experimental results of all the monitored sites has been conducted in this chapter. Results showed that internal hydraulics are significantly affected by design parameters and by smooth operational conditions, such as even inflow influent distribution. Furthermore, it was demonstrated that the outlet configuration can improve significantly the mixing and hydraulic performance. Moreover, it was evidenced that internal configuration, such as retrofit using baffles curtains, yields in enhanced performance of the system's hydraulics, while it was inferred that seasonal vegetation variation affects the mixing and flow pattern in high plant ages.

Overall, results pinpointed that hydraulic performance is intrinsically connected with the treatment performance, and should not be overlooked. Of significant value is the outcome that to-date hydraulic optimisation guides do not necessarily conform with hydraulic parameters and values obtained from large full-scale units, indicating the necessity of investigating more full-sized applications to cover the gap between simulations and reality (e.g. field effects).

8. Conclusions & Recommendations

8.1 Conclusions

The aim of this research was to investigate the impact of seasonal vegetation variation on mixing characteristics and on flow structure in emergent planted, and full-size constructed wetlands (CWs). Intrinsic to this approach was the assessment of the hydrodynamic behaviour and physical flow characteristics of those CWs, including four additional full-scale aqueous systems of different design characteristics (i.e. shape, size, outlet and internal configurations) across the UK. Following a literature review, Section 2.7 identified the specific research questions concerning: i) seasonal vegetation variation effect on mixing and flow characteristics in full-scale CWs within emergent real vegetation, and ii) physical flow characteristics in six full-scale treatment units of different scales, shapes and configurations (internal, inflow, outlet).

Thus, an outdoor tracer field study was undertaken in two full-sized aqueous systems (south wetland 1 (SW1), and south wetland 2 (SW2)). An intelligent automated tracer injection system was developed, which allowed autonomous remote measurements to be made. The fieldwork study measured longitudinal mixing, differential advection, and physics of flow, while it also monitored vegetation characteristics under natural ageing for a particular vegetation type, Phragmites australis. Concerning the hydrodynamic behaviour and physical flow characteristics, in addition to the two main wetlands, four extra full-scale systems were investigated, including two CWs (i.e. NW and A-WMTS), and two lagoons (i.e. Control and Baffled). The main conclusions drawn from this study concerning the main research questions of this study are presented as follows.

8.1.1 Seasonal vegetation variation

Seasonal vegetation variation was investigated in two similarly designed and sized CWs in-series, namely SW1 and SW2. Longitudinal mixing coefficients were obtained under the

seasonal plant growth and discharge variation within real vegetation in full-scale CWs, which contribute to the current body of knowledge. Furthermore, investigation of the physical flow characteristics and mixing processes under the seasonal vegetation variation and flow rate variation was achieved. Results indicated different impact of seasonal vegetation variation on mixing characteristics and flow profile in each CW, despite their similar size and design. The difference was attributed to the irregular bed channel topography (thus to internal design) in SW2, as a result of natural sediment deposition and accumulation over years.

Seasonal vegetation variation in SW1 influenced the mixing and flow pattern, especially at the end of the annual plant cycle, i.e. February and March. Seasonal plant variation displayed flow retardation, increased longitudinal mixing coefficients (D_x), and created large quantities of stagnant backwaters during February-March. Moreover, D_x showed affinity to the stem ageing (i.e. stem deflection degree), and displayed a range on the y axis, depending on the plant season (i.e. month) and the discharge. In particular, D_x was found to range up to four times between the two extremes of seasonal vegetation variation, i.e. February and June. Similarly, pollutant peak concentration was found to reduce up to three times in high plant age (i.e. February). Concerning discharge, as this study was carried out with different flow rates, a decrease in D_x with increase in discharge was indicated in all seasons, as shown in Figure 60. The overall impact of seasonal plant variation on the mixing and flow pattern for the current CW design suggests that seasonal vegetation variation influences the mixing and flow characteristics, and most notably at low discharges. It is inferred that seasonal plant variation has a dominant impact on the pollutant transport, on mixing and hydrodynamics of larger full-scale units operating at low discharges.

However, SW2 was less influenced by seasonal plant variation. D_x ranged over a minimal band, and showed a decrease with increase in flow rate (Figure 80), whilst it was consistently demonstrated that some other design-related element had a greater impact on the mixing and flow pattern (Figure 79, Figure 81, and Figure 88). That was particularly attributed to the bed channel irregularity, where accumulated sediment deposition supported the formation of a deeper and a shallower part in the system, hence promotion of a preferential path. Overall, it was demonstrated that design-related aspects (such as dammed outlet, regular

channel topography) have a greater impact on mixing characteristics, on flow structure, and on the overall hydraulic performance, compared to seasonal vegetation variation.

Summarising, it was deduced that field data through tracer tests on the actual site are important to optimise determination of model coefficients, because they incorporate the field effects, such as boundaries, irregular shape, wind interference, and natural seasonal plant variation.

8.1.2 Hydrodynamic Behaviour – Hydraulic Performance

Six full-scale aqueous systems of variable geometries (i.e. shape, size) and design characteristics (i.e. internal, outlet and inflow configurations) were investigated for their physics of flow and hydraulic behaviour. This work aimed at applying and assessing the current theoretical understandings developed in idealised system conditions of pilot-scale or laboratory units, on the actual site in full-size aqueous systems, thus incorporating the field effects. In order to achieve this, tracer tests were undertaken, obtaining hydraulic performance parameters, and gaining an understanding of the underlying physical flow characteristics in the systems.

A comparative evaluation among various systems was conducted to establish good practices of design aspects to improve hydraulics. Results underpinned the importance of measuring physical flow characteristics and mixing characteristics in large-scale non-ideal shaped systems, and demonstrated that physics and hydraulic performance play a central role in the treatment performance, thus should not be overlooked. A summary of the main findings of this study are presented as follows.

a. Outlet Configuration

Controlled outlet conditions have proved to be pivotal in increasing the HRT, thus the treatment efficiency of the unit. Comparison of results between the bunded NW and the unbunded SW1 and SW2, showed that downstream control of the flow depth within the treatment unit, e.g. using a dam or embankment, significantly enhances the hydraulic performance, hence increases the treatment capacity of the treatment unit. The three

systems compared are of same size, shape and design, however, the different outlet configuration in NW (i.e. bunded) achieves increased HRTs (i.e. from minutes to several hours), dissipates flow velocities, and notably augments pollutant spread.

b. Inflow Configuration

Achieving even inflow conditions is a good recommended practice to maintain enhanced internal mixing and flow characteristics. Disturbance of inflow uniformity resulted in poor mixing and slow internal recirculations of the pollutant in the A-WMTS, thus reduction of the treatment efficiency. Results in A-WMTS demonstrated that inflow conditions appear pivotal in the design stage of CWs to optimise the hydraulic and treatment performance of large units. The two-inlet and single-inlet inflow schemes tested, showed a notable difference in flow pattern, and thus on the treatment efficiency in large-scale units. The single-inlet inflow condition resulted in slow internal recirculations, which caused insufficient mixing of the solute in the system, as shown in Figure 111. This entails reduced hydraulic and treatment performance. The normal two-inlet inflow condition allowed for more even distribution of the tracer and enhanced mixing conditions. Therefore, during the design or remediation stage of CWs, even inflow conditions should be secured because of the drastic effects they have in full-size units.

c. Internal Configuration

Baffles curtains retrofitting in the lagoon had a distinct effect on flow and mixing characteristics, and demonstrated enhancement of the hydraulic performance. In particular, through the baffle retrofit hydraulic efficiency and HRT increased significantly, larger proportion of the total volume became active, while plug flow conditions prevailed enhancing contaminant spread. The use of baffles as a remediation measure is considered useful to ameliorate internal hydraulics and treatment performance in full-size aqueous systems.

Seasonal plant variation and distribution, as well as bed topography are another aspects of internal configurations investigated in this study, conclusions of which were presented in Section 8.1.1. Overall, seasonal vegetation variation should not be overlooked by practitioners, as it affects both the flow and mixing characteristics seasonally.

d. Shape and Scale Effects

Hydraulic transport parameters obtained through tracer tests showed similar characteristics between smaller and larger full-scale units. The relative comparison between the systems does not appear to have scale effects between the six treatment units, as shown Figure 122, where 1/Pe against D_x/Wu^* receives approximately a linear response. Therefore, it appears that hydraulic transport parameters and hydraulic performance in smaller systems, i.e. SW1, SW2, NW, are comparable to larger systems, i.e. A-WMTS, and Clough Foot lagoons. Moreover, it was observed that the width of the treatment unit is a dimension that affects significantly the mixing characteristics especially in larger full-scale units.

8.2 Future Work & Recommendations

- This thesis has demonstrated that seasonal vegetation variation may influence significantly the mixing properties and flow patterns, and has pinpointed the shortfall of related data around this topic. It was shown that whilst studies using artificial or real vegetation have been useful in characterising the underlying mechanisms of vegetated flows, seasonal vegetation variation effect on hydrodynamics has been largely overlooked. Studies with artificial vegetation cannot represent natural properties, such as stem flexibility or deflection due to ageing, therefore future work should focus on monitoring and describing the behaviour of real vegetation as well as natural seasonal plant variation. Future work could include investigation of seasonal plant variation on a variety of plant types.
- Other areas of future work could include collection of field empirical data in full-size CWs and application of numerical works and modelling to improve prediction of water quality models, incorporating parameters related to irregular system shapes, real vegetation, and seasonal vegetation variation. Moreover, validation of models should use primarily field empirical datasets to allow calibration of the model parameters. Furthermore, development of a catchment model, incorporating the

hydrological, hydraulic and chemical data, as well as the ratio between the CW area over the catchment area, would be of interest for many stakeholders.

- This work has shown that whilst studies using simulated tracer tests and simulated hypothetical cases (i.e. system shapes, vegetation layout), as well as small-scale laboratory units have been useful in characterising the hydraulic performance and in setting thresholds and establishing values of good practice for design criteria, in-situ tracer tests are still important, because they do not ignore the field effects, e.g. the extra variables introduced either by boundary effects or secondary currents, or by the presence of real vegetation. Studies with simulated design parameters cannot characterise accurately important variables, such as secondary velocities and boundary effects of non-ideal or irregular system shapes. Therefore, future work should concentrate on investigating full-size systems, in order to provide more realistic design values.
- Hydraulic performance and physical flow characteristics should not be neglected or undervalued when investigating (or aiming at good) practices to improve or optimise treatment performance. Results of this study highlighted the importance of physics and hydraulics in the treatment efficiency of full-size units, and showed that there is an intrinsic link between hydraulic and treatment performance. This underlines the need to link the physical, chemical and biological (e.g. biodegradation) fields of science in the wetland or pond design, in order to reflect the 100% capacity of treatment processes.

References

Agunwamba, J.C. (2006). Effect of the location of the inlet and outlet structures on short-circuiting: Experimental investigation. *Water environment research*, **78**(6), 580-589.

Anderson, S. M. & Charters, A. C. (1982). A fluid dynamics study of seawater flow through Gelidium nudifrons. *Limnology and Oceanography*, **27**(3), 399-412.

Aquatic and Wetland Plants in Florida. UF-IFAS. Aquatic Macrophytes. University of Florida – Institute of Food and Agricultural Sciences. URL: http://plants.ifas.ufl.edu/ [Date accessed: 03/07/2015].

Ayyoubzadeh, S.A., Faramarz, M. & Mohammadi, K. (2004). Estimating longitudinal dispersion coefficient in rivers. *Proceedings of the 6th international conference on hydroinformatics*.

Beer, T. & Young, P.C. (1983). Longitudinal dispersion in natural streams. *Journal of environmental engineering*, **109**(5), 1049-1067.

Beutel, M. W., Newton, C. D., Brouillard, E. S., & Watts, R. J. (2009). Nitrate removal in surface-flow constructed wetlands treating dilute agricultural runoff in the lower Yakima Basin, Washington. *Ecological Engineering*, **35**(10), 1538-1546.

Bianchi, M., & Harter, T. (2002). *Nonpoint sources of pollution in irrigated agriculture: Farm Water Quality Planning Series*. Division of Agriculture and Natural Resources, University of California, USA.

Billy, C., Birgand, F., Ansart, P., Peschard, J., Sebilo, M., & Tournebize, J. (2013). Factors controlling nitrate concentrations in surface waters of an artificially drained agricultural watershed. *Landscape ecology*, **28**(4), 665-684.

Blackwell, M.S.A, Hogan, D.V. & Maltby, E. (2002) 'Wetlands as Regulators of Pollutant Transport', in Haygarth , P.M. & Jarvis, S.C. (ed.) *Agriculture, Hydrology and Water Quality*. Wallingford, UK: CAB International, pp. 321-339.

Blankenberg, A. G. B., Braskerud, B., & Haarstad, K. (2006). Pesticide retention in two small constructed wetlands: treating non-point source pollution from agriculture runoff. *International Journal of Environmental Analytical Chemistry*, **86**(3-4), 225-231.

Bodin, H., Mietto, A., Ehde, P.M., Persson, J. & Weisner, S.E.B. (2012). Tracer behaviour and analysis of hydraulics in experimental free water surface wetlands. *Ecological Engineering*, **49**, 201-211.

Bodin, H., & Persson, J. (2012). Hydraulic performance of small free water surface constructed wetlands treating sugar factory effluent in western Kenya. *Hydrology Research*, **43**(4), 476-488.

Bollmann, U. E., Tang, C., Eriksson, E., Jönsson, K., Vollertsen, J., & Bester, K. (2014). Biocides in urban wastewater treatment plant influent at dry and wet weather: concentrations, mass flows and possible sources. *Water research*, **60**, 64-74.

Borgvang, S. A., & Tjomsland, T. (2001). Nutrient supply to the Norwegian coastal areas (1999) calculated by the model TEOTIL. *NIVA-report*, 4343-2001.

Borin, M., & Tocchetto, D. (2007). Five year water and nitrogen balance for a constructed surface flow wetland treating agricultural drainage waters. *Science of the Total Environment*, *380*(1), 38-47.

Boxall, J.B. & Guymer, I., (2003). Analysis and Prediction of Transverse Mixing Coefficients in Natural Channels, (February), 129–139.

Braskerud, B. C. (2002). Factors affecting phosphorus retention in small constructed wetlands treating agricultural non-point source pollution. *Ecological Engineering*, *19*(1), 41-61.

Branger, F., Tournebize, J., Carluer, N., Kao, C., Braud, I., & Vauclin, M. (2009). A simplified modelling approach for pesticide transport in a tile-drained field: The PESTDRAIN model. *Agricultural water management*, **96**(3), 415-428.

British Standard 3680 Part 2C. Measurement of Liquid Flow in Open Channels – Dilution Methods – Methods of Measurements using Chemical Tracers. British Standards Institution. London, 1993.

Brix, H. (1994). Functions of macrophytes in constructed wetlands. *Water Science Technology*, **29**(4), 71-78.

Buccola, N., & Spolek, G. (2011). A pilot-scale evaluation of greenroof runoff retention, detention, and quality. *Water, Air, & Soil Pollution*, **216**(1-4), 83-92.

Chamberlain, S., & Moorhouse, A. M. (2016). Baffle Curtain Installation to Enhance Treatment Efficiency for Operational Coal Mine Water Treatment Schemes. *Proceedings of the International Mine Water Association (IMWA) conference*.

Chanson, H., (2004). Environmental hydraulics of open channel flows. Oxford: Elsevier Butterworth-Heinemann.

Chen, X. (1994). Effects of hydrodynamic and sediment transport processes on nutrient dynamics in shallow lakes and estuaries. PhD dissertation, University of Florida, Gainesville, FL.

Chikwendu, S.C. (1986). Calculation of longitudinal shear dispersivity using an N-zone model as N->∞. *Journal of Fluid Mechanics*, **167**, 19-30.

Coffey, S. (1997). Selected agricultural best management practices to control nitrogen in the Neuse River basin. North Carolina State University, Raleigh, NC, USA. *Technical Bulletin*, 1-50.

Cooper, P. (1999). A review of the design and performance of vertical-flow and hybrid reed bed treatment systems. *Water Science and Technology*, **40**(3), 1-9.

Crossan, A. N. (2002). *Remediation of pesticides on cotton farms: studies of the environmental distribution, transport and fate of five pesticides*. PhD Thesis. Department of Agricultural Chemistry and Soil Science, Faculty of Science, University of Sydney.

Danckwerts, P. V. (1953). Continuous flow systems: distribution of residence times. *Chemical Engineering Science*, **2**(1), 1-13.

Deng, Z.Q., Singh, V.P. & Bengtsson, L. (2001). Longitudinal dispersion coefficient in straight rivers. *Journal of Hydraulic Engineering,* **127**(11), 919-927.

Diaz, F.J., O'Geen, A.T., Dahlgren, R.A. (2012). Agricultural pollutant removal by constructed wetlands: Implications for water management and design. *Agricultural Water Management*, **104**, 171-183.

Dunne, E. J., Coveney, M. F., Hoge, V. R., Conrow, R., Naleway, R., Lowe, E. F., Battoe, L. E., & Wang, Y. (2015). Phosphorus removal performance of a large-scale constructed treatment wetland receiving eutrophic lake water. *Ecological Engineering*, **79**, 132-142.

Editorial (2009). Pollution control by wetlands. *Ecological Engineering*, **35**, 153-158.

Elder, J.W. (1959). The dispersion of a marked fluid in turbulent shear flow. *Journal of Fluid Mechanics,* **5**(4), 544-560.

EPA (Environmental Protection Agency), (2014). Water: Polluted Runoff. What is Nonpoint source pollution. URL: http://water.epa.gov/polwaste/nps/whatis.cfm [Date accessed: 17/07/2014].

Etemad-Shahidi, A. & Taghipour, M. (2012). Predicting longitudinal dispersion coefficient in natural streams using M5' model tree. *Journal of Hydraulic engineering*, **138**(6), 542-554.

European Commission, 2006. Bathing water quality - Legal Obligations under the EU Bathing Water Directive 2006/7/EC. Available at: http://ec.europa.eu/environment/water/water-bathing/summary.html

European Commission, 2014. Introduction to the new EU Water Framework Directive. Available at: http://ec.europa.eu/environment/water/water-framework/info/intro_en.htm#top-page

European Commission, 2000. The EU Water Framework Directive - integrated river basin management for Europe. Available at: http://ec.europa.eu/environment/water/water-framework/index_en.html

Faulwetter, J.L., Gagnon, V., Sundberg, C., Chazarenc, F., Burr, M.D., Brisson, J., Camper, A.N. & Stein, O.R. (2009). Microbial processes influencing performance of treatment wetlands: A review. *Ecological Engineering*, **35**, 987-1004.

Feng, Y. Z., Xie, X. J., Qin, X. W., Yang, G. H., Cao, Y. C., & Yang, S. Q. (2011). Features and treatment of non-point source pollution in the Ningxia Yellow River area. *African Journal of Agricultural Research*, **6**(24), 5541-5550.

Fennel, K., Brady, D., DiToro, D., Fulweiler, R. W., Gardner, W. S., Giblin, A., & Tobias, C. (2009). Modeling denitrification in aquatic sediments. *Biogeochemistry*, **93**(1-2), 159-178.

Fia, R., Matos, A. T., Ferreira, P. A., Teodoro, P. E. P., Schuery, F. C., & Luiz, F. A. R. (2008). Desempenho agronômico da thypha sp. e alternanthera philoxeroides mart utilizadas no tratamento de águas residuárias da lavagem e descascamento/despolpa dos frutos do cafeeiro em sistema alagado construído. *Engenharia na Agricultura*, **16**(4), 436-448.

Fia, R., Matos, A. T. D., Fia, F. R., Matos, M. P. D., Lambert, T. F., & Nascimento, F. S. (2010). Performance of forage crops in wetlands used in the treatment of wastewater of coffee processing. *Revista Brasileira de Engenharia Agrícola e Ambiental*, **14**(8), 842-847.

Fischer, B.H. (1967). The mechanics of dispersion in natural streams. *Journal of Hydraulic Division,* ASCE*,* **93**(6), 187-216.

Fischer, B.H. (1975). Discussion of 'simple method for predicting dispersion in streams. *Journal of the Environmental Engineering Division,* ASCE*,* **101**(3), 543-455.

Fischer, H.B., List, J.E., Koh, R.C.Y., Imberger, J. & Brooks, N.H. (1979). Mixing in inland and coastal waters. New York: Academic Press.

Gagnon, V., Chazarenc, F., Kõiv, M., & Brisson, J. (2012). Effect of plant species on water quality at the outlet of a sludge treatment wetland. *Water research*, **46**(16), 5305-5315.

Gao, J.P., Maguhn, J., Spitzauer, P. & Kettrup, A. (1997). Distribution of pesticides in the sediment of the smaill Teufelweiher pond (Southern Germany). *Water Resources*, **32**, 2811-2819.

Gao, J.P., Maguhn, J., Spitzauer, P. & Kettrup, A. (1998a). Sorption of pesticides in the sediment of the Teufelweiher pond (Southern Germany). I: Equilibrium assessments, effect of organic carbon content and pH. *Water Resources*, **32**, 1662-1672.

Gao, J.P., Maguhn, J., Spitzauer, P. & Kettrup, A. (1998b). Sorption of pesticides in the sediment of the Teufelweiher pond (Southern Germany). II: Competitive adsorption, desorption of aged residues and effect of dissolved organic carbon. *Water Resources*, **32**, 2089-2094.

German, J., Jansons, K., Svensson, G., Karlsson, D. & Gustafsson, L. G. (2005). Modelling of different measures for improving removal in a stormwater pond. *Water Science & Technology*, **52**(5), 105-112.

Ghermandi, A., Bixio, D. & Thoeye, C. (2007). The role of free water surface constructed wetlands as polishing step in municipal wastewater reclamation and reuse*Science of the Total Environment*, **380**, 247-258.

Google Maps. Location of RSPB Hope Farm in Knapwell, Cambridgeshire. National Grid Reference: TL 333625 62549.

Gordon, N.D., McMahon, T.A., Finlayson, B.L., Gippel, C.J. & Nathan, R.J. (2004). Stream Hydrology: An Introduction for Ecologists. John Wiley & Sons, Ltd, 2nd edition. Chichester, UK.

Gottschall, N., Boutin, C., Crolla, A., Kinsley, C. & Champagne, P. (2007). The role of plants ine the removal of nutrients at a constructed wetland treating agricultural (dairy) wastewater, Ontario, Canada. *Ecological Engineering*, **29**, 154-163.

Gregoire, C., Elsaesser, D., Huguenot, D., Lange, J., Lebeau, T., Merli, A., Mose, R., Passeport, E., Payraudeau, S., Schuetz, T., Schulz, R., Tapia-Padilla, .G.,Tournebize, J., Trevisan, M., Wanko, A. (2009). Mitigation of agricultural nonpoint-source pesticide pollution in artificial wetland ecosystems. *Environmental Chemistry Letters*, **7**, 205-231.

Guymer, I. (2002). A national database of travel time, dispersion and methodologies for the protection of river abstractions. R AND D TECHNICAL REPORT-ENVIRONMENT AGENCY P.

Guymer, I., Wilson, C. & Boxall, J. (2009). Modelling Solute Transport Processes in Free Surface Flow CFD Schemes 1. Lecture 1.

Hammer, D.A., (1992). Designing constructed wetlands systems to treat agricultural nonpoint source pollution. *Ecological Engineering*, **1**, 49–82.

Haygarth, P.M. & Jarvis, S.C. (2002): Agriculture, hydrology, and water quality. CABI Publishing, Wallingford, Oxfordshire, UK.

Headley, T.R. & Kadlec, R.H., (2007). Conducting hydraulic tracer studies of constructed wetlands: a practical guide. *Ecohydrology & Hydrobiology*, **7**(3-4), 269–282.

Hey, D.L., Kenimer, A.L., Barrett, K.R., 1994. Water quality improvement by four experimental wetlands. *Ecological Engineering,* **3**,381-397.

Holland, J.F., Martin, J.F., Granata, T., Bouchard, V., Quigley, M. & Brown, L. (2004). Effects of wetland depth and flow on residence time distribution characteristics. *Ecological Engineering*, **23**, 189-203.

Horne, A. J. (2002). Potential value of constructed wetlands for nitrate removal along some large and small rivers. *Internationale Vereinigung fur Theoretische und Angewandte Limnologie Verhandlungen*, **27**(7), 4057-4062.

International Association for the Properties of Water and Steam (IAPWS), R12-08. Release on the IAPWS Formulation 2008 for the Viscosity of Ordinary Water Substance, September 2008. Available at: http://www.iapws.org/

Iwasa, Y. & Aya, S. (1991). Predicting longitudinal dispersion coefficient in open-channel flows. *Proceedings of International Symposium on Environmental Hydraulics,* Hong Kong, 505-510.

Johannesson, K. M., Kynkäänniemi, P., Ulén, B., Weisner, S. E. B., & Tonderski, K. S. (2015). Phosphorus and particle retention in constructed wetlands—A catchment comparison. *Ecological Engineering*, **80**, 20-31.

Jordan, T. E., Whigham, D. F., Hofmockel, K. H., & Pittek, M. A. (2003). Nutrient and sediment removal by a restored wetland receiving agricultural runoff. *Journal of environmental quality*, **32**(4), 1534-1547.

Kadlec, R. H. (1990). Overland flow in wetlands: vegetation resistance. *Journal of Hydraulic Engineering*, **116**(5), 691-706.

Kadlec, R.H. (1994). Detention and mixing in free water wetlands. *Ecological Engineering*, **3**, 345-380.

Kadlec, R. (1995). Overview: Surface flow constructed wetlands. *Water Science Technology,* **32**, 1-12.

Kadlec, R. H., & Knight, R. L. (1996). Treatment wetlands. CRC. *Baca Raton, FL*.

Kadlec, R.H. (2009). Comparison of free water and horizontal subsurface treatment wetlands. *Ecological Engineering*, **35**, 159-174.

Kadlec, R.H. & Wallace, S.D. (2009). Treatment wetlands, 2nd edition. Boca Raton, CRC Press.

Kiely, G. 1997. Environmental engineering. London: McGraw-Hill.

Kladivko, E. J., Brown, L. C., & Baker, J. L. (2001). Pesticide transport to subsurface tile drains in humid regions of North America. *Critical Reviews in Environmental Science and Technology*, **31**(1), 1-62.

Knight, R.L. (1987). Effluent distribution and basin design for enhanced pollutant assimilation by freshwater wetlands. In Reddy K.R., Smith W.H. (Eds.), *Aquatic plants for water treatment and resource recovery*, 913-921. Orlando, Florida, USA: Magnolia Publishing Company.

Knobeloch, L., Salna, B., Hogan, A., Postle, J., & Anderson, H. (2000). Blue babies and nitrate-contaminated well water. *Environmental Health Perspectives*, **108**(7), 675.

Koskiaho, J. (2003a). Flow velocity retardation and sediment retention in two constructed wetland-ponds. *Ecological Engineering*, **19**, 325-337.

Koskiaho, J., Ekholm, P., Räty, M., Riihimäki, J., & Puustinen, M. (2003b). Retaining agricultural nutrients in constructed wetlands—experiences under boreal conditions. *Ecological Engineering*, **20**(1), 89-103.

Kotti, I.P, Gikas, G.D. & Tsihrintzis, V.A. (2010). Effect of operational and design parameters on removal efficiency of pilot-scale FWS constructed wetlands and comparison with HSF systems. *Ecological Engineering*, **36**, 862-875.

Kuschk, P., Wiessner, A., Kappelmeyer, U., Weissbrodt, E., Kästner, M., & Stottmeister, U. (2003). Annual cycle of nitrogen removal by a pilot-scale subsurface horizontal flow in a constructed wetland under moderate climate.*Water Research*, **37**(17), 4236-4242.

Lange, J., Schuetz, T., Gregoire, C., Elsässer, D., Schulz, R., Passeport, E., & Tournebize, J. (2011). Multi-tracer experiments to characterise contaminant mitigation capacities for different types of artificial wetlands. *International Journal of Environmental and Analytical Chemistry*, **91**(7-8), 768-785.

Lau, S. T. D. (2007). Scaling dispersion processes in surcharged manholes (Doctoral dissertation, University of Sheffield).

Laurent, J., Bois, P., Nuel, M., & Wanko, A. (2015). Systemic models of full-scale Surface Flow Treatment Wetlands: Determination by application of fluorescent tracers. *Chemical Engineering Journal*, **264**, 389-398.

Levenspiel, Octave, 1966. Chemical Reaction Engineering. First Edition. John Wiley & Sons, Inc, New York.

Lightbody, A. F. & Nepf, H. M. (2006). Prediction of velocity profiles and longitudinal dispersion in emergent salt marsh vegetation. *Limnology and Oceanography*, **51**(1), 218-228.

Lightbody, A.F., Avener, M.E. & Nepf, H.M., (2008). Observations of short-circuiting flow paths within a free-surface wetland in Augusta, Georgia, U.S.A. *Limnology and Oceanography,* **53**(3), 1040-1053.

Lightbody, A.F., Nepf, H.M. & Bays, J.S. (2009). Modeling the hydraulic effect of transverse deep zones on the performance of short-circuiting constructed treatment wetlands. *Ecological Engineering,* **35**, 754-768.

Lin, A.Y.C., Debroux, J.F., Cunningham, J.A. & Reinhard, M. (2003). Comparison of rhodamine WT and bromide in the determination of hydraulic characteristics of constructed wetlands. *Ecological Engineering,* **20**, 75-88.

Liu, H. (1977). Predicting dispersion coefficient of streams. *Journal of Environmental Engineering Division,* ASCE*,* **103**(1), 59-69.

Liu, J. J., Dong, B., Guo, C. Q., Liu, F. P., Brown, L., & Li, Q. (2016). Variations of effective volume and removal rate under different water levels of constructed wetland. *Ecological Engineering*, **95**, 652-664.

Locke, M.A., Weaver, M.A., Zablotowicz, R.M., Steinriede, R.W., Bryson, C.T., Cullum, R.F., 2011. Constructed wetlands as a component of the agricultural landscape: Mitigation of herbicides in simulated runoff from upland drainage areas. *Chemosphere*, **83**, 1532-1538.

Lu, S. Y., Wu, F. C., Lu, Y. F., Xiang, C. S., Zhang, P. Y., & Jin, C. X. (2009). Phosphorus removal from agricultural runoff by constructed wetland. *Ecological Engineering*, **35**(3), 402-409.

Lv, T., Zhang, Y., Zhang, L., Carvalho, P. N., Arias, C. A., & Brix, H. (2016). Removal of the pesticides imazalil and tebuconazole in saturated constructed wetland mesocosms. *Water research*, **91**, 126-136.

Mackenzie, S.M., & McIlwraith, C.I. (2015). Constructed farm wetlands – treating agricultural water pollution and enhancing biodiversity (2nd edition). Available from: www.wwt.org.uk/farmwetlands/

Mander, Ü., Tournebize, J., Soosaar, K., Chaumont, C., Hansen, R., Muhel, M., Teemusk, A., & Vincent, B. (2015, April). Nitrous oxide and methane emission in an artificial wetland treating polluted runoff from an agricultural catchment. In *EGU General Assembly Conference Abstracts* (Vol. 17, p. 13911).

Masters, G. M., & Ela, W. (1991). *Introduction to environmental engineering and science* (Vol. 3). Englewood Cliffs, NJ: Prentice Hall.

McElroy, A. D., Chiu, S. Y., Nebgen, J. W., Aleti, A., & Vandegrift, A. E. (1975). Water pollution from nonpoint sources. *Water Research*, **9**(7), 675-681.

Miller, C.T. & Weber, W.J. (1986). Sorption of hydrophobic organic pollutants in saturated soil systems. *Journal of Contaminant Hydrology*, **1**, 243-261.

Min, J. H. & Wise, R. W., (2009). Simulating short-circuiting flow in a constructed wetland: the implications of bathymetry and vegetation effects. *Hydrological Processes*, **23**, 830-841.

Mitsch, W.J., Gosselink, J.G. (2007). Wetlands, 4th edition, John Wiley & Sons, Inc., New York, p.582.

Mitsch, W. J., Horne, A. J., & Nairn, R. W. (2000). Nitrogen and phosphorus retention in wetlands-ecological approaches to solving excess nutrient problems. *Ecological Engineering*, **14**(1-2), 1-7.

Moreno, M.D. (1990). A tracer study of the hydraulics of facultative stabilization ponds. *Water Resources*, **24**(8), 1025-1030.

Murphy, E., Ghisalberti, M. & Nepf, H. (2007). Model and laboratory study of dispersion in flows with submerged vegetation. *Water Resources Research*, **43**, W05438, doi:10.1029/2006WR005229.

Nepf, H.M. (1999). Drag, turbulence, and diffusion in flow through emergent vegetation. *Water Resources Research*, **35**(2), 479-489.

Nepf, H., Ghisalberti, M., White, B., & Murphy, E. (2007). Retention time and dispersion associated with submerged aquatic canopies. *Water Resources Research*, **43**(4).

Nepf, H. M., & Vivoni, E. R. (2000). Flow structure in depth-limited, vegetated flow. *Journal of Geophysical Research: Oceans*, **105**(C12), 28547-28557.

Nepf, H. M. (2004). Vegetated flow dynamics. *The ecogeomorphology of tidal marshes*, 137-163.

Nepf, H.M. (2012). Flow and transport in regions with aquatic vegetation. *Annual Review of Fluid Mechanics*, **44**, 123-142.

Nepf, H.M., Mugnier, C.G. & Zavistoski, R.A. (1997). The effects of vegetation on longitudinal dispersion. *Estuarine, Coastal and Shelf Science*, **44**, 675-684.

Nowell, L.H, Capel, P.D. & Dileanis, P.D. (1999) *Pesticides in Stream Sediment and Aquatic Biota*, United States of America: CRC Press LLC.

Pappalardo, S. E., Otto, S., Gasparini, V., Zanin, G., & Borin, M. (2016). Mitigation of herbicide runoff as an ecosystem service from a constructed surface flow wetland. *Hydrobiologia*, *774*(1), 193-202.

Plazas, L., Rosero, .E., Solarte, E,. Sandoval, J. & Pena, M. (2009). Losses in the Fluorescent Tracer used in Hydrodynamic Modelling of Constructed Wetlands by Laser Induced Fluorescence. *Proceedings of SPIE*, Vol.7462.

Persson, J., Somes, N.L.G. & Wong, T.H.F. (1999). Hydraulics efficiency of constructed wetlands and ponds. Water Science and Technology, **40**(3), 291-300.

Persson, J. (2000). The Hydraulic Performance of Ponds of Various Layouts. *Urban Water*, **2**, 243-250.

Persson, J., & Wittgren, H. B. (2003). How hydrological and hydraulic conditions affect performance of ponds. *Ecological Engineering*, *21*(4), 259-269.

Poach, M. E., Hunt, P. G., Reddy, G. B., Stone, K. C., Johnson, M. H., & Grubbs, A. (2004). Swine wastewater treatment by marsh–pond–marsh constructed wetlands under varying nitrogen loads. *Ecological Engineering*, **23**(3), 165-175.

Poe, A. C., Piehler, M. F., Thompson, S. P., & Paerl, H. W. (2003). Denitrification in a constructed wetland receiving agricultural runoff. *Wetlands*, **23**(4), 817-826.

Polprasert, C. & Bhattarai, K.K. (1985). Dispersion model for waste stabilization ponds. *Environmental Engineering*, **111**(1), 45-59.

Reed, S. C. (1990). *Natural systems for wastewater treatment*. Water Pollution Control Federation.

Reed, S. C., & Brown, D. (1995). Subsurface flow wetlands—a performance evaluation. *Water environment research*, **67**(2), 244-248.

Reichenberger, S., Bach, M., Skitschak, A. & Frede, H.G. (2007). Mitigation strategies to reduce pesticide inputs into ground- and surface water and their effectiveness; A review. *Science of the Total Environment*, **384**, 1-35.

Reinhardt, M., Gächter, R., Wehrli, B., & Müller, B. (2005). Phosphorus retention in small constructed wetlands treating agricultural drainage water. *Journal of Environmental Quality*, **34**(4), 1251-1259.

Rodgers, J.H. & Dunn, A. (1992). Developing design guidelines for constructed wetlands to remove pesticides from agricultural runoff. . *Ecological Engineering,* **1**, 83-95.

Rose, M. T., Sanchez-Bayo, F., Crossan, A. N., & Kennedy, I. R. (2006). Pesticide removal from cotton farm tailwater by a pilot-scale ponded wetland. *Chemosphere*, **63**(11), 1849-1858.

Rossmann, M., de Matos, A. T., Abreu, E. C., e Silva, F. F., & Borges, A. C. (2012). Performance of constructed wetlands in the treatment of aerated coffee processing wastewater: removal of nutrients and phenolic compounds. *Ecological Engineering*, **49**, 264-269.

Rossmann, M., Matos, A. T., Abreu, E. C, Silva, F. F. & Borges, A. C. (2013). Effect of influent aeration on removal of organic matter from coffee processing wastewater in constructed wetlands. *Journal of Environmental Management*, **128**, 912-919.

Roux, L., Tournebize, J., Chaumont, C, Hocine, H. & Ginzburg, I. (2013). Modelling of a constructed wetland for pesticide mitigation. *13th Edition of the World Wide Workshop for Young Environmental Scientists*, Arcueil, France.

Runes, H. B., Jenkins, J. J., Moore, J. A., Bottomley, P. J., & Wilson, B. D. (2003). Treatment of atrazine in nursery irrigation runoff by a constructed wetland. *Water Research*, **37**(3), 539-550.

Rutherford, J.C. (1994). River mixing. Chapter 4, Longitudinal Dispersion. John Wiley & Sons, Inc., Chichester, U.K.

Schulz, R. (2004). Field studies on exposure, effects and risk mitigation of aquatic nonpoint-source insecticide pollution: A review. *Journal of Environmental Quality*, **33**, 419-448.

Schulz, R. & Peall, S.K.C. (2001). Effectiveness of a constructed wetland for retention of nonpoint-source pesticide pollution in the Lourens River Catchment. *Environmental Science Technology*, 35, 422-426.

Selvamurugan, M., Doraisamy, P., & Maheswari, M. (2010). An integrated treatment system for coffee processing wastewater using anaerobic and aerobic process. *Ecological Engineering*, **36**(12), 1686-1690.

Seo, I.W. & Cheong, T.S. (1998). Predicting longitudinal dispersion coefficient in natural streams. *Journal of Hydraulic Engineering,***124**(1), 25-32.

Seo, I.W., Baek, K.O. & Jeon, T.M. (2006). Analysis of transverse mixing in natural streams under slug tests. *Journal of Hydraulic Research*, **44**(3), 350–362.

Serra, T., Fernando, H.J.S., Rodriguez, R.V. (2004). Effects of emergent vegetation on lateral diffusion in wetlands. *Water Resources*. **38**, 139–147.

Schaffranek, R. W., Riscassi, A. L., Rybicki, N. B., & Lombana, A. V. (2003). Fire effects on flow in vegetated wetlands of the Everglades. In *Greater Everglades Ecosystem Restoration Conference, Palm Harbor, FL, USA*.

Scholz, M., Harrington, R., Carroll, P., & Mustafa, A. (2007). The integrated constructed wetlands (ICW) concept. Wetlands, **27**(2), 337-354.

Schuetz, T., Weiler, M., & Lange, J. (2012). Multitracer assessment of wetland succession: effects on conservative and nonconservative transport processes. *Water Resources Research*, **48**(6).

Schulz, R. (2004). Field studies on exposure, effects, and risk mitigation of aquatic nonpoint-source insecticide pollution. *Journal of Environmental Quality*, **33**(2), 419-448.

Shih, S.F. & Rahi, G.S. (1982). Seasonal variations of Manning's foughness coefficient in a subtropical marsh. *Transactions of the American Society of Agricultural Engineers*, **25**(1), 116-120.

Shilton, A., (2005). *Pond treatment technology*. London: IWA Publishing.

Shucksmith, J. D. (2008). *Impact of vegetation in open channels on flow resistance and solute mixing*. PhD Thesis. Sheffield.

Shutes, B., Revitt, M., Scholes, L., 2010. Constructed wetlands for flood prevention and water reuse. In: Proceedings of the 12th International Conference on Wetland Systems for Water Pollution Control, 4th-8th Oct 2010, Venice, Italy.

Somes, N.L.G., Persson, J. & Wong, T.H.F. (1998). Influence of Wetland Design Parameters on the Hydrodynamics of Stormwater Wetlands. *Hydrastorm*, Adelaide, 27-30 September, 1998, 123-128.

Søvik, A. K., & Mørkved, P. T. (2008). Use of stable nitrogen isotope fractionation to estimate denitrification in small constructed wetlands treating agricultural runoff. *Science of the Total Environment*, **392**(1), 157-165.

Stangroom, S. J., Collins, C. D., & Lester, J. N. (2000). Abiotic behaviour of organic micropollutants in soils and the aquatic environment. A review: II. Transformations. *Environmental technology*, **21**(8), 865-882.

Stanton, E. A., & Taylor, M. (2012). Valuing Florida's clean waters. *Stockholm Environment Institute–US Center*.

Stern, D.A., Khanbilvardi, R., Alair, J.C. & Richardson, W. (2001). Description of flow through a natural wetland using dye tracer tests. *Ecological Engineering,* **18**, 173-184.

Stottmeister, U., Wiessner, A., Kuschk, P., Kappelmeyer, U., Kaestner, M., Bederski, O., Mueller, R.A. & Moormann, H. (2003). Effects of plants and microorganisms in constructed wetlands for wastewater treatment. *Biotechnology Advances*, **22**, 93-117.

Su, T.M., Yang, S.C., Shih, S.S. & Lee, H.Y. (2009). Optimal design for hydraulic efficiency on free-water-surface constructed wetlands. *Ecological Engineering*, **35**, 1200-1207.

Ta, C.T. & Brignal, W.J. (1998). Application of computational fluid dynamics technique to storage reservoir studies. *Water science and technology*, **37**(2), 219-226.

Tang, X., Yang, Y., Tao, R., Chen, P., Dai, Y., Jin, C., & Feng, X. (2016). Fate of mixed pesticides in an integrated recirculating constructed wetland (IRCW). *Science of The Total Environment*, **571**, 935-942.

Tanino, Y., & Nepf, H. M. (2008). Laboratory investigation of mean drag in a random array of rigid, emergent cylinders. *Journal of Hydraulic Engineering*, **134**(1), 34-41.

Tanner, C. C., Nguyen, M. L., & Sukias, J. P. S. (2005). Nutrient removal by a constructed wetland treating subsurface drainage from grazed dairy pasture. *Agriculture, ecosystems & environment*, **105**(1), 145-162.

Tao, B. & Fletcher, A.J. (2013). Metaldehyde removal from aqueous solution by adsoption and ion exchange mechanisms onto activated carbon and polymeric sorbents. *Journal of Hazardous Materials*, **244-245**, 240-250.

Taylor, G.I. (1953). Dispersion of soluble matter in solvent flowing slowly through a tube. Proceedings of the Royal Society A, **219**, 186-203.

Taylor, G.I. (1954). The Dispersion of Matter in Turbulent Flow Through a Pipe. *Proceedings of the Royal Society of London. Series A. Mathematical and Physical Sciences*, **223**(1155), 446-468.

Tediosi, A., Whelan, M.J., Rushton, K.R., Thompson, T.R.E., Gandolfi, C. & Pullan, S.P. (2012). Measurement and conceptual modelling of herbicide transport to field drains in a heavy clay soil with implications for catchment-scale water quality management. *Science of the Total Environment*, **438**, 103-112.

Thackston, E.L., Shields, D. & Schroeder, P.R. (1987). Residence time distributions of shallow basins. Journal of Environmental Engineering, **113**(6), 1319-1332.

Tournebize, J., Passeport, E., Chaumont, C., Fesneau, C., Guenne, A., & Vincent, B. (2013). Pesticide de-contamination of surface waters as a wetland ecosystem service in agricultural landscapes. *Ecological engineering*, **56**, 51-59.

Tournebize, J., Chaumont, C., Fesneau, C., Guenne, A., Vincent, B., Garnier, J., & Mander, Ü. (2015). Long-term nitrate removal in a buffering pond-reservoir system receiving water from an agricultural drained catchment. *Ecological Engineering*, **80**, 32-45.

Tournebize, J., Chaumont, C., & Mander, Ü. (2016). Implications for constructed wetlands to mitigate nitrate and pesticide pollution in agricultural drained watersheds. *Ecological Engineering*. In press.

Veolia Water Technologies (2014). Removing Metaldehyde from Drinking Water. URL: http://veoliawatertechnologies.com/news-media/articles/metaldehyde-removal.htm. [Accessed on 05/09/2014].

Verhoeven, J.T.A. & Setter, T.L. (2010). Agricultural use of wetlands: opportunities and limitations. *Annuals of Botany*, **105**, 155-163.

Villaverde, J., Kah, M. & Brown, C.D. (2008). Adsorption and degradation of four acidic herbicides in soils from southern Spain. *Pest Management Science*, **64**, 703-710.

Volkmar, E. C., & Dahlgren, R. A. (2006). Biological oxygen demand dynamics in the lower San Joaquin River, California. *Environmental science & technology*, **40**(18), 5653-5660.

Vymazal, J. (2010). Constructed wetlands for wastewater treatment: five decades of experience. *Environmental Science & Technology*, **45**(1), 61-69.

Vymazal, J. (2013). Emergent plants used in free water surface constructed wetlands: A review. *Ecological Engineering*, **61**, 582-592.

Vymazal, J., 2007. Removal of nutrients in various types of constructed wetlands. *Science of the Total Environment*, **380**, 48-65.

Vymazal, J., Brix, H., Cooper, P. F., Green, M. B., & Haberl, R. (1998). *Constructed wetlands for wastewater treatment in Europe*. Backhuys Publishers, Leiden, The Netherlands.

Vymazal, J., Greenway, M., Tonderski, K., Brix, H., & Mander, Ü. (2006). Constructed wetlands for wastewater treatment. In *Wetlands and natural resource management* (pp. 69-96). Springer Berlin Heidelberg.

Walker, D.J. (1998). Modelling residence time in stormwater ponds. *Ecological Engineering,* **10**, 247-262.

Wallach, R. (1991). Runoff contamination by soil chemicals: Time scale approach. *Water resources research*, **27**(2), 215-223.

Wallis, S.G., Guymer, I. & Bilgi, A. (1989). A Practical Engineering Approach to Modelling Longitudinal Dispersion. Proceedings of International Conference on Hydraulic and Environmental Modelling of Coastal, Estuarine and River Waters, Bradford, England. 19-21 Sept., 291-300.

Wang, R., Korboulewsky, N., Prudent, P., Baldy, V., & Bonin, G. (2009). Can vertical-flow wetland systems treat high concentrated sludge from a food industry? A mesocosm experiment testing three plant species. *Ecological Engineering*, **35**(2), 230-237.

Wang, R., Baldy, V., Périssol, C., & Korboulewsky, N. (2012). Influence of plants on microbial activity in a vertical-downflow wetland system treating waste activated sludge with high organic matter concentrations. *Journal of environmental management*, **95**, S158-S164.

Wauchope, R. D. (1978). The pesticide content of surface water draining from agricultural fields—a review. *Journal of environmental quality*, **7**(4), 459-472.

Werner, T.M. & Kadlec, R.H. (2000). Wetland residence time distribution modelling. *Ecological Engineering,* **15**, 77-90.

Whelan, M.J. *10th Annual Technical Meeting on Environmental Risk Assessment Research ERAR CRD*. June 2016. University of York.

Wong, T. H. F., & Somes, N. L. G. (1995). A stochastic approach to designing wetlands for stormwater pollution control. *Water Science and Technology*, **32**(1), 145-151.

Woods-Ballard, B, Kellagher, R., Martin, P., Jefferies, C., Bray, R., & Shaffer, P. (2007). The SUDS manual (C697). Available from: http://www.ciria.org/Resources/Free_publications/the_suds_manual.aspx

Worman, A. & Kronnas, V. 2005. Effect of pond shape and vegetation heterogeneity on flow and treatment performance of constructed wetlands. *Journal of Hydrology*, **301**, 123–128.

Wu, M., Tang, X., Li, Q., Yang, W., Jin, F., Tang, M., Scholz, M. (2013a). "Review of Ecological Engineering Solutions for Rural Non-Point Source Water Pollution Control in Hubei Province, China." Water, Air, & Soil Pollution, **224**(5), 1-18.

Wu, H., Zhang, J., Li, C., Fan, J., & Zou, Y. (2013b). Mass balance study on phosphorus removal in constructed wetland microcosms treating polluted river water. *CLEAN–Soil, Air, Water*, **41**(9), 844-850.

Yates, C. R., & Prasher, S. O. (2009). Phosphorus reduction from agricultural runoff in a pilot-scale surface-flow constructed wetland. *Ecological Engineering*, **35**(12), 1693-1701

Young, P.C. & Wallis, S.G. (1986). The aggregated dead zone (ADZ) model for dispersion in rivers. International Conference on Water Quality Modelling in the Inland Natural Environment, Bournemouth, England, L1, 421-433.

Zhang, L., Scholz, M., Mustafa, A., & Harrington, R. (2008). Assessment of the nutrient removal performance in integrated constructed wetlands with the self-organizing map. Water Research, **42**(13), 3519-3527.

Zhang, X., & Zhang, M. (2011). Modeling effectiveness of agricultural BMPs to reduce sediment load and organophosphate pesticides in surface runoff. *Science of the Total Environment*, **409**(10), 1949-1958.

Zhang, J., Shen, T., Liu, M., Wan, Y., Liu, J., & Li, J. (2011). Research on non-point source pollution spatial distribution of Qingdao based on L-THIA model. *Mathematical and Computer Modelling*, **54**(3), 1151-1159.

9. Appendices

9.1 Appendix I: Related to Chapter 3 – *Methodology*

a. Flow Measurements at Hydraulic Control Structures

Simultaneous flow measurements were undertaken at the hydraulic control structures of each CW (locations of the hydraulic control structures are seen in Figure 24). The results showed that there is no time lag between the inlet and outlet of each wetland at the time of the tracer test. The monitoring period of the simultaneous flow measurements at the V-notch weir and Venturi flumes (inlet and outlet of the CWs) is presented in Figure 125. Results refer to flow rate at SW1 inlet (V-notch weir), at SW1 outlet (Venturi Flume 1), and at SW2 outlet (Venturi Flume 2), and cover DWF and storm flow conditions. Two flow conditions were selected from Figure 125 to be shown in detail, as representative of the flow rate range of this study; a DWF condition (Figure 126), and a storm flow condition (Figure 127).

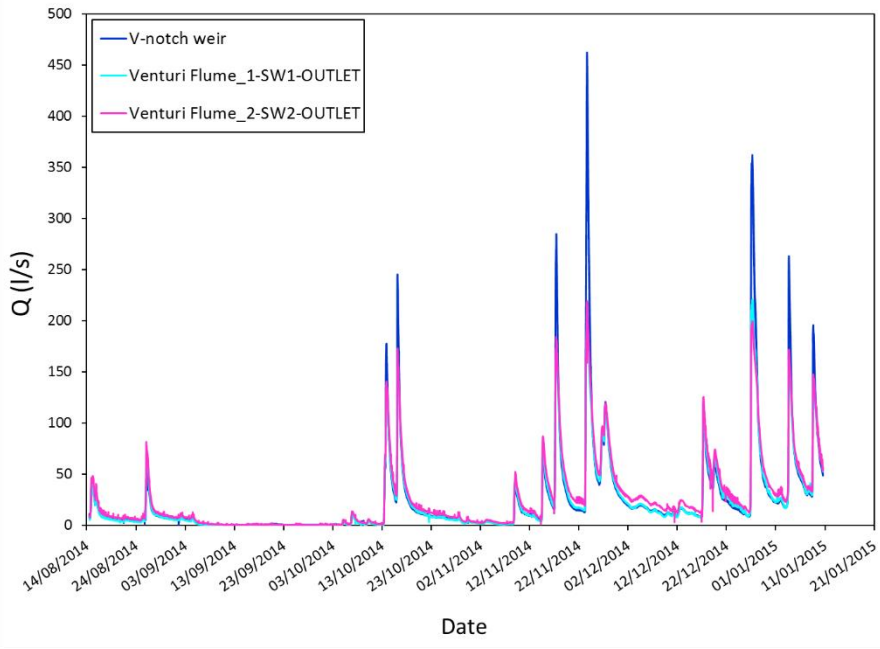

Figure 125: Simultaneous monitoring of flow rate at the hydraulic control structures in SWs (inlet and outlet).

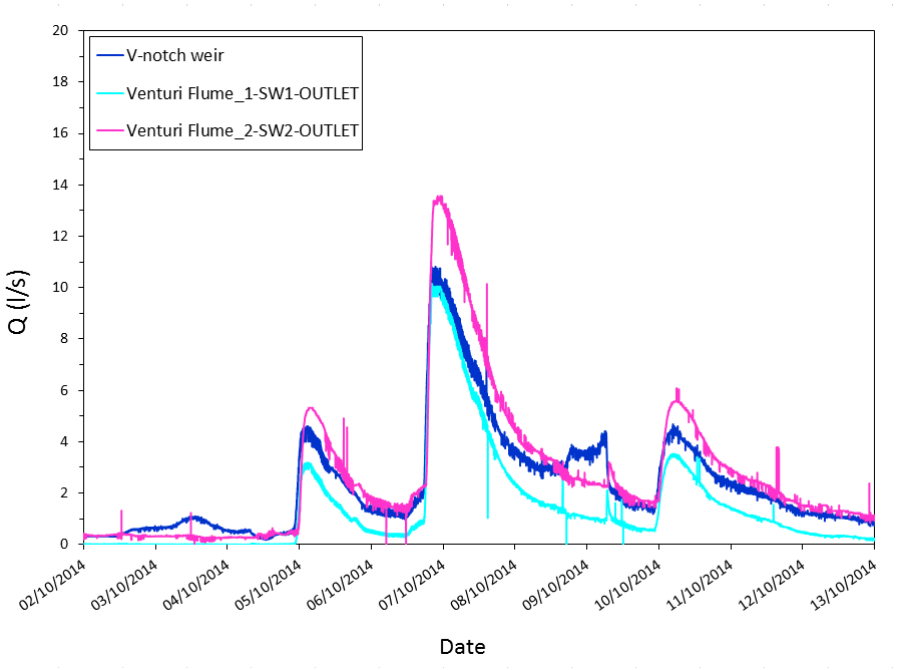

Figure 126: Simultaneous flow rate measurements at inlet and outlets of SWs under dry weather flow.

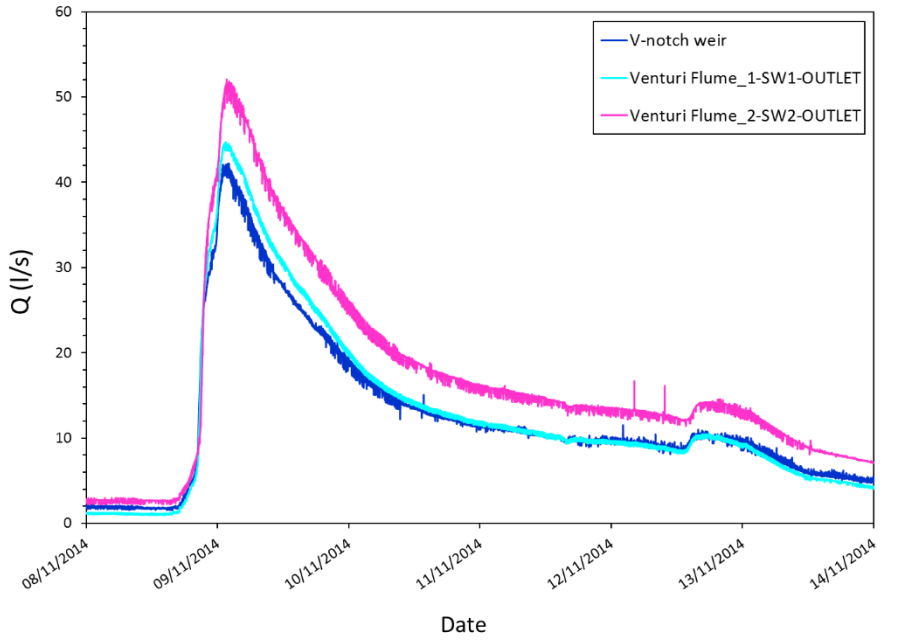

Figure 127: Simultaneous flow rate measurements at inlet and outlets of SWs under storm flow.

b. Site Surveying

Wetlands surveying helped to obtain total volumes of water stored in the CWs at different water levels, bottom topography, and vegetation boundaries. Surveying work took place in June 2014. Surveying works are generally preferred to be done in lightly cloudy days. This is because either sun rays or fog may have a distortion impact on the results. Due to the minimal flow in the wetlands during summer months, surveying works were conducted in June. Despite the dry conditions, there was some minimal flow in SWs, where some hyporheic water exchange was present creating a thick layer of mud on the wetlands' bed (see Figure 128). The equipment used was a robotic total station and a prism. To take correct level measurements, as precisely as possible, an extra cap of 2 cm thickness was attached at the bottom of the prism pole to prevent from sinking the prism sharp end deeply into the soil.

Besides the muddy bed at the middle of the wetlands, a second challenge encountered was the extreme vegetation growth in and out of the systems, making the working conditions tough. Despite the ongoing development in height, Phragmites stems height and density (see Figure 129) induced problems in accessing and taking measurements in all parts of the wetland bed, and especially towards the middle. Furthermore, surrounding plants and tree foliage were at their culmination growth stage, adding visual problems during the surveying works, and accessing the surrounding area.

Measurements were taken along sections of the wetland length at approximately 2-3 m apart. The extra cap was added or removed accordingly depending on whether the bed was muddy or dry.

Figure 128: Bed muddy soil in the wetlands during surveying works was deeper than expected, approximately 15 cm depth.

Figure 129: Stems in June 2014 during the surveying works. Stems are packed in density and still developing while there is still some quantity of the previous year's decaying stems.

c. Solid volume fraction calculations for stems

This section provides information about the calculations involved for the solid volume fraction, Φ, in the two extreme cases of stems deflection.

Case I refers to 0% stem deflection (i.e. upright stems), and is considered to occur between April and January for this micro-climate. The usual equation that calculates Φ is defined as:

$N_t \pi d_m^2 / 4$. In Case II, when stems are fully deflected, the methodology followed to calculate Φ in each wetland is described by the following steps:

- The cross-sectional stem area, α, was computed as $\pi d_m^2 / 4$.
- The product of α·H was computed to give the volume of the deflected stems, where H = average stem height (m).
- The stem population density, N_t, was multiplied by α·H, to incorporate the packing density of the stems deflected in the wetland.
- Normalisation of the product of α·H·N_t (which gives length units) was achieved by dividing over the mean water depth, h = 0.2 m.

d. <u>Flow measurements through hydraulic structures and associated conversions</u>

The water level readings from the pressure transducer were converted into flow rate through the standard Kindvater & Carter free water surface equation (BS3680–4A, 1981), given by Equation 9.1. Given the in-series arrangement of SWs, and the short HRT, and the negligible time lag from inlet to outlet, the discharge in the stream and in SW2 was considered same as SW1.

$$Q = \frac{8}{15} C_e \sqrt{2g} \cdot \tan\frac{\theta}{2} \cdot h_e^{\frac{5}{2}} \qquad \text{Equation 9.1}$$

where θ is in rad; h_v is the measured head; C_e is coefficient of discharge; h_e is the effective head; K_h is a head correction factor that compensates for the combined effects of viscosity and surface tension and is found from the following equation, $K_h = 0.001 \cdot (\theta \cdot (1.395 \cdot \theta - 4.296) + 4.135)$, where θ in rad. K_h is 0.0012m in this study.

Accordingly, the calculation of the flow in the Venturi flumes was achieved using the free water surface standard Equation 9.2.

$$Q_f = C_{ft}(h_u)^{n_{ft}} \qquad \text{Equation 9.2}$$

In which C_{ft} = 2.63 (free-flow coefficient for the flume); n_{ft} = 1.83 (exponent depending on the flume size); h_u = water depth in ft; Q_f = flow rate in cfs (cubic foot per second) (Utah State University, 2008).

e. Flow measurements through dilution gauging in SW2

Flow rate obtained from dilution gauging in SW2 is plotted against flow rate from the pressure transducer in Figure 130. The mass balance is not consistently good in all months, i.e. January and February present good tracer mass recovery, whereas December results are out of range. The outliers are mainly attributed to the lack of robustness of the automated tracer injection system, and in particular to the pump's robustness to inject the proper amount of tracer in the system. Recall that tracer tests paused in March due to SW2 tracer injection equipment malfunction, thus tracer tests ceased in SW2 in March. This decision was made because SW2 data analysis to that date, had not shown any particular affinity to seasonal plant variation, therefore it was decided that tests continue in SW1, as far as weather permits.

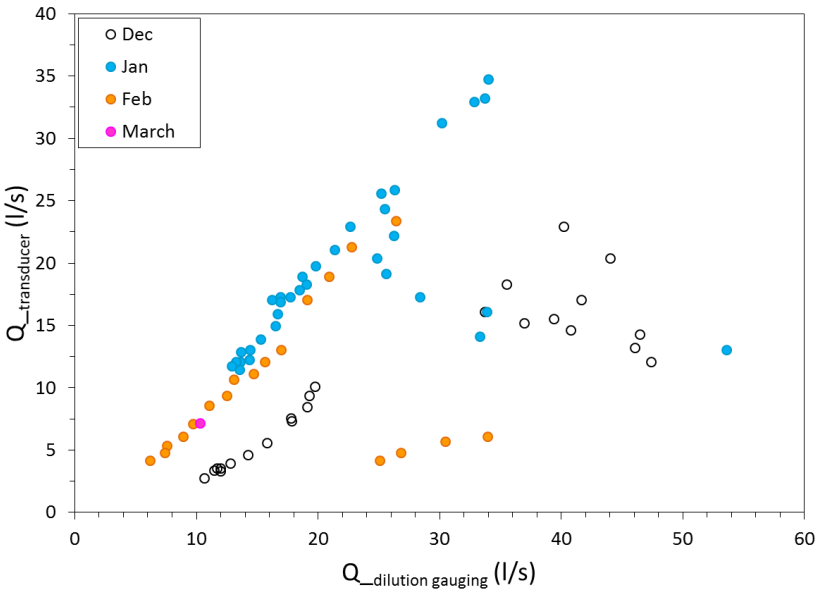

Figure 130: Mass balance of dye between discharges measured from the pressure transducer and from the dilution gauging in SW2 in different months.

f. Calibration values for longitudinal mixing study in SW1 & SW2 for different gain settings

Calibration values for the three fluorometers used for the longitudinal mixing study in SW1 - SW2 are presented Figure 131, Figure 132, and Figure 133 for gain 1, 10, & 100 respectively.

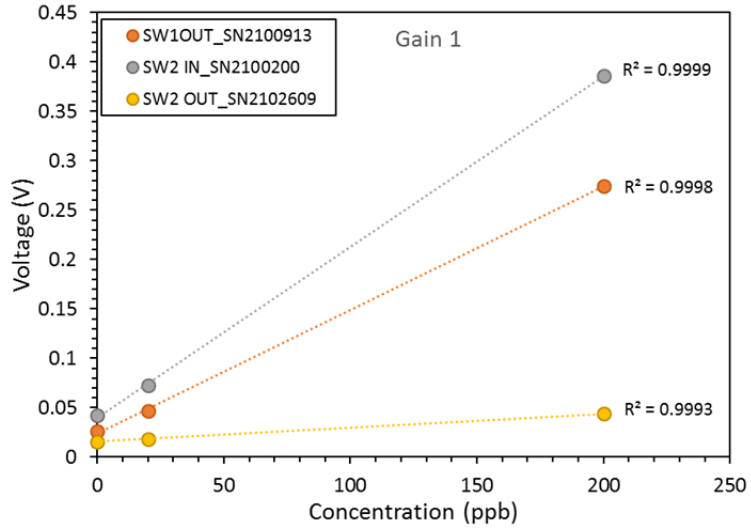

Figure 131: Calibration values of fluorometers for longitudinal mixing study in SWs at Gain 1 sensitivity.

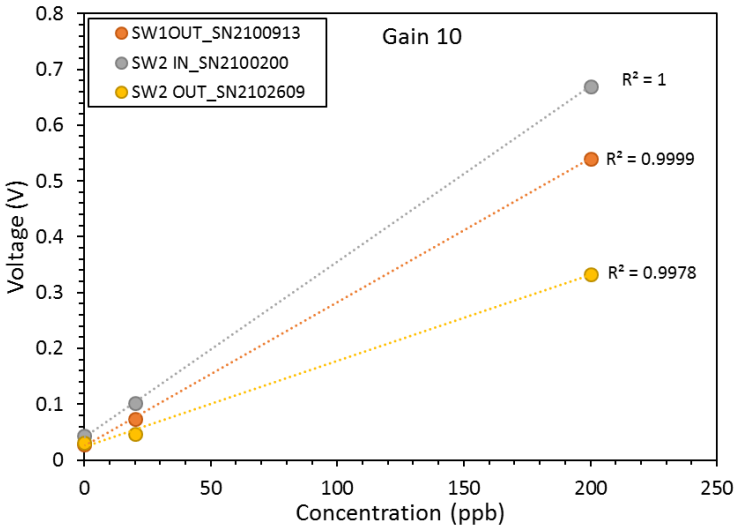

Figure 132: Calibration values of fluorometers for longitudinal mixing study in SWs at Gain 10 sensitivity.

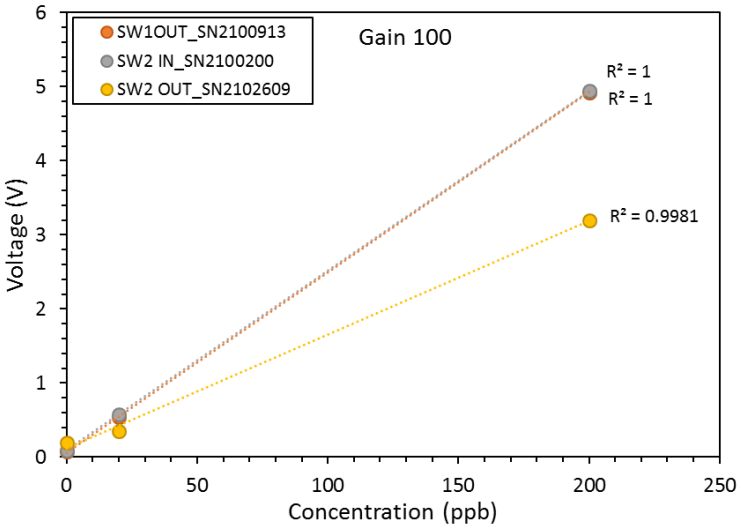

Figure 133: Calibration values of fluorometers for longitudinal mixing study in SWs at Gain 100 sensitivity.

g. Calibration values for differential advection study in SW1 & SW2

Calibration values for the extra four fluorometers used for the differential advection study are provided in Table 9.1 and refer to both SW1 and SW2 tracing tests.

Table 9.1: Calibration values of the four fluorometers used for the differential advection study in SW1 & SW2.

	GAIN 1							
Location	**L1**		**L2**		**L3**		**L4**	
Instrument SN	SN2103148		SN2100670		SN2100912		SN2100911	
Concentration (ppb)	mV	V	mV	V	mV	V	mV	V
0	26	0.026	65	0.065	31	0.031	31	0.031
250	108	0.108	918	0.918	130	0.13	132	0.132
500	193	0.193	1808	1.808	236	0.236	236	0.236

9.2 Appendix II: Related to Chapter 4 – *Experimental Results*

This section shows a compilation of the tracer tests for the stream, and a compilation of the RTDs and CRTDs for actual and for normalised time for SW1 and SW2.

a. Compilation of RTDs & CRTDs in SW1

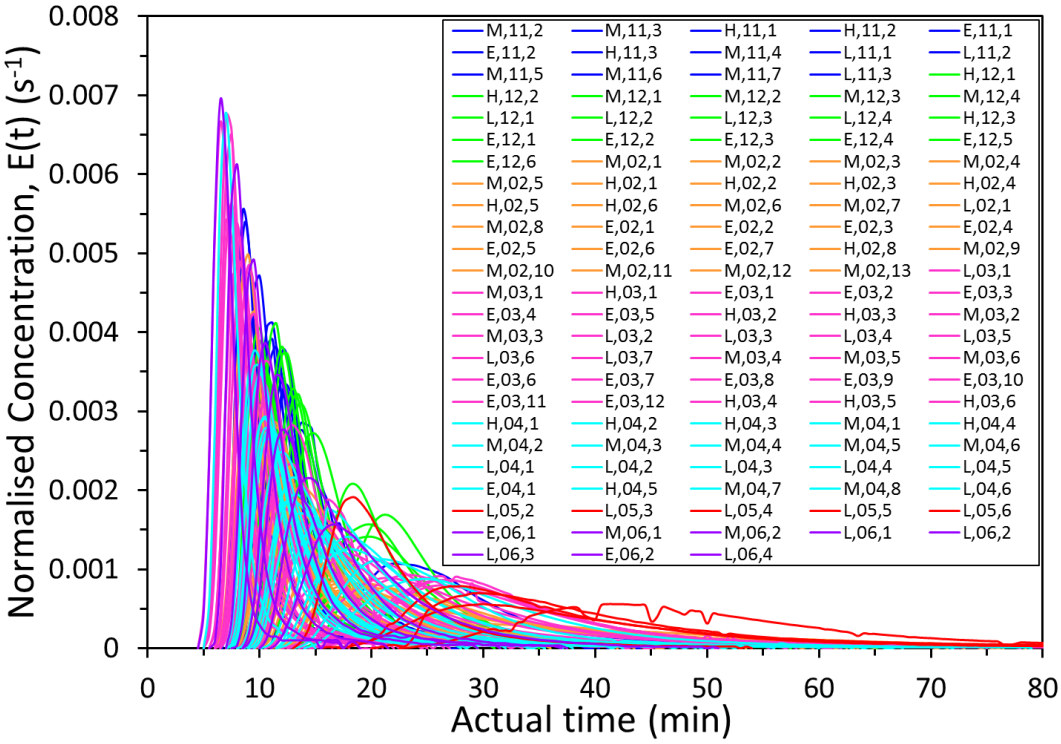

Figure 134: Compiled RTDs at actual time for SW1.

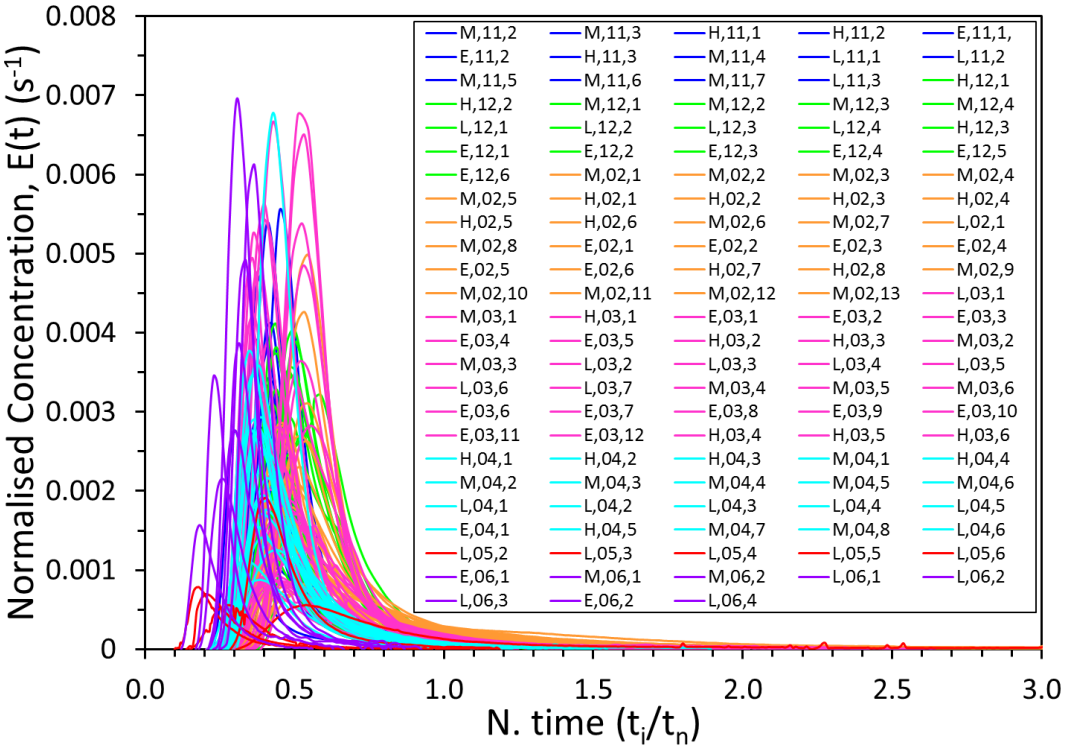

Figure 135: Compiled RTDs at normalised time for SW1.

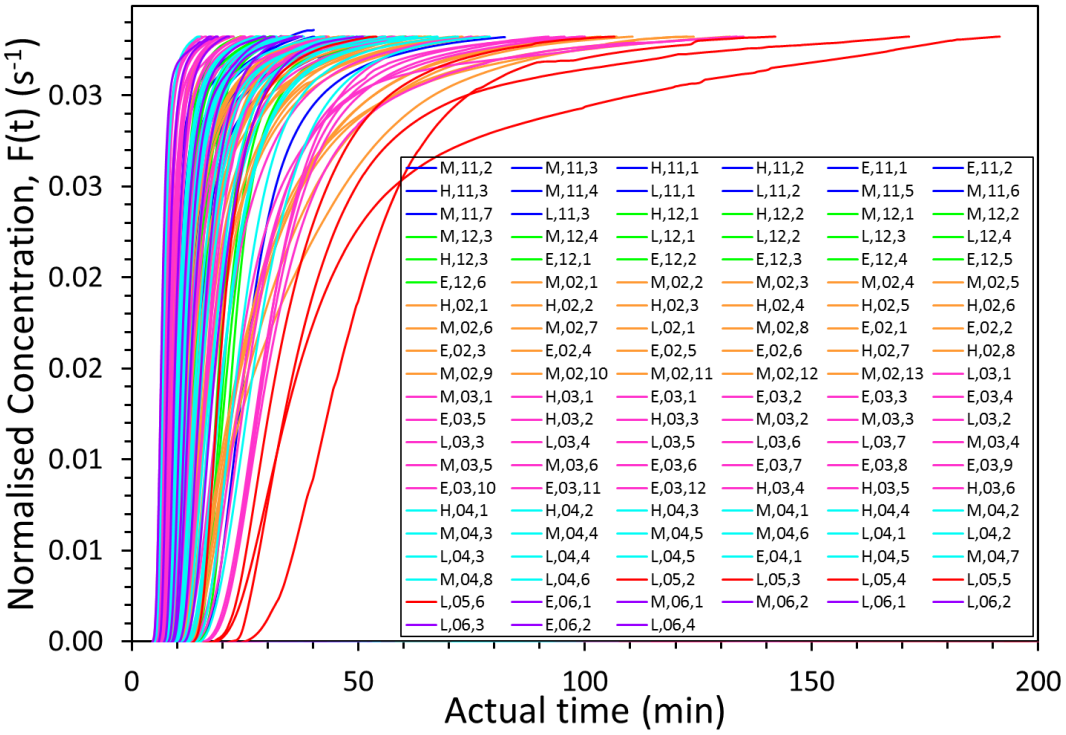

Figure 136: Compiled CRTDs at actual time for SW1.

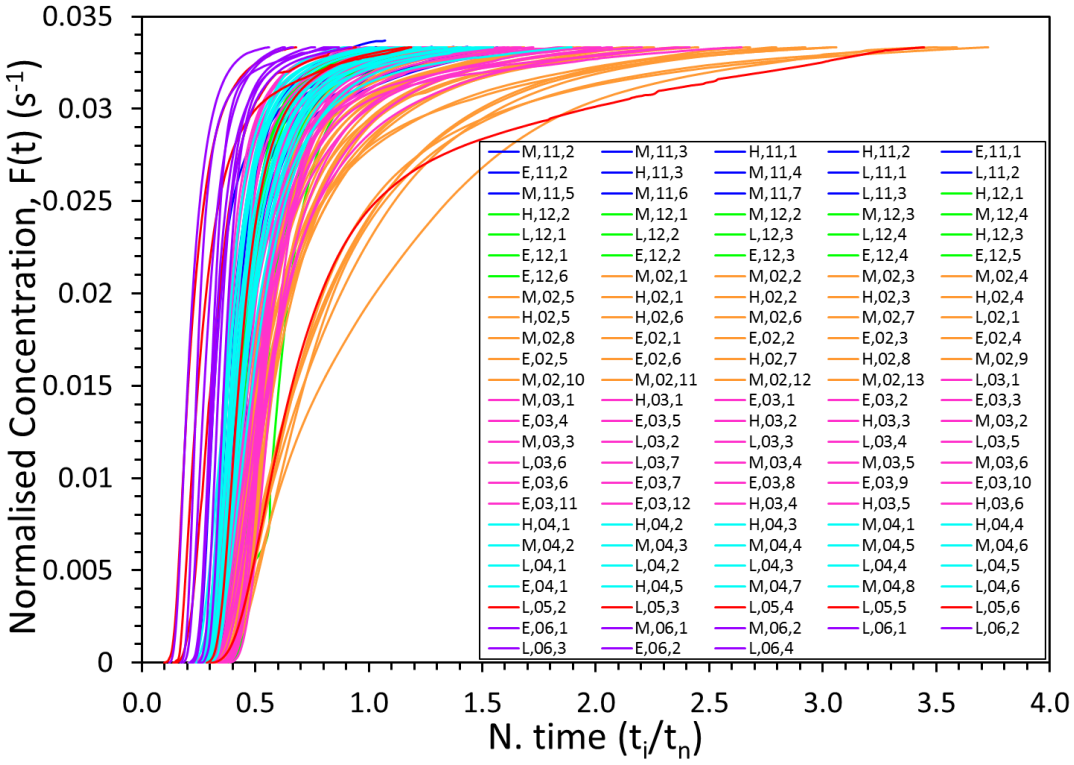

Figure 137: Compiled CRTDs at normalised time for SW1.

b. Compilation of RTDs & CRTDs in SW2

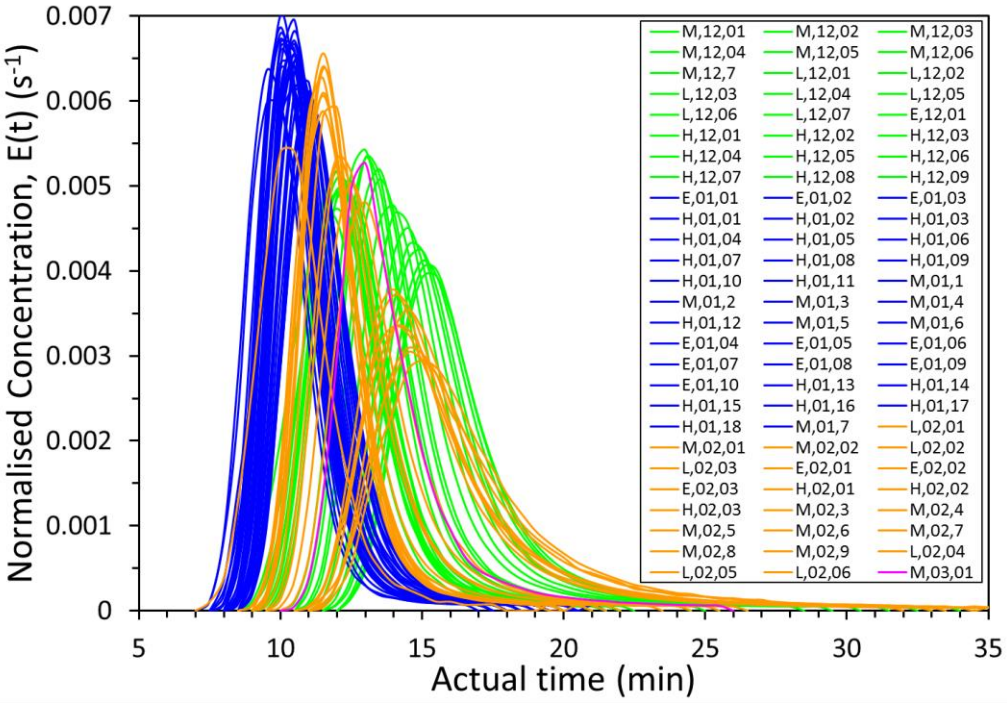

Figure 138: Compiled RTDs at actual time for SW2.

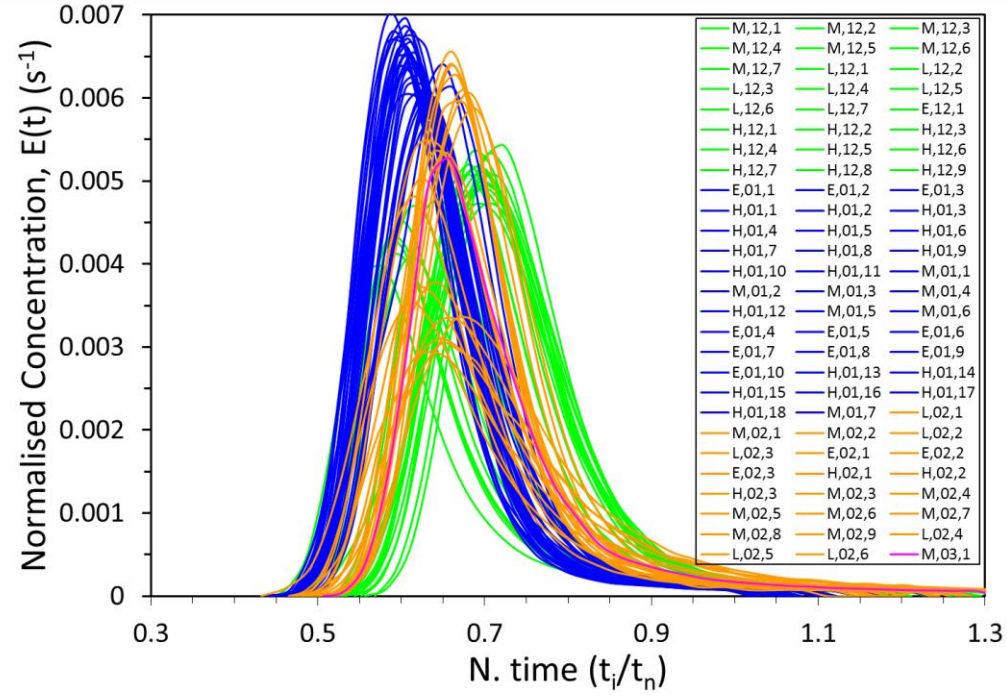

Figure 139: Compiled RTDs at normalised time for SW2.

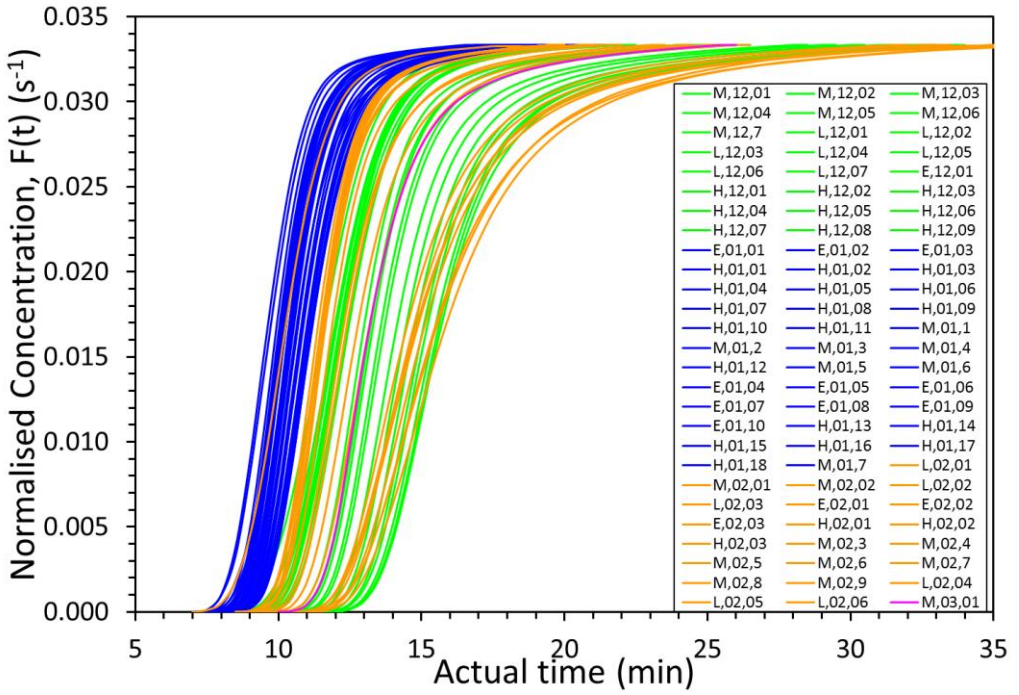

Figure 140: Compiled CRTDs at actual time for SW2.

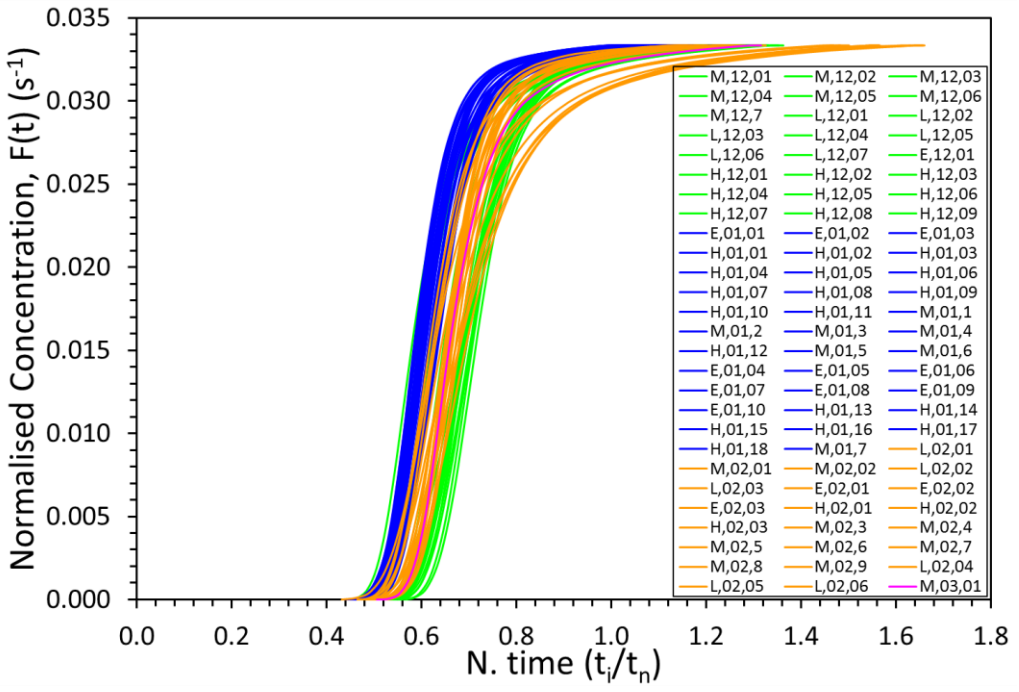

Figure 141: Compiled CRTDs at normalised time for SW2.

9.3 Appendix III: Related to Chapter 5 – Summary of SW1 & SW2 Results & Discussion

This section presents SW2 results for data processing at a lower cut-off value, i.e. 0.2%, and is used as a reference to the basic consistent analysis using 1% cut-off. Figure 142 shows the relationship between D_x and Q, and suggests an inverse trend, albeit not strong. Figure 143 illustrates the dimensionless D_x against Q, connoting a strong inverse trend. Plant deflection, thus ageing, does not appear to affect the degree of longitudinal mixing.

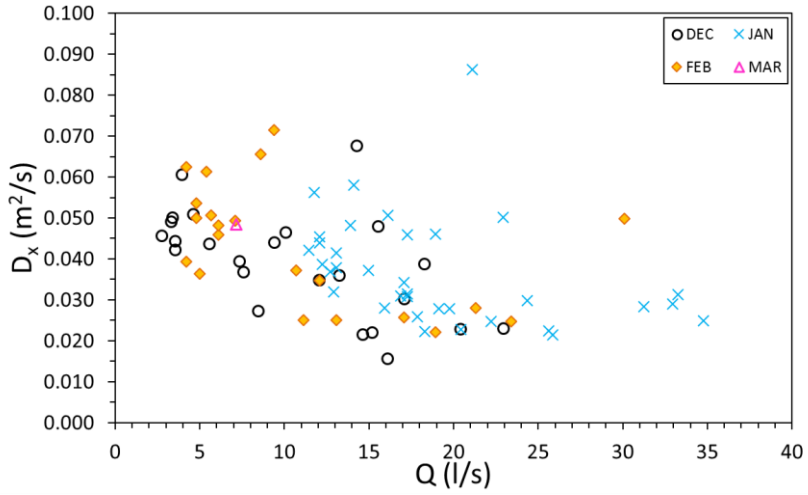

Figure 142: Longitudinal dispersion coefficient against discharge in SW2, for lower cut-off value, i.e. 0.2%.

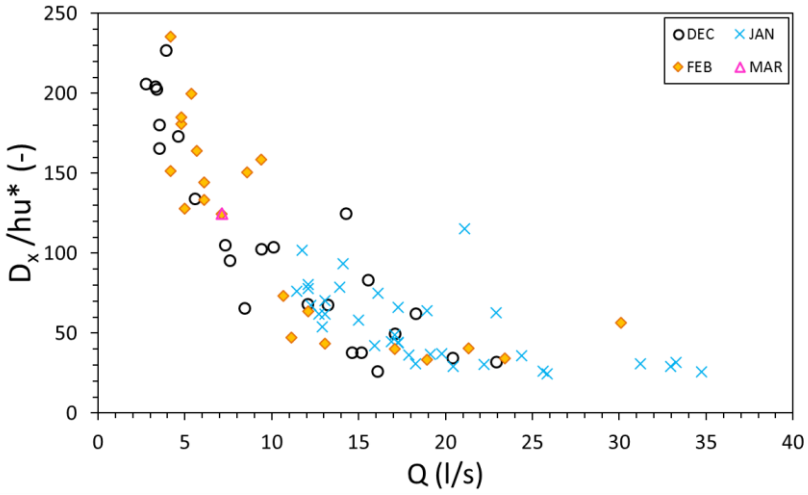

Figure 143: Normalised longitudinal dispersion coefficient against discharge in SW2, for lower cut-off value, i.e. 0.2%.

A comparison between the dimensionless D_x coefficients against Q for the South Wetland systems is presented in Figure 144. SW2 presents the lowest D_x values and minimal variation in D_x, where SW2 D_x coefficients become comparable with SW1 ones only for the low flow rates.

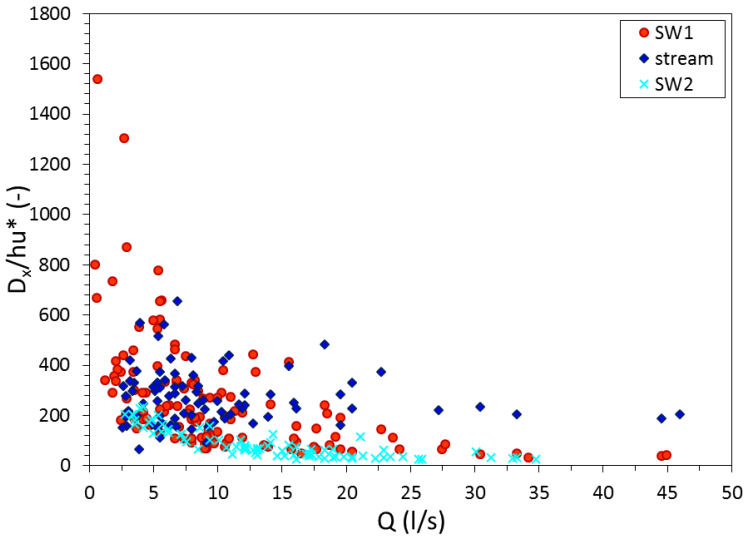

Figure 144: Normalised longitudinal dispersion coefficient against discharge in South Wetlands, where SW2 analysis uses lower cut-off value, i.e. 0.2%.

Peclet number is presented against Q in Figure 145 and against the Mo mixing index in Figure 146 respectively. It is observed that greater advection occurs in SW2 (Figure 145) compared to SW1 for the same flow rates, verifying the greater short-circuited flows. Figure 146 indicates that variation in mixing is minimal in SW2, suggesting that neither flow rate nor seasonal plant variation affect mixing characteristics in this system. However, Figure 146 indicates that a different mechanism occurs in SW1, as mixing and Pe number follow a strong negative correlation, suggesting that increase in flow velocity or discharge, reduces mixing in the wetland.

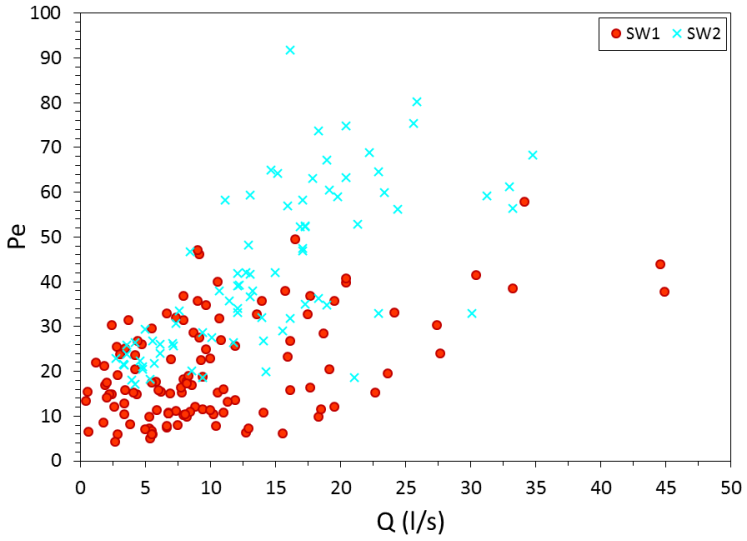

Figure 145: Peclet number against discharge in South Wetlands, where SW2 analysis uses lower cut-off value, i.e. 0.2%.

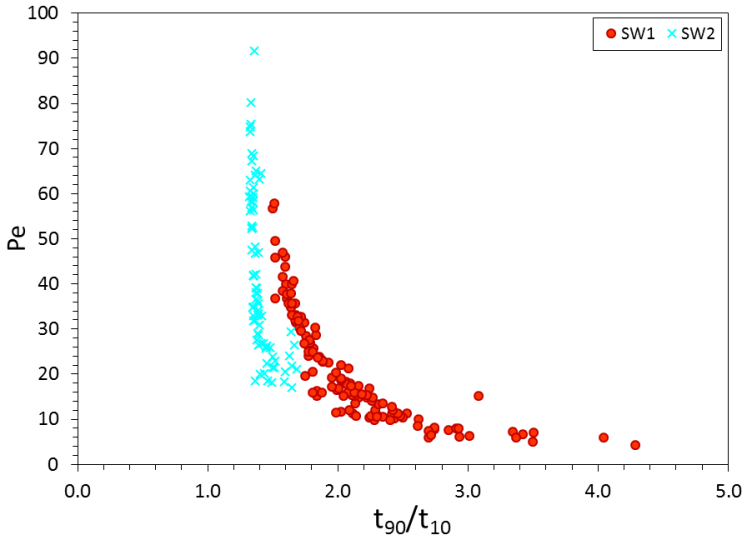

Figure 146: Peclet number against mixing index in South Wetlands, where SW2 analysis uses lower cut-off value, i.e. 0.2%.

9.4Appendix IV: Related to Chapter 6 – Further Applications & Experimental Results

a. Vegetation characteristics in NW

Despite the lack of rainfall and the intermittent flow regime in NW during the monitoring period 2015-2016, vegetation characteristics were monitored, and are presented in Table 9.2, including stem diameter, population density, plant biomass, and plant porosity expressed through two extreme stem deflection positions.

Table 9.2: Record of vegetation characteristics measurements in NW.

NW				
Mean stem diameter, d_m (mm)	4.73		Stem deflection	
Population density, N_t (no./m^2)	114		*Upright,* η_g	0.998
Plant biomass, B_p (gr/m^2)	284 (281)		*Fully-deflected,* η_{dc}	0.979

Note that values in brackets refer to the dry weights of the plant biomass.

b. Calibration values for longitudinal mixing study and differential advection study in NW during Campaign II

Calibration values of fluorometers for longitudinal mixing and differential advection studies undertaken during Campaign II in NW are shown in Figure 147. Gain 1 sensitivity was used. The corresponding location for the serial number of each fluorometers is given in Table 9.3. Locations can be seen in Figure 94.

Table 9.3: Fluorometer locations & corresponding serial numbers (SN) for the NW mixing study.

	Longitudinal mixing		**Transverse Locations**			
Location	**Before pipe**	**After pipe**	**L1**	**L2**	**L3**	**L4**
Instrument SN	SN2100911	SN2100912	SN2100670	SN2100913	SN2103148	SN2101038

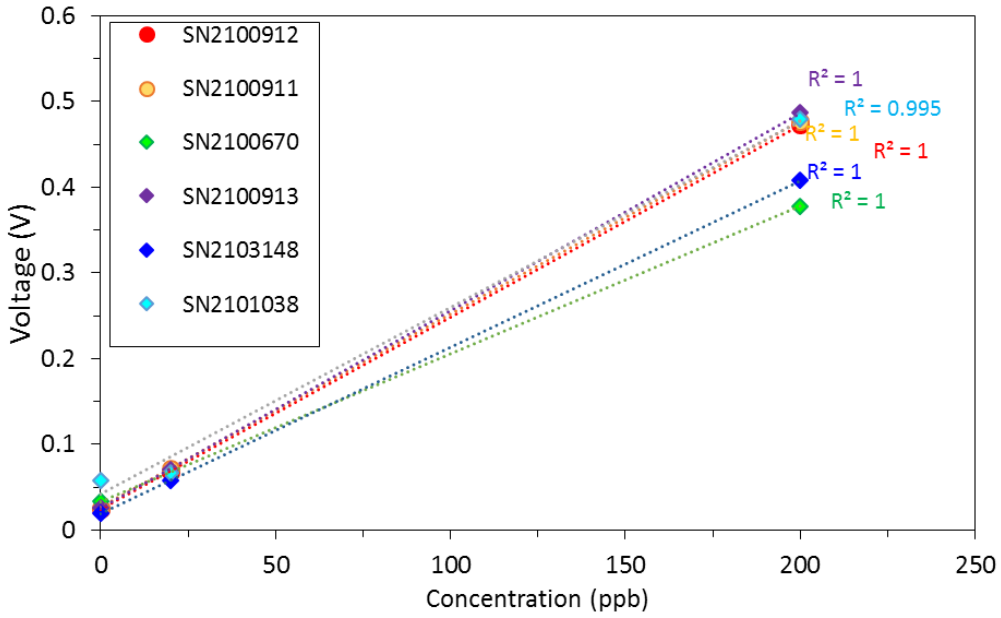

Figure 147: Calibration values of fluorometers for longitudinal mixing and differential advection studies in NW at Gain 1 sensitivity.